

Proteoglycans in the Corneal Stroma and their Role in Development and Pathology

Thesis submitted to Cardiff University for the degree of
Doctor of Philosophy in the discipline of Biophysics

Barbara Paulina Palka (MSc)

The Structural Biophysics Group
School of Optometry and Vision Sciences
Cardiff University
2010

UMI Number: U517541

All rights reserved

INFORMATION TO ALL USERS

The quality of this reproduction is dependent upon the quality of the copy submitted.

In the unlikely event that the author did not send a complete manuscript and there are missing pages, these will be noted. Also, if material had to be removed, a note will indicate the deletion.



UMI U517541

Published by ProQuest LLC 2013. Copyright in the Dissertation held by the Author.
Microform Edition © ProQuest LLC.

All rights reserved. This work is protected against
unauthorized copying under Title 17, United States Code.



ProQuest LLC
789 East Eisenhower Parkway
P.O. Box 1346
Ann Arbor, MI 48106-1346

DECLARATION

This work has not previously been accepted in substance for any degree and is not concurrently submitted in candidature for any degree.

Signed Marine Palle (candidate) Date 01.03.11

STATEMENT 1

This thesis is being submitted in partial fulfillment of the requirements for the degree of PhD.

Signed Marine Palle (candidate) Date 01.03.11

STATEMENT 2

This thesis is the result of my own independent work/investigation, except where otherwise stated. Other sources are acknowledged by explicit references.

Signed Marine Palle (candidate) Date 01.03.11

STATEMENT 3

I hereby give consent for my thesis, if accepted, to be available for photocopying and for inter-library loan, and for the title and summary to be made available to outside organisations.

Signed Marine Palle (candidate) Date 01.03.11

Summary

The unique structure of the cornea is essential for this connective tissue to be transparent. Any disruption in the spatial arrangement or size of collagen fibrils results in cornea becoming opaque. Thus, ultrastructure is closely linked to transparency. Proteoglycans in the corneal stroma are widely believed to influence its ultrastructure.

This thesis will focus on two situations in which proteoglycan changes are potentially linked to corneal structural change and transparency loss. In developing chick cornea, changes in stromal architecture, hydration and content of extracellular matrix molecules such as proteoglycans accompanies the onset of transparency in the last week of development. Conversely, in patients suffering from genetic malfunctions in the proteoglycan synthesis pathway, corneal structure is often changed and transparency lost. These model systems will be studied to shed light on possible roles of proteoglycans for the control of corneal fibril structure and thus transparency.

In the developing chick cornea and in macular cornea dystrophy (MCD) it was found that the progressive close packing of collagen fibrils is not homogenous. Microbeam small angle X-ray diffraction revealed that in MCD collagen fibrils are more closely packed in the deep stromal layers, which was attributed to differential distribution of proteoglycans. In the developing chick cornea, compaction of collagen fibrils starts in the deep stromal layers, to be followed by the outer layers so that spacing becomes uniform across the corneal depth before hatch. These changes are most likely associated with preferential sulphation of proteoglycans.

Transmission electron microscopy of a human cornea with excess chondroitin sulphate/dermatan sulphate glycosaminoglycan showed that changes in proteoglycan structure, content and sulphation lead to the formation of abnormally large collagen fibrils. The lack of sulphation of keratan sulphate in MCD also led to abnormally large fibrils, which are present in the deep stromal layers. These findings suggest overlapping roles of the two proteoglycan populations in the corneal stroma with possible feedback mechanisms, too.

Taken together, the findings of this thesis indicate the central role played by proteoglycan-collagen interactions in the development and maintenance of properly formed corneal stroma.

Acknowledgements

I would like to thank my supervisors Professor Andrew Quantock and Professor Keith Meek for all their time, advice and encouragement. Without their support I would not have been able to start or to complete this doctoral research.

I am also grateful to Dr. Rob Young and Dr. Melody Liles for their countless help inside and outside the laboratory and for their effort to always keep my spirits high. I would also like to thank Dr. Craig Boote for solving all my X-ray problems.

Thank you to Professor Shigeru Kinoshita, Dr. Naoto Yagi, and especially Dr. Hidetoshi Tanioka from Kyoto Prefectural University of Medicine and Japan Synchrotron Radiation Research Institute for making experiments in Spring8 possible.

Thank you to Dr. Cecilie Bredrup and Professor Eyvind Rodahl from the University of Bergen for fruitful collaboration.

I would also like to thank Dr. Clair Gealy and Professor James Ralphs from the School of Biosciences for help with the immuno experiment.

Thank you to all support staff in the School of Optometry and Vision Sciences.

And finally, I would like to thank my family and friends for their unconditional love and believe in me.

List of contents

1 Introduction.....	1
1.1 The eye	1
1.2 Cornea	4
1.3 Collagen.....	6
1.3.1 Collagen structure and biosynthesis	6
1.3.2 Types of collagen.....	9
1.3.2.1 Fibrillar collagen.....	10
1.3.2.2 FACIT	11
1.3.2.3 Other collagens	12
1.4 Collagen arrangement and corneal transparency.....	13
1.5 Proteoglycans	16
1.5.1 Small leucine-rich proteoglycans	17
1.5.2 Glycosaminoglycans.....	18
1.5.3 Proteoglycans of the cornea.....	20
1.5.4 Proteoglycans collagen interaction.....	23
1.6 Chick eye development	25
1.7 Human corneal disorders.....	27
1.7.1 Dystrophies	27
1.7.2 Mucopolisaccharidoses.....	29
1.8 Aims and objectives	30
2 General methods	32
2.1 X-ray diffraction.....	32
2.1.1 Principals of method.....	33
2.1.2 Data collection and analysis of patterns	35
2.2 Transmission electron microscopy	41
2.2.1 Tissue preparation.....	42
2.3 Spectrophotometry	44
2.4 Immunofluorescence microscopy.....	46
3 Light transmission through developing chick cornea.....	48
3.1 Methods	49

3.2 Results	50
3.3 Discussion	53
4 Spatial and temporal alterations in collagen architecture in developing chick cornea.....	57
4.1 Methods	58
4.1.1 Specimens	58
4.1.2 Synchrotron X-ray diffraction	58
4.2 Results	59
4.2.1 Ultrastructural fibril changes from corneal centre to periphery with development	59
4.2.2 Depth-profiled ultrastructural fibril changes with development	62
4.2.2.1 Depth-profiled data set #1	64
4.2.2.2 Depth-profiled data set #2.....	66
4.3 Discussion	67
5 Spatial and temporal alterations in proteoglycan content in developing chick cornea.....	71
5.1 Methods	72
5.1.1 Immunofluorescence microscopy	72
5.1.2 Electron microscopy	73
5.2 Results	74
5.2.1 Immunofluorescence microscopy	74
5.2.2 TEM.....	76
5.3 Discussion	82
6 Collagen architecture in human pathologies with proteoglycan defects	85
6.1 Macular corneal dystrophy	85
6.1.1 Case report and methods.....	86
6.1.2 Results	88
6.1.3 Discussion.....	95
6.2 Congenital stromal corneal dystrophy.....	97
6.2.1 Case report and methods.....	97
6.2.2 Results	98
6.2.3 Discussion.....	100
6.3 Sly syndrome – mucopolysaccharidosis VII.....	100
6.3.1 Case report and methods.....	101

6.3.2 Results	102
6.3.3 Discussion.....	105
7 Concluding remarks	107
Appendix.....	113
References	134

List of figures

1 Introduction

Figure 1.1	Schematic of a cross-section of a human and an avian eye.....	2
Figure 1.2	Figure showing a section of the cornea through its depth and the five main layers.	4
Figure 1.3	Schematic of a single collagen α -chain and a triple helical conformation.	7
Figure 1.4	Representation of collagen biosynthesis.	8
Figure 1.5	Schematic of collagen molecules assembled into a fibril with overlap and gap zones.	9
Figure 1.6	Diagram of FACIT collagen type IX along a type II fibrillar collagen.	11
Figure 1.7	Scanning electron micrograph of a stack of lamellae in the corneal stroma showing collagen fibrils running parallel to each other within a lamella, but with lamellae rotated compared to each other.....	14
Figure 1.8	Preferential collagen orientation in the cornea.....	15
Figure 1.9	Small leucine-rich core proteins organised into 5 subfamilies.....	17
Figure 1.10	Simplified structures of corneal matrix glycosaminoglycans attached to the core protein via a linkage region.....	18
Figure 1.11	Decorin core protein interacting with collagen fibril surface via hydrogen bonds between amino acid residues.	24
Figure 1.12	Pictures presenting first 7 days of chicken corneal development while cornea is created and the most significant changes occur	25

2 General methods

Figure 2.1	A) The SPring8 synchrotron and a schematic representation of the facility B) Inside the 40XU beam-line and a holder with attached microscope.	33
Figure 2.2	Schematic diagram of an X-ray beam being scattered from an array of cylindrical fibrils.....	34
Figure 2.3	Transect taken through the centre of a diffraction pattern obtained from human cornea.....	36
Figure 2.4	Projection of the transect image as a graph of intensity against pixel position.....	36
Figure 2.5	An intensity profile of the diffraction pattern with a visible first order equatorial peak used for the calculation of the collagen interfibrillar spacing.....	37
Figure 2.6	An intensity profile of the diffraction pattern with background scatter removed.....	37
Figure 2.7	Schematic representation of the diffraction angle, θ , for rat tail tendon (blue) and a cornea θ_1 (pink) and their interrelationship.....	39
Figure 2.8	Schematic of a transmission electron microscope.....	41

Figure 2.9	Representation of the Lambert-Beer law for the transmission of a beam of light through a cuvette with the sample.....	45
Figure 2.10	Schematic antibody containing heavy and light chains and visible constant and variable regions.....	46
Figure 2.11	Schematic interaction between an epitope of the antigen plus primary and secondary antibodies in the process of labelling a specimen for immunofluorescence microscopy.	47

3 Light transmission through developing chick cornea

Figure 3.1	Part of the light spectrum of visible light in the wavelength range, 400-700nm, with absorption spectra for various corneal components.	49
Figure 3.2	Spectrophotometer cuvette filled with silicone oil containing suspended chick cornea, ~4mm in diameter.....	50
Figure 3.3	Three-dimensional graph of light transmission as a function of development and wavelength.....	51
Figure 3.4	Light transmission as a function of development at different wavelengths (400-700nm).....	51
Figure 3.5	Light transmission as a function of wavelength for corneas of developmental stage E12-E18.	52
Figure 3.6	Light transmission at 500nm wavelength as a function of development.	53
Figure 3.7	Transmission electron micrographs of developing chick cornea (E12-E18).	55

4 Spatial and temporal alterations in collagen architecture in developing chick cornea

Figure 4.1	Front-on and edgeways scan of the chick corneaindicating the path of the beam and direction of raster scan.	59
Figure 4.2a	Collagen fibril spacing as a function of development and radial position.	60
Figure 4.2b	Collagen fibril spacing as a function of radial position in the front-on scan.....	61
Figure 4.3	Data from experiment #1: Fibril interspacing as a function of stromal depth in the developing chick cornea.	63
Figure 4.4	Data from experiment #2: Fibril interspacing as a function of stromal depth in the developing chick cornea.	65

5 Spatial and temporal alterations in proteoglycan content in developing chick cornea

Figure 5.1	Immunofluorescence staining with antibody 7D4 for chondroitin sulphate glycosaminoglycan chains in the chick cornea E12 and E18.....	75
Figure 5.2a-b	Collagen fibrils in the mid corneal stroma at E12 and E13 with visible GAG chains of proteoglycans.....	77
Figure 5.2c-d	Collagen fibrils in the mid corneal stroma at E14 and E15 with visible GAG chains of proteoglycans.....	78

Figure 5.2e-f	Collagen fibrils in the mid corneal stroma at E16 and E17 with visible GAG chains of proteoglycans.....	79
Figure 5.2g-h	Collagen fibrils in the mid corneal stroma at E18 and skin with visible GAG chains of proteoglycans.....	80
Figure 5.3	Accumulation of keratan sulphate proteoglycans in the developing chick cornea at E12-E18.....	81

6 Collagen architecture in human pathologies with proteoglycan defects

Figure 6.1	Clinical appearance of the MCD cornea examined in this thesis. Diffuse ground-glass-like stromal opacities were observed on slit-lamp examination, with irregular patches visible in the cornea by the scleral scattering technique.	87
Figure 6.2	The tissue holder with two mounted strips of cornea.....	88
Figure 6.3	Small angle x-ray diffraction patterns of a human eye bank cornea and MCD cornea, with visible meridional and equatorial reflections.	89
Figure 6.4	Centre-to-centre collagen fibril spacing measured across the strip of human eye bank cornea and MCD cornea in the central region.	90
Figure 6.5	Centre-to-centre collagen fibril spacing measured across the human eye bank cornea and MCD cornea from epithelium to endothelium.	91
Figure 6.6	Transverse-section electron microscopic images of collagen fibrils in the anterior and posterior stroma in MCD. Focal pockets of collagen fibrils of abnormally large diameter are present in the posterior stroma.	92
Figure 6.7	Transverse-section electron microscopic images of collagen fibrils in the posterior stroma in MCD. Visibly enlarged collagen fibrils are in evidence.....	93
Figure 6.8	Histograms showing the range of collagen fibril diameters in regions of MCD stroma which contain abnormally large diameter fibrils, and in the normal human cornea.....	94
Figure 6.9	Transmission electron micrographs of the human sclera before and after chondroitinase ABC digestion.	98
Figure 6.10	Transmission electron microscope of CSCD cornea. In the break in between the lamellae there are visible GAG filaments.	99
Figure 6.11	Electron microscope micrographs of the CSCD cornea treated with chondroitinase ABC to remove CS and DS GAG chains.	99
Figure 6.12	Transmission electron micrograph of a keratocyte in the Sly syndrome cornea with visibally enlarged vacuoles filled with proteoglycan and enlarged filaments of PG amongst collagen fibrils. Image courtesy of Dr Rob Young.....	102
Figure 6.13	Transmission electron micrographs of the outer, mid and deep corneal stroma in Sly syndrome with different sized collagen fibrils visible. Histograms represent fibril diameter measurements in all three parts of the stroma.	104

List of tables

1 Introduction

Table 1.1	Differences between the human and avian eye.	3
Table 1.2	Types of corneal epithelial cells.	5
Table 1.3	Vertebrate collagen classes.	10
Table 1.4	Distribution of the main collagen types in the corneal layers.	13
Table 1.5	General structure of corneal GAGs.	20
Table 1.6	Chick corneal development.	26
Table 1.7	Corneal dystrophies.	28
Table 1.8	The mucopolisaccharidoses, with indicated enzyme malfunctions and type of GAG accumulated in the lysosomes.	29

4 Spatial and temporal alterations in collagen architecture in developing chick cornea

Table 4.1	Table of collagen interspacing in the developing cornea (E15-E18) in the 75µm closest to the epithelium and endothelium for data set #1 and #2.	67
-----------	--	----

List of abbreviations

Ab	antibody
Ala	alanine
Asp	asparagine
BSA	bovine serum albumine
C	carbon
CB	cuprolinic blue
ch'ase ABC	chondroitinase ABC
Col	triple helical collagenous domain
CS/DS	chondroitin/dermatan sulphate
CSCD	congenital stromal corneal dystrophy
Cys	cysteine
E	embryonic day
ECM2	extracellular matrix protein 2
FACIT	fibril-associated collagen with interrupted triple helices
Fuc	fucose
GAG	glycosaminoglycan
Gal	galactose
GalNAc	N-acetyl-galactosamine
GlcNAc	N-acetyl-glucosamine
GluA	glucuronic acid
Gly	glycine
HS	heparan sulphate
I	intensity
IduA	iduronic acid
Ig	immunoglobulin
KS	keratan sulphate
LRR	leucine-rich repeats
MACIT	membrane-associated collagen with interrupted triple helices
Man	mannose
MCD	macular corneal dystrophy
MIM	mendelian inheritance in man
MPS	mucopolisaccharidosis
MULTIPLEXIN	multiple triple-helix domain and interruptions
NC	non-collagenous domain
PBS	phosphate-buffered saline
PG	proteoglycan
PRELP	proline arginine-rich end leucine-rich repeat protein
PTA	phosphotungstic acid
R	radial position
SD	standard deviation
Ser	serine
SLRP	small leucine-rich proteoglycan
UA	uranly acetate
Xyl	xylose

Chapter One

1 Introduction

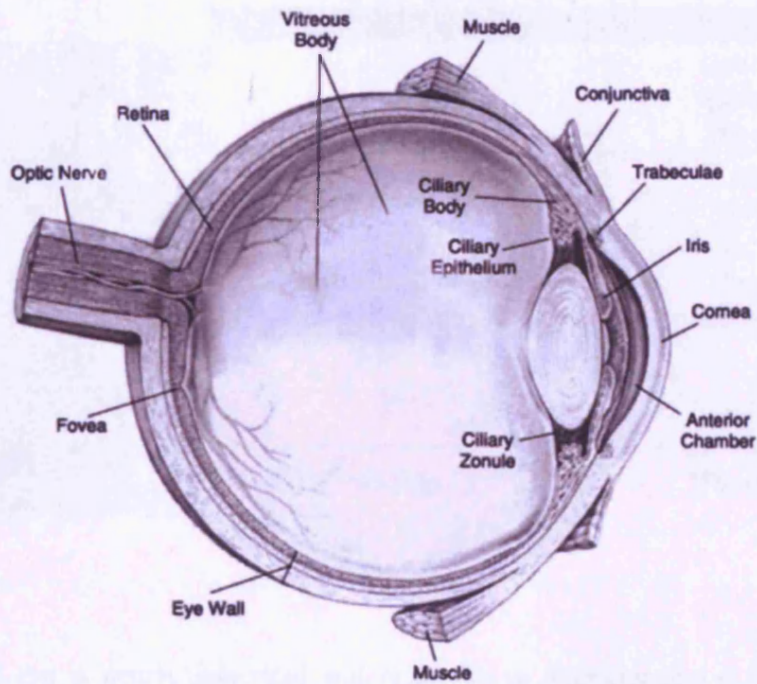
This chapter presents a brief description of the ocular system with emphasis on corneal structure. To act as a basis for the research presented and discussed in this thesis, it provides information about proteoglycans, collagen structure and biosynthesis, as well as the interactions and functions of these molecules. Brief introductions to chick eye development and human ocular disease affecting the structure of the cornea are also included.

1.1 The eye

The eye is the organ of photoreception in the animal kingdom. The structure of vertebrate's eyes, including human and bird eyes share fundamental similarities (Figure 1.1). In the eye, the incoming light has to pass through four transparent media: the cornea, aqueous humor, lens and vitreous humor before reaching the retina, where photoreceptors convert light energy into electric impulses. These impulses are sent via the optic nerve to the brain's cortex, where a visual image emerges. Several extraneous structures and layers give the eye the strength to resist injuries, withstand intraocular pressure and help in accommodation. For example, the eye is suspended and moved in the orbit of skull by six extra-ocular muscles attached to the white outer coat of the eye, called the sclera. The conjunctiva lines the eyelids and folds back to attach to the eye. The back eye's nourishment is provided by a vascular layer called the choroid. The front of the eye is nourished by the turnover of aqueous humor produced by the ciliary body and tear film. Small ciliary body muscle are responsible for the movement of the lens causing changes in accommodation, with the amount of light entering the eye controlled by small ring muscle of the iris which changes its aperture.

Inevitably some differences occur between avian and human eye, mainly due to avian adaptation to various habitats and avian nature in general. The main differences are presented in Table 1.1, which I created based on a selection of anatomical books.

A



B

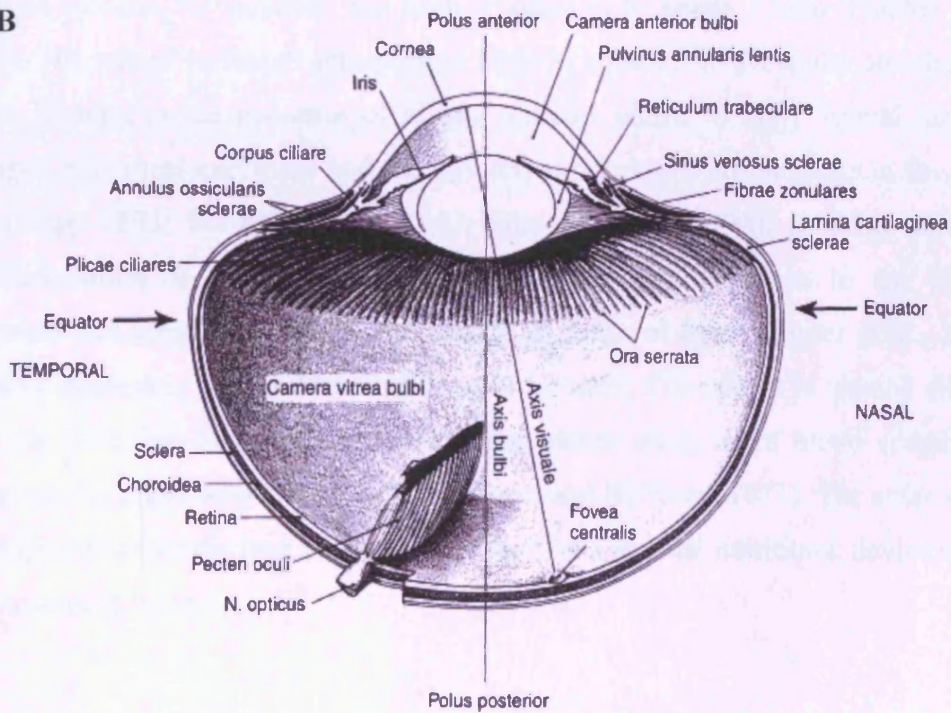


Figure 1.1 Schematic diagram of a cross-section of (a) a human eye (after Mac and Joy, 2000) and (b) an avian eye (after Güntürkün, 1998).

Table 1.1 Differences between the human and avian eye.

	Human eye	Avian eye
Shape	sphere	flattened globose tubular
Accommodation organ	lens	lens cornea
Nutrition provider	choroid aqueous humor tear film	pecten choroid aqueous humor
Number of eyelids	2	3
Transmitted light	visible	UV-visible

The human eye is nearly spherical and is 25mm in diameter and 6.5ml in volume (Forrester et al., 2002). Avian eyes differ in shape and size but are always large in comparison to their body size. The equatorial diameter of a 3-week-old White Leghorn chicken, for example, has been reported to be nearly 13mm (Prashar et al., 2009). The retinal surface is increased in birds to enhance visual acuity and depth of focus. Thanks to the presence of ciliary muscles attach to bony scleral ossicles, changes in corneal curvature and thereby refractive power are possible in the avian eye (Beer, 1893; Schaffel et al., 1987; Glasser et al., 1994). In adult chick an accommodation of 25 Dioptres can be induced, with 40% due to the corneal curvature and remaining 60% to the change in shape of lens (Glasser et al., 1994). Another interesting feature in a bird's eye is a pecten. The pecten is located directly over the optic disc near the retina and is completely made up of blood vessels and extravascular pigmented stroma cells (Bellhorn and Bellhorn, 1975). The avian retina is completely avascularised and the presence of this unusual nutritional device seems to compensate for this.

1.2 Cornea

The most outer layer in the front of the eye has to combine an optical function with structural strength. For that reason, cornea has to be fully transparent to focus incoming light and be tough to counter trauma and infections from the outside environment. The cornea bulges from the sclera in the transition region called the limbus. This highly vascularised area is rich in stem cells that are responsible for an epithelial layer turnover (Davanger and Evensen, 1971) and wound healing (Huang and Tseng, 1991).

The human cornea is roughly spherical, although its diameter is slightly smaller in the vertical (9.0-11.0mm) than in the horizontal (10.6-11.7mm) direction, and it is thicker at the periphery (0.67mm) in comparison with the centre (0.52mm) (Tovee, 2008). The chick cornea continues to grow after hatch and from 0.16mm thick at hatch it reaches 0.25mm in the young hen (Hay and Revel, 1969). Corneal curvature and axial length are maintained by pressure from the fluids inside the eye (Oyster, 1999).

Chick and human cornea differ in size, however, their basic structure manifests considerable similarity. In the normal physiological state the cornea has no blood vessels, but has tightly packed nerve endings on the surface (Rózsa and Beuerman, 1982). The fully developed human and avian cornea consists of five layers (Figure 1.2).

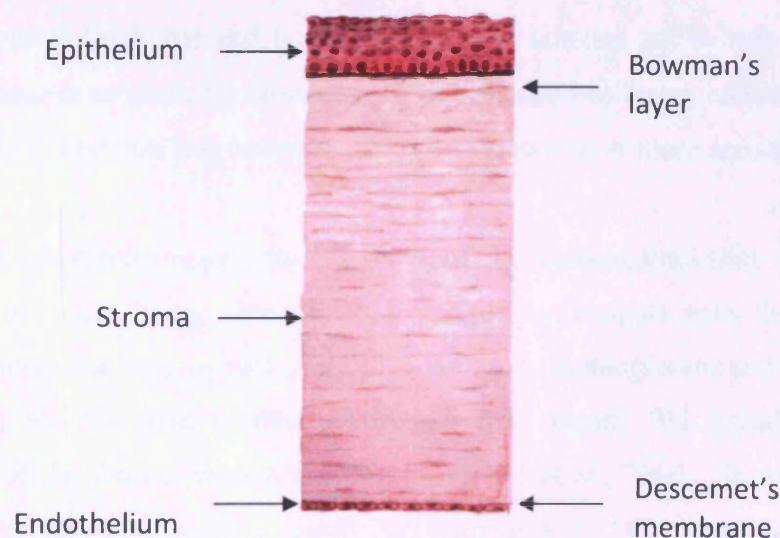


Figure 1.2 Image of the section of the cornea divided into five layers.

(Modified from [://education.vetmed.vt.edu/curriculum/VM8054/EYE/CRNSCLRA.HTM](http://education.vetmed.vt.edu/curriculum/VM8054/EYE/CRNSCLRA.HTM))

The human epithelium is around 50µm thick, which is approximately 10% of the whole thickness of the cornea and it consist of different types of cells described in Table 1.2.

Table 1.2 Types of corneal epithelial layers based on selection of books.

Cells type	Number of layers	Characteristics
surface cells	2	flattened squamous non-keratinised
polygonal cells	2-3	wing shaped
basal cells	1	cuboid

The basal cells constantly proliferate and thus push existing epithelial cells upwards. With each division the most superficial layer of surface cells is removed. Total epithelial turnover takes around 2 weeks (Cenedella and Fleschner, 1990). All epithelial cells are held together by desmosomes, and the epithelium is attached to the stroma by an attachment complex. The lamina densa is anchored to the Bowman's layer by a meshwork of anchoring collagen VI and VII filaments and hemidesmosomes (Gipson et al., 1987).

The most anterior part of the corneal stroma is Bowman's layer. It takes up to 2% of the total corneal thickness and is 8-14µm thick in humans and 4-5µm thick in the hen. This layer is an acellular meshwork of disorganised collagen, consisting of short and thin fibrils, and this is believed to make Bowman's layer more resistant to strain.

The stroma constitutes approximately 90% of the corneal thickness. It is mainly composed of water being about 75% hydrated (by weight) with the biological material comprising various collagens, glycoproteins, proteoglycans and keratocytes. Keratocytes are flattened corneal fibroblasts that occupy 9% (middle) to 17% (posterior) of the human stroma's volume (Hahnel et al., 2000). Stromal collagen fibrils are organised into approximately 200 (Hogan et al., 1971) 2µm thick lamellae that lie parallel to the corneal surface in the central cornea (Komai and Ushiki, 1991). Within the lamellae run regularly arranged collagen fibrils of small uniform

diameter. The stroma's unique structure makes the cornea the only connective tissue which is transparent. The architecture of the stroma and the theories of transparency will be presented in Section 4.

Descemet's membrane is produced by the endothelium to separate it from the stromal matrix. It constitutes less than 2% of corneal thickness. It can be divided into zones: one of which is granular and amorphous and the other, well organised and banded with nodes linked together with strands into hexagons (Jakus, 1956). This membrane is rich in fibronectin or laminin, and in collagen types IV, V, VI and VIII.

The corneal endothelium is a single layer of hexagonal cells that form the posterior surface of the cornea. These cells have a long life but low regenerative capacity. Cell density decreases with age in normal adult cornea at a rate of 0.6% per year (Bourne et al., 1997). The remaining cells compensate for this loss by stretching and changing shape (Yee et al., 1985). The endothelium, via a system of pumps, controls the maintenance of the right corneal hydration, and thus transparency (Maurice, 1972). It controls the flow of fluids and ions between the stroma and aqueous (Hodson and Miller, 1976; Bonanno, 2003).

1.3 Collagen

Collagen is the most abundant protein in the animal kingdom and a prevalent component of the corneal stromal extracellular matrix. It plays not only a structural role but is involved in cell attachment, differentiation, and also in immunopathological, developmental and physiological processes.

To date, 28 collagen types have been identified, of which 18 can be found in human cornea and 11 take part in the process of corneal development (Linsenmayer et al., 1998; Ihanamäki et al., 2004; Gordon and Hahn, 2010).

1.3.1 Collagen structure and biosynthesis

There are two characteristics that all collagen molecules have in common, that is being composed of three α -chains and having at least one domain in which these

chains are arranged in a left-handed triple helix by being closely wrapped around one another (Figure 1.3).

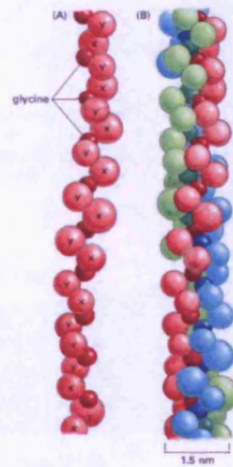


Figure 1.3 Schematic of a single collagen α -chain and a triple helical conformation (after Alberts et al., 2002).

This conformation is stabilised by inter-chain hydrogen bonds. The peptide bonds linking adjacent amino acids are hidden in the interior of the molecule. To fold α -chains into the proper helical conformation, glycine must be present as every third amino acid. The chains are therefore composed of a series of triplets Gly-X-Y, where X and Y can be any amino acid but are often proline and hydroxyproline, respectively (Ramshaw et al., 1998). Triple helical regions (Col domains) are flanked by non-collagenous domains, which are non-glycine-X-Y regions (NC domains or telopeptides). The significance of the triplet with Gly to form the triple helix becomes obvious when mutation of a single residue (replacing Gly with Ala) results in the formation of crystals rather than fibrils (Bella et al., 1994). The hydroxyproline in the position Y but not X, increases dramatically the thermal stability of triple helices (Berg and Prockop, 1973).

Collagen is firstly synthesised in the rough endoplasmic reticulum of stromal keratocytes (Ruggiero et al., 1996). Then procollagen molecules undergo a series of modifications and folding that involves activity of glycosyltransferases, isomerases and collagen-specific chaperone Hsp47 (Nagata, 1998). Procollagen molecules are transported then to the Golgi apparatus where molecules are stacked laterally and are secreted into the extracellular space (Figure 1.4).

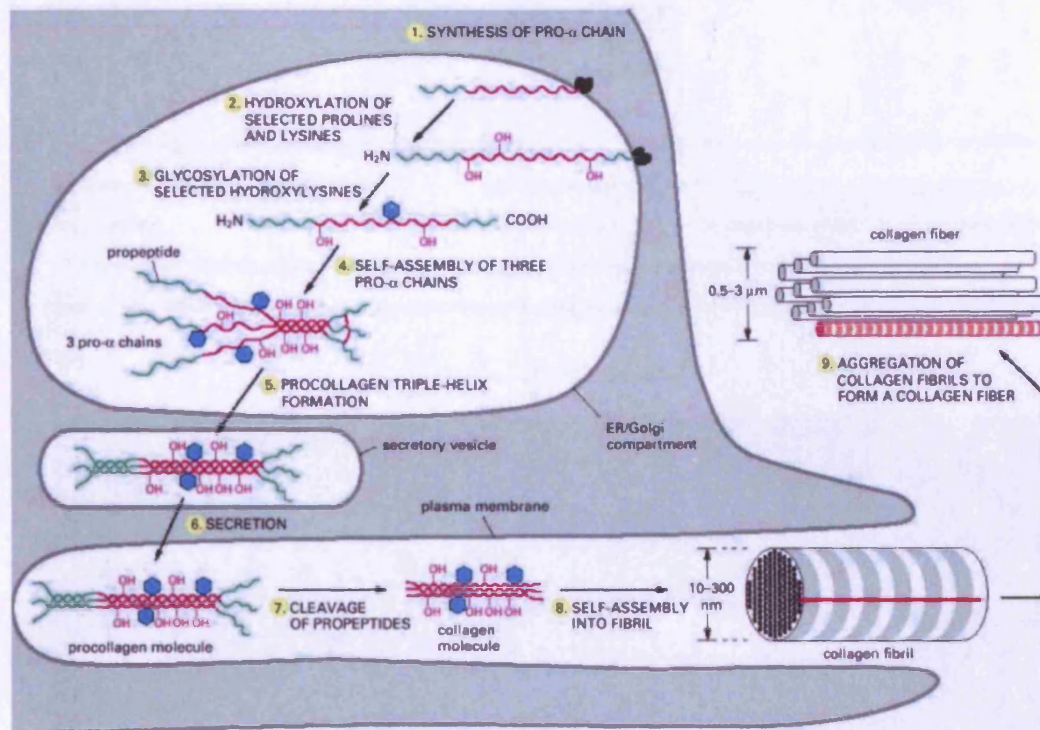


Figure 1.4 Representation of collagen biosynthesis (after Alberts et al., 2002).

At this stage molecules are composed of a central triple helical domain and non collagenous domains at N- and C- terminal ends. Both of these domains are cleaved by propeptidase enzymes generating mature collagen molecules. However, only removing C-propeptides is required for the correct course of events where mature triple helical collagen molecules assemble into fibrils (Kadler et al., 1987). Fibrillogenesis is a self-assembly process, but in vivo, the presence of fibronectin, fibronectin-binding and collagen-binding integrins and collagen V or XI is required (Linsenmayer et al., 1993; Wenstrup et al., 2004; Kadler et al., 2008).

Fibril forming collagen has an axial D-periodicity of 67nm and displays a staining pattern comprising a gap (dark) and an overlap (light) zone (Petruska and Hodge, 1964). However, D-periodicity in different tissues can vary and has been reported to be 65nm in corneal collagen (Meek et al., 1981). This light and dark pattern is a reason for calling fibril forming collagen a banded fibrils. The positive staining pattern shows even more intense banding along the fibrillar axis. Bands within each D-periodicity have designated letters "a" to "e" (Figure 1.5) (Smith and Frame, 1969).

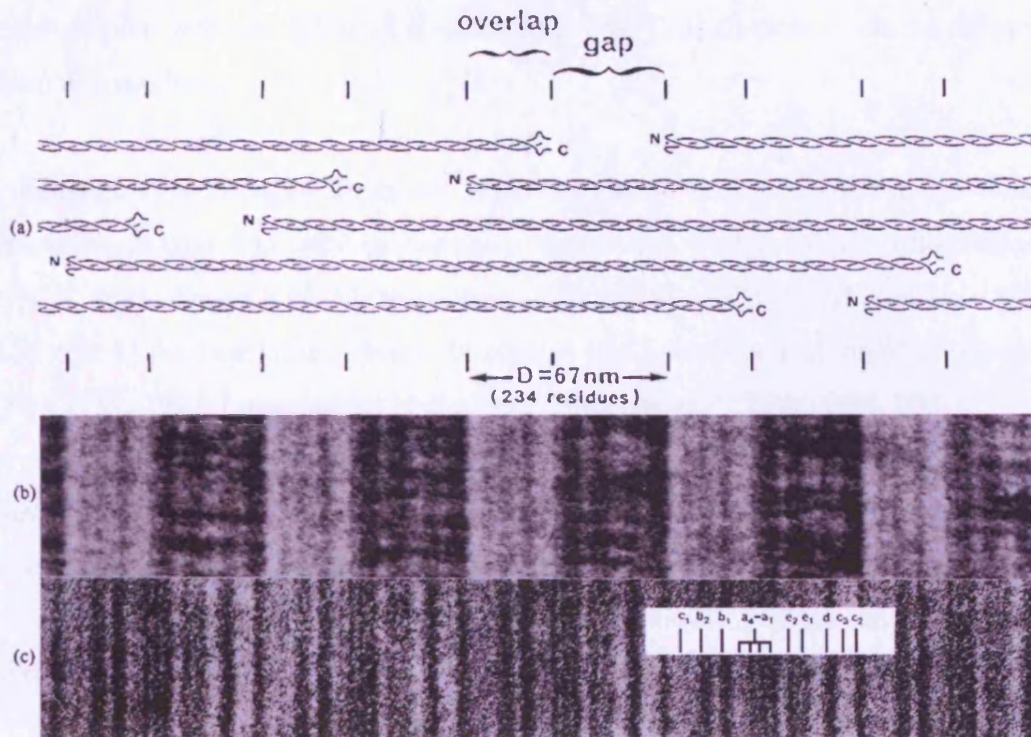


Figure 1.5 Schematic of collagen molecules assembled into a fibril with overlap and gap zones visible (a). Fibrils negatively (b) and positively (c) stained with PTA show collagen binding sites (after Kadler et al., 1996).

The stability of the collagen fibril comes from its coiled coil three-dimensional structure. A single collagen α -chain is a right-hand helix, which with two other α -chains form a left-hand triple helical structure. These triple helices are organised into microfibrils arranged in the way that they form another right-hand helix by being tilted $\sim 15^\circ$ to the fibril long axis (Wess et al., 1998; Holmes et al., 2001). Microfibrils show a quasi-hexagonal cells packing (Orgel et al., 2000) and a separation of intact microfibrils is virtually impossible, because of an interaction between N- and C-termini of collagen molecules, which creates covalent cross-links within and in between microfibrils (Orgel et al., 2000).

1.3.2 Types of collagen

It is now well established that most connective tissues are composed of several collagen types. Collagen of a specific type can consist of homotrimeric molecules (e.g. type II, III) where all three α chains are the same, or can be formed of

heterotrimers with one different α -chain (e.g. type I) or all three α -chains different from one another (e.g. type IX).

Pure single-type collagen fibrils are unlikely to exist. Collagen type I in the cornea and collagen type II in cartilage are paired to create heterotypic fibrils with collagen type V and collagen type XI, respectively (Birk et al., 1986, Mendler et al., 1989). The role of the two latter types is to control fibril diameter and longitudinal growth (Birk et al., 1990; Linsenmayer et al., 1993; Blaschke et al., 2000; Birk, 2001).

Several classes of collagenous molecules can be distinguished based on size, domain structure and supramolecular organisation. 27 collagen types are presented in Table 1.3. The most recent collagen type XXVIII has been identified but cannot be clearly assign into any collagen subgroup (Veit et al., 2006).

Table 1.3 Vertebrate collagen classes (Shoulders and Raines, 2009).

Collagen class	Collagen types
Fibrillar	I, II, III, V, XI, XXIV, XXVII
FACIT	IX, XII, XIV, XVI, XIX, XX, XXI, XXII, XXVI
Network	IV, VI, VIII, X,
Anchoring fibrils	VII
MACIT	XIII, XVII, XXIII, XXV
MULTIPLEXIN	XV, XVIII

Abbreviations:

FACIT – fibril-associated collagen with interrupted triple helices

MACIT – membrane-associated collagen with interrupted triple helices

MULTIPLEXIN – multiple triple-helix domains and interruptions

1.3.2.1 Fibrillar collagen

The most abundant and broadly studied collagen class is fibrillar collagen. Structure, biosynthesis and fibrillogenesis of this classic striated collagen are described in part 3.1 of this chapter as a representative model of collagen. In the cornea, which is the subject of all the research included in this thesis, type I, II, III and V can be found.

Type I collagen has been isolated from many adult connective tissues, including the primary and secondary corneal stroma and Bowman's layer. Its function is to give tissue tensile strength. Type II collagen is mainly found in cartilage (Miller and Matukas, 1969) and vitreous (Trelstad and Kang, 1974). In an avian developing cornea type II is present in the primary stroma, although it disappears by E20 and is visible in hen cornea only in Descemet's membrane (Hendrix et al., 1982). The proportion of type III collagens is low in healthy cornea but increases during wound healing or inflammation (Mally et al., 1990). Detectable collagen III in mature tissue is associated with the stroma and epithelial substratum. Type V collagen is a part of a heterotypic fibril with collagen type I in mature corneal stroma (Fitch et al., 1984). Type V in the native form retains a large pepsin-sensitive NH_2 -terminal domain at the end of its α -chains, which regulates fibrillogenesis and fibril diameter (Linsenmayer et al., 1993; Andrikopoulos et al., 1995; Linsenmayer et al., 1998) and in Bowman's layer its function may be the anchoring of basement membranes to the underlying stromal matrix (Adachi and Hayashi, 1986).

1.3.2.2 FACIT

Fibril associated collagens with interrupted triple helices (FACITs) are a class of molecules designed for interaction with fibrils and other matrix components. Each FACIT molecule contains multiple triple helical domains interrupted by non-triple helical domains (Figure 1.6). Some domains lie along the fibril surface and anchor the molecule to the underlying fibrillar collagens. Other domains protrude from the fibril to support interactions with adjacent fibrils or matrix components (Shaw and Olsen, 1991).

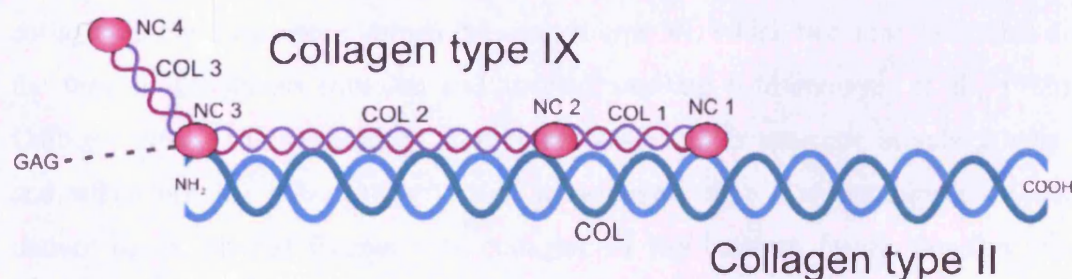


Figure 1.6 Diagram of FACIT collagen type IX along a type II fibrillar collagen. COL-triple helical collagen domain, NC-non collagenous domain.

Type IX collagen is associated with type II collagen molecules of fibrils in the primary corneal stroma, the vitreous and cartilage (Fitch et al., 1988). Collagen type IX consists of three Col domains and four NC domains (Figure 1.6) (van der Rest et al., 1985). One of the NC domains may have a chondroitin sulphate side chain attached, which provides another potential functional group for interaction with matrix components (van der Rest and Mayne, 1988; Fitch et al., 1995). Type IX function in cornea is probably to stabilise the primary corneal matrix; hence this collagen type disappears after stromal swelling (Cai et al., 1994; Fitch et al., 1998).

Type XII and XIV are structurally similar and are associated with fibrils containing collagen type I (Gordon et al., 1990; Keene et al., 1991). In the developing avian cornea both types are temporally and spatially separated. Collagen type XIV is detectable throughout the stromal thickness in early development and during tissue compaction, while collagen type XII is deposited near Bowman's layer and Descemet's membrane regions where matrices interface with one another throughout development (Gordon et al., 1996; Akimoto et al., 2002). This may suggest that type XII collagen has a role in development of stromal architecture and maintenance of fibril organisation, while type XIV collagen may play a role in the regulation of fibrillogenesis (Young et al., 2002).

1.3.2.3 Other collagens

In the cornea there are three types of network-forming collagens: IV, VI and VIII. Type IV collagen makes a three-dimensional structure in basement membranes (Yurchenco and Ruben, 1988) and is present in the developing avian stroma as strings and plaques of basement-like material (Fitch et al., 1991). Another common collagen in the developing cornea is collagen type VI, which becomes detectable at the time of fibroblasts invasion and stromal swelling (Linsenmayer et al., 1986). Collagen type VI is secreted by fibroblasts; however, its presence in subepithelial and subendothelial areas suggests that those layers may also participate. In the mature tissue, beaded filaments of collagen VI run between layers, bundles and fibrils, and in the less dense matrix interact with striated fibrils of collagen I (Bonaldo et al., 1990). Collagen type VIII (Sage et al., 1983) forms hexagonal lattices in Descemet's membrane of the cornea (Sawada et al., 1990). Collagen type

VII is a part of the anchoring filaments which form an attachment complex adhering the corneal epithelium to the anterior stroma (Burgeson et al., 1990; Gipson, 1992). Recently it also has been shown merging into the banded collagen fibrils in dermis (Villone et al., 2008), whereas type XVII is involved in a hemidesmosomal attachment complex (Li et al., 1993; Gordon et al., 1997).

The types of collagen detected in the cornea are shown in the Table 1.4 according to their position in the cornea, except collagen type XX. Although expression of this type of collagen has been found in the layer of corneal epithelium, insufficient information is available to place this FACIT into any of categories below (Koch et al., 2001).

Table 1.4 Distribution of the main collagen types in the corneal layers (Marshall et al., 1993; Linsenmayer et al., 1998; Michelacci, 2003).

	I	II	III	IV	V	VI	VII	VIII	IX	XII	XIII	XIV	XVII	XVIII
Anchoring complex				×		×	×						×	
Bowman's layer	×		×		×	×								
Primary stroma	×	×		×		×			×					
Secondary stroma	×		×		×	×				×	×	×		
Descemet's membrane				×		×		×						×

1.4 Collagen arrangement and corneal transparency

Collagen fibrils are arranged in the corneal stroma into lamellae stacked on one another and especially in the developmental stage, they are organised into orthogonal lattices. Most fibrils have a uniform diameter (25-35nm) and run nearly parallel to each other with regular spacing, forming bundles that coalesce into flat lamellae throughout development (Figure 1.7) (Trelstad and Coulombre, 1971; Birk and Trelstad, 1984; Meek and Leonard, 1993; Hirsch et al., 1999).

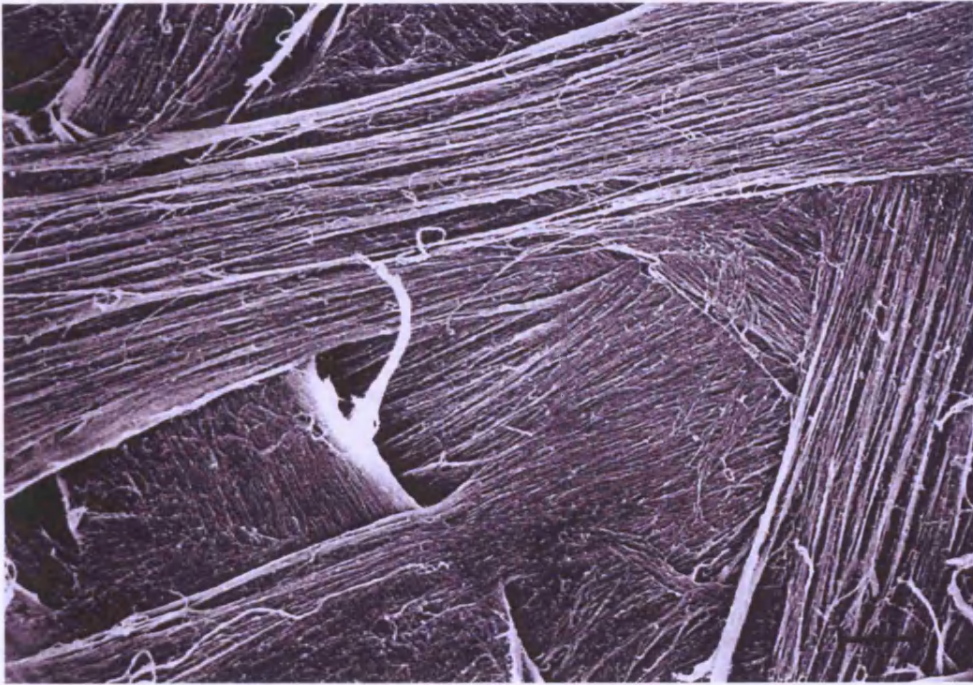


Figure 1.7 Scanning electron micrograph of a stack of lamellae in the corneal stroma showing collagen fibrils running parallel to each other within a lamella, but lamellae rotated compared to each other. Calibration bar = 10 μ m (after Radner et al., 1998).

In the central region of the human cornea, there are approximately 240 stacked lamellae and this number increases to 500 at the limbus (Hamada et al., 1972; Bergmanson et al., 2005). Each lamella is rotated in the plane of the cornea at a certain degree (between 0 and 90°) compared to the adjacent lamella. In the anterior stroma, collagen lamellae are thin (0.2-1.2 μ m), sometimes splitting into two or three sublayers that become interwoven. Sometimes lamellae split not only in the horizontal direction but also in the anterior to posterior direction (Radner et al., 1998). In the posterior stroma, collagen lamellae tend to be parallel to the corneal surface and are thicker (0.2-2.5 μ m) than in the anterior stroma. In a thin layer near Descemet's membrane collagen fibrils run in various directions and form a loose fibrillar network (Komai and Ushiki, 1991). In the plane of the cornea, collagen fibrils run in different directions, although it is possible to distinguish a preferential spatial organisation. In the central cornea fibrils are orientated in the inferior-superior and nasal-temporal directions, while near the limbus collagen run along the circumference (Meek et al., 1987; Boote et al., 2005) (Figure 1.8). The preferential orientation of highly aligned collagen is restricted to the posterior stromal layers (Kamma-Lorger et al., 2010).

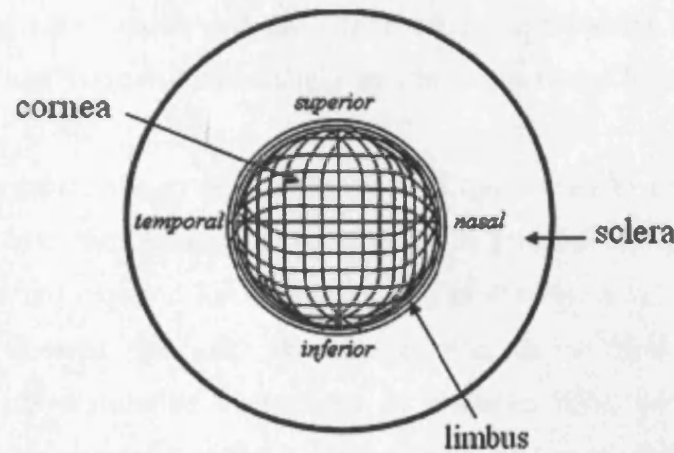


Figure 1.8 Preferential collagen orientation in the human cornea (after Boote et al., 2005).

Unlike all other collagen-rich tissues, the cornea is transparent and, as I will describe later, the characteristic fibrillar architecture of the stroma is responsible for this. The stroma, apart from collagen fibrils, also includes keratocytes and other matrix components. Corneal fibroblasts in the normal healthy state produce corneal crystallins, which make them weak light scatterers by reducing refractive index inhomogeneities in the cytoplasm and make keratocytes more transparent (Jester et al., 1999; Jester, 2008). For that reason, in most of the transparency theories, an important feature is the arrangement, centre-to-centre spacing, and size of the collagen fibrils.

The lattice arrangement of corneal collagen fibrils inspired the first explanation of corneal transparency by Maurice (1957). It proposed that the small size and uniform spacing leads to destructive interference between the light scattered by individual fibrils, thus limiting the intensity of scattered light and resulted in only forward transmission of light. Goldman et al. (1968) modified the lattice theory of Maurice and included the fluctuation in the index of refraction within the media as a function of distance. In general, it proposed that incident light scattering in the media is dependent on the wavelength of light and the magnitude of the refractive index fluctuations. When the distance between scattering structures is less than half the wavelength of visible light (approximately 200nm), the medium is transparent. Another model was suggested by Smith (1969) in which he assumed that all corneal components have a uniform refractive index and light propagates through the tissue unscattered. This model proved to be unsound based on evidence including X-ray

diffraction data, which confirmed the difference in the refractive indices between collagen fibrils and the rest of extracellular matrix (Leonard and Meek, 1997).

The pioneering lattice theory of Maurice (1957) has proved to be a basis for the current models of corneal transparency, although the geometrically perfect regularity of the lattice is not required for transparency (Goodfellow et al., 1978). Hart and Farrell (1969) showed that only short-range order in the fibril arrangement is necessary for the destructive interference of scattered light, while Feuk (1970) developed a long-range order model based on small, random displacements from the ideal lattice. Twersky (1975) assumed a two-dimensional fibril arrangement and distribution based on the volume fraction occupied by fibrils, whilst Benedek (1971) focused on the fibril number density. Hart and Farrell (1969) presented as concept of a radial distribution function that helped Freund to develop a statistical method called the Direct Summation of Fields to predict transmission by a short-range order distribution of different-sized fibrils (Freund et al., 1986). Based on these studies it is believed that corneal transparency depends on incident light wavelength, density of fibril packing, fibril diameter, refractive index of collagen, interfibrillar matrix and their ratio, light scattering angle and thickness of the cornea (Farrell and McCally, 2000). Some of those can be influenced by components of corneal extracellular matrix, mainly proteoglycans.

1.5 Proteoglycans

Proteoglycans (PGs) are molecules associated with the extracellular matrix in many tissues, and in cornea are composed of a core protein with covalently attached glycosaminoglycan (GAG) chains. The exception is hyaluronan which is a GAG not linked to the protein. PGs can be divided into three main categories: small leucine-rich PGs, modular PGs and cell-surface PGs.

PGs are structural proteins; thus, they play a major role in signal transduction, adhesion, migration, and proliferation of cells, fibril assembly, degradation and inflammation (Fullwood et al., 1996; Merline et al., 2009; Schaefer and Schaefer, 2010). PGs are so functionally diverse due to the numerous differences in size and structure of protein between molecules. The size of a core protein is in the range 20

to 450kD. GAG chains, which are repeating disaccharides with sulphate esters, can be up to 70kD large and can be divided into three main types: chondroitin/dermatan sulphate (CS/DS), keratan sulphate (KS) and heparan sulphate.

1.5.1 Small leucine-rich proteoglycans

Corneal proteoglycans belong to the small leucine-rich proteoglycans (SLRP) family, which consist of 5 subfamilies and is expanding (Figure 1.9). Members of SLRP PGs share some common characteristics. For example, the central domain of the core protein constitutes leucine-rich motifs repeats (LRR) flanked by two conserved cysteine-rich regions. In all SLRP PGs, the C-terminal cysteine motif forms a disulfide bond between Cys 284 and Cys 317 causing the extended LRR to fold creating the structure called an “ear repeat”. N-terminal contains a cluster of four cysteines capping motif and GAG chain attachment sites (Scott et al., 2004; McEwan et al., 2006).

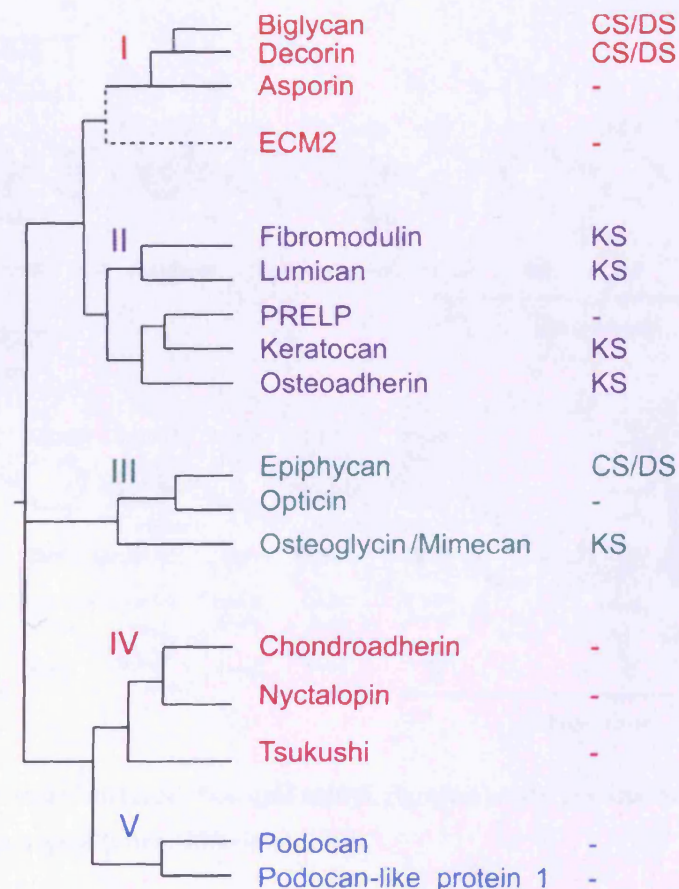


Figure 1.9 Small leucine-rich core proteins organised into 5 subfamilies (Scheaffer and Iozzo, 2008). Next to proteins, GAG chains that can be attached to the core to form PGs.

In the healthy adult corneal stroma, four main PGs can be found: decorin (Li et al., 1992), lumican (Blochberger et al., 1992b; Kao, 2006), keratocan (Corpuz et al., 1996; Chakravarti, 2006) and mimecan (Funderburgh et al., 1997).

The core proteins of all corneal PGs have a similar size of 40-52kD (Blochberger et al., 1992b). Decorin has a single 55-60kD CS/DS chain, while lumican, keratocan and osteoglycin/mimecan have 2-3 KS chains of 10-15kD each (Hassell et al., 1979; Midura and Hascall, 1989; Dunlevy et al., 1998).

1.5.2 Glycosaminoglycans

GAG chains are made of repeating disaccharide regions containing acetylated amino sugar moieties (N-acetyl-galactosamine or N-acetyl-glucosamine) and uronic acid (D-glucuronic acid or L-iduronic acid). KS GAGs are based on repeating disaccharides $[-4 \text{ N-acetyl-glucosamine-}\beta 1,3\text{-galactose}\beta 1]_n$ (Neame and Kay, 2000).

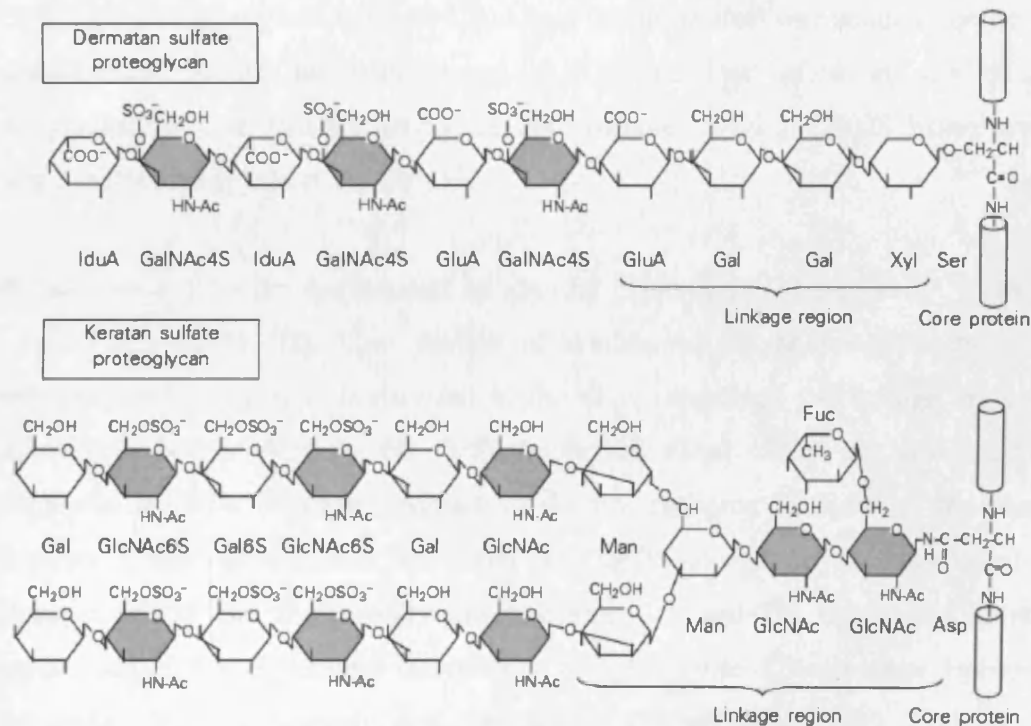


Figure 1.10 Simplified structures of corneal matrix glycosaminoglycans attached to the core protein via linkage region (after Michelacci, 2003).

CS/DS GAG chains are O- attached to the serine in a Ser-Gly pair near the N-terminal of core protein via tetrasaccharide glucuronic acid-galactose-galactose-

xylose (Chopra et al., 1985) (Figure 1.10), while KS is N-linked to asparagine of the core protein via a mannose-N-acetyl-glucosamine complex. The extended KS chain links to the 6-position of mannose while the 3-position branches into the short non-sulphated chain capped by sialic acid (Stein et al., 1982; Oeben et al., 1987). In cartilage, the KS chain is O-linked to serine or threonine (Funderburgh, 2000) and in brain Man-O-Ser linkages may exist (Krusius et al., 1986).

Under normal physiological conditions, GAG chains have a hydrophilic nature, are highly negatively charged and exhibit varying sulphation patterns. Sulphation of KS occurs on C6 of the N-acetylglucosamine and an additional sulphate may occur on C6 of galactose (Scudder et al., 1986). Distribution of sulphation along the KS chain has been characterised in detail for porcine KS. It shows that 4-6 N-acetylglucosamine disaccharide moieties nearest the protein are unsulphated, the next 10-12 disaccharides are sulphated only on the glucosamine, and the additional 2-10 disulphated disaccharides occur on non-reducing termini of the chains (Oeben et al., 1987). CS chains are less sulphated and have no more than one sulphate group per disaccharide. Sulphation may occur at C4, or less often at C6 of N-acetylgalactosamine. In a human cornea, approximately 64% of CS/DS disaccharides stay unsulphated (Plaas et al., 2001).

In the cornea, PGs are synthesised by stromal keratocytes (Midura et al., 1989; di Iorio et al., 2010). The core protein is synthesised in the rough endoplasmic reticulum and while it is transferred to the Golgi apparatus the linkage region is attached to Ser or Asp. In the Golgi apparatus, GAG chains are elongated by sequential addition of sugar residues to the non-reducing terminus of the chain. Separate glycosyltransferases are active in CS/DS elongation for attachment of glucuronic acid and for N-acetylgalactosamine. CS and DS GAGs are initially synthesised as CS GAG, and the activity of the enzyme C5-epimerase isomerise glucuronic acid into iduronic acid creating DS (Silbert et al., 1989; Little et al., 2008). In KS chains, elongation different glycosyltransferases attach alternately galactose and N-acetylglucosamine to the growing chain (Calabro et al., 2000; Funderburgh, 2000).

The GAG chain elongation process is coordinated with chain sulphation (Uchimura et al., 1998). Sulfotransferases add sulfoesters to 4- or 6-hydroxyl of the GalNAc residues in CS/DS. KS chains are sulphated by two sulfotransferases, one of which adds sulphate to GlcNAc. The other one is able to add sulphate to galactose of KS and to GalNAc of CS/DS (Ruter and Kresse, 1984; Habuchi et al., 1996; Fucuta et al., 1997). The final synthesised structure of corneal GAGs is presented in Table 1.5.

Table 1.5 General structure of corneal GAGs.

	Disaccharide	Sulphation position
Dermatan sulphate	L-iduronic acid + GalNAc	4
Chondroitin sulphate	D-glucuronic acid + GalNAc	4 or 6
Keratan sulphate	galactose + GlcNAc	6

1.5.3 Proteoglycans of the cornea.

Decorin and biglycan

Decorin and biglycan were first identified in bovine bone and cartilage (Rosenberg et al., 1985; Fisher et al., 1987). Both decorin and biglycan have a similar gene structure and have CS/DS GAG attachment sites at the N-terminal domain. The structure of the GAG depends on the tissue in which decorin is expressed. CS chains exist in developing bone, DS in skin or tendon, and a mixture of CS/DS in cartilage and cornea. Decorin usually carries one GAG chain, while biglycan has two attached chains; however, a few exceptions can be found. In a chicken cartilage, decorin exists with two GAG chains (Blaschke et al., 1996), and in a mammalian cartilage, decorin protein without GAG substitutions has been identified (Sampaio et al., 1988). It has also been suggested that biglycan with only one GAG chain exists in embryonic chick and human cornea (Funderburgh et al., 1998). Another reported dissimilarity in the structure of decorin in adult hen and in bovine cornea is that the GAG chain may contain KS as well as DS (Blochberger et al., 1992a).

Decorin is one of the most abundant PGs in ocular tissue, while biglycan has only been detected in the normal corneal epithelium of, and in very small quantities in the

stroma of mostly older corneal tissues (Bianco et al., 1990; Funderburgh et al., 1998). Stromal deposition of biglycan is more common diseases such as keratoconus and bullous keratopathy and in corneal scarring (Cintron et al., 1990; Funderburgh et al., 1998).

The presence or lack of decorin influences collagen fibril assembly, diameter and mechanical strength (Danielson et al., 1997; Corsi et al., 2002). It has been reported that decorin inhibits fibrillogenesis of collagen I and II in tendon and cartilage (Vogel et al., 1984). In the process of collagen assembly, an increase in the amount of decorin increases the density of the collagen fibril network (Iwasaki et al., 2008).

Decorin knock-out mice demonstrate a wide range of collagen fibril diameters accompanied by skin fragility but not corneal clouding (Danielson et al., 1997). Later, it was discovered that during the absence of decorin, expression and deposition of biglycan increases, resulting in nearly normal fibrillogenesis. Double-deficient mice (decorin and biglycan null mice) show dysfunctional fibrillogenesis during the development of the cornea causing changes in the structure and organisation, with abnormal fibrils mainly in the posterior stroma. This shows that decorin has a role in regulating stromal fibril assembly and lateral fibril growth that can be fine-tuned by biglycan during early development (Zhang et al., 2009). In case of decorin-deficiency, biglycan is up-regulated, but not the reverse (Birk et al., 2006).

Decorin GAG chains also play an important role in maintaining normal corneal structure. The presence of β -D xyloside during development affects the process of attaching the PG linkage region to the core protein, which results in production of decorin without GAG chains. Corneas treated in this way show disruptions in collagen fibril packing and lamellar disorganisation, but with no collagen fibril diameter alterations (Hahn and Birk, 1992). However, a reducing effect of decorin GAG chains on collagen fibril diameter, in the vitro study, been reported (Vogel and Trotter, 1987; Ruhland et al., 2007). In the developing chick cornea, mRNA of decorin is expressed from E9 and increases until E18 (Dunlevy et al., 2000).

Lumican

Lumican expression is highest, but not exclusively so, in the cornea because it has been found in other tissues and organs, such as kidneys and lungs (Schaefer et al., 2000, Ying et al., 1997). Bovine lumican carries one KS chain (Funderburgh et al., 1991). However, in mature chick cornea, lumican protein has five potential KS attachment sites (Blochberger et al., 1992a); thus, only three of those oligosaccharides are substituted with KS chains (Midura and Hascall, 1989; Dunlevy et al., 1998). Corneal lumican is ordinarily expressed by keratocytes, but during the early stages of wound healing it is expressed by the corneal epithelium (Saika et al., 2000). Lumican-null mice manifest opaque corneas and skin fragility. In the posterior cornea abnormally thick collagen fibrils are formed probably by fibril fusion, and this suggests that lumican may be needed to limit fibrils lateral growth (Chakravarti et al., 2000). In the developing chick cornea, a switch from a glycoprotein to a sulphated proteoglycan form of lumican is detected between E12 and E15, which is synchronised with the onset of corneal transparency (Cornuet et al., 1994). Expression of lumican is coupled with expression of keratocan and, in corneas of lumican deficient mice, keratocan expression decreases, which is a sign of a regulatory function of lumican on the transcription of keratocan (Carlson et al., 2005).

Keratocan and mimecan

Keratocan is expressed early in development and is present across the entire thickness of the stroma (Liu et al., 1998). Only in the cornea does keratocan contain large sulphated KS chains. In other tissues keratocan is primarily non-sulphated (Corpuz et al., 1996). Expression of keratocan mRNA in chick development is found to be at similar levels to lumican at E9 but decreases as the cornea becomes transparent (Dunlevy et al., 2000). Keratocan-null mice manifest a less severe phenotype from lumican-null mice. The cornea is clear and yet thinner, and has abnormal collagen fibril diameter and spacing compared with the wild type (Meek et al., 2003b; Kao and Liu, 2003).

Osteoglycin, later renamed mimecan, initially was isolated from bovine bone, and then from the cornea (Funderburgh et al., 1997). Mimecan mRNA is expressed during chick corneal development at low levels and is undetectable in adult hen corneas (Dunlevy et al., 2000). Mimecan core protein carries KS GAGs in human, bovine and developing chick cornea but not in the murine cornea (Funderburgh et al., 1997), which explains why mimecan-null mice do not manifest loss in corneal transparency or a decrease in thickness (Tasheva et al., 2002).

1.5.4 Proteoglycans collagen interaction

Proteoglycans are associated with corneal collagen, specifically at the a and c (KS PG) and d and e (DS PG) bands visible on positive fibril staining (Scott and Orford, 1981; Scott and Haigh, 1985; Meek et al., 1986; Scott and Haigh, 1988a). In the absence of any of the PGs, the binding sites of these PGs stay unoccupied (Scott, 1988). The core protein is non-covalently attached to the collagen fibril with GAG chains reaching outwards from the fibril into the interfibrillar space, regulating collagen spacing where, it has been proposed, they form duplexes with each other (Scott, 1991a; Rada et al., 1993). It has been also indicated that CS/DS filaments are able to form periodic interactions with collagen fibrils even without a protein core (Raspani et al., 2008).

To explain how PG core protein interacts with much bigger collagen fibrils, an insight into the protein structure is required. The structure of the core protein of all SLRP exhibits similarities due to the leucine repeats. The most studied structure is that of the decorin core protein. The first decorin model was based upon the crystal structure of the porcine ribonuclease inhibitor (Weber et al., 1996). LRR region is composed of alternating short β -strands and α -helices which run parallel to the common axis and form an arched structure with β -sheets linking concave surface of the molecule and the α -helices positioned at the convex face (Kobe and Deisenhofer, 1993; 1995). It was originally proposed that the inner concave surface is of a size and shape able to accommodate only one collagen triple helix, 3nm in length (Weber et al., 1996). It is at this surface through which decorin has been proposed to dimerise (Scott et al., 2004). More recent study shows that one molecule of decorin core protein interacts with four to six collagen molecules, and a large number of hydrogen

bonds and electrostatic interactions with d and e₁ bands of collagen can determinate binding specificity and protein conformation (Figure 1.11) (Orgel et al., 2009).

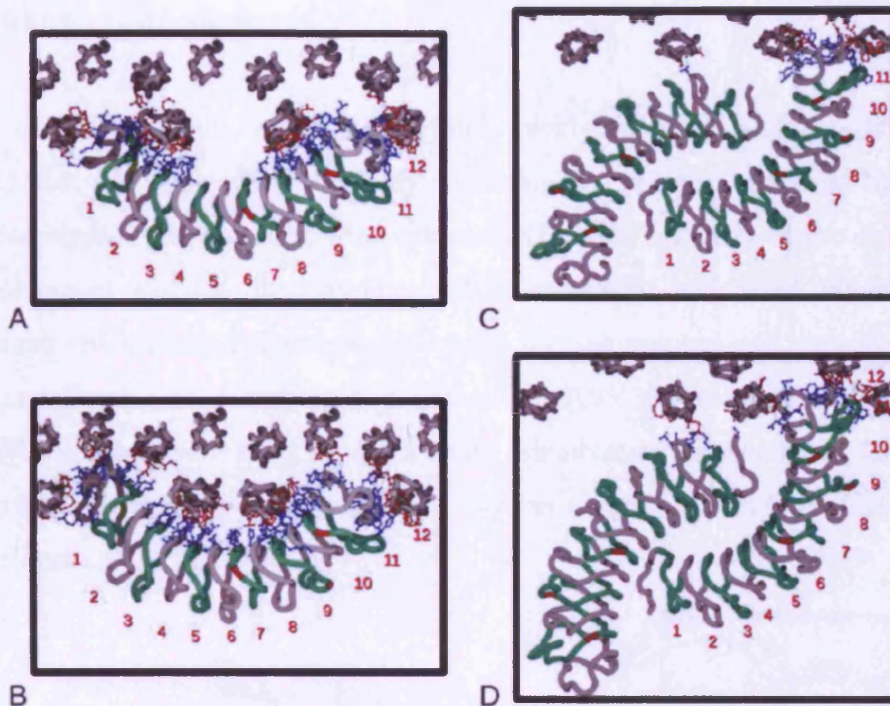


Figure 1.11 Decorin core protein interacting with the collagen fibril surface via hydrogen bonds between amino acid residues. A and B represents PG binding at the e band in common and wide conformation respectively, and C and D represents a decorin dimer binding at the d band in common and wide conformation (after Orgel et al., 2009).

The most recent three-dimensional electron tomography of bovine and murine corneal stroma (Lewis et al., 2010; Parfitt et al., 2010) led to the idea of a new model of collagen-PG interactions. It is apparent that stained PG filaments can extend between two or more collagen fibrils. However, PG filaments are not long enough to span this distance (Scott, 1992), and it was suggested that GAG chains from separate PGs may join together. Pre-incubation of corneal tissue with specific GAG-degrading enzymes has shown that that CS/DS chains in the cornea are longer and can create bridges among several collagen fibrils, whereas KS chains connect adjacent fibrils. Proteoglycans are likely to optimise the spacing by contracting and expanding space between individual collagen fibrils. It is postulated that less sulphated proteoglycans pull in fibrils to restrict and stabilise interfibrillar spacing, and highly sulphated proteoglycans are capable of attracting an influx of water and

push out fibrils. This model postulates that proteoglycans control interfibrillar spacing through thermal motion and osmotic pressure.

1.6 Chick eye development

The eye of the chick develops early and quickly reaches a relatively large size in comparison to the rest of the body. Additionally, an easy access to the embryos means birds are often chosen for eye research. Detailed study of the chick corneal development was described by Hay and Revel (1969), and based primarily on this research chick corneal development events are summarised and presented in Table 1.6 and figure 1.12. Hamburger and Hamilton (1951) divided chicken development into 46 stages, where stage 46 is hatching (Hamburger and Hamilton, 1992). These stages are used along with embryonic days to describe the main events in corneal development.

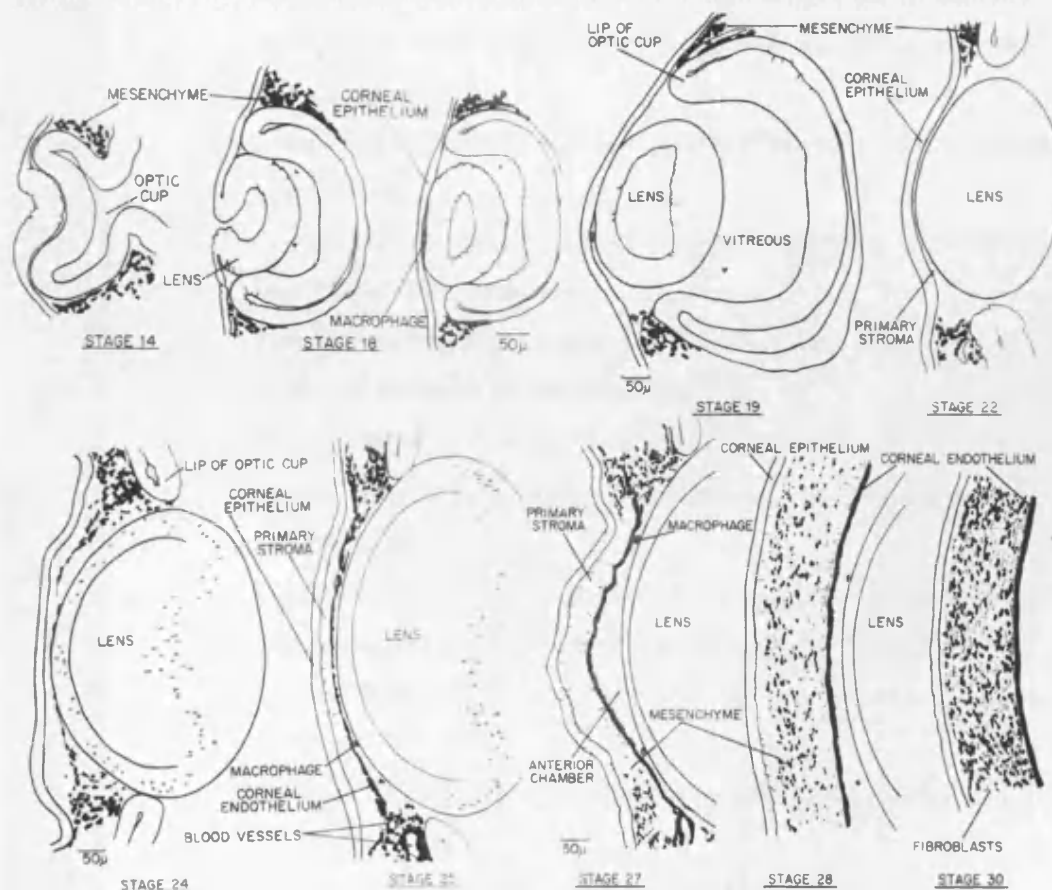


Figure 1.12 Diagrams representing the first 7 days of chicken corneal development when the cornea is created and the major changes occur (after Hay and Revel, 1969).

Corneal development can be divided into four main stages:





- 1st  events leading to formation of the primary stroma
- 2nd  development of primary stroma
- 3rd  development of secondary stroma
- 4th  dehydration and compaction of the stroma

Table 1.6 Chick corneal development.

Day/ stage	Stromal thickness	Event
2 14		Optic vesicle forms a cup shaped structure
2.5 16		Overlying ectoderm forms lens placode
3 18		Lens vesicle detaches from the ectoderm
3 18		Ectoderm differentiates into a 2 cell thick corneal epithelium
		Basal cells of epithelium increase in height
3.5 22		Corneal epithelium synthesise fibrous and acellular matrix between itself and the basal surface of the anterior lens epithelium called the primary stroma
		Long isoform of collagen IX is expressed (Fitch et al., 1995; Svoboda et al., 1988)
		Corneal endothelium arises from vascular mesenchyme and is placed near the lip of the optic cup
4 23		Endothelium migrates between primary stroma and lens to form
4.5 24		Brille (epithelium + stroma + endothelium)
5 25	10 μ m	Short isoforms of collagen IX expressed (Fitch et al., 1995)
5 26		Stroma invaded by secondary mesenchymal cells (Linsenmayer et al., 1998)
5.5 27	60 μ m	Disappearance of fibril-associated IX collagen which let lamellae separate during later swelling (Cai et al., 1994, Fitch et al., 1995)
6 28	110 μ m	Mesenchymal cells differentiate into fibroblasts (Garrett and Conrad, 1979)
		Collagen XII and XIV synthesised by epithelial cells (Gordon et al., 1996)
		Collagen XII expressed in the long form (Akimoto et al., 2002)
		Secretion of hyaluronate by epithelium or endothelium (Conrad, 1970; Toole and Trelstad, 1971)
6.5 29		Secretion of hybrid collagen I/V fibrils (Brik et al., 1986)

7	30	140 μ m	Fibroblasts penetrate lamellae of the stroma, although not the part adjacent to epithelium
8	34	170 μ m	Formation of vitreous humor, thus presence of intraocular pressure and first signs of corneal curvature (Coulombre and Coulombre, 1958b)
9	35		
10	36	190-220 μ m	Endothelium forms Descemet's membrane
11	37		Anterior-most 1 μ m thick layer of stroma not invaded by fibroblasts Collagen type XIV mRNA expression reaches high level (Young et al., 2002)
12	38	200 μ m	Anterior stroma becomes Bowman's layer (Fitch et al., 1994)
13	39		Stroma undergoes a dehydration
14	40	150 μ m	PGs synthesis increases (Nakazawa et al., 1995)
15	41		Collagen XIV expression decreases to disappear by E18 (Young et al., 2002)
16	42		
17	43		
18	44	160 μ m	Tissue becomes fully transparent (Coulombre and Coulombre, 1958a)
After hatch		250 μ m	Cornea keeps growing

1.7 Human corneal disorders

To study the biologic function of PGs in cornea, the genetically altered organisms can be created and we can study tissue structure and function when PG alterations occur. In addition, one can study the human condition by investigating the corneal stroma in selected diseases caused by genetic malfunctions. The most useful for my research are disorders in which the phenotype manifests change in corneal transparency and in which the biosynthetic pathway of the PGs is altered.

1.7.1 Dystrophies

A corneal dystrophy is defined as a heterogenous group of bilateral genetically determined non-inflammatory diseases that are restricted to the cornea and which are not manifested systemically (Klintworth, 2009).

Dystrophies can be divided into three groups based upon the anatomical location of the changes. Anterior corneal dystrophies affect the corneal epithelium, basement membrane and Bowman layer, stromal corneal dystrophies affect the corneal stroma, and posterior corneal dystrophies affect Descemet's membrane and the corneal endothelium (Table 1.7). Most dystrophies follow a Mendelian inheritance pattern, autosomal dominant, autosomal recessive and X-linked recessive (Klintworth, 2009).

Table 1.7 Corneal dystrophies (after Klintworth, 2009).

Superficial corneal dystrophies	Meesmann's dystrophy
	Reis-Bücklers' corneal dystrophy
	Thiel-Behnke dystrophy
	Gelatinous drop-like corneal dystrophy
	Lisch epithelial corneal dystrophy
	Epithelial recurrent erosion dystrophy
	Subepithelial mucinous corneal dystrophy
Corneal stromal dystrophies	Macular corneal dystrophy (MCD)
	Granular corneal dystrophy
	Lattice corneal dystrophy
	Fleck's dystrophy
	Schnyder's corneal dystrophy
	Posterior amorphous corneal dystrophy
	Congenital stromal corneal dystrophy(CSCD)
Posterior dystrophies	Fuchs' dystrophy
	Posterior polymorphous dystrophy
	Congenital endothelial dystrophy
	X-linked endothelial dystrophy

In the scope of this thesis it is the structure of the stroma which is of interest, thus I have chosen to study selected cases of stromal dystrophies. In chapter 6, MCD and CSCD will be presented in detail. Both dystrophies cause loss of corneal transparency and are characterised by structural changes within the stroma. They are chosen because their underlying genetic defect influences PGs. MCD is caused by the production of KS GAGs with altered sulphation pattern (Klintworth et al., 1986)

while CSCD characterises production of decorin with truncated core protein (Bredrup et al., 2005).

1.7.2 Mucopolisaccharidoses

The mucopolisaccharidoses (MPSs) are a group of disorders caused by inherited defects in lysosomal enzymes, resulting in widespread intra- and extra-cellular accumulation of glycosaminoglycans. Lack or reduced activity of enzymes responsible for catabolism of GAG chains results in systemic storage of GAGs in lysosomes, including ocular tissues.

MPSs are divided according to the enzyme defect and systemic manifestations and the groups are presented in Table 1.8.

Table 1.8 The mucopolisaccharidoses with indicated enzyme malfunction and type of GAG accumulated in the lysosomes (Ashworth et al., 2006).

MPS Type	Enzyme deficiency	GAG
MPS I (Hurler, Scheie, Hurler/Scheie)	α -L-Iduronidase	DS, HS
MPS II (Hunter)	Iduronate-2-sulfatase	DS, HS
MPS III (Sanfilippo)	Heparan sulfamidase (A)	HS
	N-Acetyl- α -D-glucosaminidase (B)	HS
	Acetyo-CoA: α glucosaminidase	HS
	N-acetyltransferase (C)	HS
	N-Acetylglucosamine-6-sulfatase (D)	HS
MPS IV (Morquio)	N-Acetylgalactosamine-6-sulfatase	KS
MPS VI (Maroteaux-Lamy)	N-acetylgalactosamine-4-sulfatase	DS
MPS VII (Sly)	β -D-Glucuronidase	DS, HS, CS
MPS IX (Natowicz)	Hyaluronidase	CS

MPSs as systemic diseases cause more severe changes in human phenotype. An ocular defect is only one of many abnormalities. In this thesis, MPS VII will be presented with the emphasis on the collagen fibrils in the stroma.

1.8. Aims and objectives

The aim of this thesis is to develop further our understanding of structure-function relationships in the cornea.

There is an emphasis on proteoglycans influencing structural alterations in collagen architecture by its altered composition or molecular structure. Two model systems will be investigated: development and disease. Embryonic chick corneas in which the PG content is altered with time will be studied along with human corneas with diseases involving genetic mutations in PG pathways.

Chapter Three

Aim:

To test the hypothesis that a developing cornea transmits light to varying degrees and that this is due to changes in the structure.

Objective:

Quantify the light transmission through the cornea at different stages of development at different wavelengths.

Chapter Four

Aim:

To test the hypothesis that collagen spacing changes with depth and laterality during corneal development.

Objective:

Use microbeam X-Ray diffraction to investigate the collagen centre-to-centre spacing across the cornea (periphery-centre-periphery) and across the corneal depth (epithelium-endothelium).

Chapter Five

Aim:

To test the hypothesis that localisation of proteoglycans (CS/DS) changes within the depth of the corneal stroma during development.

Objective:

Detect native CS/DS PGs in the stroma of developing chick by immunolabeling and enzymatically digest CS/DS PGs to visually distinguish the population of CS/DS PGs from KS PGs on the electron micrograph.

Chapter Six

Aim:

To test the hypothesis that changes in proteoglycan structure is associated with structural abnormalities in human corneal disease.

Objective:

Bring together the techniques used to investigate the chick model to study structural changes in collagen size and arrangement in MCD, CSCD and MPSVII.

Chapter Two

2 General methods

In this chapter the principles of the methods used in the thesis will be presented. Four main techniques were used as research tools: small-angle X-ray fibre diffraction, electron microscopy, spectrophotometry and immunofluorescence microscopy. More detailed description of the methods, including the protocols, is an integral part of each result chapter.

2.1 X-ray diffraction

All small angle X-ray diffraction studies included in this thesis were conducted at the Spring8 synchrotron in Hyogo, Japan (Figure 2.1). This facility is a 3rd generation synchrotron opened in 1997 and it provides the most powerful synchrotron radiation currently available. Storage ring circumference is 1436m and the generated energy reaches 8 GeV.

A synchrotron is a type of particle accelerator generating a high-intensity light, which is an electro-magnetic wave emitted from an electron travelling at almost the speed of light when its path is bent by a magnet creating a uniform magnetic field. There are two types of a light source at Spring8: an insertion device and bending magnets. There are two insertion devices: an undulator and a wiggler. The beam size and angular spread of synchrotron radiation from the undulator is much lower than that from the bending magnets and wiggler. In my experiment the insertion device was the undulator. Synchrotron radiation is characterised by features like brightness, high directionality and variable polarisation.

Along the circumference of the storage ring, there are 53 experimental hutches. Each of the beam line is used for a different purpose. My small angle X-ray diffraction study was performed on a 40XU High Flux beam line. This beam line is being used for:

- time-resolved diffraction and scattering experiments
- X-ray speckle experiments
- Microbeam x-ray diffraction experiments
- X-ray fluorescence analysis.

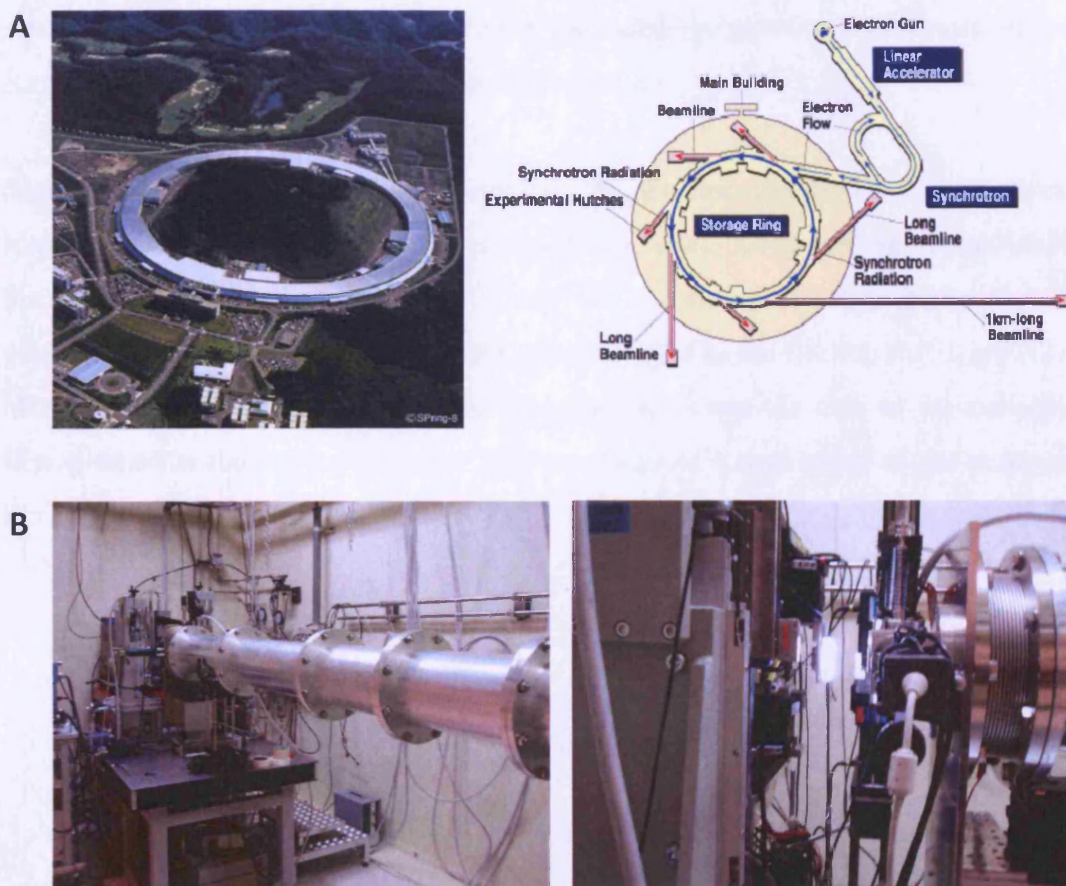


Figure 2.1 A) The SPring8 synchrotron and a schematic representation of the facility B) Inside the 40XU beam-line, and a holder with attached microscope.

The beam line 40XU is equipped with x-ray shutters, a fast CCD camera, an X-ray image intensifier, YAG laser and a vacuum path for small angle X-ray scattering.

2.1.1 Principals of method

When a focused beam of monochromatic X-rays passes through biological tissue, the majority of rays pass straight through without an interaction. However, some rays are absorbed by the tissue itself, whilst the remainder of X-rays are scattered at various angles by the components of the sample. For my experiments the incident beam is

blocked by a lead backstop placed behind the sample, and the scattered rays form a diffraction pattern on a detector. Because X-rays are scattered through large and small angles, it is important to locate the detector an adequate distance away from the sample to record the desired part of the X-ray pattern. In the case of a small scattering angle, the low-angle pattern is recorded with a detector separated by several metres from the sample, while the wide-angle pattern for experiments on the cornea is detected at a distance of tens of centimetres.

Scatter raised from the sample is a function of the electron distribution in the sample. If collagen fibrils are held vertically in an X-ray beam, X-rays scattered parallel to the fibril axis give rise to what is called a meridional pattern. An equatorial pattern is produced by the X-rays being scattered at right angles to the fibril axis (Figure 2.2). Meridional reflections arise from the D-periodicity along the axis of the collagen fibrils, whereas the equatorial reflection is a result of lateral order of the collagen fibril packing within the lamellae.

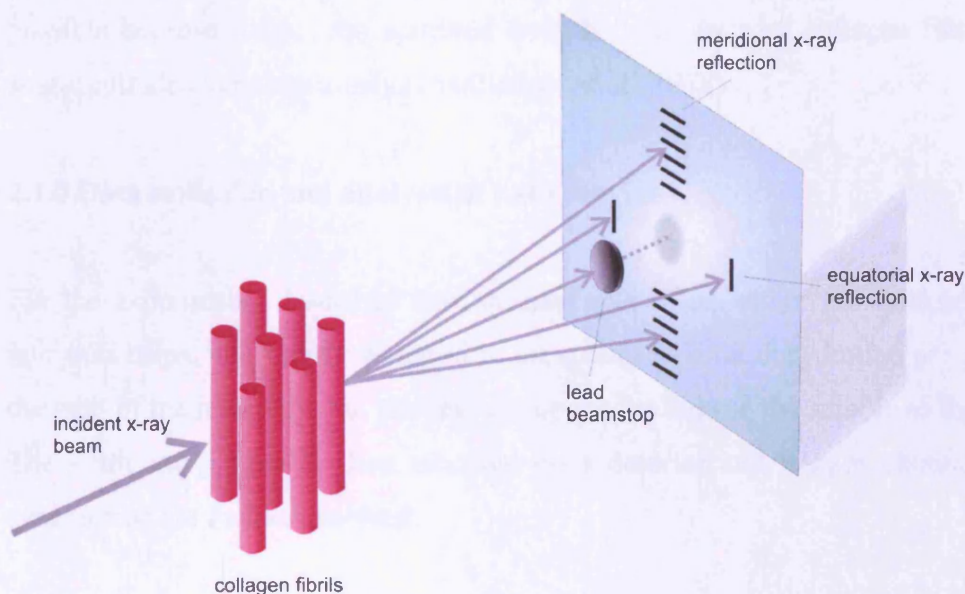


Figure 2.2 Schematic diagram of an X-ray beam being scattered from an array of cylindrical fibrils. The scattered beam gives rise to meridional and equatorial reflections.

In the cornea, if the X-rays pass through the whole thickness of the cornea from front to back several hundred lamellae are traversed, with collagen running in all directions within the plane perpendicular to the optical axis. The beam is scattered

form each lamellae in a different direction and as a result the meridional pattern appears as a series of concentric circles of intensity.

Depending on the degree of order in the structure that is a subject for an X-ray experiment; different levels of interference between the scattered rays will take place. The higher the degree of order, the sharper the interference maxima will be. Completely disorganised structures will give rise to diffused scattering, called background scatter.

Though meridional and equatorial patterns of the cornea are superimposed, they still can be distinguished from each other. The equatorial reflection is broader than the meridional, and their positions in the pattern also differ.

Important information like position of the collagen centre-to-centre spacing and collagen fibril radius can be estimated from equatorial small angle patterns. This is possible because X-rays are scattered from both an array of collagen fibrils and a single cylinder, simultaneously (Goodfellow et al., 1978).

2.1.2 Data collection and analysis of patterns

For the experiments described here corneal specimens, either full-thickness or cut into thin strips, and tightly wrapped in cling film to limit dehydration are placed in the path of the beam and the shutters are opened to expose the sample to the X-rays. The scattering pattern is then recorded on a detector and images obtained in the synchrotron are further analysed.

Before the start of each experiment, a pattern of rat tail tendon is obtained. The D-periodicity of the collagen fibrils in this tissue is known and equals 67nm (Goodfellow et al., 1978) therefore the pattern is used for the calibration which is described in detail later in the text. Collected data stored as images can be further analysed elsewhere using Unix based software (Fit2d) and statistics packages (Microsoft Excel, Statistica).

My studies focus mainly on a collagen interfibrillar spacing of the samples, however if it is necessary, the fibril diameter can be calculated. The way to obtain fibril centre-to-centre spacing is shown below.

From the recorded images showing the diffraction pattern, a vertical transect (20 pixel in width is found to be suitable) is taken throughout the centre (Figure 2.3) to produce a profile of X-ray intensity (I) against radial position (R).

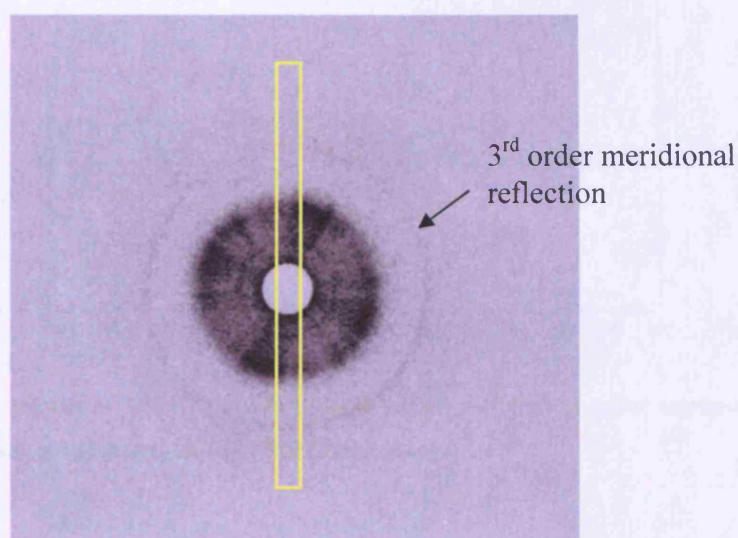


Figure 2.3 Transect taken through the centre of a diffraction pattern obtained from human cornea.

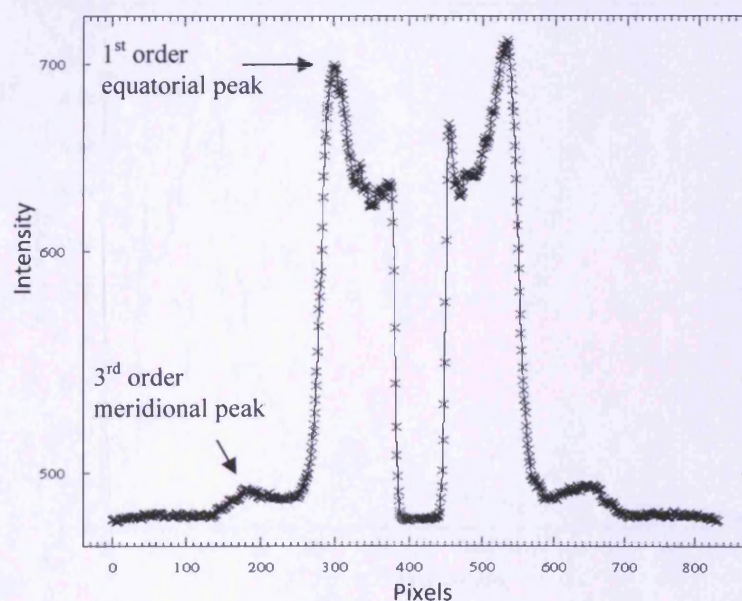


Figure 2.4 Projection of the transect image as a graph of intensity against pixel position.

To increase the signal and minimise the noise the symmetrical pattern (Figure 2.4) is folded along the centre point to generate the plot R versus IR with a clearly visible first order equatorial peak in the X-ray intensity profile (Figure 2.5). I is multiplied by R to minimise the error of taking a linear scan across a circular X-ray pattern.

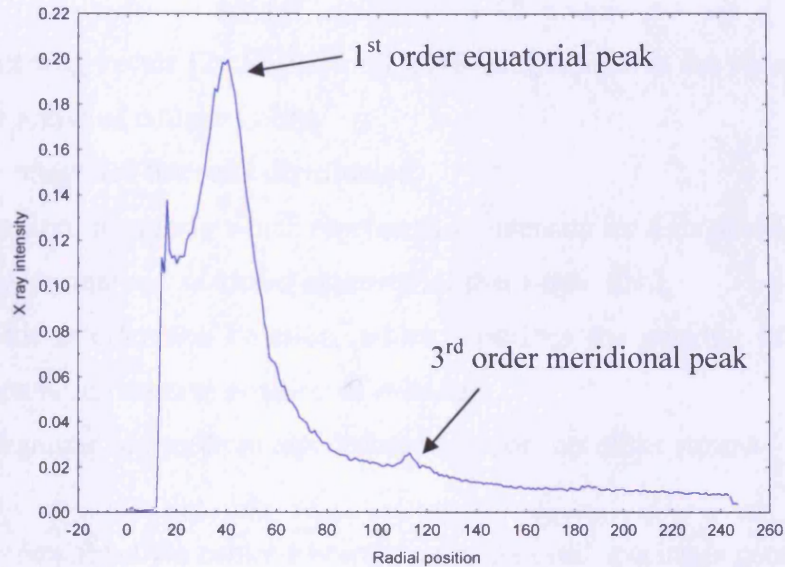


Figure 2.5 An intensity profile of the diffraction pattern with a visible first order equatorial peak used for calculation of the collagen interfibrillar spacing.

To remove scattering arising from other stromal matrix components different from collagen fibrils, a background curve is fitted and subtracted from the plot (Figure 2.6).

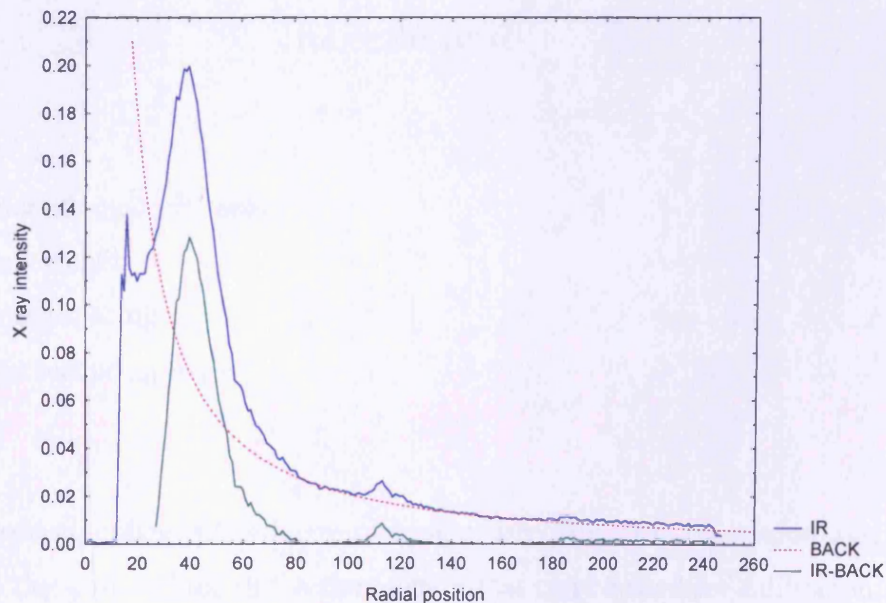


Figure 2.6 An intensity profile of the diffraction pattern with background scatter removed (green).

The intensity distribution is calculated from the equation:

$$I(K) = F^2(K)G(K) + B$$

Where,

- K is a scattering vector [$2\pi/d$ or $(4\pi/\lambda)\sin\theta$] and represents the phase difference between the arrays of collagen fibril
- $I(K)$ is the integrated intensity distribution,
- $F(K)$ is the fibril transform which represents an intensity for a single collagen fibril,
- $F^2(K)$ is the normalised scattered intensity for that single fibril,
- $G(K)$ is the interference function, which describes the packing of fibrils and depends upon K and relative position of cylinders,
- B is a background scatter from less ordered components of the stroma

The information about the centre-to-centre collagen fibril spacing is contained in the interference function.

$$G(K) = I(K) - B/F^2(K)$$

For a crystalline lattice, $G(K)=0$, except sharp peaks when $K=2\pi/d$. Then the position of the Bragg peak is a function $I(K)-B$ and is an equivalent of the Bragg equation.

$$n\lambda = 2d \sin \theta$$

Where,

- n is an order of equatorial peak
- λ is the wavelength
- d is the Bragg spacing
- θ is half the scattering angle

In rat tail tendon, collagen fibrils are running nearly parallel to the tendon axis and give rise to the well defined diffraction pattern that can be used for calibration. For the rat tail tendon the scattering angle 2θ could be easily calculated from Bragg's

equation because spacing arising from the 67nm D-periodic repeat was obtained by the X-ray beam of a wavelength equal 1.18Å. This scattering angle was then used to calculate the centre-to-centre collagen fibril Bragg spacing of the samples.

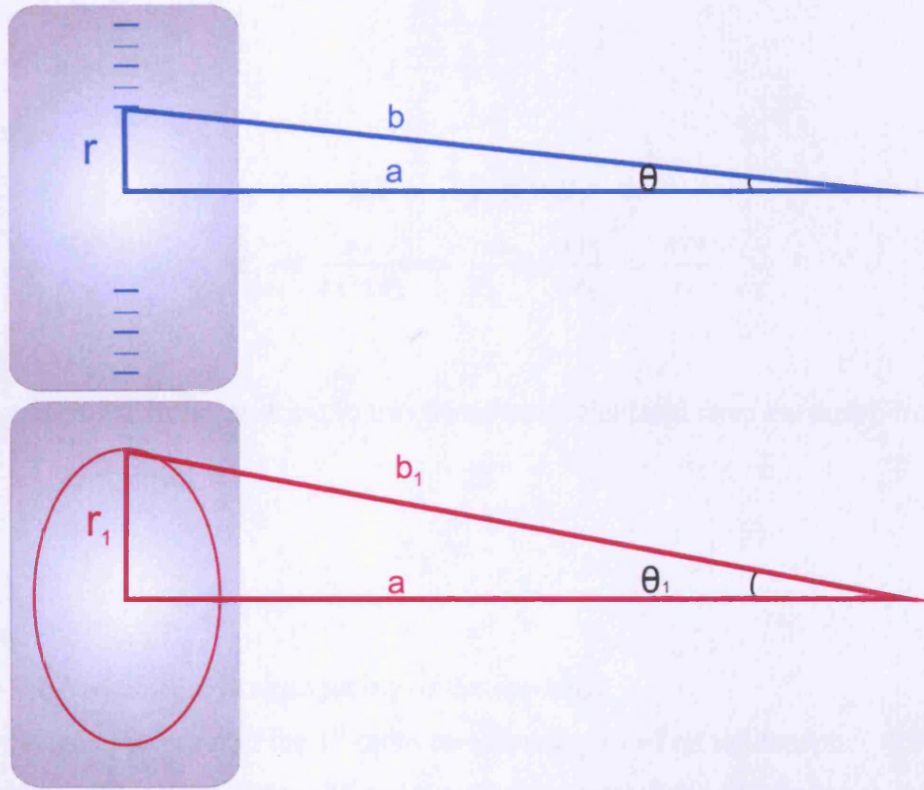


Figure 2.7 Schematic representation of the diffraction angle, θ , for rat tail tendon (blue) and a cornea θ_1 (pink) and their interrelationship. r and r_1 represent the radial distance of a peak from the centre of the pattern. a is a distance from the sample to the detector.

From figure 2.7 it is deduced that $\sin \theta = \frac{r}{b}$ and $\sin \theta_1 = \frac{r_1}{b_1}$. Because the scattering angle is low and the distance from the sample to the detector is long we make the small-angle assumption that $a = b = b_1$.

Therefore, $\sin \theta = \frac{r}{a}$ and $\sin \theta_1 = \frac{r_1}{a}$.

From Bragg's law:

Rat tail tendon:

$$\begin{aligned}
 n\lambda &= 2d \sin \theta \\
 d &= \frac{n\lambda}{2 \sin \theta} = \frac{n\lambda}{2 \frac{r}{a}} = 67 \\
 \frac{n\lambda a}{2r} &= 67 \\
 \frac{n\lambda a}{2} &= 67r
 \end{aligned}$$

Specimen:

$$\begin{aligned}
 n\lambda &= 2d_1 \sin \theta_1 \\
 d_1 &= \frac{n\lambda}{2 \sin \theta_1} = \frac{n\lambda}{2 \frac{r_1}{a}} = \frac{n\lambda a}{2r_1} = \frac{67r}{r_1}
 \end{aligned}$$

The interfibrillar Bragg spacing in this thesis was calculated from the equation:

$$d_1 = \frac{67r}{r_1}$$

Where:

d_1 – is the interfibrillar Bragg spacing of the specimen

r – is the radial position of the 1st order meridional pick of rat tail tendon

r_1 – is the radial position of the 1st order equatorial pick of the specimen

Interfibrillar Bragg spacing is a theoretical value for a crystal-like distribution of the fibrils. Worthington and Inouye made an assumption that collagen fibrils in the cornea are packed into a two-dimensional liquid-like arrangement and, therefore, the Bragg spacing should be multiplied by 1.12 to obtain closer-to-real collagen interfibrillar value (Worthington and Inouye, 1985).

In this thesis, for the comparative study of the developing chick cornea centre-to-centre fibril spacing values are presented as an interfibrillar Bragg spacing. However, in the MCD cornea study values are corrected by the 1.12 factor for better comparison with the literature.

2.2 Transmission electron microscopy

In transmission electron microscopy, electrons are projected through a thin section of a resin-embedded sample creating a two-dimensional image on the fluorescent screen. The bright area represents regions where more electrons are transmitted through the specimen. In the area where electrons are deflected from the original path, dark shadows appear.

The first transmission electron microscope was developed in Germany by Max Knoll and Ernst Ruska in 1932. The parameters of the microscope changed over time but the principle of operation stayed the same.

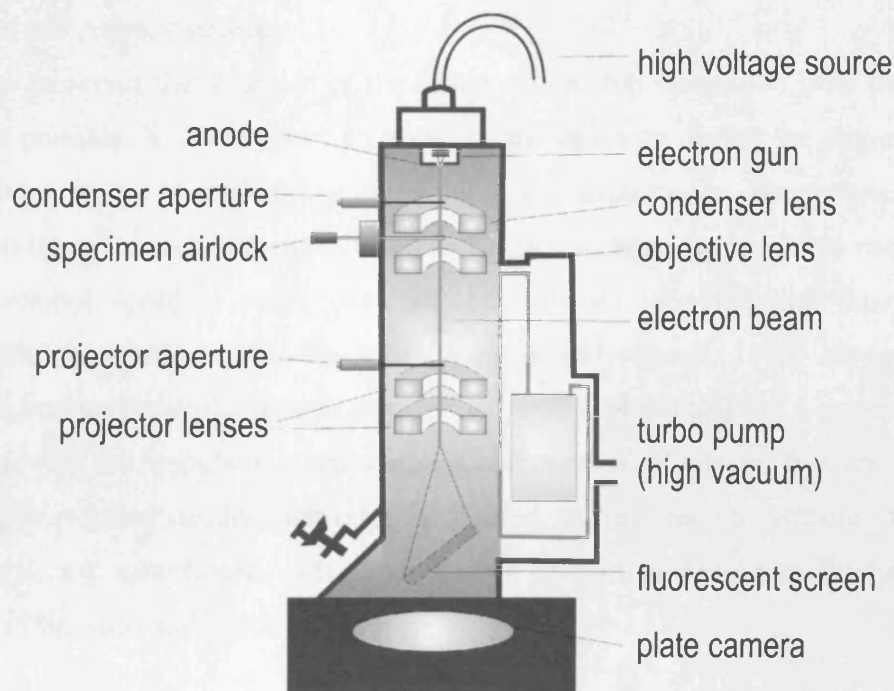


Figure 2.8 Schematic of a transmission electron microscope.

An electron beam of uniform current density is emitted in the electron gun. A tungsten wire filament is superheated by an electric current and a beam of electrons is emitted and accelerated down the column by an anode.

Lenses in the electron microscope are magnetic coils tuned to focus and direct the passing electron beam. Electrons are converged onto the specimen by the condenser

lenses, and the image is magnified and then focused on a screen at the bottom of the column by a set of objective and projector lenses. Along the microscope column are apertures which are holes designed to limit the size of the electron beam. To minimise an interaction between the electron beam and the air molecules, the inside of the column is kept at a high vacuum.

Electrons strongly interfere with atoms and for that reason specimen sections inserted into the electron microscope have to be very thin (5-100nm). To achieve such thin sections, specimens have to be specially processed.

2.2.1 Tissue preparation

Fixation and primary staining

Fixation preserves the structure of the tissue with as little alteration from the living state as possible. It is necessary to preserve the structure during the complex and damaging process of embedding, sectioning and exposure to the electron beam. Osmium tetroxide was historically used as the first fixation agent but the commonly used protocol nowadays was developed by Sabatini in 1963, and this uses a glutaraldehyde-osmium tetroxide mix (Bozzola and Russell, 1992; Hayat et al., 1989). Osmium tetroxide (atomic number 76) works additionally as a general stain, reacting with cell membranes and cellular components. However, if more specific staining is required osmium tetroxide is omitted. In this thesis a protocol for GAG staining uses glutaraldehyde with a cationic dye - cuproline blue in the fixation stage (Scott, 1980; Scott and Orford, 1981).

Washing

Washing is used to remove any excess of glutaraldehyde that remains in the tissue. As a wash we use a buffer in which the fixative was made. The buffer prevents the production of artefacts by controlling pH. Additionally, osmolarity can be adjusted by sodium or magnesium chloride.

Dehydration

Dehydration replaces the water in cells with a fluid that acts as a solvent for the hydrophobic embedding medium. Ordinarily a gradient of ethanol solutions (from the lowest to highest concentration) is used.

Infiltration with transitional solvents

After replacing water with ethanol, another solvent with high affinity to the liquid plastic medium is introduced to ensure a good infiltration of tissue. The standard solvent is propylene oxide.

Infiltration with resin

In this stage the transition fluid is gradually replaced by liquid plastic monomer. In this thesis Araldite resin was a monomer. To make it active, a hardener and accelerator were added.

Embedding and curing

Specimens infiltrated with pure resin are transferred into silicone moulds and placed into an oven heated up to 60°C for minimum 24h. In this time, resin components polymerise to form solid blocks.

Cutting

Blocks are trimmed and shaped to obtain a trapezoid surface in the area of our interest in the specimen. Sections ~90nm thick are cut on an ultramicrotome using a glass knife and collected on the water in the form of a gold ribbons. Sections are fished out onto copper grids.

Staining to enhance contrast

Dark and bright areas on the electron micrograph arise from the differences in the density of the specimen. Stain is additionally applied on the section to add greater density to the structure we are interested in. The higher atomic number of the stain, the darker shadows appear; therefore, commonly used stains are heavy metal ions.

Phosphotungstic acid (PTA) is an anionic positive stain. The electron density arises from the tungsten atoms which each have an atomic number of 74. An aqueous

solution of PTA shows an affinity for polysaccharides and carbohydrate moiety of glycoproteins and it is used for enhancing contrast while examining PGs in the cornea. Uranyl acetate (UA) is a general unspecific stain used in most procedures in electron microscopy. It can act as a positive and a negative stain. Uranium is the heaviest metal used as a stain in electron microscopy with an atomic number 92. Uranyl ions react with phosphate and amino groups and stain nucleic acids and certain proteins. At high concentration, such as those used in the experiments described in this thesis, this stain shows an affinity to positively charged groups. Lead citrate is a positive stain used for the cell examination. Lead, of atomic number 82, binds to negatively charged components like hydroxyl groups and osmium-reacted areas.

A corneal specimen that has undergone all the preparation stages outlined above is ready for examination with the electron microscope. Specific protocols are provided in the relevant chapters.

2.3 Spectrophotometry

Spectrophotometry is a method that detects the intensity of light transmitted through a sample, or absorbed by the sample, as a function of wavelength. A single beam monochromatic spectrophotometer measures the relative light intensity of the beam before and after the cuvette with the sample is inserted. To calibrate a single beam spectrophotometer, a blank probe is inserted first and the reading is set as a 100% transmission (absorption = 0). Generally in spectrophotometry any electromagnetic radiation spectrum can be used for measurements. I am using a wavelength range in the visible spectrum (400-700nm) because transmission in my study is intended to give an indication of corneal transparency for visible light.

A transmission spectrum is obtained by successively changing the wavelength of monochromatic light passing through the sample (by 10nm in the experiments described in chapter 3) and recording the change of light transmitted.

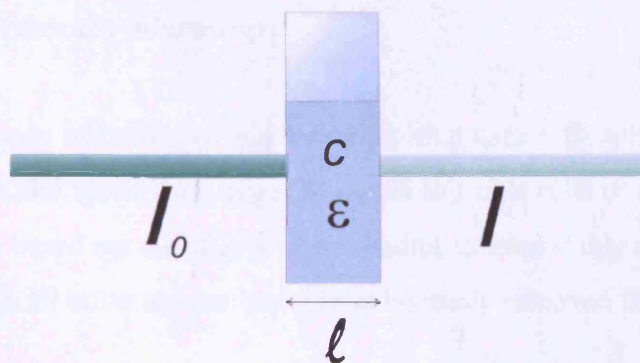


Figure 2.9 Representation of the Lambert-Beer law for transmission of a beam of light through a cuvette with a sample. I_0 is incident light intensity, I is transmitted light intensity, l is the distance the light travelled through the sample, c is the concentration of absorbing sample and ϵ is the molar absorptivity.

The basis for the spectrophotometry measurements is a law stating that there is a logarithmic dependence between the transmission of light through a substance and the product of the absorption coefficient of the substance, α , and the distance the light travels through the material l (Lambert's law). The absorption coefficient, α , can be written as a product of the molar absorptivity, ϵ , of the absorber, and the concentration, c , of absorbing species (Beer's law) (Figure 2.9).

$$T = \frac{I}{I_0} = 10^{-\alpha l} = 10^{-\epsilon l c}$$

$$A = -\log_{10} \left(\frac{I}{I_0} \right) = -\log_{10} T$$

$$A = \epsilon l c = \alpha l$$

T – is the transmission (transmittance)

I_0 – is the intensity of an incident light

I – is the intensity of a transmitted light

α – is the absorption coefficient

l – is the distance the light travels through the material (cuvette thickness)

c – is the concentration of the absorbing sample

ϵ – is the molar absorptivity

A – is the absorbance

2.4 Immunofluorescence microscopy

Immunofluorescence microscopy is a technique that uses a fluorescent dye-coupled antibody to locate and visualise a target molecule in single cells or in tissue sections. This technique is based on the ability of antibodies to bind stably and specifically to their antigen while all unbound antibodies can be easily removed from the tissue.

Antibodies are a class of immunoglobulins – proteins used by the immune system to identify and fight foreign molecules. All types of antibodies share the same basic Y shape structure. They are made of two heavy chains and two light chains (Figure 2.10). The different types of heavy chain define the immunoglobulin class. In my study I used only one type of antibody, IgG, which contain γ heavy chains and this is the most abundant immunoglobulin. At the tip of the each protein is located a highly variable region which allows specific binding to a different target – the antigen.

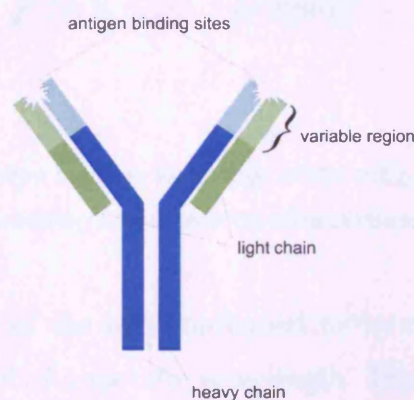


Figure 2.10 Schematic antibody containing heavy and light chains and visible constant and variable regions. At the end of the variable regions antigen binding sites are positioned.

To obtain an antibody which is directed against a desirable molecule, the antigen is injected into a small mammal such as a mouse or rabbit. To produce large quantities however, goats, sheep or horses may be immunised. In the blood of the animal, a natural mixture of antibodies known as polyclonal antibodies can be found. They all recognise the same molecule (antigen) but are produced by different B-cells and may bind to different parts (epitopes) of the antigen. To obtain a monoclonal antibody that will recognise a particular epitope, B-cells are removed from the animal's spleen and are fused with tumor cells. The tissue cultures grow quickly and produce large quantities of monoclonal antibodies.

Immunofluorescence employs two sets of antibodies: a primary antibody that identifies the antigen of interest and a secondary antibody which is fluorophore-conjugated and recognises the primary antibody (Figure 2.11).

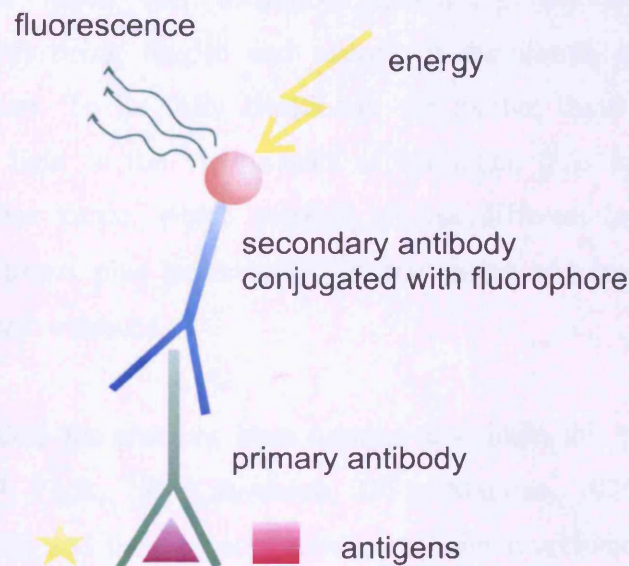


Figure 2.11 Schematic interaction between an epitope of the antigen plus primary and secondary antibodies during labelling a specimen for immunofluorescence microscopy.

To visualise the location of the immunostained molecules, a dye attached to the antibody is excited by light of a specific wavelength. This radiation causes electrons in the fluorophore to become excited to a higher energy level. One of the ways to return to a basic state of energy is to release energy via fluorescence. The emitted light has a lower energy (longer wavelength) compared to the excitation light and the two types of light have to be separated by an emission filter. That makes the emitted light visible to a human eye. Under the microscope, a fluorescing area is displayed as a collection of bright spots which stand out against a dark background.

Chapter Three

3 Light transmission through developing chick cornea

The cornea is a tissue that undergoes dramatic structural changes during development. From being fragile and opaque it transforms into a strong and transparent structure. To be fully functional, the mature tissue must be able to transmit incident light in the visible part of spectrum. It is interesting that the structurally complex tissue, which consists of five different layers, hundreds of lamellae in the stroma plus keratocytes, is transparent and is the only example amongst all connective tissues.

Several mathematical theories has been created to explain this phenomenon (Hart and Farrell, 1969; Feuk, 1970; Benedek, 1971; Maurice, 1975; Twersky 1975; Freund et al., 1986) and they all concentrate on stromal architecture and the light scattered from the collagen fibrils. According to the theory of a direct summation of fields suggested by Freund (1986), transparency depends on the:

- order of a fibrillar arrangement
- fibril diameter
- fibril number density
- balance between the refractive index of the hydrated fibrils and the extrafibrillar matrix
- corneal thickness

One of the other reasons for the loss of light transmission is absorption. Although, the majority of corneal components absorb light in the ultraviolet, this is below the visible wavelength, which means it would not affect the corneal transparency (Lerman, 1984) (Figure 3.1). The only chromophore present in the cornea is a cytochrom c in reduced and oxidised form, absorbing light at 400-420nm and at 520-600nm (Butt and Keilin, 1962).

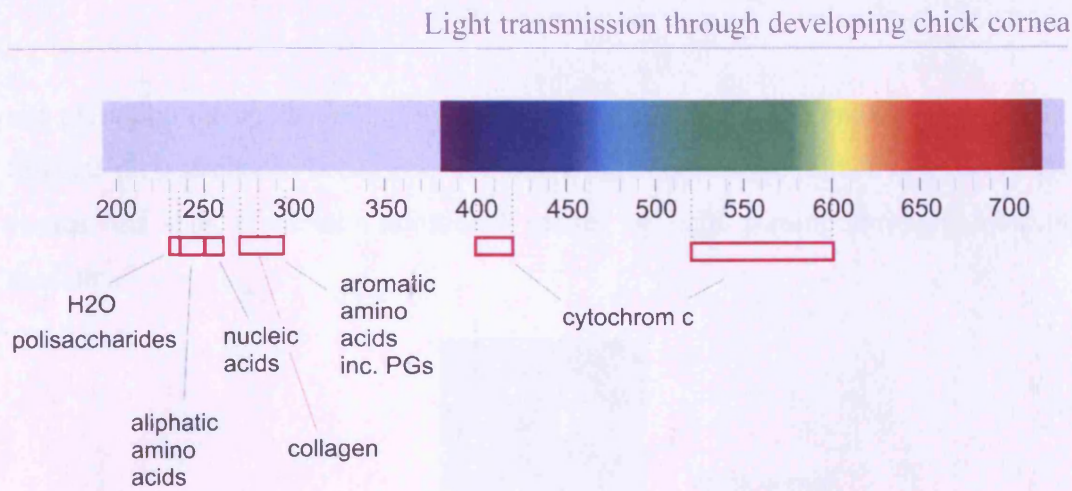


Figure 3.1 Part of the spectrum of visible light in the wavelength range, 400-700nm, with absorption spectra for various corneal components marked by pink rectangulars.

Developing chick cornea is a good model for studying transparency because all light scatter-dependent factors change during embryogenesis. The last study of transparency in visible light in chicks was conducted in the late 1950s. It showed a rise in the light transmission from about 40% before developmental day 14 to 95% the day before hatching (Coulombre and Coulombre, 1958a). Since then, there have been other light transmission studies of human, rabbit and bovine cornea (Algere et al., 1993; Kostyuk et al., 2002; Douth et al., 2008), but no chick developmental studies. I present here a detailed wavelength dependency study of a developing chick cornea in the 400-700nm wavelength spectrum.

3.1 Methods

All animals involved in this study were used in accordance with the Association for Research in Vision and Ophthalmology statement for the Use of Animals in Ophthalmic and Vision Research.

White leghorn fertilised eggs were obtained from Henry Stewart Commercial Hatchery. Eggs were placed in the incubator with regulated humidity (Octagon 100, Stanford, England) every day for six days to produce chicks at the developmental stage 12 to 18 on the same day. Each chick was sacrificed immediately before the spectroscopy measurements were taken to minimise the time between the death of the animal and transmission reading. This was done to avoid dehydration and post-mortem changes within the tissue. Corneas were dissected with laboratory scissors

and placed on the inside wall of a plastic cuvette containing silicone oil (Figure 3.2). Silicone oil was chosen because its refractive index equals the refractive index of the cornea and thus eliminates additional scatter of light passing through different mediums.

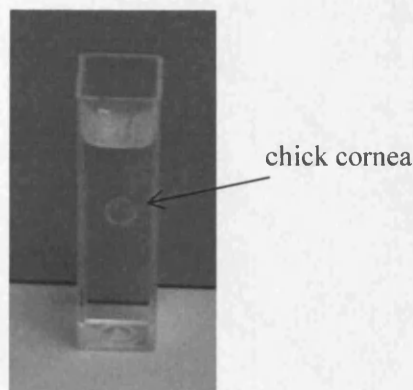


Figure 3.2 Spectrophotometer cuvette filled with silicone oil with a suspended chick cornea, ~4mm in diameter.

The cuvette with the cornea positioned on the centre of the inside wall was placed in a spectrophotometer (Pye Unicam SP8-100 UV/VIS, Cambridge, UK). The spectrophotometer was firstly calibrated against a blank probe, which was a cuvette containing silicone oil (Dow Corning 200/5cS, BDH Laboratory Supplies, Poole, UK). The position of the 1mm x 1mm beam in the centre of the cornea was found and a series of transmission readings were taken at wavelengths in the range 400 – 700nm in intervals of 10nm.

3.2 Results

Transmission measurements were taken from the centres of chick corneas at E12 (n=12), E13 (n=12), E14 (n=12), E15 (n=12), E16 (n=8), E17 (n=12) and E18 (n=12). Changes of transmittance as a function of development showed similar patterns at all recorded wavelengths. At the first three recorded stages (E12-E14) transmission is on a similar level, then from E15 increases significantly (Figure 3.3 and Figure 3.4). This supports previous white light measurements which indicate that the main onset of transparency take place from E14 onwards.

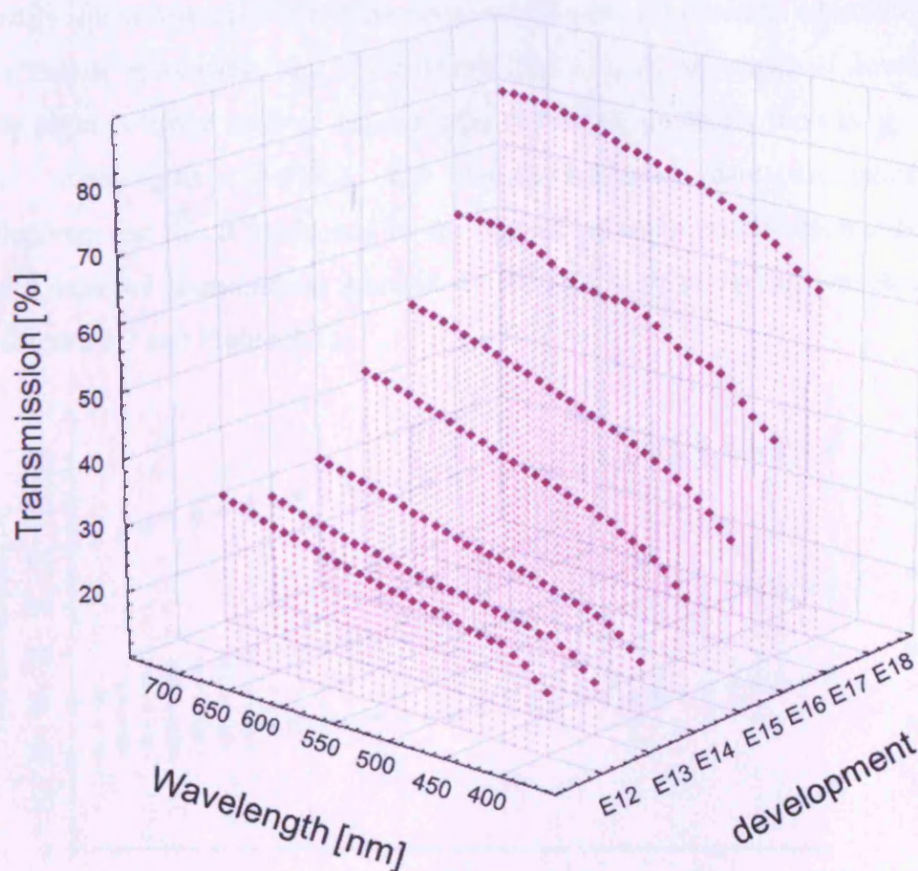


Figure 3.3 Three-dimensional graph of light transmission as a function of development and wavelength.

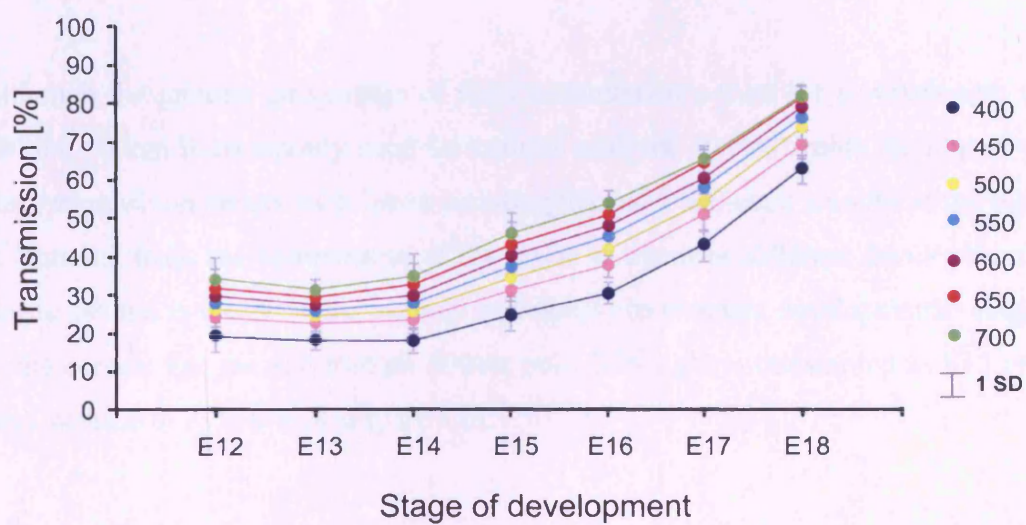


Figure 3.4 Light transmission as a function of development at different wavelengths (400-700nm).

Transmission measured in 10nm intervals reveals some absorbance, especially at E17 in the ranges 460-510nm and 560-610 nm (Fig.3.5). At all stages of development transmission is lower at short wavelengths (19-62%), gradually increasing towards longer wavelengths (34-81%). The cornea becomes more transparent with development and this is evidenced by the highest values of transmission at E18. The highest recorded transmission reached 81.5% (SD=2.9) at 700nm wavelength for E18 (Figure 3.3 and Figure 3.5).

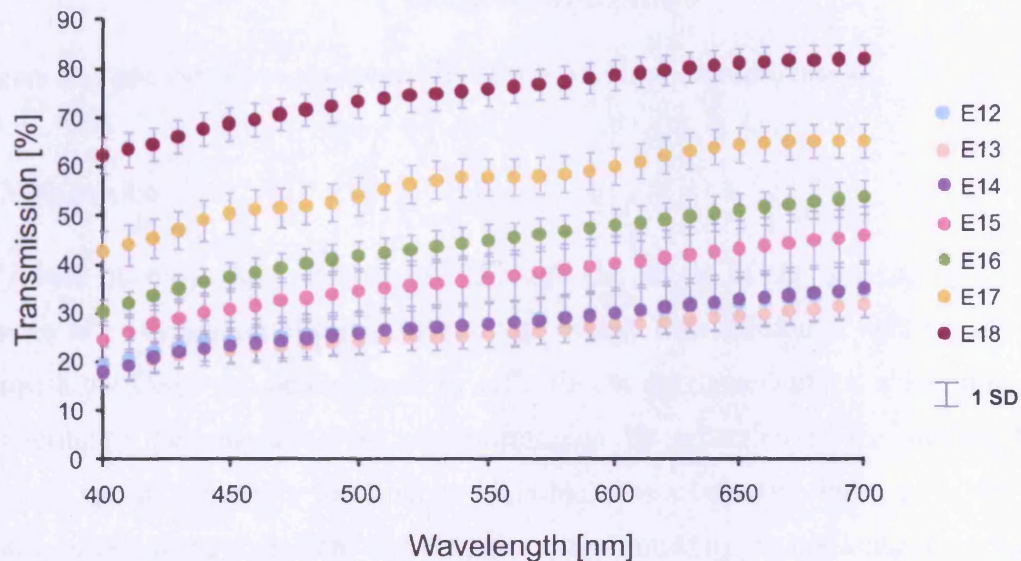


Figure 3.5 Light transmission as a function of wavelength for corneas of developmental stage E12-E18.

Although the greatest percentage of light transmission occurs for a wavelength of 700nm, 500nm is commonly used for corneal analysis. 500nm avoids the impact of absorption which occurs with lower wavelengths and a sufficient amount of the light is scattered from the components of the tissue to compare different developmental stages. 500nm is therefore the optimal wavelength to compare developmental stages in the cornea. For the wavelength 500nm only 26% light is transmitted at E12 and then increase to 73% at E18 (Figure 3.6).

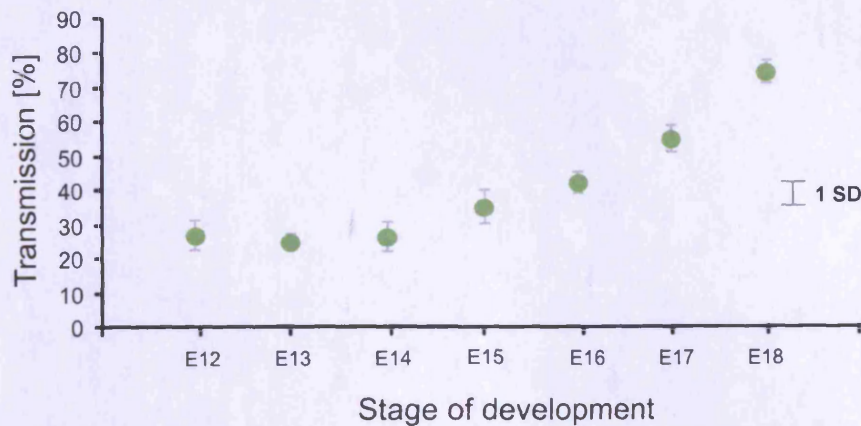


Figure 3.6 Light transmission at 500nm wavelength as a function of development,.

3.3 Discussion

My data quantify light transmission through the centre of the developing chick cornea as an indication of the level of transparency. Transmission of light travelling through the tissue can be disrupted by reflection at the tissue surface, absorption or scattering. I minimised a loss of transmission by reflection at the surface by immersing the corneas in the silicone oil, which has a refractive index of 1.397. It has been calculated elsewhere that the loss of transmitted light when isolated corneas are held in silicone oil is only 0.006% and can be omitted (Kostyuk et al., 2002). The majority of corneal components absorb light in wavelengths shorter than violet light and light transmission, thus transparency, in visible light is not affected (Lerman, 1984). The only pigment absorption in the visible light spectrum was recorded at wavelengths characteristic for the reduced and oxidised cytochrome c localised in the mitochondria of cells. This caused low readings of transmission for corneas at all developing stages at 400-420nm and 520-600nm. The strongest absorption is visible at E17. At this stage there is also an additional absorption visible at 460-490nm, although it cannot be explained what causes it.

It can be assumed then that a main reason of the transmission loss in my experiment is light scattering. During corneal development the tissue becomes more transparent, which means that light scattering decreases. Scattering in developing tissue, cells aside, is reduced by fibrils being arranged in a more ordered fashion, thinning of the cornea, a decrease in the fibril number density, and probably changes in the

refractive index between hydrated fibrils and the extracellular matrix (Hart and Farrell, 1969; Freund et al., 1986; Meek et al., 2003a). A refractive index imbalance between the fibrils and extracellular matrix must have an impact on the scattering of light, and we know that the amount and type of proteoglycans in the stromal matrix changes significantly during development (Anseth, 1961; Zhang et al., 2005). According to Benedek a large amount of light is scattered by so called “lakes” in the corneal stroma and that is a reason for swollen corneas to be opaque (Benedek, 1971). The same lakes are present in the stroma of developing chicks and only with time do the number of lakes decrease significantly, reducing scatter of light and making the cornea more transparent (Figure 3.7).

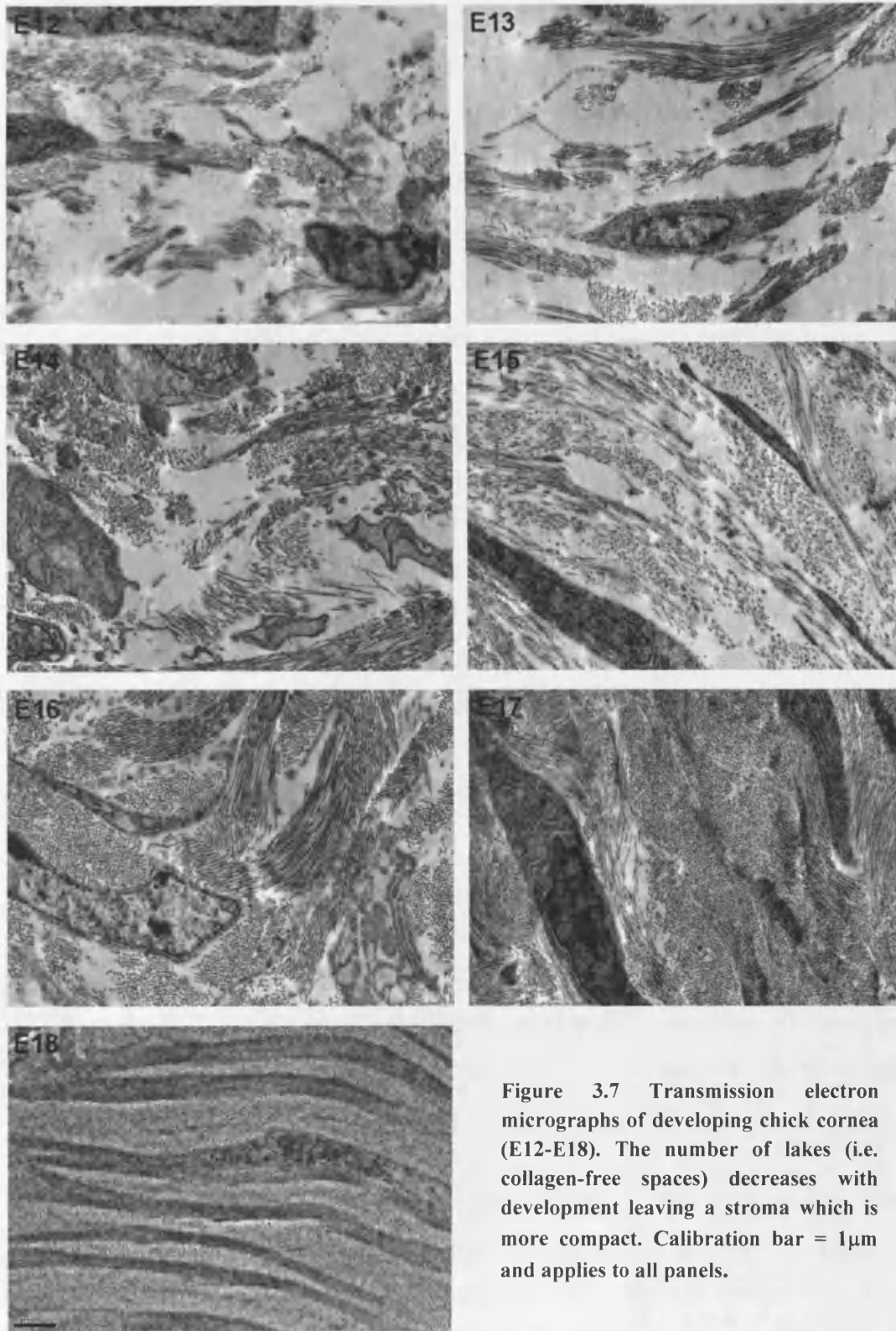


Figure 3.7 Transmission electron micrographs of developing chick cornea (E12-E18). The number of lakes (i.e. collagen-free spaces) decreases with development leaving a stroma which is more compact. Calibration bar = 1μm and applies to all panels.

In the developing chick cornea Coulombre and Coulombre (1958a) report 39% transmission of incident light at E12. At E18 this was 80% and the maximum is reached a day before hatching at E20 and equals 95%. This white-light transmission data is in line with our measurement for the 700nm wavelength measurements in which transmission increases from 35% at E12 to 81% at E18. Light transmission at 500nm is lower than at 700nm reaching only 73% at E18.

Previous light transmission studies have reported nearly 90% transmission in human cornea (Doutch et al., 2008) and over 90% in rabbit cornea (Algvere et al., 1993) and bovine cornea (Kostyuk et al., 2002), although the measurements were taken under different conditions than in the present experiment. Bovine and human corneas were stripped of their epithelium and endothelium layers, thus measurements apply only to the corneal stroma. Additionally, transmission in rabbit cornea was measured *in vivo*, and the other corneas had pressure applied to simulate intraocular pressure of an eyeball. Chick corneas are too small and too fragile to attempt measurements under pressure. Previously it was reported that a lack of pressure results in a decrease of light transmission at around 4% in a large animal with a thicker cornea (Kostyuk et al., 2002). In the case of very thin chick corneas a transmission loss is expected to be much less and not that significant.

Farrell described the wavelength dependence in normal cornea to be an inverse-cubic, and a pathological swollen cornea to show an inverse-square dependence (Farrell et al., 1973). In the developing chick cornea at E18, wavelength dependency is an inverse-square that fits the model of a swollen cornea. It could be caused by still high water content of a cornea and not full maturation of a tissue.

To summarise, light transmission through the chick cornea increases with development, especially after E14. Transmission values in the longer wavelengths (near red) are higher than in the shorter wavelengths (near violet) because blue light scatters more than the red light. Additionally, at 400-420nm, transmission is lower because of an absorption of light by cytochrome c. The biggest impact on transparency is the scatter of light caused by the presence of lakes in the stroma, changes in interspacing and in fibril arrangement, changes of thickness and imbalance of refractive indices between collagen fibrils and extrafibrillar substance.

Chapter Four

4 Spatial and temporal alterations in collagen architecture in developing chick cornea

The cornea requires the development of strength and transparency at the same time and undergoes a series of events during the period of development to obtain the required structure (Hay and Revel, 1969). To reach full transparency, collagen fibrils must be arranged in a well organised manner (Maurice, 1957; Benedek, 1971). Fibrils of a uniform diameter and regularly spaced, are arranged into lamellae. Within the lamella, fibrils are running parallel to each other, but adjacent lamellae are tilted by a few degrees within the plane of the cornea. All the changes of the corneal ultrastructure are important to obtain and to keep functionality of the tissue.

During tissue development, compaction of the lamellae occurs in the corneal stroma and the spacing between the collagen fibrils decreases (Quantock et al., 1998). In the developing chicken cornea, the stroma reaches maximal thickness by E10 and then undergoes a process of compaction between E14 and E18 (Quantock et al., 2003). Compaction is caused mainly by a water loss which leads to a concentration of the matrix components. The content of proteoglycans within the stromal extracellular matrix also changes and all events happen simultaneously with the tissue becoming more transparent.

At E18 of development, the cornea reaches nearly 90% of transparency of the mature cornea (Coulombre and Coulombre, 1958a). Previous studies show that centre-to-centre interfibrillar spacing decreases while the cornea develops (Quantock et al., 1998; Quantock et al., 2003). The measurements were obtained by synchrotron X-ray diffraction throughout the whole depth of the cornea in the central region. Thus values are the average throughout all lamellae. To investigate if there is any difference in the collagen fibril interspacing between central and periphery of the cornea and if there is any difference according to the depth of the cornea, an X-ray diffraction ultrastructure study was conducted using a 25µm-diameter beam.

4.1 Methods

All animals involved in this study were used in accordance with the Association for Research in Vision and Ophthalmology statement for the Use of Animals in Ophthalmic and Vision Research.

4.1.1 Specimens

Corneas were obtained from white leghorn chicks (Henry Steward Commercial Hatchery) on developing day 14 (E14) to 18 (E18) in daily intervals. Tissue was dissected round the limbus with scissors after which corneas were immediately fixed in eppendorf tubes in 4% paraformaldehyde in a 0.1M Sörens phosphate buffer. After 24 hours, corneas were moved to 0.5% paraformaldehyde in a 0.1M Sörens phosphate buffer for transport to the Spring8 synchrotron in Japan. All work was conducted in accordance with the ARVO Resolution for the Use of Animals in Ophthalmic and Vision Research.

4.1.2 Synchrotron X-ray diffraction

X-ray diffraction study was performed at the SPring8 synchrotron in Hyogo, Japan, on the 40XU beam line with a millisecond exposure times. Corneas from E14 to E18, previously fixed, were wrapped in clingfilm to prevent hydration loss and mounted on a holder that was placed in the path of the X-ray beam.

First, a scan was performed on the whole cornea positioned such that the surface of the cornea was perpendicular to the direction of the beam (Figure 4.1A). This front-on scan was conducted on one cornea of each developmental day. The scan started above the tissue, ran through the diameter of the cornea with the 25 μ m beam moving in 50 μ m steps and finished below the tissue.

The second type of scan was performed on a thin strip of cornea around 400 μ m thick that was cut free-hand with a laboratory blade from the central area of the cornea and orientated in the holder in such a way that the edge of the corneal strip was facing the

beam. The scan was run throughout the depth of the cornea starting above the epithelium down to endothelium with the 25 μ m beam in 25 μ m steps thus sampling the whole of the stromal depth. The available optical system allowed the choice of the position of the scan in the area of the strip where no visible tilting occurred (Figure 4.1B).

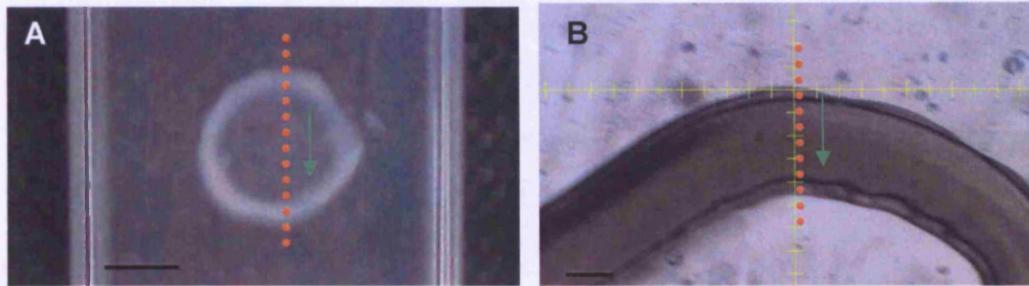


Figure 4.1 Front-on (A) and edgewise (B) scan of the chick cornea indicating path of the beam and direction of raster scan. Calibration bar = 2mm (A) and 100 μ m (B).

The obtained patterns (1024 x 1024 pixels) were analyzed using Unix based software (Sun Microsystems, Mountain View, CA) and statistical software (Statistica7) as previously described (Meek and Quantock, 2001).

Based on the position of the first order equatorial reflection and calibrated against the 67nm D-periodicity of collagen fibrils in wet rat tail tendon, fibril centre to centre spacing was calculated across the corneal button and across the depth of the cornea for the developmental period E14-E18.

4.2 Results

4.2.1 Ultrastructural fibril changes from corneal centre to periphery with development

X-ray diffraction patterns of scans through the front of the cornea from E14 to E18 were analysed. The results of over 350 patterns analysed show that with development, mean centre-to-centre fibril spacing steadily decreases. Due to the orientation of the tissue towards the X-ray beam, the values of the fibril interspacing registered show an average of the collagen in all lamellae within the stroma. From

the data presented in Figure 4.2a and 4.2b it can be seen that the compaction of collagen fibrils between E14 and E18 reaches 25% in the central and peripheral regions.

Compaction of the fibrils with development occurs across a whole corneal diameter, but additionally there is a noticeable reduction in the fibrillar interspacing in the central region of each cornea. This is especially notable in the earlier stages of the development (Figure 4.2b). At E14 the reduction between the peripheral and central 250 μ m of the cornea is 18% and at E15 and E16 it is 15%. In the later developmental stages the difference between collagen fibril interspacing in the centre and periphery of the cornea is lower and reaches 7% by E18.

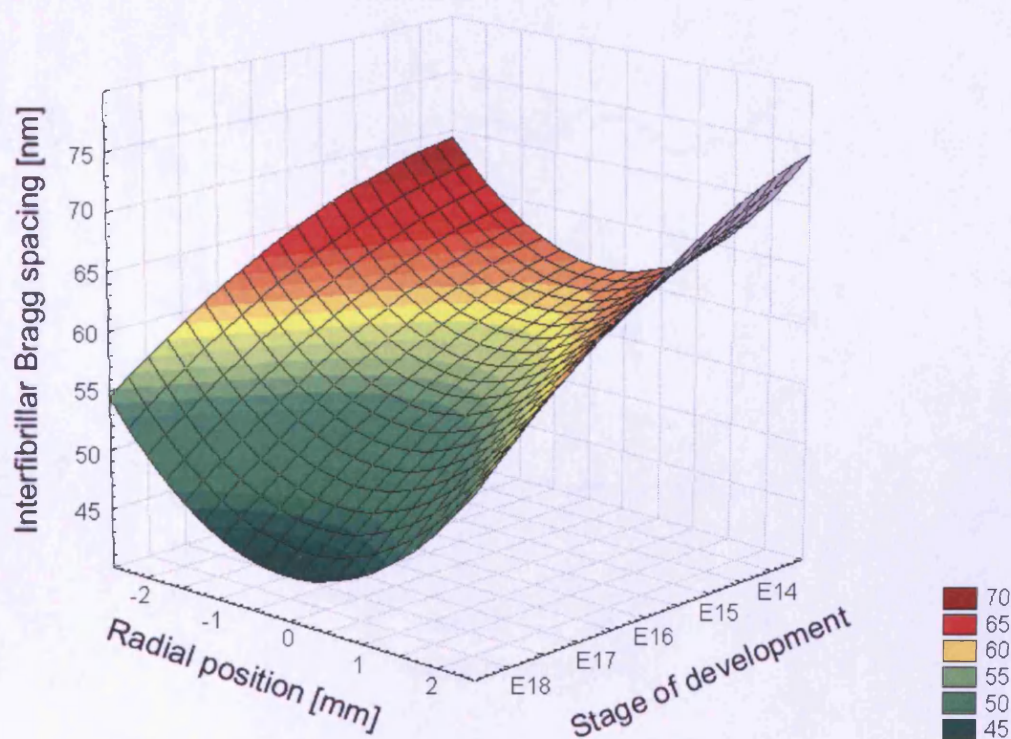


Figure 4.2a Collagen fibril spacing as a function of development and radial position in the front on scan.

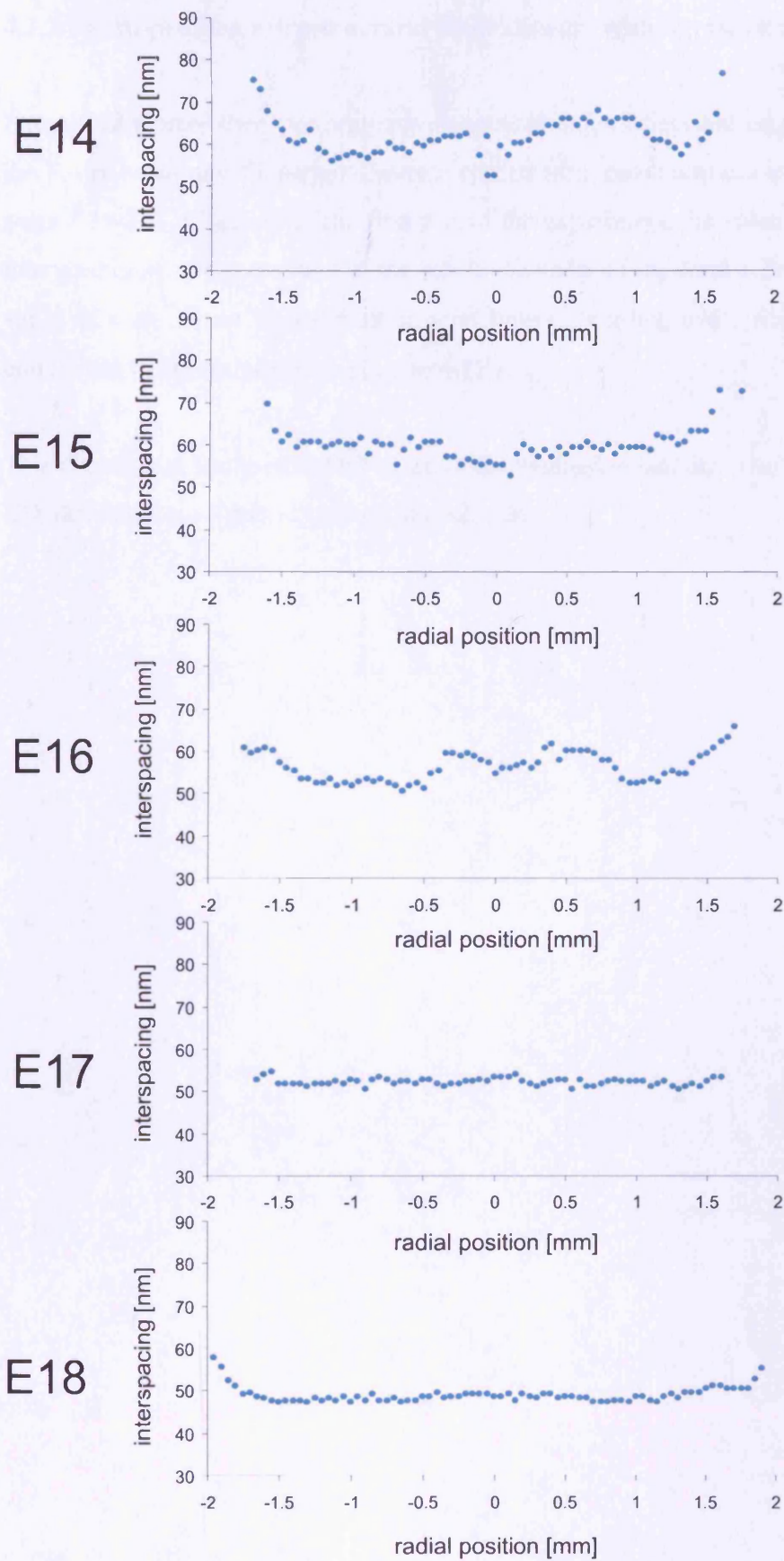


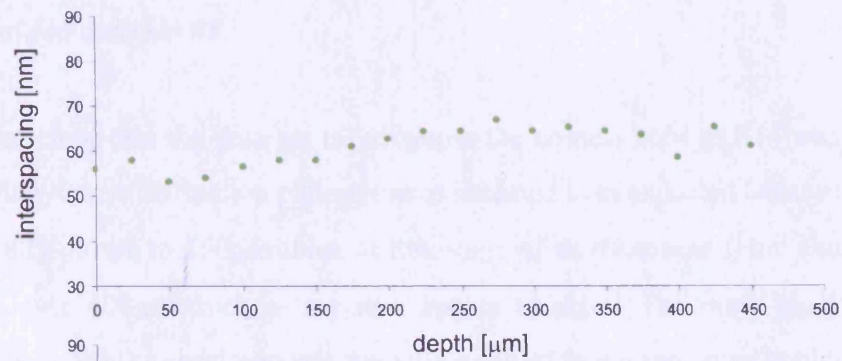
Figure 4.2b Collagen fibril spacing as a function of radial position in the front-on scan.

4.2.2 Depth-profiled ultrastructural fibril changes with development

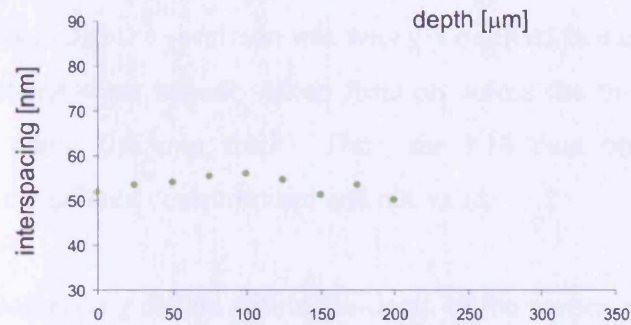
Experiments were then performed with corneal strips orientated edge wise towards the X-ray beam and 51 patterns were recorded from chick corneas at developmental stage E14-E18. Contrary to the first part of the experiment, the value of the collagen interspacing is not an average of the whole thickness of the cornea, but represents the value of each of the 25 μ m thick stromal layers recorded, while scanning from the epithelium to the endothelium (Figure 4.1B).

This experiment was performed twice at the SPring8 synchrotron with the full E14 - E18 developmental period studied in each case.

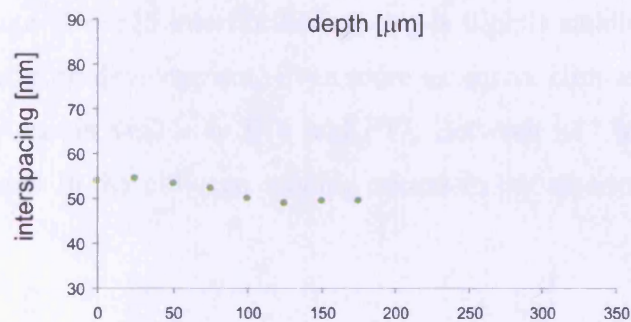
E14



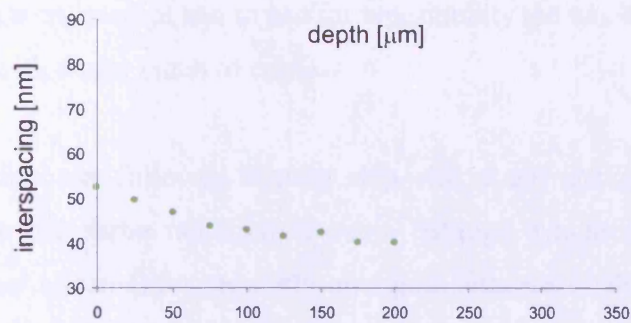
E15



E16



E17



E18

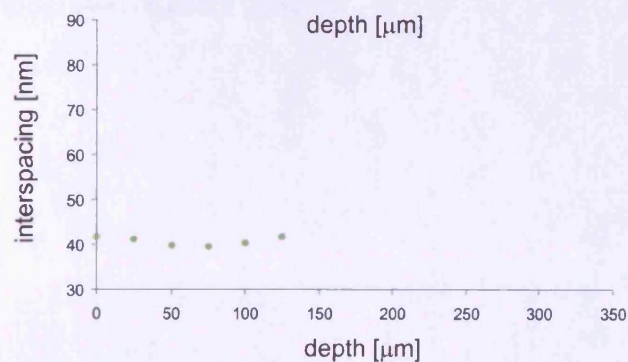


Figure 4.3 Data from experiment #1: Fibril interspacing as a function of stromal depth in the developing chick cornea. 0 indicates starting point of the scan at the anterior surface of the stroma.

4.2.2.1 Depth-profiled data set #1

On analysis, it was clear that the data set taken across the corneal strip at E14 was highly unusual. Many more diffraction patterns were obtained than expected because the stroma is usually closer to 150 μ m thick at this stage of development (Hay and Revel, 1969) not over 400 μ m thick as my data appear to show. The most likely explanation for this is that the specimen was wrongly oriented in the specimen holder so that X-ray patterns were actually taken front-on across the thin strip (which is estimated to be about 0.4 mm thick). Thus, the E14 data presented here for completeness are considered compromised and not valid.

Collagen fibril interspacing differs within the depth of the cornea, and changes with developmental stage. On E15 interfibrillar spacing is slightly smaller in the posterior stroma and later during development. Even more extensive compaction in the deep regions of the stroma is visible in E16 and E17. Between E17 and E18 the most significant reduction in the collagen spacing occurs in the anterior stroma (around 10nm).

Because E14 data were corrupt and to test for repeatability the whole experiment was conducted again with a new batch of corneas.

The original protocol was followed in every step without any changes and the repeat was conducted in the same radiation source - SPring8 synchrotron. Another 51 diffraction patterns arisen from regularly arranged collagen in the corneal stroma were analyzed in the E14-E18 chick corneas.

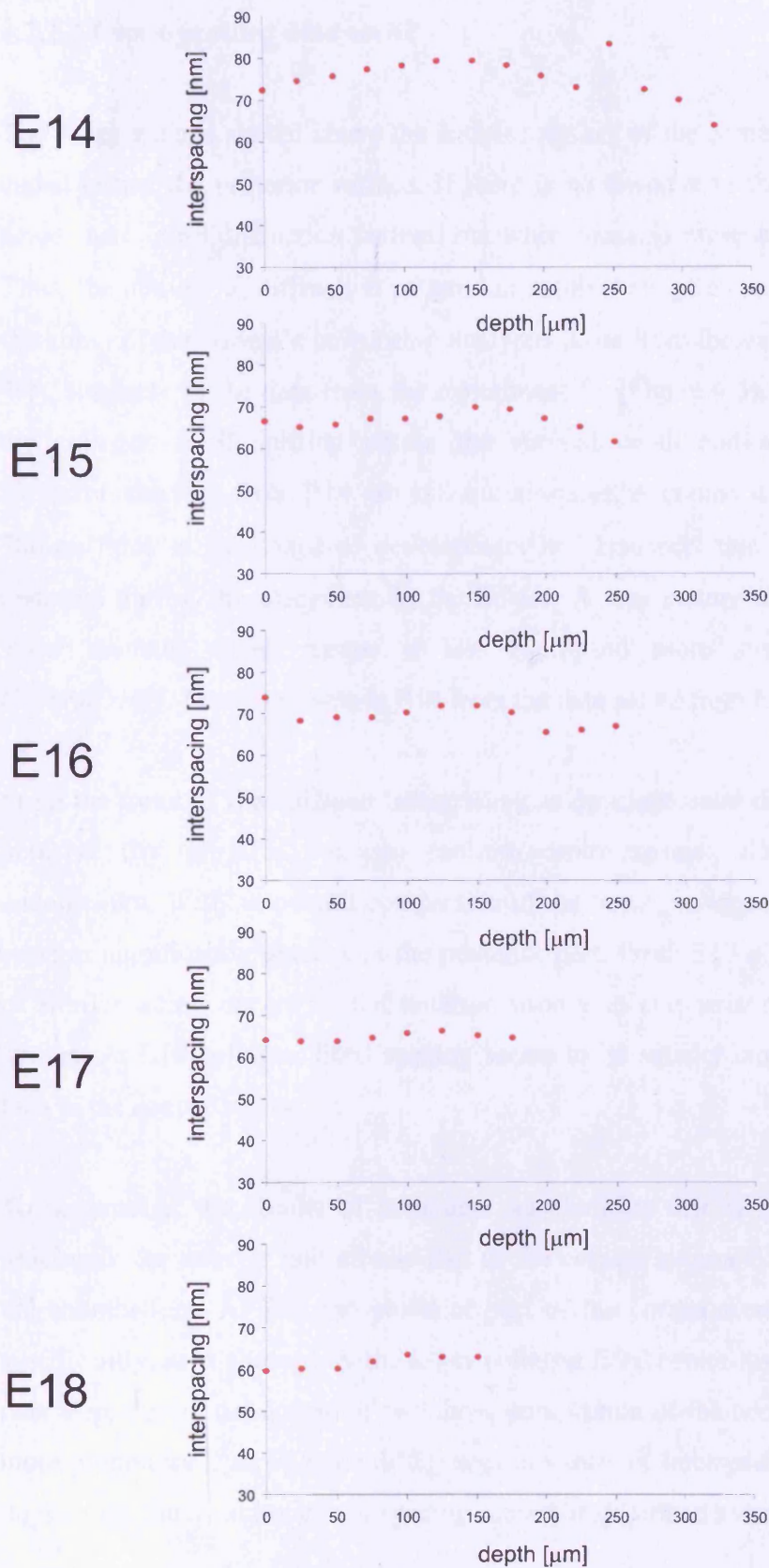


Figure 4.4 Data from experiment #2: Fibril interspacing as a function of stromal depth in the developing chick cornea. 0 indicates starting point of the scan at the anterior surface of the stroma.

4.2.2.2 Depth-profiled data set #2

The X-ray scan is started above the anterior surface of the cornea (Figure 4.1B) and ended below the posterior surface. If there is no tissue in the path of the X-ray beam there is no diffraction pattern, but when tissue is present, the pattern occurs. Thus, the number of diffraction patterns in 25µm steps gives us an indication of the thickness of the stroma's strip being analysed. Data from the experiment #2 (Figure 4.4), similarly to the data from the experiment #1 (Figure 4.3), shows variations in the collagen fibril spacing within the stromal depth and across development. However, the data from E14 are still questionable. A cornea is unlikely to be over 300µm thick at this stage of development and I suspect that the tissue has been distorted during the placement in the holder. A less mature tissue has the higher water content, which makes it less rigid and more susceptible to tilting. Unfortunately, I have to exclude E14 from the data set #2 from further analysis.

From the trend of the collagen interspacing in developmental day E15-E18, we can perceive that at E15, collagen centre-to-centre spacing decreases toward the endothelium. With an overall compaction of the tissue, collagen interspacing at E16 remains significantly smaller in the posterior part. From E17 a more rapid decrease of fibril spacing occurs in the anterior stroma in comparison with the posterior stroma. At E18 collagen fibril spacing seems to be smaller close to the epithelium than in the deeper layers.

To summarise, the results of both data sets indicate that at E15 the interfibrillar spacing in the anterior and middle part of the corneal stroma is higher than close to the endothelium. At E16 the posterior part of the cornea seems to compact more significantly, as is showed by the lower collagen fibril centre-to-centre spacing. As a next step, during the course of two days, compaction of the near epithelial layers is more pronounced. At E18 the differences in values of interspacing within the depth do not vary much, although the spacing cannot be described as uniform.

Collagen fibril centre-to-centre spacing decreases between E15 and E18 altogether more in the region close to the epithelium than close to the endothelium (Table 4.1).

When taken the nearest 75µm to epithelium and 75µm to endothelium, data set #1 and data set #2 show bigger collagen interspacing reduction near epithelium by 1nm and 2.5nm accordingly.

Table 4.1 Table of collagen interspacing in the developing cornea (E15-E18) in the 75µm closest to the epithelium and the endothelium for data set #1 and #2.

Stage of development	Data set #1		Data set #2	
	75µm closest to the epithelium	75µm closest to the endothelium	75µm closest to the epithelium	75µm closest to the endothelium
E15	53.0 nm	51.5 nm	65.7 nm	64.5 nm
E16	54.0 nm	49.3 nm	70.4 nm	66.2 nm
E17	49.4 nm	40.7 nm	63.8 nm	65.2 nm
E18	40.9 nm	40.4 nm	62.1 nm	63.4 nm

Both data sets seems to show the same trend for the collagen fibril spacing in the depth of the developing stroma, however the absolute values differ. Any possible mistakes during data analysing has been excluded and I am not sure, why the absolute values difference occurred.

4.3 Discussion

Compaction of the developing stroma and reduction of the collagen centre-to-centre spacing within the lamellae leads to the onset of the transparency in the cornea. Assembly of the collagen fibrils, thinning of the tissue and the changes in the composition of the extracellular matrix were broadly studied by previous workers (Hay and Revel, 1969; Conrad, 1970; Trelstad and Coulombre, 1971; Quantock et al., 1998; Meek and Quantock, 2001). In my experiment I am concentrating on the later stages of the development (after E14) when more settled changes occur.

All structural changes that happen across the cornea from centre to periphery and throughout its depth were of interest. The study shows that the collagen fibril spacing, while taken as an average across the whole depth of the stroma, increases while measured away from the prepupillary region and it applies to each stage

between E14 and E18. A similar study was performed on the human cornea (Boote et al., 2003) which showed the mean fibril spacing in the central cornea was 5-7% lower than that in the peripheral cornea. My aim was to investigate in an animal model of development whether or not central versus peripheral differences in collagen spacing are present during tissue morphogenesis. What was interesting was a chance to study if the structure of the developing cornea resembles the mature tissue at each stage between E14 and E18. My data shows that, on average, the fibrillar spacing decreases across the whole extent of the cornea, but the difference between central and peripheral region in each stage is not constant. While tissue develops, the difference in collagen interspacing between central and peripheral region is 17% at E14 and only 7% at E18. This could be a result of changes in the collagen alignment. Mature normal chicken cornea has got collagen fibrils aligning circumferentially in the peripheral cornea and limbus that is lost in the chickens affected by rethinopathy globe enlarge (rge) mutation (Boote et al., 2008). This mutation causes the cornea to flatten and collagen fibril spacing to increase rapidly towards the corneal periphery comparison to the unaffected tissue (Boote et al., 2009). At E14 and E15, tissue is not fully structurally established and collagen fibrils in the periphery have probably not reached the final alignment. In support of this, up to E16, when dissecting cornea, it is still possible to separate the cornea by peeling off with a tweezers. In the later stages, scalpels or scissors have to be used. The structural development in the limbal area, mainly circumferentially alignment of collagen, causes the decrease of collagen fibril spacing and emerging of corneal curvature. This could be a reason why the collagen fibril spacing does not compact at the same rate in the centre and in the periphery of the cornea.

The result of the in-depth micro scan showed that at E15, the corneal stroma is slightly more compact close to the endothelium. E16 brings further, even more noticeable, collagen interspacing reduction in the posterior stroma. At E17 compaction slows in the posterior stroma but fibril spacing near the epithelial region starts to rapidly decrease.

In the developing chick's eye, the compaction that starts at E14 in the posterior stroma has been previously reported (Trelstad and Coulombre, 1971) and that is in line with my findings where the collagen fibril spacing decreases towards the

posterior at E15 and E16. Unfortunately, data of E14 from both sets of scans has to be excluded, because the thickness of the cornea is too great to be real. A tilting of the tissue, hence the increase of the thickness is suspected.

Connon's study on the developing chick cornea reported a decrease of the interfibrillar spacing both in the anterior and the posterior between E16 and E18. It also shows that fibril arrangement in the stroma becomes homogenous around day 18 (Connon et al., 2004). I cannot fully relate my finding to the published data, as more repeats of the depth scans are needed to obtain a reliable and clear pattern of collagen compaction during the chick development.

From the former experiment I can clearly say that a link exists between the tissue swelling or compacting and the content of the extracellular matrix. Study of the water gradient and proteoglycan content in the bovine and rabbit cornea showed that the posterior stroma is more hydrated and in this part the concentration of the keratan sulphate proteoglycan is greater than in the anterior part (Castoro et al., 1988; Bettelheim and Goetz, 1976). It happens because the two types of proteoglycan seem to have a different water affinity. CS/DS PGs have bigger affinity power than KS PGs that is why the latter release water easier and accumulates water easier (Bettelheim and Ehrlich, 1963; Plessy and Bettelheim, 1975).

Early experiments on localisation of KS PGs in chick developing cornea showed accumulation of KS first in the posterior stroma and then uniform throughout the stroma (Funderburgh et al., 1986; Takahashi et al, 1999). Although, the latest most comprehensive immunohistochemical study revealed KS PGs to appear in the opposite manner to previous findings and opposite to the bovine and rabbit cornea. It shows, that by E14, KS PGs are mainly accumulated in the anterior part of the cornea, especially highly sulphated KS and then the distribution becomes more uniformly spread across the stroma by day 18 (Young et al., 2007b; Gealy et al., 2007). That would suggest that the anterior part of the stroma has higher water content in early stages of development. That is in line with my findings that the greater compaction in total occurs in the outer layer of the stroma.

While KS is spreading from the anterior to the posterior, CS/DS is first accumulated in the posterior part near day 12-14 of development and then spreads towards the epithelium, which is based on my observations further presented in Chapter Five. Each study presents two different kinds of PGs, with different affinity to the water, that are localised at the opposite sides of corneal stroma and then spread uniformly across the corneal depth and is simultaneous with closer uniform interfibrillar spacing by the developing tissue.

The corneal structure is mainly shaped by the dehydration triggered by the activation of the endothelial pumps. However, equally important is the sulphation of the GAG chains present in the corneal stroma and changes in the ratio and the location of the PGs. All of the above changes happen during development and most likely contribute towards the differences in the collagen spacing within the depth of the stroma.

It is known that while cornea becomes more dehydrated, it accumulates more sulphated KS (Hart, 1976; Cornuet et al., 1994). In the human cornea, in the central region there are 24% more acidic glycosaminoglycans, mostly KS, than in the periphery (Brocherding et al., 1975). This may contribute to the higher values of collagen fibril interspacing in the periphery of the cornea. In developing chicks, KS becomes more sulphated with development (Liles et al., 2010). Sulphation of the CS/DS also changes. Chondroitin-6-sulphate decreases while chondroitin-4-sulphate increases near day 14 of development (Zhang et al., 2005). There is no information how the PGs are distributed in the stroma so we cannot incorporate these changes into our model of depth related collagen interfibrillar changes.

Chapter Five

5 Spatial and temporal alterations in proteoglycan content in developing chick cornea

During the process of development, changes in the level of biosynthesis of GAG chains occur along with changes in the sulphation patterns. Additionally, proteoglycans are not uniformly distributed across the corneal stroma. Localisation of sulphated KS has been broadly studied (Funderburgh et al., 1986; Takahashi et al., 1999; Young et al., 2007b; Gealy et al., 2007), but there are no reports about localisation of CS/DS. Here I use the monoclonal antibodies raised against native proteoglycans carrying CS chains to visualise spatial distribution of CS in the stroma.

In the extracellular matrix of the developing chick stroma, two groups of proteoglycans are present. One has keratan sulphate GAG chains attached to the core protein of which there are three types: keratocan (Corpuz et al., 1996; Liu et al., 1998), lumican (Blochberger et al., 1992b) and mimecan (Funderburgh et al., 1997). The other proteoglycans carry chondroitin/dermatan GAG chains and they are decorin (Li et al., 1992) and biglycan (Bianco et al., 1990).

For a better differentiation between the two groups of proteoglycans, for the second part of experiment, I removed one population using an enzyme called chondroitinase ABC. This enzyme cleaves mainly next to 4- sulphated disaccharides from the non-reducing terminal of CS chains (Hardingham et al., 1993) but taking into consideration that in developing chick cornea the majority of sulphated CS are 4 – sulphated (Hart, 1976; Nakazawa et al., 1995; Zhang et al., 2005), it makes this enzyme suitable for the experiment. After enzyme digestion we can investigate the developing stroma under transmission electron microscope to search for compositional and spatial differences between KS and CS/DS.

5.1 Methods

All animals involved in this study were used in accordance with the Association for Research in Vision and Ophthalmology statement for the Use of Animals in Ophthalmic and Vision Research.

5.1.1 Immunofluorescence microscopy

16 fertilised white leghorn chicken eggs were collected from a commercial hatchery (Hy-line UK, Warwickshire) and placed in the incubator to develop. At day 12, 14, 16 and 18 of development, embryonic corneas were dissected (n=8 for each stage). Corneas were then embedded in Tissue Tek (O.C.T. compound, Sakura Finetek) on cork disks, snap-frozen by dipping in liquid nitrogen-cooling isopentane and then stored at -80°C until use.

Sectioning was carried out on a cryostat at -20°C and tissue sections 8µm thick were obtained and collected on glass slides (RaLamb, UK). Sections were allowed to thaw and circumscribed with the “Immegde pen” that prevents cross contamination of the antibody by leaving water repellent rings around individual sections on the slide. On each section 200µl 0.01M phosphate-buffered saline (PBS) without Tween 20 was applied and left for 10 min to rehydrate samples and then removed.

Non-specific binding was eliminated by coating slides with a blocking agent – 1% bovine serum albumin (BSA) for 30 min using 150µl per section at room temperature. Blocking serum was washed out with PBS. Primary antibodies (Ab) 6C3, 4C3 and 7D4 of working dilution 1:100 and at a volume of 200µm per circle were applied. As a negative control, slides with no primary Ab and with naïve mouse immunoglobuline (mIgG) used at a dilution of 1:200 instead of CS/DS mouse antibody (mAb) were prepared. Slides with primary Ab were incubated for 2 hours in a humid box at room temperature and then washed.

A goat anti-mouse IgG FITC conjugate antibody diluted 1:400 was used as a secondary antibody. 150µl of secondary antibody solution per section was applied and incubated for an hour in the dark at room temperature before washing in PBS.

Corneal sections were mounted in a drop of Vectashield (mounting medium for fluorescence with DAPI, H-1200) under glass coverslips and examined using a Leica TCS SP2 fluorescence microscope (Leica, Vienna, Austria). DAPI excites at 360nm and emits at 460nm when bound to DNA. This allows visualisation not only of the location of secondary antibodies but nuclei of cells in the corneal slice. Images were taken using an Olympus AX470 camera (Olympus, UK)

5.1.2 Electron microscopy

21 corneas from white leghorn chickens (Henry Stewart & Co. Ltd., Louth, Lincolnshire, UK) at developmental stages E12 to E18, along with biopsies of chick skin from E18 as a positive control were dissected with scissors, handled carefully to avoid structural deformation and prepared for electron microscopy.

One batch of E12 to E18 corneas was quartered and fixed overnight in 2.5% glutaraldehyde in 25 mM sodium acetate buffer with 0.05% cuproline blue (0.1 M $MgCl_2$, pH 5.7) to stain the sulphated PGs (Scott, 1980).

Another series was fixed for 10 minutes in 4% paraformaldehyde in Tris/sodium acetate buffer (pH 7.2) to make the tissue more resistant to swelling during a period of incubation with enzyme. These corneas were then washed twice in chondroitinase buffer, which is the buffer used to reconstitute the chondroitinase ABC (50 mM Tris, pH 8, 60 mM sodium acetate and 0.02% BSA) and cut into quarters. Corneal pieces were then incubated for 4 hours at 37°C in chondroitinase buffer containing 2.5 U/ml chondroitinase ABC (from *Proteus vulgaris*; Sigma-Aldrich) to remove the chondroitin- and dermatan-sulfate GAG chains from the tissue. Commercially prepared protease inhibitor cocktail for general use (Sigma-Aldrich) was added to the chondroitinase buffer (1% of total volume) to inhibit endogenous PG degradation.

The third, control, series of E12 to E18 corneal quarters was similarly processed but the chondroitinase buffer contained only protease inhibitor cocktail and no chondroitinase ABC. This was done to investigate if the incubation period had any negative impact on the PG content. After incubation, samples from the second and third series were washed in chondroitinase buffer (without enzyme), before fixation and staining overnight in 2.5% glutaraldehyde in 25 mM sodium acetate buffer with

0.05% cuproinic blue (0.1 M MgCl_2 , pH 5.7) in an identical manner to which non-digested tissue had been treated.

Skin biopsies were treated simultaneously with all three series of cornea quarters to represent a control for chondroitinase ABC activity. All tissues were then rinsed in 25mM sodium acetate buffer (pH 5.7) and contrast enhanced with 0.5% sodium tungstate. The tissue was then dehydrated in 0.5% sodium tungstate in 50% ethanol which was followed by 70% ethanol, 90% ethanol, 100% ethanol and finished with propylene oxide before embedding in Araldite resin. Individual pieces of tissue were placed in moulds in more Araldite resin and cured in the oven in 60°C for 2 days.

Ultrathin sections (approx 90nm thick) were cut on glass knives on an Ultracut E microtome (Reichert-Jung, Vienna, Austria), collected on copper grids (300 square mesh, Agar), and stained with 1% aqueous phosphotungstic acid and saturated aqueous uranyl acetate before examination by transmission electron microscopy (JEM-1010; JEOL, Tokyo, Japan) equipped with an 11-megapixel CCD camera (Orius SC1000 CCD camera; Gatan Ltd., UK, Cambridge, UK).

5.2 Results

5.2.1 Immunofluorescence microscopy

Immunofluorescence microscopy of the developing cornea shows an accumulation of CS/DS during the later stages of incubation. Staining with the monoclonal antibody 7D4 revealed chains of chondroitin/dermatan sulphate through the corneal stroma (Figure 5.1). Images of the negative control confirmed lack of non-specific binding of the secondary antibody. Staining with the two other monoclonal antibodies 6C3 and 4C3 displayed the same pattern. Neither of the antibodies used is fully characterised and for the analysis only one out of three sets of staining was chosen to be presented.

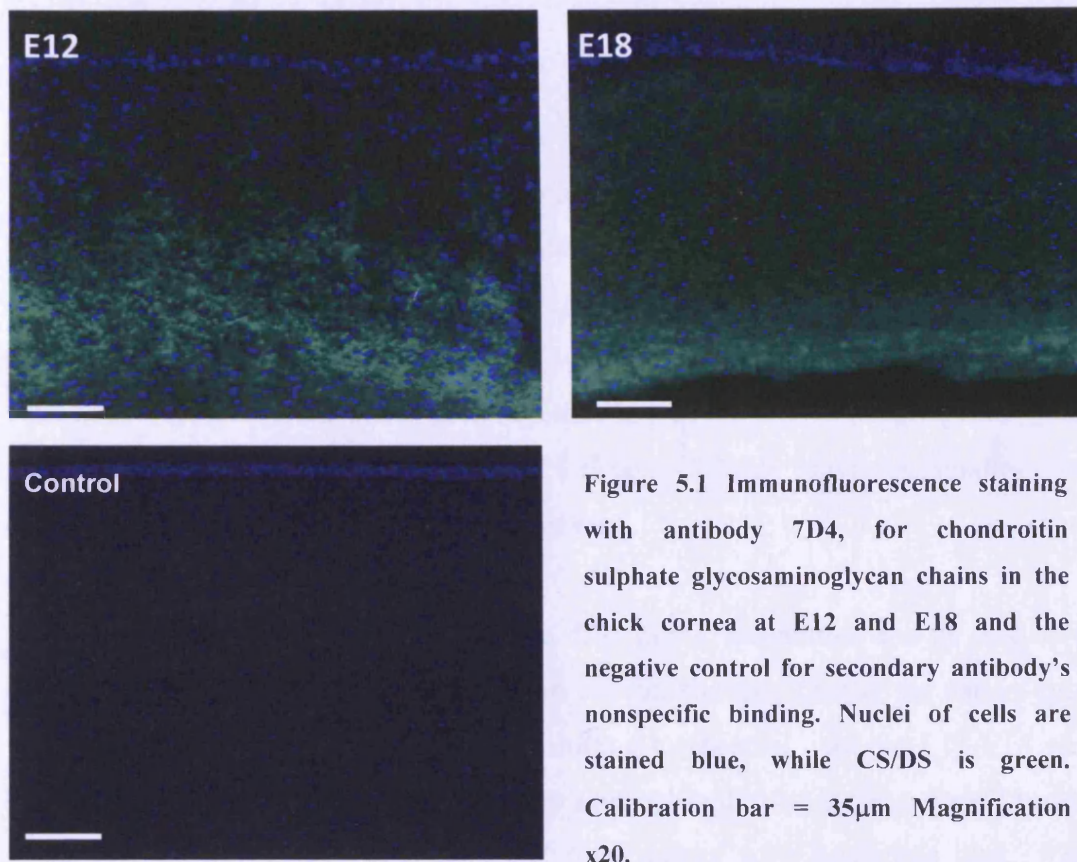


Figure 5.1 Immunofluorescence staining with antibody 7D4, for chondroitin sulphate glycosaminoglycan chains in the chick cornea at E12 and E18 and the negative control for secondary antibody's nonspecific binding. Nuclei of cells are stained blue, while CS/DS is green. Calibration bar = 35 μ m Magnification x20.

At day 12 of development, CS/DS has clearly accumulated in the posterior region of the stroma with a clear unstained region in the anterior part of the stroma. During the next stages (E14 and E16), chondroitin/dermatan sulphate chains are present as well in the anterior part. Interestingly, only on day 16 of development does immunofluorescence staining appear to be homogenous. At the final stage (E18), CS/DS are visible throughout the whole thickness of the tissue with easy to distinguish layers of higher intensity near the epithelium and the endothelium.

Corneal matrix compaction and dehydration by day 15 cause sections to become thinner from this stage onwards (Siegler and Quantock, 2002). This allows a full thickness image on E18 to be obtained at x20 magnification in comparison to E12.

5.2.2 TEM

The stroma of developing chick corneas in daily intervals E12 – E18 was studied using electron microscopy. Cuproinic blue stain made sulphated GAG chains in both KS and CS/DS PGs visible. To distinguish KS PGs from CS/DS PGs an enzymatic digestion using chondroitinase ABC was performed. In the tissue stained with cuproinic blue PGs are visible as long and thick GAG chains running along collagen fibrils as well as in between adjacent fibrils. They are most prominent in the earlier stages of development – up to E15 (Figure 5.2a-d). However, smaller GAG chains are also present in the developing matrix.

Enzymatic digestion process requires a few hours incubation and it has to be established if this causes any proteoglycan content changes. One of the causes could be a PGs leaching out into the bathing fluid. As a control, corneas E12-E18 were incubated in the buffer used to reconstitute an enzyme, for the same period of time as tissue ongoing enzymatic digestion, and then stained with cuproinic blue. When compared with untreated corneas, there are no visible, significant differences in proteoglycan content at any studied stage of development. There are still two different types of proteoglycans noticeable. It is likely that the brief pre-fixation helped prevent this loss of PGs.

To test chondroitinase ABC activity, skin biopsies from the skin of chick (E18) were treated in the same way corneas were treated. Skin was chosen as a control because its extracellular matrix contains one type of proteoglycans: decorin. After enzyme digestion there are only bare collagen fibrils visible with no PGs left in the tissue (Figure 5.2h). It shows that following the protocol we are able to remove all chondroitin/dermatan sulphate from the tissue.

In chick corneas in the E12-E18 timeframe which underwent the enzymatic digestion we can no longer observe long and thick GAG chains (Figure 5.2a-g). That indicates that the large filaments often linking adjacent collagen fibrils are CS/DS proteoglycans. Remaining small enzyme resistant filaments on the surface of fibrils are KS proteoglycans in developing chick cornea. Comparing chondroitinase ABC digested corneas E12-E18 shows that amount of visible KS PGs increases in the mid section of the extracellular matrix of the stroma while tissue develops (Figure 5.3).

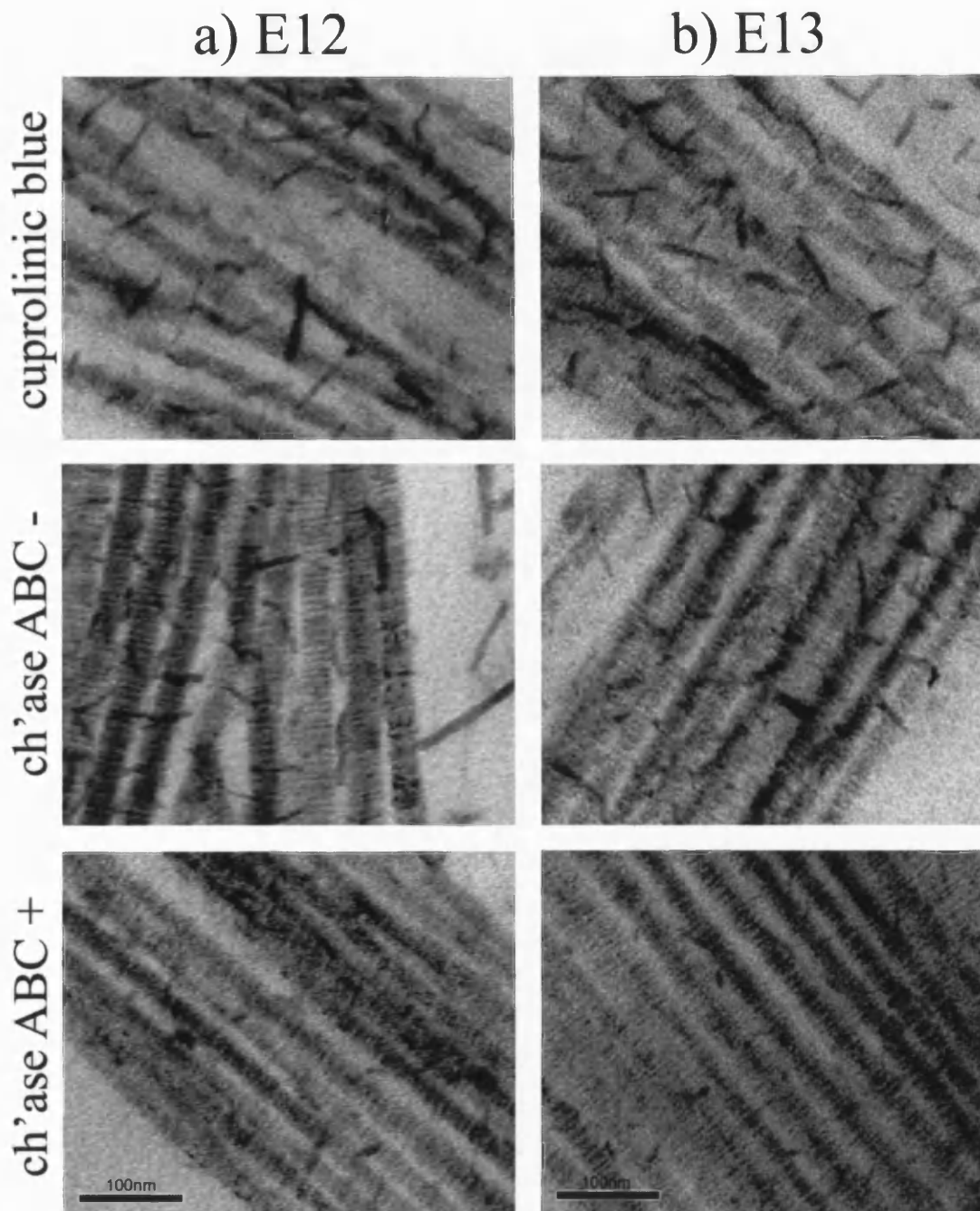


Figure 5.2a-b Collagen fibrils in the mid corneal stroma at E12 and E13 with visible GAG chains of proteoglycans. The 3rd row shows tissue with CS/DS removed by chondroitinase ABC and no large filaments are evident. Micrographs taken at x20k magnification.

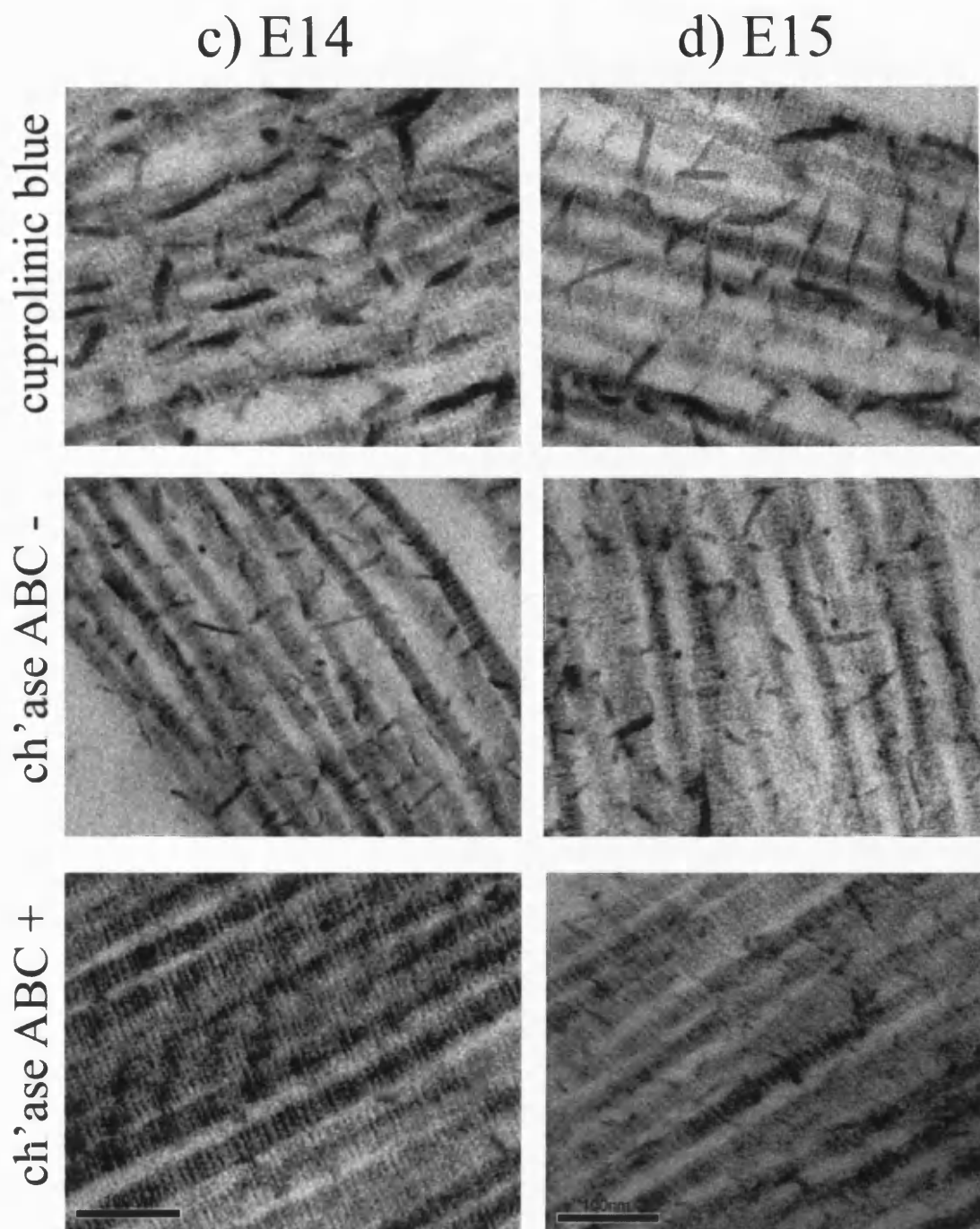


Figure 5.2c-d Collagen fibrils in the mid corneal stroma at E14 and E15 with visible GAG chains of proteoglycans. The 3rd row shows tissue with CS/DS removed by chondroitinase ABC and no large filaments are evident. Micrographs taken at x20k magnification.

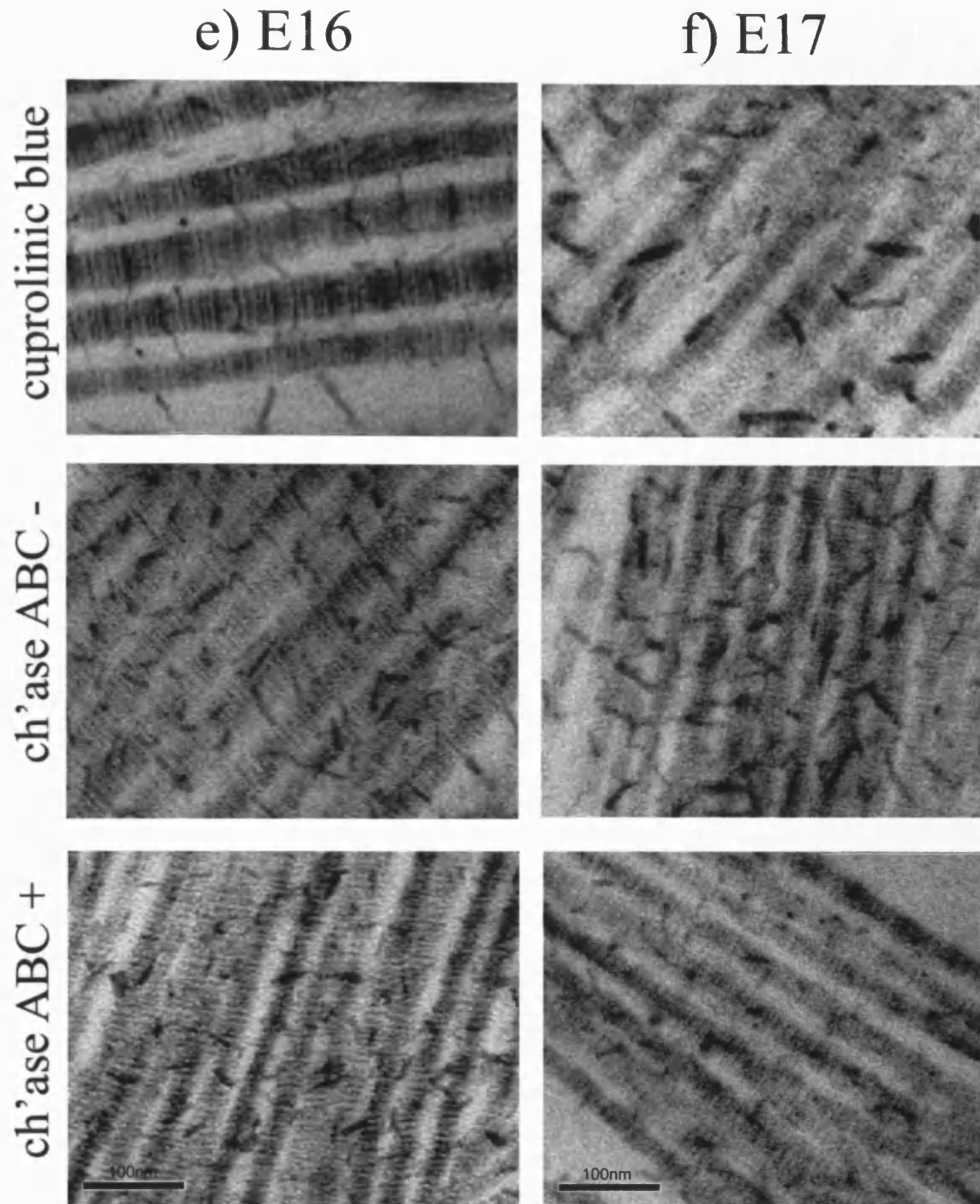


Figure 5.2e-f Collagen fibrils in the mid corneal stroma at E16 and E17 with visible GAG chains of proteoglycans. The 3rd row shows tissue with CS/DS removed by chondroitinase ABC. No large filaments are evident, but more small collagen associated PG filaments are seen. These are of the KS variety. Micrographs taken at x20k magnification.

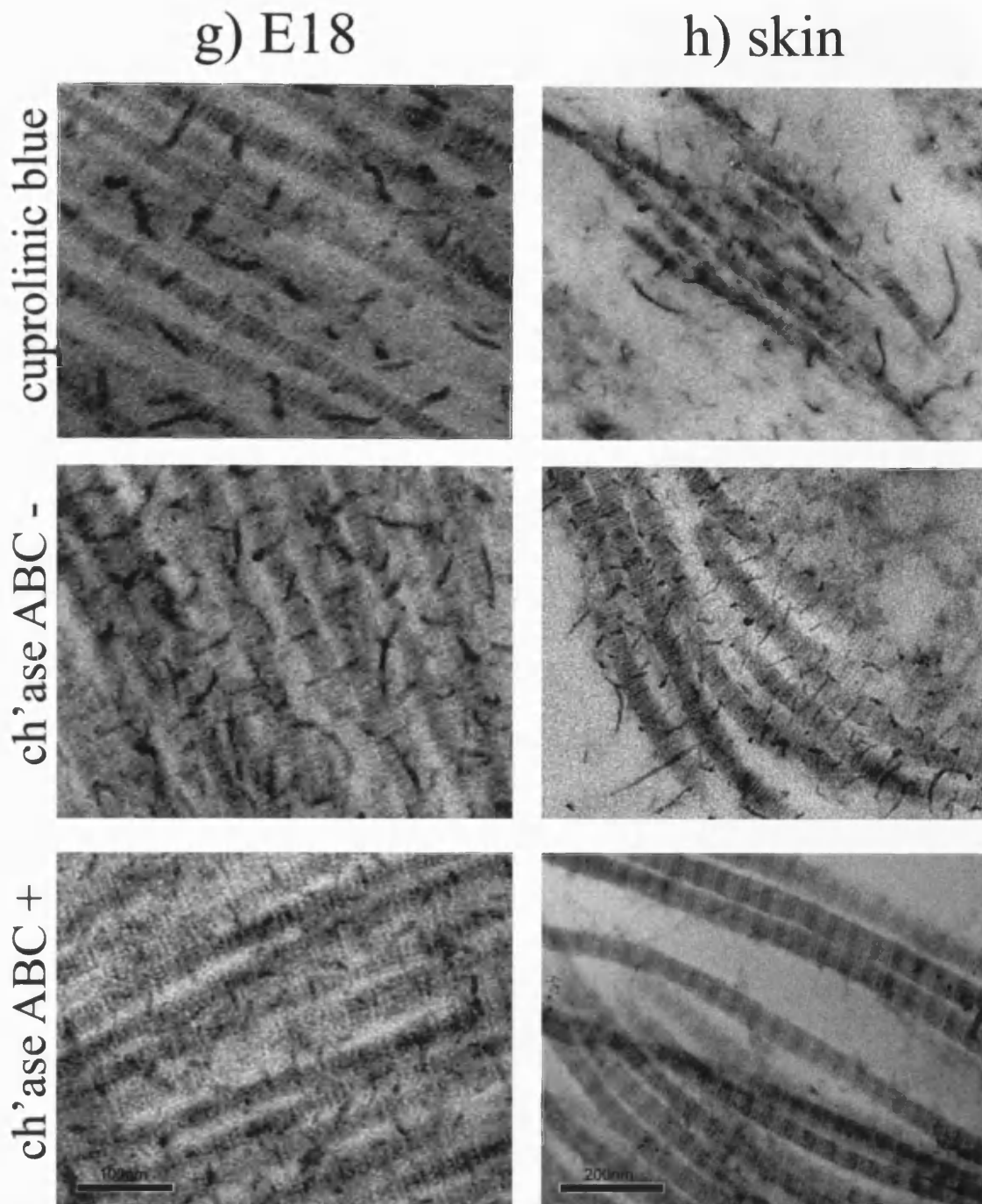


Figure 5.2g-h Collagen fibrils in the mid corneal stroma at E18 and skin with visible GAG chains of proteoglycans. The 3rd row shows tissue with CS/DS removed by chondroitinase ABC. No large filaments are evident in the cornea, but more small collagen associated PG filaments are seen. These are of the KS variety. No PGs are visible in the skin control confirming good enzyme activity. Micrographs taken at x20k magnification for the cornea and at x10k for the skin.

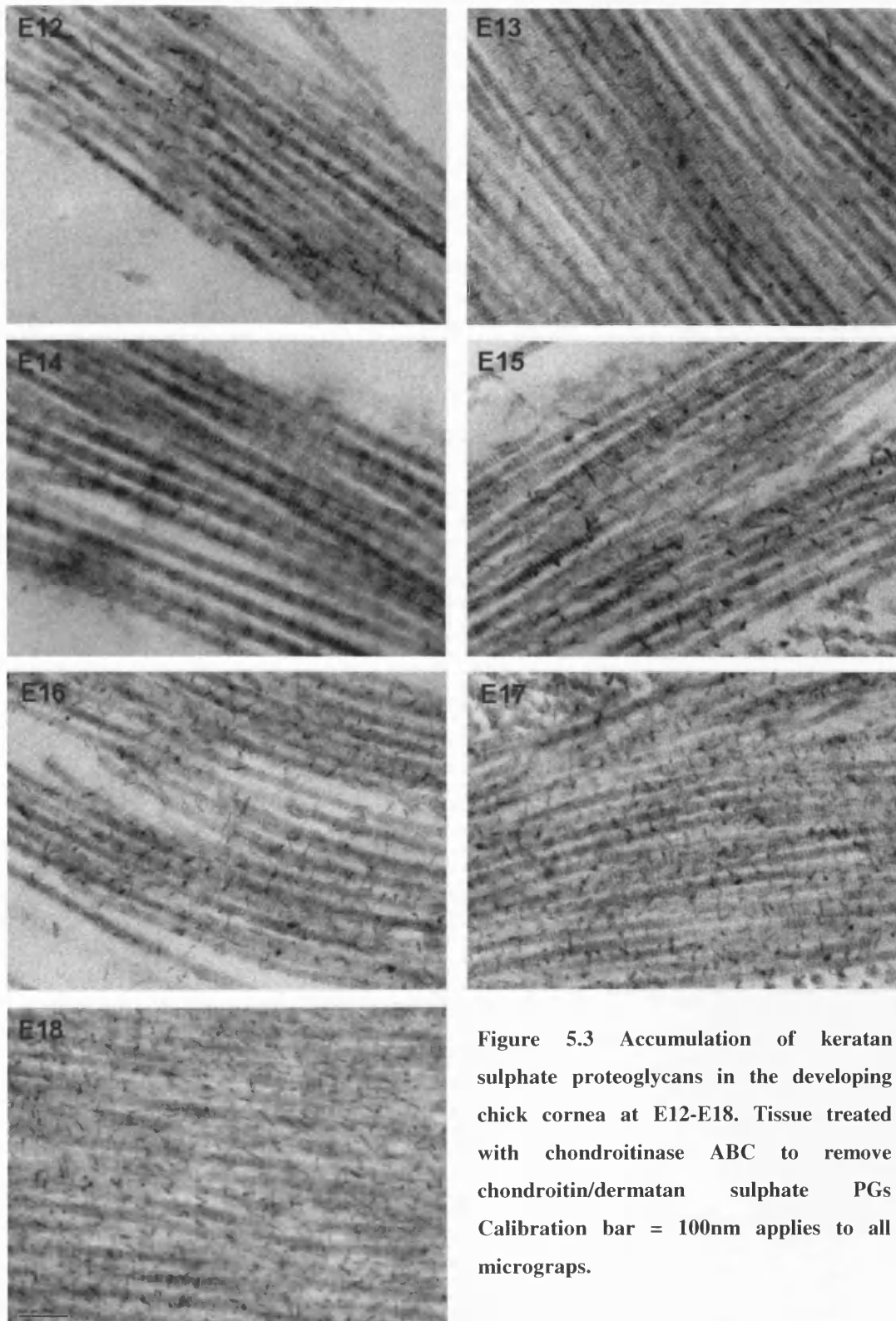


Figure 5.3 Accumulation of keratan sulphate proteoglycans in the developing chick cornea at E12-E18. Tissue treated with chondroitinase ABC to remove chondroitin/dermatan sulphate PGs. Calibration bar = 100nm applies to all micrographs.

5.3 Discussion

In the developing chick cornea proteoglycans are first synthesised after invasion of the primary stroma by fibroblasts. Those synthesised on E5 are mainly CS/DS PGs, and then on E7 an increase in synthesis of KS PGs occurs (Hart, 1975; Nakazawa et al., 1995; Takahashi et al., 1999). With development the total amount of glycosaminoglycans per dry weight of cornea increases (Anseth, 1961), but it is not a uniform process. Synthesis of KS PGs increases until E14 when it peaks and then starts to decline until E18 (Nakazawa et al., 1995; Zhang et al., 2005). The biosynthesis of CS/DS PGs is highest in the early stages of development, decreases until E18, and is lower still in adult chickens (Nakazawa et al., 1995; Zhang et al., 2005). However, not only does the biosynthesis and ratio of PGs change with development, but also its spatial accumulation in the stroma.

Results of the immunofluorescence study suggest that the accumulation of CS/DS throughout the corneal stroma proceeds in a posterior to anterior manner. In the early stages of development CS/DC appears on the posterior side of the stroma and around E14 spreads out in an anterior direction. That is in opposite to the accumulation of high-sulphated KS (Young et al., 2007b). Unfortunately, the types of antibody that were used in experiment do not provide us with information about how accumulation of CS/DS refers to its sulphation. Antibodies 7D4, 4C3 and 6C3 were raised against native chick bone marrow proteoglycans and recognise CS chains, however, the epitopes have not been fully characterised (Sorrel et al., 1990). It is known that native CS epitopes for these antibodies are more structurally complex than the 0-, 4-, 6-sulfated disaccharide repeats of CS chains and are distributed within the linear framework of chains (Sorrel et al., 1993). Additionally, the presence and location of the epitopes may vary with source, developmental stage and pathological status of the tissue (Caterson et al., 1990). For that reason, the presented data show only overall CS/DS PG distribution within the depth of the cornea without providing any information about the GAG chains sulphation.

There are no studies on the location of CS/DS according to its sulphation pattern in chick cornea, but in the case of mice, a presence of chondroitin chains rich in 4-sulphated disaccharides in corneal PGs was revealed (Young et al., 2005). However,

previous studies on other connective tissues have shown that the ratio of 6:4 sulphated CS PGs increases with age (Lauder et al., 2001) and epitopes for antibody that recognise 6-sulphated disaccharides may be present at a later stage.

Chondroitinase ABC digestion and transmission electron microscopy of the developing chick corneas has been performed to distinguish between two types of proteoglycans in the stroma. On micrographs there are usually two types of filament visible. In one group PGs are small and associated with collagen fibrils surface. Another one are larger and lie along collagen fibrils or extend out into the extracellular matrix, connecting with adjacent fibrils (Connon et al., 2003). In this study all PGs with large filaments were removed from the tissue during enzymatic digestion in all stages of development, indicating that they are CS/DS PGs.

Additionally, it can be noticed that GAG chains of CS/DS PGs are longer and thicker in the early stages of development – until E15. This might be due to the sulphation changes, although I can only speculate. The ratio of 4 - sulphated to 6 – sulphated CS/DS increases in chick development and reaches a maximum at E14 (Hart, 1976; Zhang et al., 2005). Thus, the majority of the visible CS/DS are probably 4 – sulphated CS/DS because chondroitin 6 – sulphate is synthesised only in the very early and very late developmental stages (Nakazawa et al., 1995). These large filaments, approximate 65nm long but being even 100nm long, found in the chick cornea resemble filaments in the mouse cornea, which are describe as 4 – sulphated CS/DS. However, murine filaments are much longer and are able to connect more than 2 collagen fibrils (Young et al., 2005).

The number of small filaments of KS on the surface of collagen fibrils which remain after digestion with chondroitinase ABC increases between E12 and E18. This is probably the result of PGs accumulation and increase in KS chains sulphation which happens during development (Nakazawa et al., 1995). Especially highly sulphated KS GAG epitopes are detectable in the last week of chick development (Liles et al., 2010), which is our studied period. The character of used cationic dye supports an increase in KS detection with increase of sulphation, because cuproinic blue complexes with negative charges of sulphated GAG chains (Scott, 1972). However, the accumulation of KS PGs presented in this study is only a qualitative, not a

quantitative representation, of the process. To quantify the amount of PG within the stroma based on the electron micrographs, all three areas of the stromal depth (anterior, mid, posterior) have to be represented. I showed only PGs in the middle stroma. This may not be representative of the entire depth of the stroma.

Chapter Six

6 Collagen architecture in human pathologies with proteoglycan defects

This chapter presents studies of three diseased human corneas with different genetic mutations in PG pathways, 1) Macular corneal dystrophy in which sulphation of KS GAGs is disrupted (Hassell et al., 1980), 2) Sly syndrome where GAG chains are accumulated due to the inability of the organism to catalyse them (Sly et al., 1973), and 3) Congenital Stromal Corneal Dystrophy (CSCD) in which a truncated decorin core protein is produced (Berdrup et al., 2005). All of these abnormalities lead to the opacification of the cornea. The structural changes in size and spacing of collagen fibrils in the corneal stroma will be described.

6.1 Macular corneal dystrophy

Macular corneal dystrophy (MCD; MIM 217800) is an autosomal recessive disease characterised by progressive corneal cloudiness and focal opacities caused by an anomaly in the production of KS GAG (Klintworth and Vogel et al., 1964; Klintworth and Smith, 1983; Hassell et al., 1980; Nakazawa et al., 1984; Midura et al., 1990; Plaas et al., 2001).

Three main immunophenotypes of MCD can be distinguished (type I, type IA and type II) based on the reactivity of corneal tissue and/or serum to a monoclonal antibody (5D4) which recognises high-sulphated KS (Caterson et al., 1983; Mehmet et al., 1986). Sulphated KS, which is present in the cornea and serum of non-affected individuals, is absent from the serum and cornea in the majority of MCD patients, and these are categorised as MCD type I (Thonar et al., 1986; Klintworth et al., 1986). Initially, all MCD patients were believed to have defective, unsulphated KS-GAG systemically, but in the late 1980s it was discovered that some patients had immunodetectable KS in their serum and cornea (designated MCD type II), even though the different MCD types are clinically indistinguishable (Yang et al., 1988; Edward et al., 1988). Further studies have identified MCD type IA, in which there is

no detectable KS in sera of affected individuals, but a 5D4-positive signal in keratocytes (Klintworth et al., 1997).

As mentioned in earlier chapters KS, in the cornea is an important matrix molecule, which forms PG by binding to one of three core proteins, lumican, keratocan or mimecan (Blochberger et al., 1992b; Corpuz et al., 1996; Funderburgh et al., 1997). KS PGs bind to collagen fibrils via their core proteins at defined locations along the fibril axis (Scott and Haigh, 1985; Meek et al., 1986) with the hydrophilic, sulphated GAG chains occupying the extrafibrillar space where they help control the swelling properties of the stroma and the structural arrangement of the collagen fibrils (Bettelheim and Plessy, 1975; Bettelheim and Goetz, 1976; Castoro et al., 1988; Borcharding et al., 1975). The cornea affected by MCD is thinner than normal (Ehlers and Bramsen, 1978; Donnenfeld et al., 1986) and, unlike in other conditions such as keratoconus where a slippage of lamellae is suspected to be responsible for the reduction in central corneal thickness (Fullwood et al., 1992; Meek et al., 2005), the collagen fibrils in MCD are more closely spaced than normal (Meek et al., 1989; Quantock et al., 1990).

All previous measurements of collagen fibril spacing by small-angle X-ray diffraction represent an average value throughout the whole thickness of the stroma. KS, however, is not evenly distributed throughout the cornea (Scott and Haigh, 1988c; Scott and Bosworth, 1990), so to investigate whether or not the PG alterations manifested in MCD are associated with location-specific changes in stromal extracellular matrix architecture we conducted a series of microbeam synchrotron X-ray diffraction experiments at a spatial resolution of 25µm to ascertain the depth-dependent nature of collagen fibril spacing in MCD.

6.1.1 Case report and methods

The research described in this chapter was carried out in collaboration with colleagues in Kyoto Prefectural University of Medicine, and was approved by the Committee for Ethical Issues on Human Research of Kyoto Prefectural University of Medicine and followed the tenets of the Declaration of Helsinki.

The patient was a 50-yr-old female with bilateral MCD type I, who 11 years earlier had undergone penetrating keratoplasty in her right eye. As with the right cornea, the left cornea was affected by a diffuse ground-glass-like stromal opacity, and numerous irregularly-shaped white patches which were confined mainly to the deep part of the stroma (Figure 6.1).



Figure 6.1 Clinical appearance of the MCD cornea examined in this thesis. Diffuse ground-glass-like stromal opacities were observed on slit-lamp examination (A), with irregular patches visible in the cornea by the scleral scattering technique (B).

The edges of the opacities were dull and indistinct. A penetrating keratoplasty was performed in the patient's left eye in September 2007, after which the excised button (7mm-diameter) was immediately wrapped in Clingfilm to prevent dehydration, and stored at -80°C for 7 days prior to transportation on dry ice from the hospital in Kyoto to the SPring-8 synchrotron facility in Hyogo Prefecture, Japan, where small-angle X-ray scattering techniques were used to investigate the internal fine structure of the corneal stroma in its hydrated state as described in methods (Meek and Quantock, 2001).

A human eye-bank cornea deemed unsuitable for grafting because of a low endothelial cell count was similarly examined. Under a binocular microscope, two thin strips were cut across the centres of the MCD and eye bank corneas using a surgical blade, with the edge of a glass microscope slide serving as a guide for the dissection. This was done with the epithelial side up, and the cut strips were estimated to be in the region of $400\mu\text{m}$ thick.

Two thin strips of tissue were dissected across the central cornea. One strip was analysed with the X-ray beam directed through the corneal strip from front to back,

whilst the second strip was oriented so that the beam passed through the corneal strip edgewise (Figure 6.2).

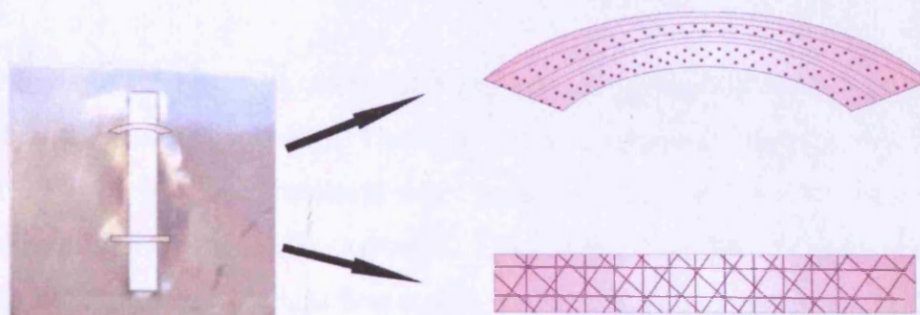


Figure 6.2 The tissue holder with two mounted strips of cornea. The one at the top is mounted facing the x-ray beam edge wise while the bottom corneal strip is mounted face-on. The right hand schematic shows corneal strips with the approximate direction of the collagen fibrils indicated.

Depth-profiled data were collected from the centre of the cut-strip (i.e. at a location corresponding to the corneal centre) and at a position in the mid-periphery, approximately 3mm from the corneal centre. On the high flux beamline 40XU, a series of small-angle X-ray diffraction patterns was obtained with a 25 μ m beam ($\lambda = 1.18\text{\AA}$) in 25 μ m steps using sub-second exposure times as described previously (Quantock et al., 2007). A series of small angle diffraction patterns were recorded on the detector (4 inch II (V7739P/ION) + C4880-50) situated 3.13m behind the specimen. Patterns were analyzed to provide values for the mean collagen interfibrillar spacing, calibrated to the meridional reflection arising from the 67-nm axial repeat of collagen in rat tail tendon and adjusted by a 1.12 calibration factor to take into account the mode of packing of collagen fibrils in cornea (Worthington and Inouye, 1985), as was done in previous studies of MCD (Meek et al., 1989; Quantock et al., 1990).

After X-ray exposure, small full-thickness pieces of MCD cornea were prepared by conventional fixation in 2.5% buffered glutaraldehyde, followed by post-fixation for 1-hr each in 1% aqueous osmium tetroxide and 0.5% aqueous uranyl acetate. Tissue was then dehydrated through an ascending series of ethanol concentrations, immersed in propylene oxide, and embedded in Araldite CY212 epoxy resin. Ultrathin sections were cut with a diamond knife on a Leica UC6 ultramicrotome,

picked up on uncoated copper grids, contrasted with saturated uranyl acetate and Reynold's lead citrate, and imaged on a Philips/FEI 208 electron microscope.

On the basis of the obtained electronmicrographs, histograms of fibril diameter were prepared using ImageJ software. The scale for measurements was set using the pixel size of the scale bar. The threshold was changed to obtain the best contrast between the collagen fibril and the background. Then each individual collagen fibril was measured by drawing a straight line across the shortest diameter of fibril to eliminate an error which might have occurred from a possible tilt of the fibril.

6.1.2 Results

Comparison of raw diffraction patterns shows a decrease in the collagen centre-to-centre fibril spacing in the MCD cornea. The equatorial reflection ring in the eye bank human cornea and in the MCD cornea had different radii (Figure 6.3). In the small angle X-ray diffraction, a bigger equatorial reflection ring indicates smaller fibril interspacing. The 1st and 3rd meridional reflections which were within the collection area of the detector were unchanged, indicating that the axial order of collagen molecules or D-period is the same in both the eye bank cornea and the MCD cornea.

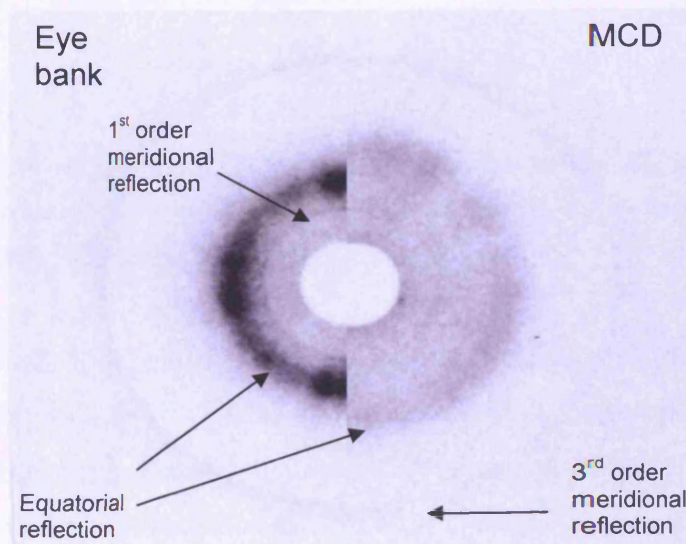


Figure 6.3 Small angle X-ray diffraction pattern of a human eye bank cornea (left) and MCD cornea (right) with visible meridional and equatorial reflections.

Collagen interfibrillar spacing, measured at 27 positions, 25 μ m apart, in the central region of the eye bank cornea and in 21 positions in the MCD cornea with the beam directed at right angles to the corneal surface and passed through the whole thickness of the tissue gave mean values of 52.0nm (SD \pm 0.3nm) and 40.7nm (SD \pm 0.7nm), respectively (Figure 6.4). Previous measurements by synchrotron X-ray diffraction of collagen fibril spacing in MCD indicated a reduction of 22% compared to the fibril spacing in a post-mortem human cornea, with the values representing an average throughout the whole thickness of the stroma (Quantock et al., 1990). A similar proportional reduction is seen in the current analysis.

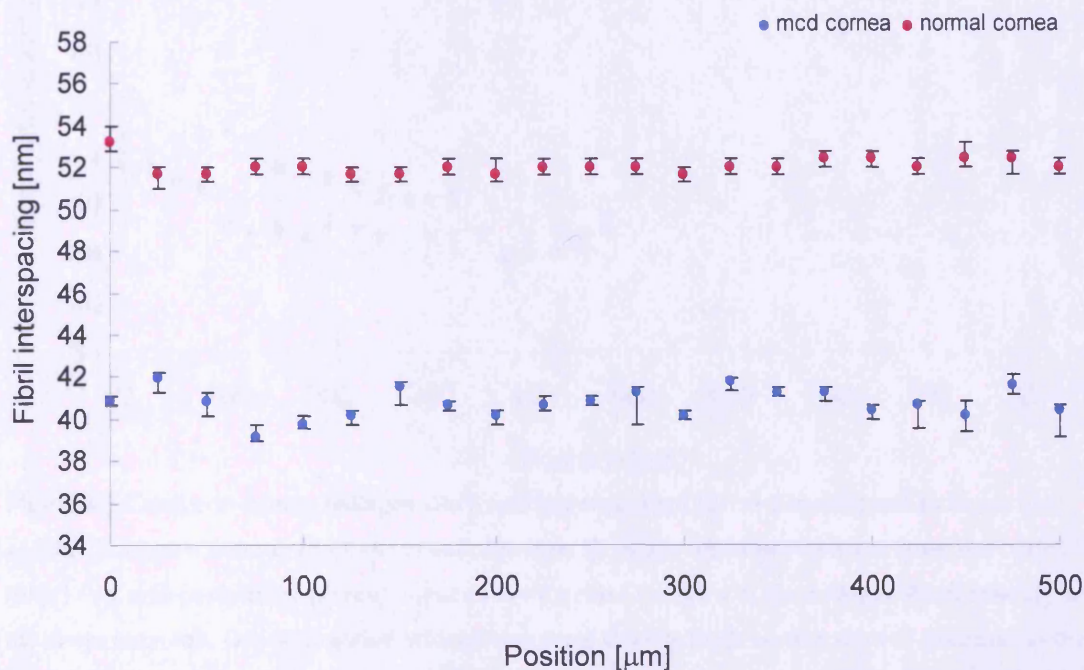


Figure 6.4 Centre-to-centre collagen fibril spacing measured across the strip of human eye bank cornea (pink) and MCD cornea (blue) in the central region. Error bars show accuracy of the reading: the longer the bar the less accurate the reading.

What is not known, however, is whether or not this reduced fibril spacing in MCD varies with stromal depth. To rectify this, measurements of collagen interfibrillar spacing were obtained in sequential steps of 25 μ m across the MCD and eye bank corneas from anterior to posterior. Eye bank data confirmed previous depth-profiled X-ray diffraction studies (Quantock et al., 2007) and showed that collagen fibrils were more widely spaced in the posterior stroma (by approximately 25%) as compared to the mid-depth or anterior stroma (Figure 6.5). The opposite was true,

however, for the MCD cornea, with collagen fibril spacing clearly lower in the posterior stroma (Figure 6.5).

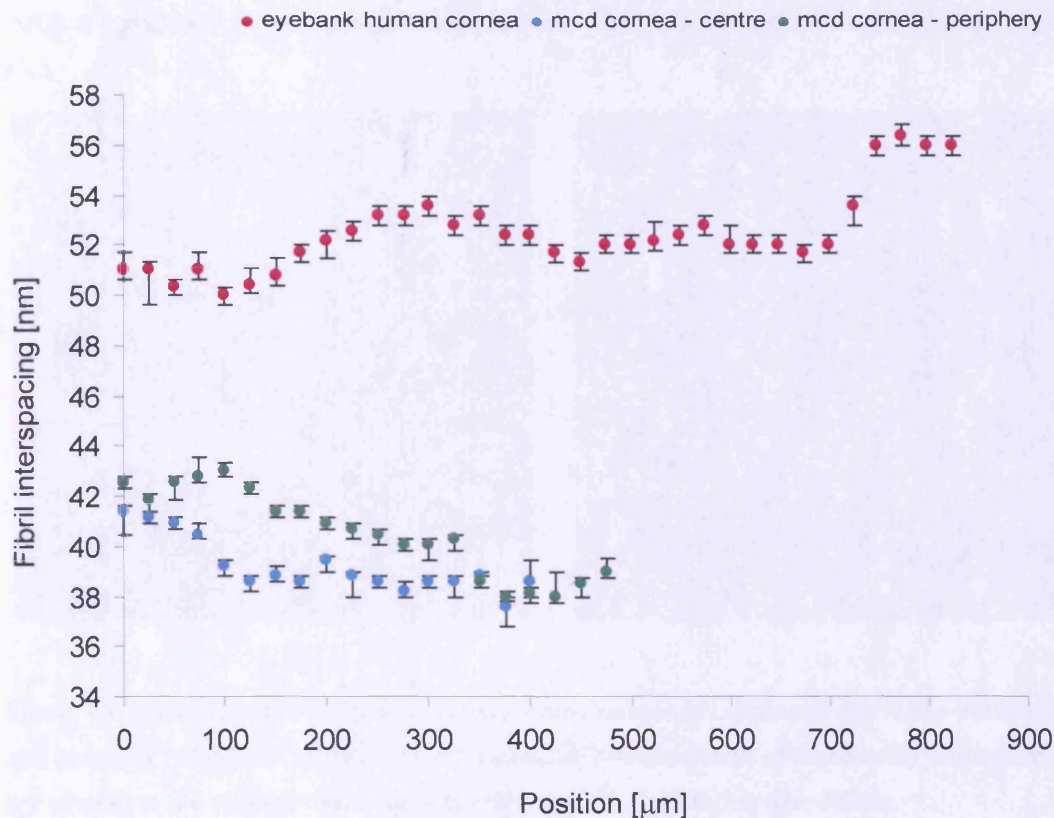


Figure 6.5 Centre-to-centre collagen fibril spacing measured across a human eye bank cornea and MCD cornea from epithelium to endothelium. Depth-profiled information from the centre (blue) and mid-peripheral (green) cornea shows a clear decrease in the collagen fibril spacing in the deeper stroma. Depth-profiled information from the eye bank cornea showed decrease in the collagen fibril spacing in the outer stroma (purple). Error bars show accuracy of the reading: the longer the bar the less accurate the reading.

This was the case in the mid-periphery too, although values are higher than in the corneal centre as tends to be the case in human cornea (Boote et al., 2003). At the centre of the MCD cornea, collagen spacing is 5.4% less in the posterior 100μm of stroma compared to the anterior 100μm ($p < 0.01$). At the mid-periphery, the posterior 100μm of the MCD stroma shows a collagen spacing which was 10.0% less than that in the anterior 100μm ($p < 0.01$). Thus, the profile of collagen fibril spacing as a function of stromal depth in a MCD cornea (lower fibril spacing in the deep stroma) is unlike that for a human cornea from the eye bank (lower fibril spacing in the anterior stroma).

Confirmation of more prevalent stromal alterations in the posterior cornea in MCD came from electron microscopic examination of the cornea. This disclosed that the collagen fibrils appear structurally normal in the anterior cornea, but that the deep stroma possesses focal pockets of abnormally large diameter collagen fibrils (Figure 6.6).

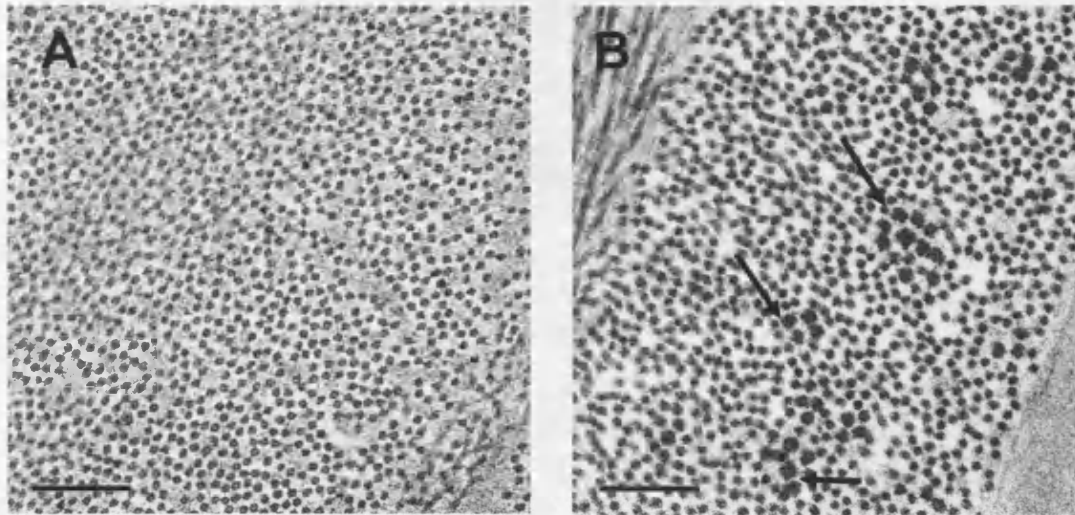


Figure 6.6 Transverse-section electron microscopic images of collagen fibrils in the anterior (A) and posterior (B) stroma in MCD. Focal pockets of collagen fibrils of abnormally large diameter are present in the posterior stroma. Magnification 32k. Calibration bar=300nm.

To exclude the possibility that unusual collagen fibrils are only an individual characteristic, electron microscopy was again carried out on the corneal biopsy of another Japanese patient suffering from MCD. I received the MCD corneal piece in January 2010. After fixation and staining in 2.5% buffered glutaraldehyde and 0.05% cuproline blue, tissue was embedded in Araldite CY212 epoxy resin. Ultrathin sections (90nm thick) were cut with a glass knife, collected on copper grids (300 square mesh, Agar scientific), and stained with 1% aqueous phosphotungstic acid and saturated aqueous uranyl acetate before examination by transmission electron microscopy (JEM-1010; JEOL, Tokyo, Japan) equipped with an 11-megapixel CCD camera (Orius SC1000 CCD camera; Gatan Ltd., UK, Cambridge, UK). Pockets with enlarged collagen fibrils were found in the posterior stroma (Figure 6.7).



Figure 6.7 Transverse-section electron microscopic images of collagen fibrils in the posterior stroma in a second patient with MCD. Visibly enlarged collagen fibrils are in evidence (arrows). Calibration bar =150nm.

Fibrils ($n=802$) in the eye bank cornea examined displayed a normal distribution of fibril diameters which ranged from 20.0nm-35.6nm (Figure 6.8B), and was centred on 26.4nm ($SD\pm 2.6$ nm), similar to published values of 26.0nm ($SD\pm 2.4$ nm) (Quantock et al., 1993a). Measurement of fibrils ($n=800$) in areas which contained the congregations of large-diameter fibrils gave a range of 20nm to 63nm, with a distribution which was not normal (one-sample Kolmogorov-Smirnov Test $p<0.001$) and skewed towards higher diameters (Figure 6.8).

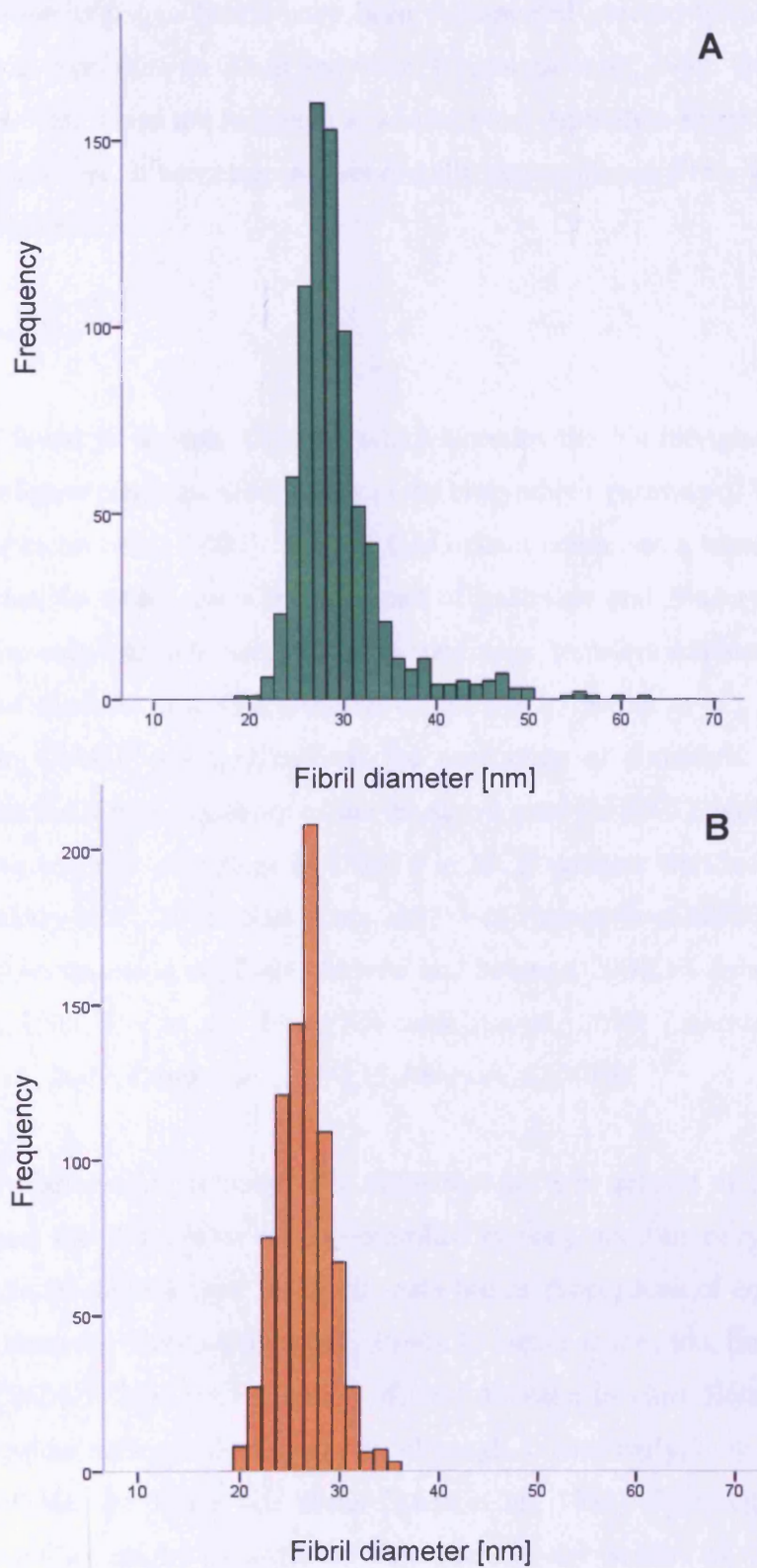


Figure 6.8 Histograms showing the range of collagen fibril diameters in regions of MCD stroma which contain abnormally large diameter fibrils (A) and in the normal human cornea (B).

Large-diameter collagen fibrils have been documented previously in MCD where they range in size between 20nm and 60nm (Quantock et al., 1993; Quantock et al., 1997). However, it was not indicated at what stromal depth they existed. In the MCD cornea studied here, it was clear that abnormally large collagen fibrils were restricted to the deep stroma.

6.1.3 Discussion

Mutations found in a gene, CHST6, which encodes the N-acetylglucosamine 6-O sulphotransferase cause an abnormality in the biosynthetic pathway of KS that occurs in MCD (Akama et al., 2000). The KS GAG chain comprises a repeating series of disaccharides, in which each is composed of galactose and *N*-acetylglucosamine. This inactive sulphotransferase, in normal conditions, transfers sulphate onto the 6-*O* positions of GlcNAc and Gal (Akama et al., 2001; Fukuta et al., 1997), thus a mutation in CHST6 adversely affects the production of a mature, sulphated KS GAG. Since the initial discovery of the causative gene for MCD, molecular genetic studies have reported mutations in CHST6 in MCD patients worldwide (Liu et al., 2000; El-Ashry et al., 2002; Niel et al., 2003; Iida-Hasegawa et al., 2003; Warren et al., 2003; Abbruzzese et al., 2004; Aldave and Sonmez, 2004; El-Ashry et al., 2005; Liu et al., 2005; Liu et al., 2006; Klintworth et al., 2006; Liskova et al., 2008; Sultana et al., 2009; Dang et al., 2009; El-Ashry et al., 2010).

KS PGs are believed to influence the ultrastructural arrangement of collagen fibrils in the cornea. Fibril diameter can be controlled by the proportion of type V collagen molecules in the hybrid type I/V fibril, with higher proportions of collagen type V leading to narrower fibrils (Birk et al., 1990). Evidence exists, too, for a role for KS PGs and CS/DS PGs in the regulation of fibril diameter in vitro. Both, lumican and decorin regulate collagen fibrillogenesis, although, interestingly, they do so with, as well as without, the GAG side chain (Rada et al., 1993). This suggests that the regulatory ability might lie with the core protein, and studies of the corneas of lumican-null mice show that collagen fibrils are sometimes abnormally large (Chakravarti et al., 2000). The presence of unusually large collagen fibrils in the corneas of MCD patients is indicative of a role for the GAG side chain of KS in the regulation of fibril diameter. Collagen intermolecular spacing appears to be

unchanged within fibrils in MCD corneas (Quantock et al., 1992), I can therefore probably assign the larger fibril diameters to the aggregation of more molecules into fibrils, and even perhaps the merging of existing fibrils, rather than the existence of more widely spaced collagen molecules within fibrils. Studies on the corneas of gene-targeted mice with a mutation of *Chst5*, a murine equivalent of *CHST6* in humans, have reported a thin stroma and closer-than-normal collagen fibril spacing, but not pockets of abnormally large collagen fibrils in the corneal stroma (Hayashida et al., 2006). I reanalysed tissue blocks from Hayashida's published study (2006) and after extensive searching did not find any evidence of large diameter collagen fibrils in the stroma. The mouse cornea, however, contains KS GAG chains that are less sulphated than those in human cornea (Young et al., 2005), so perhaps the lack of KS sulphotransferase activity in the *Chst5*-null mouse has less of an impact on collagen fibril diameter because of the lower need for sulphated KS GAG in the cornea of this species.

The low levels of sulphated KS GAG in the mouse cornea have been attributed to the thinness of the cornea, into which oxygen readily diffuses to all layers of the stroma (Scott and Bosworth, 1990). It was postulated by Scott and colleagues however, that proportionally higher levels of sulphated KS GAG found in the deeper layers of the thicker corneas of larger animals is a direct consequence of the restricted oxygen supply, and that KS GAG acts as a "stand-in" for CS/DS GAG in conditions of oxygen lack (Scott and Haigh, 1988b; Scott, 1991a; Scott, 1994). This concept has support in other tissues such as articular cartilage, in which a similarly increased prevalence of KS GAG is seen in thicker cartilages with a greater abundance in deeper layers (Stockwell and Scott, 1965; Stockwell, 1991). KS GAG is not found in sulphated form in the stroma in MCD I (Thonar et al., 1986; Klintworth et al., 1986; Yang et al., 1988; Edward et al., 1988; Klintworth et al., 1997). Rather, it is present in unsulphated or low-sulphated form (Lewis et al., 2000; Young et al., 2007a; Saito et al., 2008). The current finding that structural matrix changes (i.e. reduced collagen fibril spacing and large-diameter fibrils) are more prevalent in the deep stroma in MCD I might reflect the heightened importance of sulphated KS PGs in this part of the tissue in the human cornea.

6.2 Congenital stromal corneal dystrophy

Congenital stromal corneal dystrophy (CSCD; MIM 610048) is an autosomal dominant disorder causing cloudiness of the cornea, and like other dystrophies, affects only the cornea without any association with secondary or systemic disease (Klintworth, 2009). CSCD is a very rare disease found only in three families of Norway, French and Belgium origin (Odland, 1968; Berdrup et al., 2005, Turpin et al., 1939; Witschel et al., 1978; Van Ginderdeuren et al., 2002). The disorder is caused by frame shift mutation in the DCN gene (c. 967delT or c. 941delC) localised on chromosome 12q22 that leads to truncation of the C-terminal of decorin protein (Berdrup et al., 2005; Rødahl et al., 2006). On clinical examination small flaky or feathery opacities are visible throughout the stroma from birth after when the opacity progresses. There are only four congenital dystrophies and CSCD is the only one with affected stroma. The other three are: congenital hereditary endothelial dystrophy, polymorphous dystrophy and posterior amorphous corneal dystrophy and they manifest defects in endothelial functions. In CSCD, opacities are probably visible in the electron microscope as layers of amorphous material between the lamellae. I used an enzyme digestion to establish the character of accumulated material.

6.2.1 Case report and methods

Corneal button biopsies were obtained from the Norwegian patient who underwent a penetrating keratoplasty. Immediately after dissection, the corneal button was frozen and stored in liquid nitrogen until use. One CSCD corneal piece and one sclera piece were pre-fixed in 4% paraformaldehyde in Tris/sodium acetate buffer (pH 7.2) to prevent swelling during period of incubation with an enzyme. Then the tissue was incubated in 2.5 U/ml chondroitinase ABC from *Proteus vulgaris* for 4 hours at 37°C to remove the chondroitin GAG chains. CSCD corneal biopsies and normal human scleral biopsies, with and without enzyme treatment, were fixed overnight in 2.5% glutaraldehyde in 25mM sodium acetate buffer, pH 5.7, containing 0.1M magnesium chloride and 0.05% cuproinic blue to stain sulphated GAG chains. The tissue was then dehydrated and embedded in Araldite resin. Sections were cut on a glass knife

and picked upon copper grids were stained with 1% phosphotungstic acid and saturated uranyl acetate solution. Scleral biopsies as a control for the enzyme activity and CSCD corneal biopsies were examined by transmission electron microscopy (JEM-1010; JEOL, Tokyo, Japan) equipped with an 11-megapixel CCD camera (Orius SC1000 CCD camera; Gatan Ltd., UK, Cambridge, UK).

6.2.2 Results

Scleral extracellular matrix contains mainly aggrecan, biglycan and dermatan that carry chondroitin and/or dermatan sulphate chain (Young, 1985; Rada et al., 1997). This makes the sclera a good model for testing the activity of chondroitinase ABC, an enzyme which cleaves CS and DS chains. In this study nearly 100% of visible cuprolineic blue stained GAG chains were removed by chondroitinase ABC (Figure 6.9); this confirms high enzyme activity and justifies the use of this particular protocol for enzymatic removal of CS/DS.

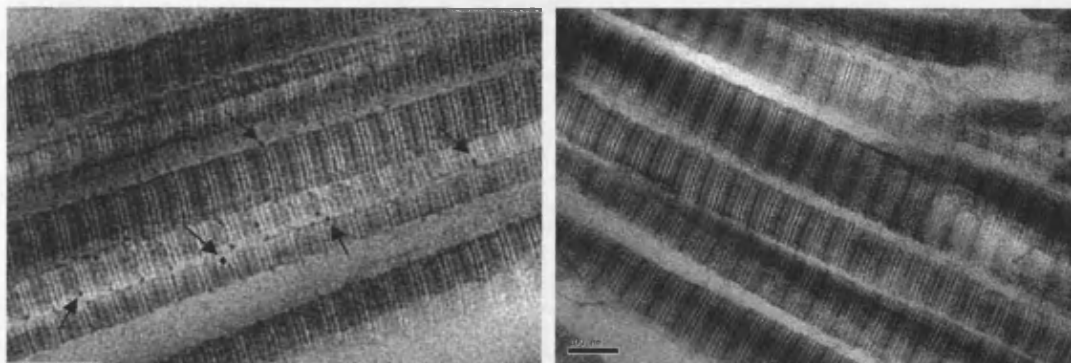


Figure 6.9 Transmission electron micrographs of the human sclera before (left) and after (right) chondroitinase ABC digestion. Arrows show cuprolineic blue stained GAG chains visible before enzyme digestion, and a lack of them after digestion which confirms chondroitinase ABC to be active as used in my digestion protocol. Magnification x20k, calibration bar =100nm and applies to both pictures.

CSCD matrix ultrastructure examined under the transmission electron microscope was severely disorganised, with break zones in-between and within lamellae. In the gap zones there are clearly visible filaments stained with cuprolineic blue, pointing to the presence of sulphated GAG chains (Figure 6.10).

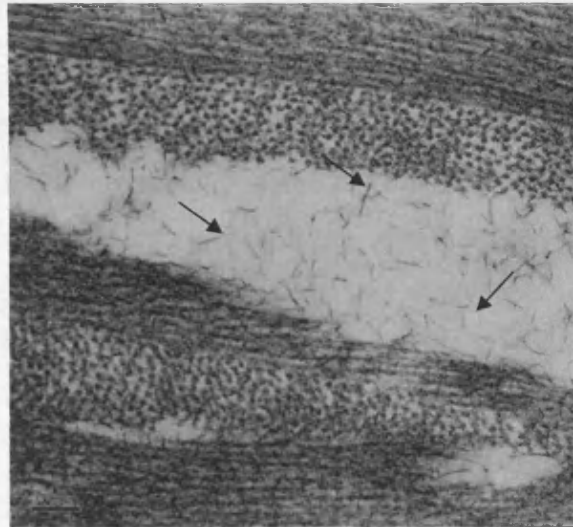


Figure 6.10 Transmission electron microscope of CSCD cornea. In the break in between the lamellae there are visible GAG filaments. Calibration bar=300nm.

After an enzymatic digestion with chondroitinase ABC, the small filaments in-between lamellae are no longer visible (Figure 6.11) suggesting that visible material in the gap area is a high sulphated CS/DS structure, presumably linked to abnormal decorin. Disruption in the structure of the stroma is clearly noticeable.

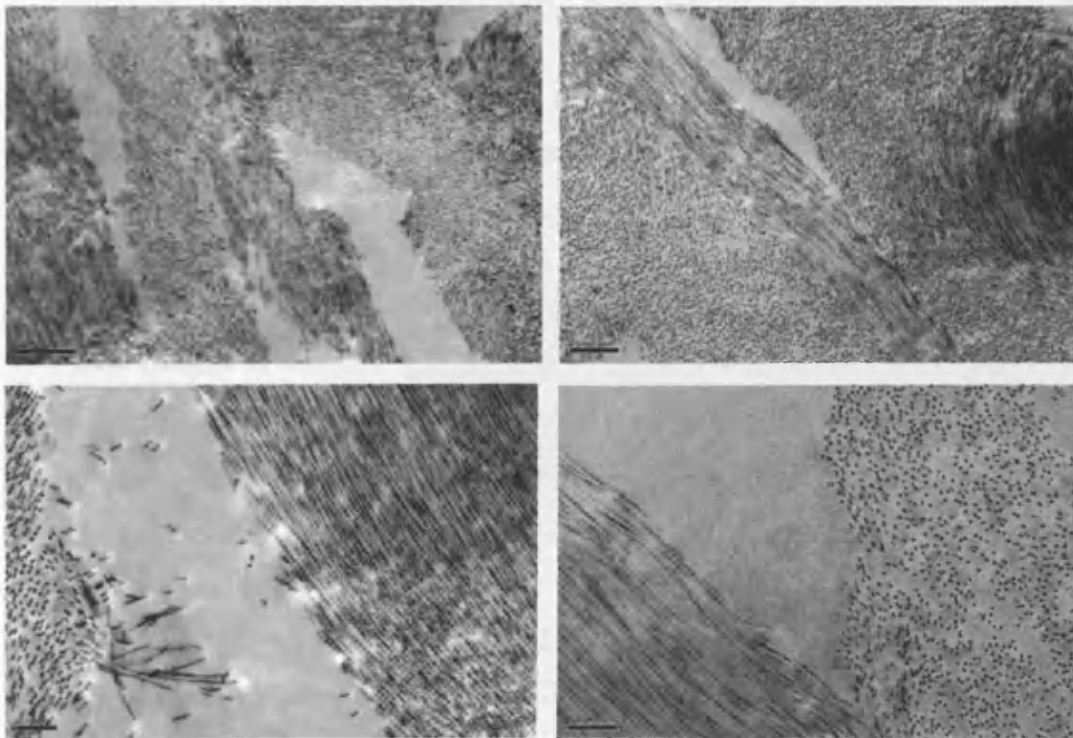


Figure 6.11 Electron microscope micrographs of the CSCD cornea treated with chondroitinase ABC to remove CS and DS GAG chains. Disrupted structure of the stroma is visible but there are no visible filaments in the gap area between lamellae.

6.2.3 Discussion

Decorin is a small extracellular matrix proteoglycan with a single CS/DS GAG chain attached to a serine residue near the N terminus (Chopra et al., 1985). A core protein of decorin contains 12 leucine-rich-repeats flanked by cysteine rich capping domains whose role is to stabilise the protein (McEwan et al., 2006). This area would not be affected by the C-terminal decorin truncation found in CSCD. However, at the C-terminal region there is a unique capping motif called the “ear repeat”. Extended leucine-rich region folds and disulfide bonds are established between Cys 284 and Cys 317 (Scott et al., 2004). Deletion of 33-C terminal amino acids in decorin core protein in CSCD is likely to disrupt this disulfide bond between cysteins which changes the protein structure. In my study I showed that filaments visible in electron micrographs in the break between lamellae are CS/DS GAG chains, which suggest the presence of decorin in this area. Truncated decorin caused by a mutation present in CSCD has an ear repeat motif which is disrupted, and this is most likely to be responsible for the susceptibility of this protein to aggregation. In the affected cornea, it is likely that decorin accumulates in the space between lamellae and even creates aggregates of protein which contributes to the disrupted structure and opacity of the cornea.

6.3 Sly syndrome – mucopolysaccharidosis VII

Mucopolysaccharidosis VII (MIM253220) was first described by Sly in 1973. It is an autosomal recessive disorder caused by the malfunction of β -glucuronidase enzyme leading to storage of heparan, dermatan and chondroitin sulphate in lysosomes (Sly et al., 1973). The disorder is manifested by slow and abnormal postnatal growth, mental problems and learning difficulties, deafness, upper airway obstruction, corneal clouding, and heart problems (Lorincz, 1978). Corneal opacification that resembles ground glass is a characteristic feature for MPS type I, IV and VI (Gosh and McCulloch, 1974; Haskins et al. 1980 and 1984; Chan et al., 1982; Klintworth, 1994; Spencer, 1996) but occurs in MPSVII only in the patient with more severe forms of the disease (Sugar, 1997; Bergwerk et al., 2000).

To date, various MPSs have been found or have been implemented into animal models of the disease. There are canine (Haskins et al., 1984; Ray et al., 1998; Silverstein Dombrowski, 2004), feline (Gitzelmann et al., 1994; Fyfe et al., 1999) and the most common murine models (Birkenmeier et al., 1989; Kyle et al., 1990; Sands and Birkenmeier, 1993; Gwynn et al., 1998; Sly et al., 2001, Vogler et al., 2001; Tomatsu et al., 2003) available for studies of MPS and for testing possible cures. Bone marrow transplant and enzyme replacement therapies are often used (Sands et al., 1993, 1994 and 1997a; Vogler et al., 1999 and 2005) and the most recent and most promising gene therapy is being also tested (Sands et al., 1997b; Kamata et al., 2001 and 2003; Grubb et al., 2010).

High magnification structural corneal studies have been carried on the tissue of Scheie's (MPS I-S), Hurler (MPS I-H), Morquio's (MPS IV) and Sanfilippo (MPS III) syndrome (Tabone et al., 1978; Zabel et al., 1989; Quantock et al., 1993a; Rummelt et al., 1992; Huang et al., 1996; Rawe et al., 1997; Alroy et al., 1999) but never Sly syndrome. Here, I undertook the first transmission electron microscope examination of high magnification corneal stroma of human MPS VII and present fibril diameter measurements from different depths of the stroma.

6.3.1 Case report and methods

A 12 years old boy suffering from MPS VII underwent penetrating keratoplasty in hospital in Prague to graft his opaque cornea. Tissue was then immediately fixed in 2% paraformaldehyde and 2.5% glutaraldehyde 1:1 mix, followed by post-fixation for 1 hour each in 1% aqueous osmium tetroxide and 0.5% aqueous uranyl acetate. Tissue was then dehydrated through an ascending series of ethanol, immersed in propylene oxide, and embedded in Araldite CY212 epoxy resin. Ultrathin sections were cut with a diamond knife on a Leica UC6 ultramicrotome, picked up on uncoated copper grids, contrasted with saturated uranyl acetate and Reynold's lead citrate, and imaged on transmission electron microscope (JEM-1010; JEOL, Tokyo, Japan) equipped with an 11-megapixel CCD camera (Orius SC1000 CCD camera; Gatan Ltd., UK, Cambridge, UK)

Fibril diameter was measured using ImageJ software. Pixel length was calibrated against the scale bar on the micrograph. Each fibril was individually measured across the shortest diameter of the fibril to eliminate the possibility of measuring an oblique fibril's surface.

6.3.2 Results

Parallel work within my group showed that the CB stained Sly syndrome cornea manifests the most significant change in morphology by the presence of keratocytes with enlarged vacuoles filled with PGs and abnormally large PG filaments between the collagen fibrils in the stroma (Figure 6.12).

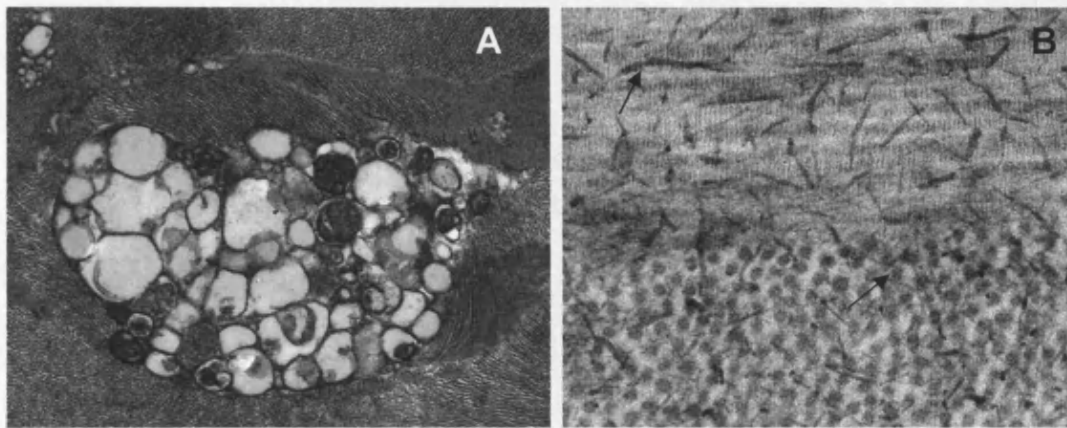


Figure 6.12 Transmission electron micrograph of a keratocyte in the Sly syndrome cornea with visibly enlarged vacuoles filled with PG (A) and enlarged filaments of PG amongst collagen fibrils (B). Image courtesy of Dr Rob Young.

I prepared osmium tetroxide stained conreal biopsy, to search for differences in size and arrangement of the collagen fibrils. Cross-sectional, high-magnification micrographs were inspected and collagen fibrils seemed to be regularly packed, although fibrils are not of a uniform diameter. Small and large collagen fibrils are visible across the corneal stroma, and abnormal diameter fibrils are localised mostly in the mid and posterior part of the stroma. In the normal cornea, fibril diameter has previously been measured in the range 19.7nm to 33.4nm (Quantock et al., 1993a). Measurements of the collagen fibrils in Sly syndrome cornea at different depths show a broader range of collagen fibrils in comparison with the normal cornea. Fibril diameter in the anterior stroma (n=681) is measured between 13.6nm and 32.2nm, in a mid stroma (n=1026) between 12.7nm and 41.6nm, and in the posterior stroma

(n=1136) between 16.6nm and 38.8nm (Figure 6.13). A one-sample Kolmogorov-Smirnov test shows that none of the fibril diameter distributions are normal at all stromal depths (anterior $p \leq 0.03$, mid $p \leq 0.01$, posterior $p \leq 0.01$). In the anterior stroma a spectrum of collagen fibril diameters is not as broad as in the mid and posterior stroma, but is still significantly different from the normal cornea.

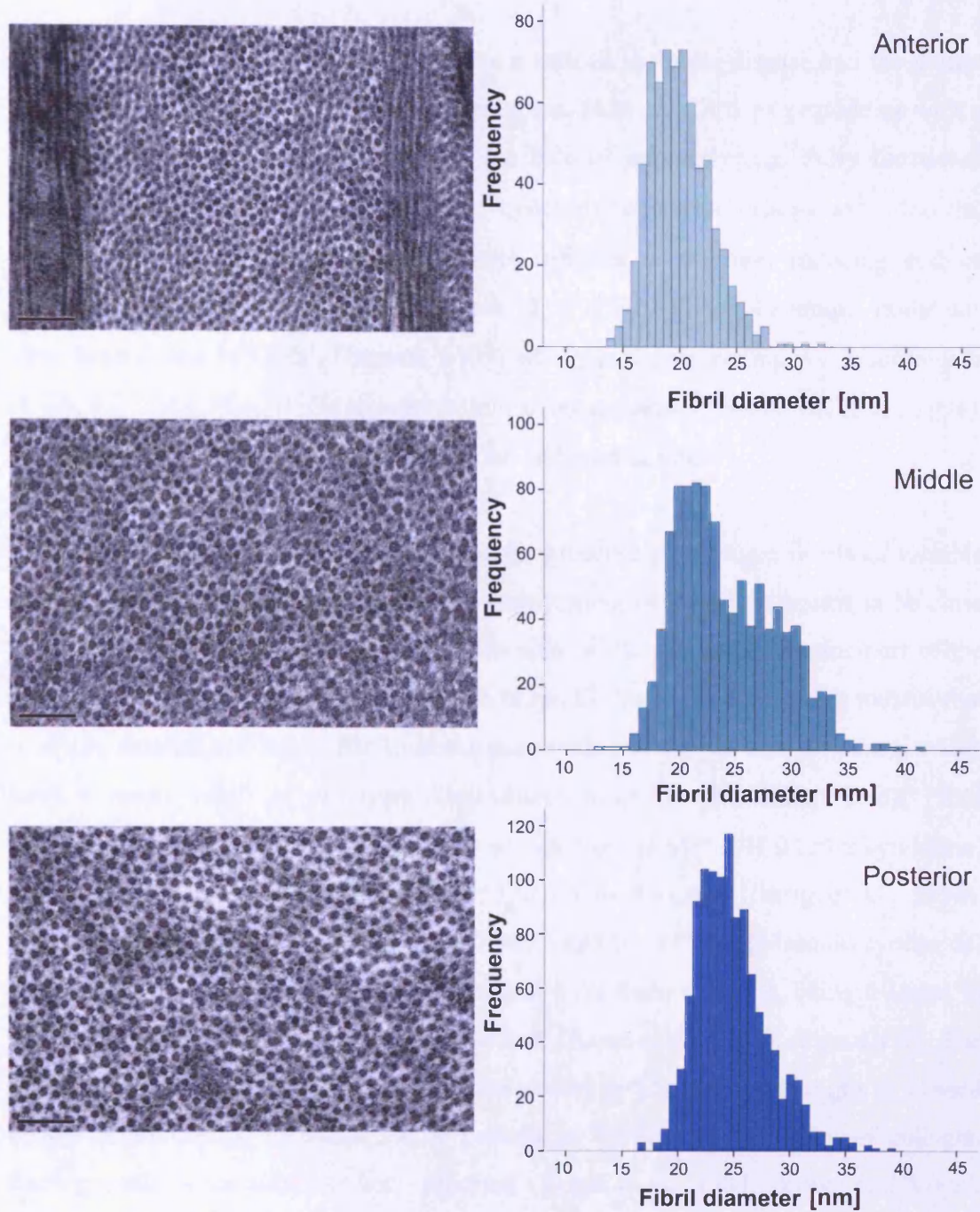


Figure 6.13 Transmission electron micrographs of the outer, mid and deep corneal stroma in Sly syndrome with different sized collagen fibrils visible. Histograms represent fibril diameter measurements ($n=2843$) in all three parts of the stroma. Calibration bars=100nm.

6.3.3 Discussion

Sly syndrome, as with the other MPSs, is a serious systemic disease and the ocular disease is only one of a multitude of symptoms. However, it does provide us with a good model to study transparency and the role of proteoglycans. Fully functional β -glucuronidase enzyme degrades glycosaminoglycans (heparan, decorin, chondroitin) by removing β -glucuronosyl residues at the non reducing end of oligosaccharides (Levy, 1953; Tomino et al., 1975). To date, 49 unique mutations have been found in GUS (Tomatsu 2009) which is a gene coding β -glucuronidase (GUS, EC 3.2.1.31, GUSB) located on chromosome arm 7 (Speleman et al., 1996). This mutation causes disease both in human and animal models.

This corneal ultrastructural study showed the presence of collagen fibrils of variable diameter throughout the stroma, but the arrangement of the fibrils seems to be close to normal. More severe changes are noticeable in the mid and posterior part of the cornea. Measured fibril diameter is in the range 12.7nm – 41.6nm which means, that there are smaller and larger fibrils in comparison to the normal human cornea, which have a mean value of collagen fibril diameter of 26.4nm (SD \pm 2.6nm). Fibril diameter's values are similar to the ones reported in the MPS I-H (Hurler syndrome) where the fibril diameters range from 12.5nm to 50.1nm (Huang et al., 1996). Interestingly, in MPS I-S (Scheie's syndrome) and in MPS IV (Morquio syndrome) only fibrils of a larger diameter than normal have been reported, being 19.9nm to 52.0nm (Quantock et al., 1993a) and 30-42nm (Rawe et al., 1997), respectively. The presence of collagen fibrils with reduced diameter in Sly syndrome might be caused by the accumulation of decorin core protein in the stroma. Inhibition of collagen fibril growth by decorin has been reported (Vogel et al., 1984; Brown and Vogel, 1989; Rada et al., 1993). Enlarged collagen fibril diameter resembles fibrils found in corneas of KS knock-out mice (Chakravarti et al., 2000). I can only speculate that an abundance of accumulated CS and DS may suppress the biosynthesis of KS. After all, suppression of sulphated KS in MCD I occurs in parallel with oversupphation of CS/DS (Meek et al., 1989; Nakazawa et al., 1984; Plass et al., 2001), possibly via some yet to be defined feedback mechanism. A lack of KS leads to the production of thick fibrils (Birk et al., 1981). Maybe there is a suppression mechanism in the

cornea. A compensation mechanism is already known when lack of decorin triggers an increased synthesis of biglycan (Zhang et al., 2009). That said, in MPS IV, where KS is accumulated, large diameter fibrils are reported (Rawe et al., 1997). Or, maybe malfunction in the PG's turnover means that even newly biosynthesised, fully functional proteoglycan cannot regulate fibrils sizes. More investigation is needed, however, to fully elucidate the molecular mechanisms and functional relationships.

The main cause of the corneal opacities in MPS remains GAG chain accumulation in the vacuoles of keratocytes (Mollard et al., 1996). Migration of the keratocytes with deposits of GAGs can even cause the reoccurrence of the cloudiness in the transplanted corneal graft (Schwartz et al., 1985; Aguirre et al., 1992). However, there are many structural changes of the cornea reported in various mucopolisaccharidosis, including increased mean collagen fibril diameter, altered fibril spacing and irregular packing (Alroy et al., 1999; Huang et al., 1996; Quantock et al., 1993a; Rawe et al., 1997; Rummelt et al., 1992; Tabone et al., 1978; Zabel et al., 1989). It has been also reported that MPS II, MPS IIIA and MPS IIIB corneas are not cloudy even when corneal epithelium, keratocytes and endothelial cells contain storage material (Topping et al., 1971; Del Monte et al., 1983; Lavery et al., 1983; Alroy et al., 1992). Another evidence for the importance of the ultrastructure is the fact that in adenovirus mediated gene therapy, which removes storage in lysosomes, lamellae disruption shows improvement only if treatment is in neonatal period, not in adulthood (Kamata et al., 2001).

Chapter Seven

7 Concluding remarks

The aim of this thesis has been to analyse the structure of the corneal stroma during development and in disease and to investigate how the change in the structure, mainly in relation to the changes in proteoglycans structure and localisation, affects the transparency of the tissue.

7.1 Chapter Three

The aim was to test the hypothesis that a developing cornea transmits light to varying degrees and that this is due to changes in the structure.

I quantified the level of transparency in late stages of chick development (E12-E18) by measuring the spectrum of light transmitted through the centre of the cornea. In the first light transmission study, Coulombre and Coulombre reported 39% transmission of incident white light at E12 increasing to 95% at E20 (Coulombre and Coulombre, 1958a). My data concur with these measurements using a 700nm wavelength, where transmission increases from 35% at E12 to 81% at E18. At shorter wavelengths the light transmission is lower. For example, at 500nm wavelength, transmission reaches only 73% at E18 which is caused by higher scattering in the blue light. Significant increase in the light transmission irrespective of the wavelength occurs after E14.

The wavelength-transmission dependency at E18 exhibits an inverse-square relationship that matches the model of a swollen human cornea (Farrell et al., 1973). Cytochrom c is responsible for the loss of transmission at some wavelengths. However, the biggest impact on transparency arises from presence of breaks in the integrity of the stroma (Benedek, 1971), from changes in fibril interspacing and arrangement and from imbalance of refractive indices between collagen fibrils and extrafibrillar substance (Hart and Farrell, 1969; Freund et al., 1986; Meek et al., 2003b). Variation in light transmission is considered to be the result of structural

changes and is presented in the panel of electron micrographs in Figure 3.7. To trace in detail those changes, an in-depth study of collagen fibril arrangement, as well as content and location of proteoglycans during chick corneal development, were undertaken and are described in Chapters Four and Five.

An important limitation of the technique used to quantify transmission is that the measurements were taken from dissected tissue. The lack of intraocular pressure could have caused structural changes in the lamellae organisation which could have affected the transmission. For that reason, a new method of measurement should be developed. Another factor that could have affected the final result is that the refractive index ratio between the collagen fibrils and the extracellular matrix for each of the developmental stages is not known.

7.2 Chapter 4

The aim was to test the hypothesis that collagen spacing changes with depth and laterally during corneal development.

I presented spatial and temporal alterations in the collagen fibril arrangement in the chick stroma during the second stage of compaction (E15-E18) using small angle X-ray diffraction. Assembly of the collagen fibrils, thinning of the cornea and changes in collagen fibril spacing within the lamellae have been extensively studied in the past (Hay and Revel, 1969; Conrad, 1970; Trelstad and Coulombre, 1971; Quantock et al., 1998; Meek and Quantock, 2001). However, I am the first to present the comprehensive study of structural changes during chick development that includes the collagen interfibrillar spacing across the cornea from centre to periphery, taken across the whole depth of the stroma.

The study showed that the collagen fibril spacing, while taken as an average across the whole depth of the stroma, decreases across the whole extent of the cornea between E14 and E18. However, the difference between the central and peripheral region in each stage is not constant. In the centre of the cornea, in each developmental day, collagen fibril spacing is smaller than in the periphery. This difference decreases with development and is 17% at E14 and only 7% at E18. The

possible cause of this change is the development of corneal curvature which causes a decrease of collagen fibril spacing in the limbal area. This is exhibited as a smaller difference between the central and peripheral collagen interspacing.

The result of the in-depth micro scan showed that at E15 the corneal stroma is slightly more compact in the near endothelial part. E16 brings further collagen interspacing reduction in the posterior stroma. At E17 compaction slows in the posterior stroma but fibril spacing close to the epithelium starts rapidly decreasing. This variation in collagen fibril spacing with depth is thought to be a result of a non-uniform distribution of proteoglycans in the stromal matrix. The two repeats of the in-depth scan confirmed the heterogeneous nature of collagen spacing and changes occurring within the depth during development. However, to an extent, the results are ambiguous. A trend can be seen in the differences in compaction; however, more repeats are needed before a final conclusion can be drawn.

7.3 Chapter Five

The aim was to test the hypothesis that localisation of proteoglycans (CS/DS) changes within the depth of the corneal stroma during development and that the appearance of the main two types of PGs differs.

It is known that KS PGs are mainly accumulated in the anterior part of the cornea (especially highly sulphated KS) and that the distribution becomes more uniformly spread across the stroma by day 18 (Young et al., 2007b; Gealy et al., 2007). While KS is spreading from the anterior to the posterior manner, CS/DS is first accumulated in the posterior part near day 12-14 of development and then spreads towards the epithelium. This was described in Chapter Five during the immunofluorescence microscopy experiment. These investigations of two different kinds of PGs localised at the opposite sides of the corneal stroma, and then spreading uniformly across the corneal depth, show that it happens simultaneously with change in the interfibrillar spacing of the stroma.

The transmission electron microscopy experiment described in Chapter Five concentrated mainly on the temporal changes in the type of PGs present in the developing stroma and on the structural changes between those two groups. From micrographs, there are usually two types of filament visible. In one group, the PGs are small and associated with the collagen fibril surface. In the other group, larger (approximately 65-100nm) filaments extend along collagen fibrils or out into the matrix, connecting with adjacent fibrils.

In this experiment, quarters of the cornea (E12-E18) were incubated with chondroitinase ABC. This procedure removed all PGs with large filaments in all stages of development, indicating that they are CS/DS PGs. The number of small filaments of KS on the surface of collagen fibrils which remain after enzymatic digestion increased between E12 and E18. This is probably the result of PGs accumulation (Anseth, 1961) and increase in KS chains sulphation during development (Nakazawa et al., 1995; Liles et al., 2010). Sulphation of the CS/DS also changes with development (Zhang et al., 2005) indicating that sulphation may play a role in the fine tuning of the stromal structure and therefore the transparency of the cornea. Unfortunately, the nature of the antibodies used for immunohistochemistry does not distinguish between different sulphation patterns. To fully understand the changes in CS/DS distribution, a different type of antibodies has to be used and the method of quantification of the PG in the various layers of cornea has to be studied.

7.4 Chapter 6

The aim was to test the hypothesis that changes in the proteoglycan structure is associated with structural abnormalities in human diseases.

A useful model of what happens in the absence of sulphation in KS PGs is macular corneal dystrophy (described in Chapter Six). A mutation in a gene, CHST6, results in the absence of sulfotransferase responsible for the production of mature sulphated KS-GAGs (Akama et al., 2000). This is the only difference between the healthy individual and the one suffering from MCD. It leads to structural changes in the

corneal stroma, mainly thinning (Ehlers and Bramsen, 1978), a decrease in collagen fibril spacing (Meek et al., 1989; Quantock et al., 1990), and finally a loss of transparency. I showed the presence of unusually large collagen fibrils in the posterior stroma of corneas of two MCD patients. This can indicate a role for the GAG side chain of KS in the regulation of fibril. Additionally, an in-depth small angle X-ray diffraction experiment showed non-uniform collagen fibril spacing across MCD I cornea. The decrease in a fibril interspacing was more prevalent in the deep stroma which, taking into consideration the presence of large fibrils, suggests the heightened importance of sulphated KS in this part of human cornea.

Another human dystrophy with a PG defect that manifests in loss of a transparency, presented in Chapter Six, is congenital stromal corneal dystrophy. In this disorder, a C-terminal of a core protein of decorin is truncated which changes a protein structure and most likely causes susceptibility of decorin protein to aggregation. In this study, I showed, by exposing a tissue's biopsy to an activity of chondroitinase ABC, that filaments which are visible in electron micrographs in the break between lamellae are the CS/DS GAG chains. After the treatment, all filaments disappeared suggesting the presence of decorin in this area, which most likely contributes to the disrupted structure and opacification of the cornea.

A final example of the cornea, in which structural changes arise from malfunction in PGs turnover, is Sly syndrome. This systemic disease fails to synthesise an enzyme responsible for catalysis of heparan, decorin and chondroitin GAG chains. I showed that collagen fibrils of variable diameter are present throughout the stroma. Fibril diameter ranged between 12.7nm-41.6nm with significantly smaller than normal fibrils present in the anterior stroma. However, most abnormal fibrils occurred in the mid and posterior part of the stroma. I can only speculate that accumulation of CS/DS may inhibit collagen fibril diameter. Sly syndrome is a very rare disease and the present study introduces the abnormal structure of the fibrils in the stroma and is only the foundation to understand the role of PGs.

7.5 Wider implications and further work

The research presented in this thesis helps to further the understanding of corneal development and structure. The knowledge of the function of proteoglycans in determining the structure of the cornea is pivotal for an attempt to create a fully functional artificial cornea. Such advances give hope to many patients awaiting corneal transplant to improve their vision.

More investigation is needed to fully understand the role of PGs, and CS/DS in particular, in the cornea. More research is needed to develop antibodies that recognise different epitops and sulphation motifs in the chick tissue. To quantify the amount of PG in different part of the stroma, three dimensional models of collagen-PG interactions need to be build. Only then, there is a possibility to distinguish with certainty between small KS filaments and larger CS/DS filaments. A method has to be developed to separate the particular layers of the cornea in order that quantification methods, such as ELISA, could be applied .In addition, to improve the transparency measurements, it would be useful to find a way to separate and then to estimate the impact factor of each of the contributors for transmission loss.

Appendix

This appendix includes publications that are the result of the work presented in this thesis.

1. *Liles M, Palka BP, Harris A, Kerr B, Hughes C, Young RD, Meek KM, Caterson B, Quantock AJ.*

“Differential relative sulfation of keratan sulfate glycosaminoglycan in the chick cornea during embryonic development.”

Invest Ophthalmol Vis Sci., 2010, 51: 1365-1372

2. *Palka BP, Sotozono C, Tanioka H, Akama TO, Yagi N, Boote C, Young RD, Meek KM, Kinoshita S, Quantock AJ.*

“Structural collagen alterations in macular corneal dystrophy occur mainly in the posterior stroma.”

Curr Eye Res., 2010, 35: 580-586

3. *Bredrup C, Stang E, Bruland O, Palka BP, Young RD, Haavik J, Knappskog PM, Rodahl E.*

“Decorin accumulation contributes to the stromal opacities found in congenital stromal corneal dystrophy.”

Invest Ophthalmol Vis Sci., 2010, 51: 5578-82

Differential Relative Sulfation of Keratan Sulfate Glycosaminoglycan in the Chick Cornea during Embryonic Development

Melody Liles,¹ Barbara P. Palka,¹ Anthony Harris,² Briedgeen Kerr,² Clare Hughes,² Robert D. Young,¹ Keith M. Meek,¹ Bruce Caterson,² and Andrew J. Quantock¹

PURPOSE. To investigate structural remodeling of the developing corneal stroma concomitant with changing sulfation patterns of keratan sulfate (KS) glycosaminoglycan (GAG) epitopes during embryogenesis and the onset of corneal transparency.

METHODS. Developing chick corneas were obtained from embryonic day (E)12 to E18 of incubation. Extracellular matrix composition and collagen fibril spacing were evaluated by synchrotron x-ray diffraction, hydroxyproline assay, ELISA (with antibodies against lesser and more highly sulfated KS), and transmission electron microscopy with specific proteoglycan staining.

RESULTS. A significant relative increase in highly sulfated KS epitope labeling occurred with respect to hydroxyproline content in the final week of chick development, as mean collagen interfibrillar distance decreased. Small KS PG filaments increased in frequency with development and were predominantly fibril associated.

CONCLUSIONS. The accumulation of highly sulfated KS during the E12 to E18 timeframe could serve to fine tune local matrix hydration and collagen fibril spacing during corneal growth, as gross dehydration and compaction of the stroma progress through the action of the nascent endothelial pump. (*Invest Ophthalmol Vis Sci.* 2010;51:1365–1372) DOI:10.1167/iops.09-4004

The cornea is a connective tissue with remarkable transparency that forms the primary refractive surface of the eye; yet, how this property arises in development remains little understood. The most widely studied model of corneal development is that of the embryonic chicken.^{1,2} In this tissue, uniformly thin collagen fibrils are laid down by stromal fibroblasts in a secondary stroma and consolidate as a series of orthogonal fibril bundles that later form into lamellae.³ At

embryonic day (E)14, the chick cornea transmits only approximately 40% of white light, but then begins to increase in transparency so that, at E19, transmission is more than 95%, similar to the adult condition.⁴ The transparency increase after E14 is accompanied by significant dehydration of the cornea, flattening of keratocytes, and compaction of stromal collagen fibrils into a spatially ordered array.^{5,6} This restructuring of the stroma is key for the acquisition of corneal transparency.^{7,8}

Small leucine-rich proteoglycans (PGs) interact with collagen fibrils in the corneal stroma and are thought to help control fibril size and spatial organization.⁹ PGs are composed of a core protein covalently bound to sulfated glycosaminoglycan (GAG) side chains. The major GAG in the cornea is keratan sulfate (KS), and three types of PG bear these side chains: lumican,¹⁰ keratocan,¹¹ and mimecan (or osteoglycin).¹² By E18, in the chick stroma KS PGs bear two to three GAG chains of approximately 15 kDa each,¹³ and the PGs lumican and keratocan have three of five potential linkage sites variably substituted with KS GAGs.¹⁴ Collagen-PG interactions are thought to occur via the PG core protein, with sulfated GAG chains extending into the interfibrillar space, where they confer stromal water-binding and sorptive tendencies that help define the hydrophilicity and swelling properties, and thus the ultrastructure, of the stromal matrix.¹⁵

Corneal PGs, especially those carrying KS chains, fulfill an important role in the establishment of a properly formed stroma during corneal embryogenesis.¹⁶ The importance of these molecules is illustrated by the fact that the corruption of sulfate motifs on KS is associated with structural matrix alterations in the corneas of humans with the inherited disease macular corneal dystrophy^{17,18} and in the corneas of mice with gene-targeted deletions in lumican^{19,20} or *Chst5*, a KS sulfotransferase enzyme.²¹ Some investigators have reported the accumulation of KS GAGs and KS PGs during embryonic development.^{22–25} Molecular studies have shown that levels of mRNA for keratocan, first expressed at E6,²⁶ exhibit a steady decline from E9 to E18, whereas, over the same time period, lumican mRNA levels remain several-fold higher.²⁷ Moreover, an approximate threefold increase in lumican core protein occurs between E7 and E9,²⁸ with a two- to threefold increase in mRNA for β -1,4-galactosyltransferase, an enzyme involved in sulfated KS synthesis, reported between E8 and E13.²⁹ Biochemical analyses have also shown that KS is synthesized by the chick cornea between E5 and E7, but that it only becomes highly sulfated by E14,³⁰ with another study indicating a switch in the production of unsulfated to sulfated KS between E12 and E15.²⁸

The current investigation was designed to test the hypothesis that sulfation of KS provides an environment of hydration conducive to the deposition of collagen fibrils and the establishment of a highly ordered stromal matrix in the developing chick. To this end, experiments were conducted to quantify

From the ¹Structural Biophysics Group, School of Optometry and Vision Sciences, and the ²Connective Tissue Biology Laboratories, School of Biosciences, Cardiff University, Cardiff, Wales, United Kingdom.

Supported by Grant EP/F034970/1 from the Engineering and Physical Sciences Research Council (AJQ, RDY, ML, KMM), Grant BBS/B/10994 from the Biotechnology and Biological Sciences Research Council (AJQ, BC), Grant G0001033 (KMM, AJQ) and Grant MRC G0800248 (AH, BK, CH, BC) from the Medical Research Council, UK, and Grant ARC 17540 from the Arthritis Research Campaign (AH, BK, CH, BC).

Submitted for publication May 19, 2009; revised July 10 and August 7, 2009; accepted August 7, 2009.

Disclosure: M. Liles, None; B.P. Palka, None; A. Harris, None; B. Kerr, None; C. Hughes, None; R.D. Young, None; K.M. Meek, None; B. Caterson, None; A.J. Quantock, None

Corresponding author: Andrew J. Quantock, Structural Biophysics Group, School of Optometry and Vision Sciences, Cardiff University, Maindy Road, Cardiff CF24 4LU, UK; quantockaj@cf.ac.uk.

collagen biosynthesis, KS sulfation status, collagen fibril spacing, and collagen-KS PG associations during the latter stages of chick corneal morphogenesis.

METHODS

Specimens

For x-ray diffraction and biochemical studies, a series of 69 embryonic chick corneas was obtained that comprised daily incremental stages from E12 to E18. Corneas were excised by an incision around the limbus in eyes of embryonic chicks obtained from Hamburger-Hamilton (HH)-staged, fertilized eggs collected from a commercial hatchery (Hy-Line UK, Warwickshire, UK) approximately 2 hours earlier, where E12 = HH38, E13 = HH39, E14 = HH40, E15 = HH41, E16 = HH42, E17 = HH43 and E18 = HH44. Immediately on excision, the corneas were sandwiched between layers of clingfilm to minimize dehydration and were placed on dry ice. Frozen corneas were transferred to -80°C storage until the synchrotron x-ray diffraction experiments could be conducted. For electron microscopy, a smaller group of fertilized eggs (Henry Stewart & Co. Ltd., Louth, Lincolnshire, UK) was incubated at 37°C until staging and excision. All work was conducted in accordance with the ARVO Statement for the Use of Animals in Ophthalmic and Vision Research, as well as with local ethics guidelines.

Synchrotron X-Ray Diffraction

Individual corneas ($n = 69$), still secured in cling film, were positioned in a sealed specimen holder between sheets of x-ray-transparent mylar where they were allowed to thaw. In turn, each cornea ($n = 8-11$ daily from E12 to E18) was then placed into the path of a focused (1×1 mm) monochromatic ($\lambda = 0.154$ nm) x-ray beam on beamline 2.1 of the Synchrotron Radiation Source, Daresbury Laboratory (Cheshire, UK). All corneas were exposed for 2 minutes each, and the resulting fiber diffraction patterns were recorded on a multiwire, gas proportional area detector plate positioned 8.25 m behind the cornea. Immediately after x-ray exposure, the corneas were refrozen and transported to the home laboratories for biochemical and immunochemical analyses (described in the following sections). Diffraction patterns (512×512 pixels) were analyzed with purpose-written software (Unix-based; Sun Microsystems, Mountain View, CA) and graphics and statistics packages (Unix; Optimas, Bothell, WA; Statistica; Statsoft, Tulsa, OK, Excel; Microsoft, Redmond, WA), as described previously.³¹ The position of the first-order equatorial (i.e., interfibrillar) reflection, calibrated to the 67-nm axial D-periodic repeat of collagen in wet rat tail tendon, was used to provide a measure of the mean center-to-center collagen fibril Bragg spacing as an average throughout the whole thickness of the central cornea. Statistical significance was ascertained by using statistical tests for large data groups: one-way ANOVA with post-hoc Tukey HSD.

After x-ray analysis, the corneas were refrozen for transportation to the home laboratory and digested for 17 hours at 60°C with 1 mg/mL papain (Sigma-Aldrich, Poole, UK) in 0.05 M sodium acetate buffer (pH 5.6), containing 0.025 M EDTA and 5 mM cysteine HCl. The enzyme was inactivated at 100°C , and the digests stored at -20°C until further analysis.

Hydroxyproline Assay

Papain digests from individual corneas were hydrolyzed by using equal volumes of 11.7 N concentration HCl to supernatant at 110°C overnight. Specimens were then lyophilized. Dried hydrolyzates were reconstituted in their starting volume of distilled water and centrifuged to remove particulate material. Hydroxyproline residues were assayed in triplicate as previously described,³² against known standards and read at 540 nm after 10 to 20 minutes incubation at 70°C . Statistical significance was ascertained by using statistical tests for large data groups: one-way ANOVA with post-hoc Tukey HSD.

KS Quantification by Competitive ELISA

Optimized, competitive ELISAs were developed to quantify pentasulfated hexasaccharides and tetrasulfated hexasaccharides as the smallest linear structures in KS chains, as recognized by the monoclonal antibodies 5D4 and 1B4, respectively.³³⁻³⁵ Ninety-six-well EIA microtiter plates (MP Biomedicals, Cambridge, UK) were coated by passive adsorption with a 250 ng/mL chondroitinase ABC-digested bovine articular cartilage aggrecan (BAC ABC core) antigen in a 20-mM sodium carbonate coating buffer (pH 9.6), for 14 hours at 37°C . Native aggrecan core protein is substituted with both chondroitin sulfate (CS) and KS chains, and CS was selectively removed by chondroitinase digestion to leave a KS-linked coating protein. The plates were washed with Tris saline azide (TSA) and the unreacted sites blocked with the addition of 1% (wt/vol) bovine serum albumin (BSA) in TSA. All incubations were performed for 1 hour at 37°C .

Papain digests from single corneas were serially diluted and allowed to bind with an equal volume of 5D4 (1:8000 dilution in 1% BSA/TSA) and incubated to compete against the BAC ABC core. A standard curve was generated from serial dilutions of BAC ABC core/5D4. The plates were then washed with TSA before incubation with alkaline phosphatase-conjugated goat anti-mouse antibody (1:5000 dilution; Promega, Madison, WI). The plates were again washed before alkaline phosphatase substrate (p-nitrophenyl phosphate, 1 mg/mL) was applied in DEA buffer (0.126 mM MgCl_2 , 1 M diethanolamine, pH corrected to 9.8). Color development was quantified on a plate reader (Multiskan MS; Labsystems, Helsinki, Finland) at 405 nm, to determine the inhibition of binding.

The same stock corneal extracts were then assayed for lesser sulfated KS by using the 1-B-4 monoclonal antibody. Optimization of conditions established that microtiter plates were coated with 125 ng/mL BAC ABC core and ELISAs performed as described above, with a 1:4000 1-B-4 dilution. Statistical significance was ascertained with statistical tests for large data groups: one-way ANOVA with post-hoc Tukey HSD.

Electron Microscopy

On excision, corneas from E12 to E18 chicks ($n = 21$) were prepared for electron microscopy, as described previously.^{21,36} A series of E12 to E18 corneas was fixed in 2.5% glutaraldehyde in 25 mM sodium acetate buffer with 0.05% cuproline blue (0.1 M MgCl_2 ; pH 5.7), to stain the sulfated PGs. Another series was fixed for 10 minutes in 4% paraformaldehyde (pH 7.2). These corneas were then washed twice in chondroitinase buffer (50 mM Tris, [pH 8], 60 mM sodium acetate, and 0.02% BSA) and quartered. Corneal pieces were incubated for 4 hours at 37°C in chondroitinase buffer containing 2.5 U/mL chondroitinase ABC (from *Proteus vulgaris*; Sigma-Aldrich) to remove the chondroitin- and dermatan-sulfate GAG chains from the tissue. Commercially prepared protease inhibitor cocktail for general use (Sigma-Aldrich) was also added to 1% total volume to inhibit endogenous PG-degradative activity. The control corneas were similarly processed in buffer minus enzyme. The samples were washed in chondroitinase buffer (minus enzyme) before fixation and staining overnight, as before. All corneas were then contrast enhanced with sodium tungstate and dehydrated and embedded in Araldite, according to standard protocols.³⁶ Ultrathin sections (~ 90 -nm thick) were cut on glass knives, collected on copper grids, and stained with 1% aqueous phosphotungstic acid and saturated aqueous uranyl acetate before examination by transmission electron microscopy (JEM-1010; JEOL, Tokyo, Japan) equipped with an 11-megapixel CCD camera (Orian SC1000 CCD camera; Gatan Ltd., UK, Cambridge, UK).

RESULTS

Mesenchymally derived presumptive keratocytes that populate the developing chick cornea are responsible for establishing the secondary stroma by synthesizing and depositing hybrid collagen type I/V fibrils.^{1,2} Quantification of collagen as hy-

TABLE 1. Average Amount of Hydroxyproline and Average Collagen Interfibrillar Spacing in Embryonic Chick Corneas

	E12 (n = 8)	E13 (n = 10)	E14 (n = 11)	E15 (n = 10)	E16 (n = 11)	E17 (n = 10)	E18 (n = 9)
Hydroxyproline, $\mu\text{g/mL}$	4.38 ± 0.18	8.06 ± 1.07	7.43 ± 0.48	17.48 ± 1.46	17.23 ± 0.74	34.52 ± 4.11	34.69 ± 1.64
Collagen fibril Bragg spacing, nm	60.8 ± 0.60	63.1 ± 1.01	63.9 ± 0.99	61.9 ± 1.22	59.8 ± 1.53	57.0 ± 0.87	53.7 ± 0.94

Embryonic days E12 to E18 are equivalent to Hamburger-Hamilton stages 38 to 44 of development. Hydroxyproline measurements are also representative of total collagen content per cornea. Data are expressed as the mean \pm SE.

droxyproline (Table 1) indicated two significant increases in hydroxyproline content, found between E14 and E15 ($P < 0.005$) and E16 and E17 ($P = 0.001$). At E16 Coleman et al.³⁷ measured $20.7 \mu\text{g}$ hydroxyproline per cornea and Conrad,³⁸ $19.5 \mu\text{g}$. Our value of $17.23 \mu\text{g/cornea}$ at this developmental stage is consistent with these published values.

X-ray diffraction patterns generated by corneas at E12 gave rise to collagen interfibrillar reflections that were consistent with a rather loose, hydrated network of formative lamellae that constitutes the tissue at this time. With development, interfibrillar reflections became more intense, presumably as a consequence of growth and the added deposition of collagen as fibrils, consistent with the results of the hydroxyproline analysis shown in Table 1. Analysis of all 69 x-ray diffraction patterns showed that the average center-to-center collagen fibril spacing from E14 to E18 decreased as the cornea thinned and became more transparent (Table 1).

These collagen spacing data were highly representative of the corneal stroma as a whole, with all fibrils in the path of the x-ray beam (which measured approximately $1 \times 1 \text{ mm}$) passing through the whole thickness of the cornea contributing to the x-ray pattern and thus the calculated values. X-ray analysis, however, could not identify how the stromal matrix was changing at the suprafibrillar level. Electron micrographs confirmed the overall nature of the stromal compaction and indicated, not a homogeneous coming together of widely and uniformly spaced fibrils with time, but rather a progressive coalescence of bundles of collagen fibrils in which the fibrils were already fairly well organized and packed laterally (Fig. 1). Based on the fundamental principles of x-ray fiber diffraction, the collagen-free spaces between fibril bundles, which were quite prevalent before E15, did not contribute to collagen interfibrillar reflection. Thus, the values displayed in Table 1 derive from collagen fibrils that are regularly spaced, whether they exist in bundles, as in the earlier stages that we investigated, or in stacked lamellae, as seen later in development. Our observations (Fig. 1), together with those of other investigators^{4,6} showed that stromal compaction during development entailed collagen fibril bundles coming together to form lamellae, whereas x-ray data indicated that fibrils within the bundles and lamellae are moving closer together from E14 onward.

As synchrotron x-ray diffraction is a noninvasive technique, the 69 corneas from which ultrastructural collagen fibril data were acquired (Table 1) were available for subsequent immunochemical quantification of KS epitope. Data were normalized to hydroxyproline content to reflect changes in lesser-

sulfated (1B4-immunoreactive) and highly sulfated (5D4-immunoreactive) KS epitope, relative to matrix deposition (Table 2). It is important to remember that these values represent relative epitope labeling between samples and that the nature of the antibodies used potentially allows multiple binding sites within the same GAG chain. KS values are relative to BAC-ABC core protein labeling equivalents.

Levels of highly sulfated KS as a proportion of hydroxyproline throughout the E12-to-E18 interval were consistently higher than corresponding amounts of the low-sulfated epitope. The amount of lesser-sulfated KS fluctuated between E12 and E18, but did not change appreciably, whereas levels of highly sulfated KS increased markedly. As can be seen in Table 2, highly sulfated KS levels remained fairly steady between E13 and E15, after which a sharp rise occurred ($P = 0.001$), such that by E16 the average amount had more than doubled from levels at E15. Although there was a reduction subsequently, it is not statistically significant ($P = 0.528$). Examination by electron microscopy of corneas in the E12-to-E18 timeframe in which chondroitin/dermatan sulfate GAG chains had been enzymatically removed from the tissue revealed cuprolinic blue-contrasted sulfated KS PGs as small collagen fibril-associated filaments that increased in abundance with time.

Discrete fibril bundles coalescing into a continuous matrix have been observed by other investigators³ and are apparent in Figures 1, 2. Measurements of (1) hydroxyproline, (2) highly and lesser sulfated KS, and (3) collagen fibril spacing were performed for each of the 69 corneas examined (Tables 1, 2). Consequently, we can seek correlations independent of developmental day. In doing so, it is evident that a positive correlation exists between hydroxyproline content and highly sulfated KS, as assessed by 5D4 binding ($R^2 = 0.682$), and between hydroxyproline content and lesser-sulfated KS, as measured by 1B4 binding ($R^2 = 0.395$), as shown in Figure 3. These parallel changes presumably reflect embryonic growth and continued matrix deposition. However, no appreciable correlation was found between the ratio of KS to hydroxyproline and collagen fibril spacing, when data from all 69 corneas were analyzed independent of developmental stage (Fig. 4).

DISCUSSION

The changing sulfation patterns of KS in the developing chick cornea raise several questions regarding the likely functional role of this molecule with respect to its sulfation status. Sulfate-

TABLE 2. The Average Amounts of 1B4- and 5D4-Labeled KS Epitope Relative to BAC-ABC Core after Normalization to Hydroxyproline Content in Embryonic Chick Corneas

	E12 (n = 8)	E13 (n = 10)	E14 (n = 11)	E15 (n = 10)	E16 (n = 11)	E17 (n = 10)	E18 (n = 9)
Lesser sulfated KS (1B4-labeled epitope/hydroxyproline)	0.125 ± 0.043	0.128 ± 0.032	0.153 ± 0.046	0.129 ± 0.024	0.109 ± 0.016	0.114 ± 0.022	0.118 ± 0.024
Highly sulfated KS (5D4-labeled epitope/hydroxyproline)	0.775 ± 0.261	0.958 ± 0.152	0.865 ± 0.160	0.840 ± 0.111	1.879 ± 0.167	1.449 ± 0.143	1.874 ± 0.206

Data are the mean \pm SE. Embryonic days E12 to E18 of development are equivalent to Hamburger-Hamilton stages 38 to 44.

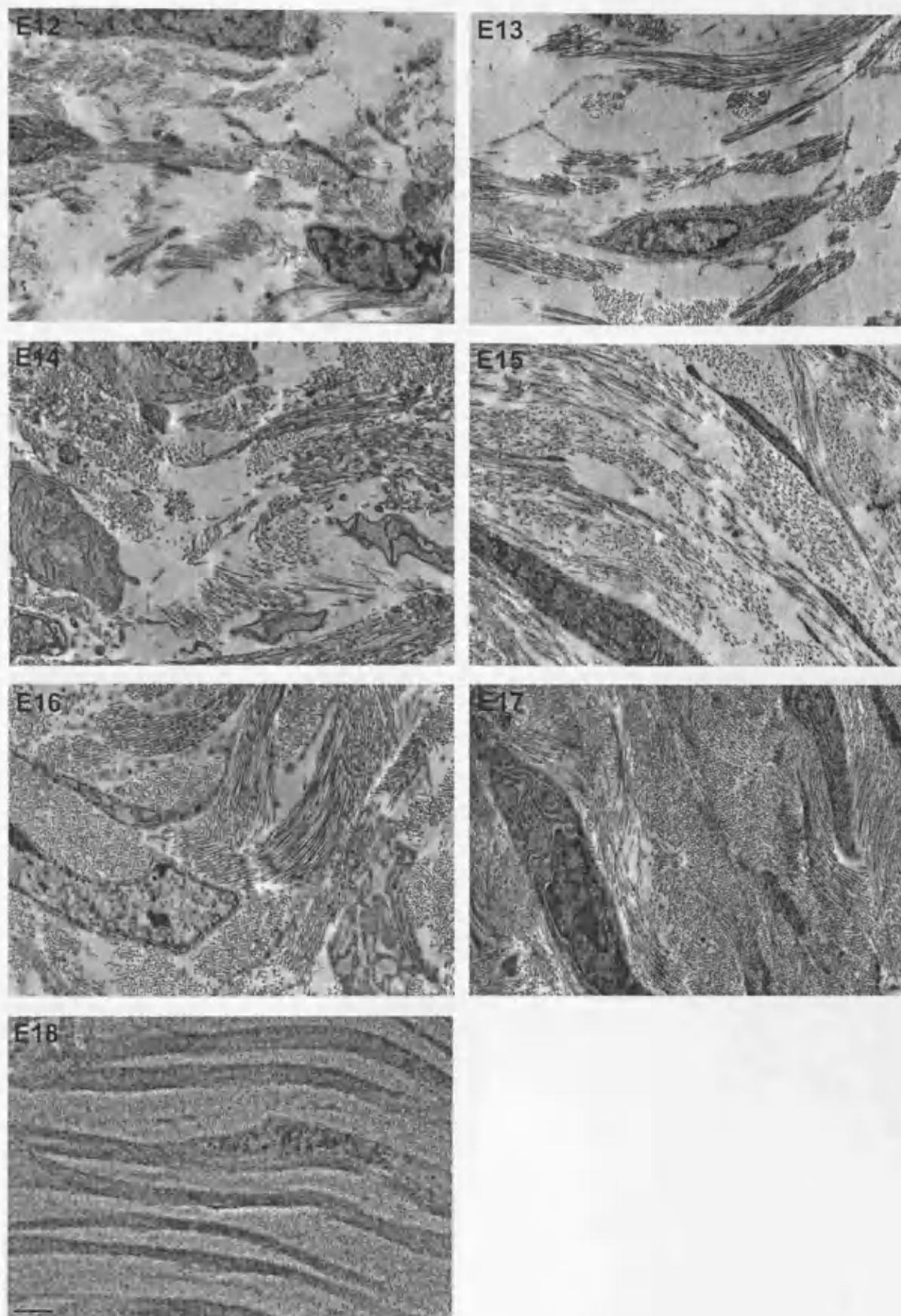


FIGURE 1. Transmission electron micrographs of developing chick corneal stroma. Tissue compaction progressed from loose bundles of collagen fibrils at E12 to a mature lamellar form at E18. Scale bar, 1 μm .

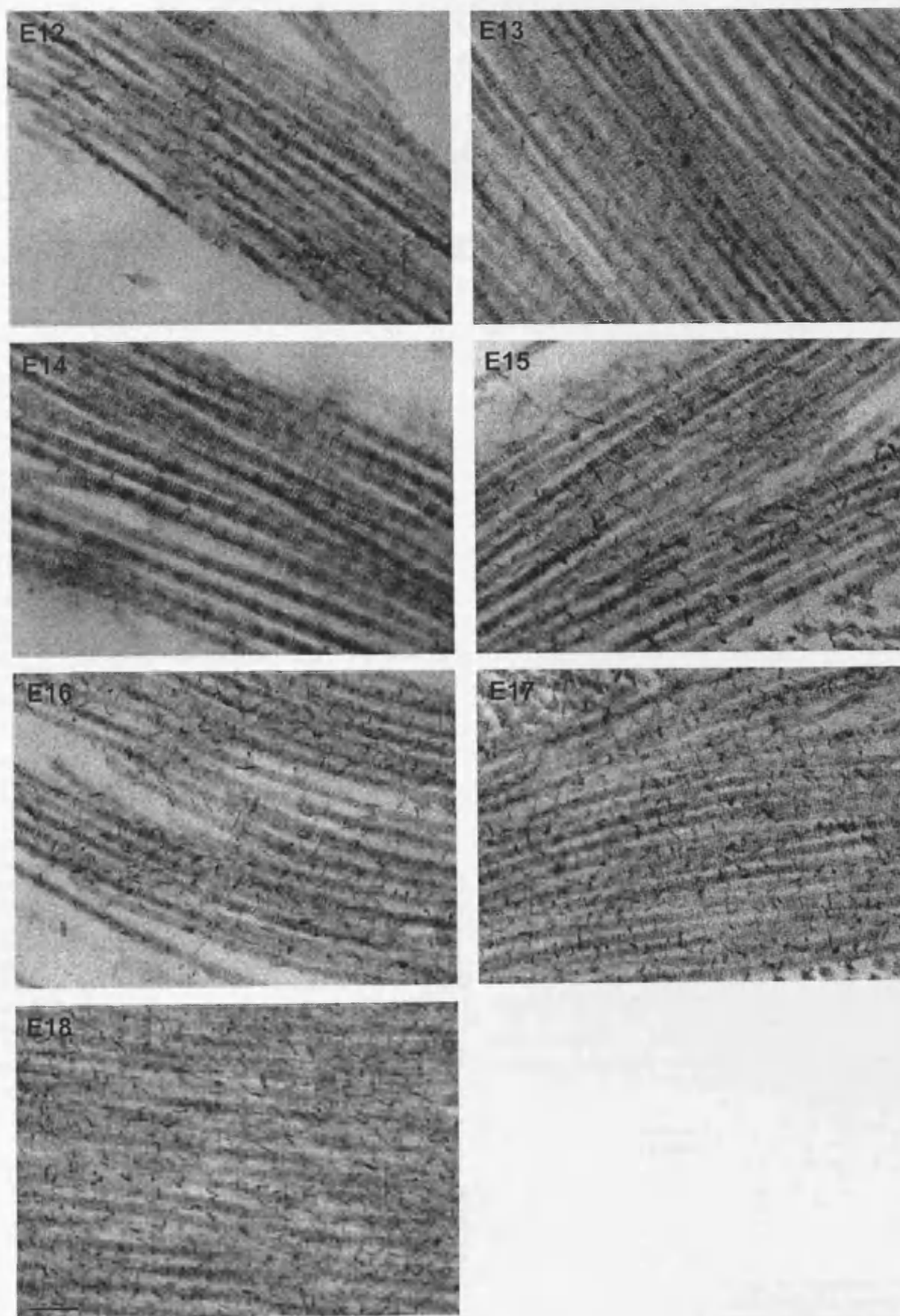


FIGURE 2. Transmission electron micrographs of chondroitinase digested developing chick corneal stroma. Increased deposition of cuprolinic blue-stained sulfated KS PG filaments occurs in the E12-E18 timeframe. Scale bar, 1 μ m.

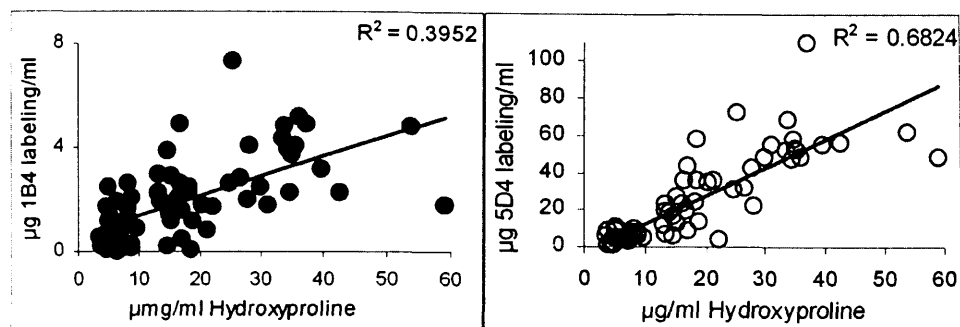


FIGURE 3. Correlation of antibody labeling in relation to BAC-ABC core against hydroxyproline content (without normalization to hydroxyproline, raw data not shown) for lesser (left, 1B4 reactive) and more highly (right, 5D4 reactive) sulfated KS.

tion of individual corneal KS chains is not homogeneous, and unsulfated disaccharides, which are predominant nearer the linkage region, become increasingly sulfated toward the non-reducing terminal.³⁹ Moreover, KS chains undergo sequential elongation and sulfation during synthesis.⁴⁰ The absence of sulfotransferase enzyme in human corneas with macular corneal dystrophy, as in mutant corneas of *Cbst5*-knockout mice, results in an immature, truncated GAG and an atypical corneal phenotype.^{18,21} Thus, KS chain length and sulfation are dictated by tissue-specific factors such as the presence of processing enzymes. During chick development, galactose-transferase activity increases with KS biosynthesis and is maintained at an unusually high level in adult cells.²⁹ The sequential mechanism of GAG subunit sulfation becomes apparent in the absence of the sulfotransferase enzyme, when neither GlcNAc nor Gal residues are sulfated.⁴¹ The negative charge provided by sulfation could serve to prevent KS GAG chain collapse during elongation and perhaps offer an explanation of the differential sulfation between shorter and longer KS chains. The presence of increasing amounts of highly sulfated KS during embryonic development is possibly linked to the appearance of the sulfate donor, 3'-phosphoadenosine-5'-phosphosulfate (PAPS).⁴² The measured elevation of 5D4 labeling at the time of increased fibrillogenesis and matrix compaction could be a result of PAPS availability facilitating increases in KS chain length and greater sulfation. The combination of these events could enhance organized stroma formation through the binding of core proteins and the hydrophilic influence of sulfate groups.

A major purpose of the present study was to investigate the structural remodeling of the stroma in relation to changing sulfation patterns of constitutive KS epitope during chick corneal morphogenesis. The results confirm previous synchrotron x-ray diffraction studies that documented the progressive compaction of corneal collagen fibrils with embryonic growth in the chick.^{43,44} In the dataset examined herein, compaction occurred after E14 (Table 1), with electron microscopy indicating that the compaction happened within bundles of collagen fibrils in which fibrils are already fairly well organized spatially (Fig. 1). The x-ray diffraction and electron microscopy

findings, when considered together, imply that collagen bundles are coalescing into lamellae, whereas, at the same time, fibrils within bundles are becoming more closely spaced. Between E15 and E16, the stroma experiences a significant increase in highly sulfated KS epitope that is disproportionate to the measured increase in hydroxyproline (Table 2). This observation is illustrative of an accelerated deposition of highly sulfated KS post-E15 which exceeds the anticipated in ovo corneal growth rate, as implied by hydroxyproline deposition. Thus, as the chick cornea develops and becomes transparent and compacted, the nature of KS antigenicity changes, with the highly sulfated KS fraction accumulating preferentially over that of the lesser-sulfated isoform and from a higher starting point. It seems counterintuitive to reason that negatively charged, highly sulfated KS GAG would accumulate as the stroma condenses and act as a biological driving force for tissue dehydration. Quite the opposite: The water-retentive properties of this hydrophilic macromolecule would be expected to swell the corneal matrix, rather than to aid in its compaction. Indeed, the current data show that the stroma was already undergoing compaction when the cornea, at E15, experienced the first sizable increase in highly sulfated KS epitope.

This result suggests that the emergence of more highly sulfated KS GAG in the chick cornea as it matures in ovo is not a driving force correlating with the homogeneous compaction of collagen fibrils in the coalescing collagen bundles and developing stromal lamellae and perhaps points to the influence of other modulating factors that help drive the structural remodeling of the developing corneal stroma in the week before hatching.

Activity of the bicarbonate pump in the corneal endothelium is critical for controlling corneal hydration and thickness and thus for maintaining transparency in the adult eye.⁴⁵⁻⁴⁷ It is also likely to be important in stromal water regulation and compaction in the developing cornea. However, the precise stage at which the endothelial pump mechanism becomes active is unknown. Histologic investigations have shown that an intact endothelial monolayer is established by E5 to E6.⁵ Stromal fluid at this time is mostly immobilized by hyaluronic

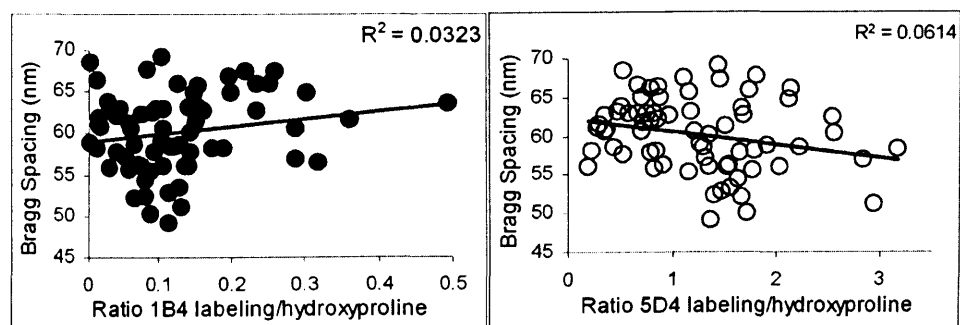


FIGURE 4. Correlation of sulfated KS antibody labeling (relative to BAC-ABC core) per hydroxyproline in relation to collagen Bragg spacing for lesser (left, 1B4 reactive) and more highly (right, 5D4 reactive) sulfated KS.

acid; later, small leucine-rich PGs, particularly KS PGs most likely influence the water-binding characteristics of the stroma. Conrad et al.,⁴⁸ studying gene expression associated with chick corneal development, including those genes involved in endothelial transport, found 5- to 10-fold increases in sodium-potassium ATPase transporter, sodium bicarbonate transporter, and carbonic anhydrase II (CA2), alongside increases in KS gene expression from E9 to E16. CA2 in particular, through increased transport of $\text{Na}^+/\text{HCO}_3^-$ and Cl^- would be expected to drive thinning of the cornea. Perhaps the accumulation of oversulfated KS during this time serves to maintain local collagen hydration, as gross dehydration and compaction progress through the action of the nascent endothelial pump.

References

- Linsenmayer TF, Fitch JM, Gordon MK, et al. Development and roles of collagenous matrices in the embryonic avian cornea. *Prog Retin Eye Res.* 1998;17:231-265.
- Quantock AJ, Young RD. Development of the corneal stroma and the collagen-proteoglycan associations that help define its structure and function. *Dev Dyn.* 2008;237:2607-2621.
- Birk DE, Trelstad RL. Extracellular compartments in matrix morphogenesis: collagen fibril, bundle, and lamellar formation by corneal fibroblasts. *J Cell Biol.* 1984;99:2024-2033.
- Coulombre AJ, Coulombre JL. Corneal development, I: corneal transparency. *J Cell Comp Physiol.* 1958;51:1-11.
- Hay ED, Revel J-P. Fine structure of the developing avian cornea. In: Wolsky A, Chen PS, eds. *Monographs in Developmental Biology*. Vol. 1. Basel, Switzerland: S. Karger; 1969:1-144.
- Trelstad RL, Coulombre AJ. Morphogenesis of the collagenous stroma in the chick cornea. *J Cell Biol.* 1971;50:840-858.
- Maurice DM. The structure and transparency of the cornea. *J Physiol (Lond).* 1957;186:263-286.
- Benedek GB. Theory of transparency of the eye. *Appl Opt.* 1971;10:459-473.
- Borcherding MS, Blacik LJ, Sittig RA, Bizzell JW, Breen M, Weinstein HG. Proteoglycans and collagen fibre organization in human corneal scleral tissue. *Exp Eye Res.* 1975;21:59-70.
- Blochberger TC, Vergnes JP, Hempel J, Hassell JR. cDNA to chick lumican (corneal keratan sulfate proteoglycan) reveals homology to the small interstitial proteoglycan gene family and expression in muscle and intestine. *J Biol Chem.* 1992;267:347-352.
- Corpus LM, Funderburgh JL, Funderburgh ML, Bottomley GS, Prakash S, Conrad GW. Molecular cloning and tissue distribution of keratocan: bovine corneal keratan sulfate proteoglycan 37A. *J Biol Chem.* 1996;271:9759-9763.
- Funderburgh JL, Corpus LM, Roth MR, Funderburgh ML, Tasheva ES, Conrad GW. Mimecan, the 25-kDa corneal keratan sulfate proteoglycan, is a product of the gene producing osteoglycin. *J Biol Chem.* 1997;272:28089-28095.
- Midura RJ, Hascall VC. Analysis of the proteoglycans synthesized by corneal explants from embryonic chicken, II: structural characterization of the keratan sulfate and dermatan sulfate proteoglycans from corneal stroma. *J Biol Chem.* 1989;264:1423-1430.
- Funderburgh JL, Funderburgh ML, Mann MM, Conrad GW. Unique glycosylation of three keratan sulfate proteoglycan isoforms. *J Biol Chem.* 1991;266:14226-14231.
- Bettelheim FA, Plessy B. The hydration of proteoglycans of bovine cornea. *Biochim Biophys Acta.* 1975;381:203-214.
- Anseth A. Glycosaminoglycans in the developing corneal stroma. *Exp Eye Res.* 1961;1:116-121.
- Hassell JR, Newsome DA, Krachmer JH, Rodrigues MM. Macular corneal dystrophy: failure to synthesize a mature keratan sulfate proteoglycan. *Proc Natl Acad Sci USA.* 1980;77:3705-3709.
- Akama TO, Nishida K, Nakayama J, et al. Macular corneal dystrophy type I and type II are caused by distinct mutations in a new sulphotransferase gene. *Nat Genet.* 2000;26:237-241.
- Chakravarti S, Magnuson T, Lass JH, Jepsen KJ, LaMantia C, Carroll H. Lumican regulates collagen fibril assembly: Skin fragility and corneal opacity in the absence of lumican. *J Cell Biol.* 1998;141:1277-1286.
- Chakravarti S, Petroll WM, Hassell JR, et al. Corneal opacity in lumican-null mice: defects in collagen fibril structure and packing in the posterior stroma. *Invest Ophthalmol Vis Sci.* 2000;41:3365-3373.
- Hayashida Y, Akama TO, Beecher N, et al. Matrix morphogenesis in cornea is mediated by the modification of keratan sulfate by GlcNAc 6-O sulfotransferase. *Proc Natl Acad Sci USA.* 2006;103:13333-13338.
- Funderburgh JL, Caterson B, Conrad GW. Keratan sulfate proteoglycan during embryonic development of the chicken cornea. *Dev Biol.* 1986;116:267-277.
- Takahashi I, Nakamura Y, Hamada Y, Nakazawa K. Immunohistochemical analysis of proteoglycan biosynthesis during early development of the chicken cornea. *J Biochem.* 1999;126:804-814.
- Zhang Y, Conrad AH, Tasheva ES, et al. Detection and quantification of sulfated disaccharides from keratan sulfate and chondroitin/dermatan sulfate during chick corneal development by ESI-MS/MS. *Invest Ophthalmol Vis Sci.* 2005;46:1604-1614.
- Young RD, Gealy EC, Liles M, Caterson B, Ralphs JR, Quantock AJ. Keratan sulfate glycosaminoglycan and the association with collagen fibrils in rudimentary lamellae in the developing avian cornea. *Invest Ophthalmol Vis Sci.* 2007;48:3083-3088.
- Conrad AH, Conrad GW. The keratocan gene is expressed in both ocular and non-ocular tissues during early chick development. *Matrix Biol.* 2003;22:323-337.
- Dunlevy JR, Beales MP, Berryhill BL, Cornuet PK, Hassell JR. Expression of the keratan sulfate proteoglycans lumican, keratocan and osteoglycin/mimecan during chick corneal development. *Exp Eye Res.* 2000;70:349-362.
- Cornuet PK, Blochberger TC, Hassell JR. Molecular polymorphism of lumican during corneal development. *Invest Ophthalmol Vis Sci.* 1994;35:870-877.
- Cai CX, Gibney E, Gordon MK, Marchant JK, Birk DE, Linsenmayer TF. Characterization and developmental regulation of avian corneal β -1,4-galactosyltransferase mRNA. *Exp Eye Res.* 1996;63:193-200.
- Hart GW. Biosynthesis of glycosaminoglycans during corneal development. *J Biol Chem.* 1976;251:6513-6521.
- Meek KM, Quantock AJ. The use of x-ray scattering techniques to determine corneal ultrastructure. *Prog Retin Eye Res.* 2001;20:95-137.
- Blain EJ, Gilbert SJ, Hayes AJ, Duance VC. Disassembly of the vimentin cytoskeleton disrupts articular cartilage chondrocyte homeostasis. *Matrix Biol.* 2006;25:398-408.
- Caterson B, Christner JE, Baker JR. Identification of a monoclonal antibody that specifically recognises corneal and skeletal keratan sulfate. *J Biol Chem.* 1983;258:8848-8854.
- Caterson B, Christner JE, Baker JR, Couchman JR. Production and characterization of monoclonal antibodies directed against connective tissue proteoglycans. *Fed Proc.* 1985;44:386-393.
- Mehmet H, Scudder P, Tang PW, Hounsell EF, Caterson B, Feizi T. The antigenic determinants recognized by three monoclonal antibodies to keratan sulfate involve hepta- or larger oligosaccharides of the poly (N-acetyllactosamine) series. *Eur J Biochem.* 1986;157:385-391.
- Young RD, Tudor D, Hayes AJ, et al. Atypical composition and ultrastructure of proteoglycans in the mouse corneal stroma. *Invest Ophthalmol Vis Sci.* 2005 46:1973-1978.
- Coleman JR, Herrmann H, Bess BJ. Biosynthesis of collagen and non-collagen protein during development of the chick cornea. *Cell Biol.* 1965;25:69-78.
- Conrad GW. Collagen and mucopolysaccharide biosynthesis in the developing chick cornea. *Dev Biol.* 1970;21(3):292-317.
- Oeben M, Keller R, Stuhlsatz H, Greiling H. Constant and variable domains of different disaccharide structure in corneal keratan sulphate chains. *Biochem J.* 1987;248:85-93.
- Akama TO, Misra AK, Hindsgaul O, Fukuda MN. Enzymatic synthesis in vitro of the disulfated disaccharide unit of corneal keratan sulfate. *J Biol Chem.* 2002;277:42505-42513.
- Akama TO, Nakayama J, Nishida K, et al. Human corneal GlcNAc 6-O-sulfotransferase and mouse intestinal GlcNAc 6-O-sulfotrans-

- ferase both produce keratan sulfate. *J Biol Chem.* 2001;276:16271-16278.
42. Conrad GW, Woo ML. Synthesis of 3'-phosphoadenosine-5'-phosphosulfate (PAPS) increases during corneal development. *J Biol Chem.* 1979;255:3086-3091.
 43. Quantock AJ, Kinoshita S, Capel MS, Schanzlin DJ. A synchrotron x-ray diffraction study of developing chick corneas. *Biophys J.* 1998;74:995-998.
 44. Siegler V, Quantock AJ. Two-stage compaction of the secondary avian cornea during development. *Exp Eye Res.* 2002;74:427-431.
 45. Hodson S, Miller F. The bicarbonate ion pump in the endothelium which regulates the hydration of rabbit cornea. *J Physiol.* 1976;263:563-577.
 46. Maurice DM. The location of the fluid pump in the cornea. *J Physiol.* 1972;221(1):43-54.
 47. Davson H. The hydration of the cornea. *J Biochem.* 1955;59:24-28.
 48. Conrad AH, Zhang Y, Walker AR, et al. Thyroxine affects expression of KS PG-related genes, the carbonic anhydrase II gene, and KS sulfation in the embryonic chicken cornea. *Invest Ophthalmol Vis Sci.* 2006;47:120-132.

ORIGINAL ARTICLE

Structural Collagen Alterations in Macular Corneal Dystrophy Occur Mainly in the Posterior Stroma

Barbara P. Palka¹, Chie Sotozono², Hidetoshi Tanioka², Tomoya O. Akama^{3,4}, Naoto Yagi⁵, Craig Boote¹, Robert D. Young¹, Keith M. Meek¹, Shigeru Kinoshita², and Andrew J. Quantock¹

¹*School of Optometry & Vision Sciences, Cardiff University, Cardiff, United Kingdom*

²*Department of Ophthalmology, Kyoto Prefectural University of Medicine, Kyoto, Japan*

³*Department of Pharmacology, Kansai Medical University, Osaka, Japan*

⁴*Tumor Microenvironment Program, Burnham Institute for Medical Research, La Jolla, California, USA*

⁵*Japan Synchrotron Radiation Research Institute, Hyogo, Japan*

ABSTRACT

Purpose: Collagen fibrils in the corneal stroma in macular corneal dystrophy, on average, are more closely spaced than in the normal cornea. This study was conducted to investigate if this occurs uniformly across the stroma or is more prevalent at certain stromal depths.

Methods: Microbeam synchrotron X-ray fiber diffraction patterns were obtained in 25 μm steps across the whole thickness of a thin strip of a macular corneal dystrophy cornea obtained at keratoplasty. Data were analyzed for mean collagen interfibrillar spacing at all positions. Serum was analyzed immunochemically to determine immunophenotype, and transmission electron microscopy was carried out to visualize stromal ultrastructure.

Results: Keratan sulphate was not detectable in blood serum, classifying the disease as macular corneal dystrophy type I. Collagen interfibrillar spacing dropped linearly with stromal depth from the anterior to posterior cornea, measuring 5–10% less in the posterior 100 μm of the MCD stroma compared to the anterior 100 μm ($p < 0.001$). Isolated pockets of collagen fibrils with unusually large diameters were identified in the deep stroma.

Conclusions: Collagen fibril spacing is reduced and large-diameter collagen fibrils are seen in macular corneal dystrophy type I, with the deep stroma affected more. We speculate that the ultrastructural abnormalities are more prevalent in the posterior stroma because the structural influence of sulphated keratan sulphate glycosaminoglycans/proteoglycans is high in this region of the cornea.

KEYWORDS: Collagen; Cornea; Glycosaminoglycans; Macular corneal dystrophy; Proteoglycans

INTRODUCTION

Macular corneal dystrophy (MCD; Mendelian Inheritance in Man (MIM) 217800), an autosomal recessive

disease characterized by progressive corneal cloudiness and focal opacities, is caused by an anomaly in the production of keratan sulphate (KS) glycosaminoglycan (GAG).^{1–7} The condition has been categorized into three main immunophenotypes (type I, type IA, and type II) based on the reactivity of corneal tissue and/or serum to a monoclonal antibody (5D4), which recognizes high-sulphated KS.^{8,9} Sulphated KS, which is present in the cornea and serum of non-affected

Received 01 December 2009; accepted 28 February 2010

Correspondence: Andrew J. Quantock, Ph.D., School of Optometry and Vision Sciences, Cardiff University, Maindy Road, Cardiff CF24 4LU, United Kingdom. E-mail: QuantockAJ@cf.ac.uk

individuals, is absent from serum and cornea in the majority of MCD patients, and these are categorized as MCD type I.^{10,11} A smaller subset of patients are designated MCD type II because of immunodetectable KS in their serum and cornea.^{12,13} Further studies have identified MCD type IA, in which there is no detectable KS in sera of affected individuals, but 5D4-positive signal in keratocytes.¹⁴

KS in cornea is an important matrix molecule,¹⁵ which is bound to one of three core proteins, lumican, keratocan, or mimecan and, thus, exists as a proteoglycan (PG).^{16–18} KS-PGs bind to collagen fibrils via their core proteins at defined locations along the fibril axis,^{19,20} with the hydrophilic, sulphated GAG chains occupying the extrafibrillar space where they help define the swelling properties of the stroma and the structural arrangement of the collagen fibrils.^{21–24} The cornea in MCD is thinner than normal,^{25,26} and unlike in other conditions, such as keratoconus where a slippage of lamellae is suspected of being responsible for the reduction in central corneal thickness,^{27,28} the collagen fibrils in MCD are more closely spaced than normal.^{29,30} Synchrotron X-ray diffraction measurements of fibril spacing in MCD corneas represent an average value throughout the whole thickness of the stroma.^{29,30} KS, however, is not evenly distributed throughout the cornea,^{31,32} so to investigate whether or not the PG alterations manifested in MCD are associated with location-specific changes in stromal extracellular matrix architecture, we conducted a series of microbeam synchrotron X-ray diffraction experiments at a spatial resolution of 25 μm to ascertain the depth-dependent nature of collagen fibril spacing MCD.

MATERIALS AND METHODS

The patient was a 50-yr-old female with bilateral MCD, who 11 years earlier had undergone penetrating keratoplasty in her right eye. As with the right cornea, the left cornea was affected by a diffuse ground-glass-like stromal opacity, and numerous irregularly-shaped white patches that were confined mainly to the deep part of the stroma (Figure 1). The edges of the opacities were dull and indistinct. A penetrating keratoplasty was performed after which the excised button (7 mm diameter) was immediately wrapped in Clingfilm to prevent dehydration, and stored at -80°C for seven days prior to transportation on dry ice to the SPring-8 synchrotron facility where small-angle X-ray scattering was used to investigate the internal fine structure of the corneal stroma in its thawed, hydrated state.³³ A human eye-bank cornea deemed unsuitable for grafting because a low endothelial cell count was similarly examined. Under a binocular microscope,

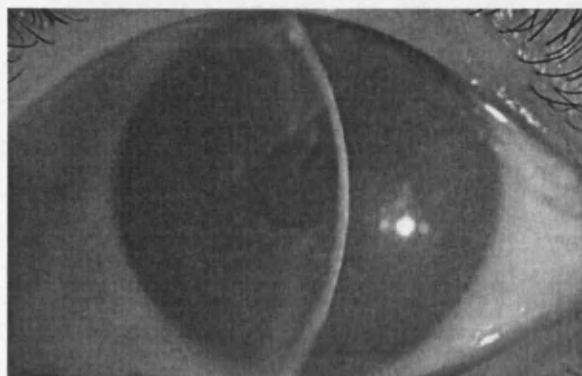


FIGURE 1 Slit-lamp examination of the MCD cornea showing diffuse ground-glass-like stromal opacification and focal deposits.

two thin strips were cut across the centers of the MCD and eye bank corneas using a surgical blade, with the edge of a glass microscope slide serving as a guide for the dissection. This was done with the epithelial side up, and the cut strips were estimated to be in the region of 400 μm thick. One strip from each cornea was analyzed with the X-ray beam directed through the tissue from front to back, while the other strips were oriented so that the beam passed through them edgewise. X-ray patterns were collected from regions of the corneas corresponding to the central pre-pupillary zone; the MCD cornea was also examined in the mid-periphery, approximately 3 mm from the corneal center. As described previously, a series of small-angle X-ray diffraction patterns was obtained on the high flux beamline, 40XU, using a 25 μm microbeam in 25 μm steps and with sub-second exposure times.³⁴ Patterns were analyzed to provide values for the mean collagen interfibrillar spacing calibrated to the meridional reflection arising from the 67 nm axial repeat of collagen in rat tail tendon, and adjusted by a 1.12 calibration factor to take into account the mode of packing of collagen fibrils in cornea³⁵ as was done in previous studies of MCD.^{29,30}

After X-ray exposure, small full-thickness pieces of MCD cornea were prepared by conventional fixation in 2.5% buffered glutaraldehyde, followed by post-fixation for 1 hr each in 1% aqueous osmium tetroxide and 0.5% aqueous uranyl acetate. Tissue was then dehydrated through an ascending series of ethanol, immersed in propylene oxide, and embedded in Araldite CY212 epoxy resin (Agar Scientific, Stansted, UK). Ultrathin sections were cut with a diamond knife on a Leica UC6 ultramicrotome (Leica, Vienna, Austria), picked up on uncoated copper grids, contrasted with saturated uranyl acetate and Reynold's lead citrate, and imaged on a Philips (Philips, Eindhoven, The Netherlands)/EM208 electron microscope.

The patient's serum KS level was measured by inhibition ELISA analysis using 5D4 anti-KS monoclonal antibody.¹⁰ In brief, a serum sample or bovine cartilage KS standard (KS-2eq, kindly provided by Prof. Eugene J.-M. A. Thonar, Rush Presbyterian-St. Luke's Medical Center, Chicago, Illinois, USA) was mixed with 5D4 antibody (Seikagaku Co., Tokyo, Japan) and incubated at 4°C overnight. The mixture was then transferred to a 96-well ELISA plate that was coated with bovine nasal septum D1 fraction, which contained KS antigen. This was incubated at 4°C for 1 hr, after which the plate was emptied and washed three times with PBS pH 5.3 containing 0.05% Tween-20 (PBST5.3). Horseradish peroxidase-conjugated goat anti-mouse IgG antibody (Thermo Scientific, Rockford, Illinois, USA) was diluted into 1% BSA in PBST5.3 and added to the ELISA plate, followed by a 1 hr incubation at room temperature. The plate was emptied and washed with PBST5.3 three times and developed with DuoSet ELISA development reagent (R&D Systems, Minneapolis, Minnesota, USA) according to the manufacturer's instructions. The patient's serum KS concentration was calculated in reference to absorbance values of the KS standard.

The research described in this article was approved by the Committee for Ethical Issues on Human Research of Kyoto Prefectural University of Medicine and followed the tenets of the Declaration of Helsinki. Informed consent was obtained from the MCD patient after she had received a detailed explanation of the procedures.

RESULTS

KS in the serum of the MCD patient was quantified by ELISA with the 5D4 antibody at less than 10 ng/ml, indicating the immunophenotype to be MCD type I. This is consistent with the genetic status, in which the patient presented the mutation C (c.631) to T in exon 1 of the *CHST6* gene.

Collagen interfibrillar spacing, measured at 27 positions, 25 μm apart, in the central region of the eye bank cornea and the MCD cornea with the beam directed at right angles to the corneal surface and passed through the whole thickness of the tissue gave mean values of 52.0 nm (SD \pm 0.3 nm) and 40.7 nm (SD \pm 0.7 nm), respectively. Previous measurements by synchrotron X-ray diffraction of collagen fibril spacing in MCD indicated a reduction of 22% compared to the fibril spacing in a post-mortem human cornea, with the values representing an average throughout the whole thickness of the stroma.³⁰ A similar proportional reduction is seen in the current analysis. What is not known, however, is whether

or not this reduced fibril spacing in MCD varies with stromal depth. To rectify this, measurements of collagen interfibrillar spacing were obtained in sequential steps of 25 μm across MCD and eye bank corneas from front to back. Eye bank data confirmed previous depth-profiled X-ray diffraction studies,³⁴ and showed that collagen fibrils were more widely spaced in the posterior stroma (by approximately 25%) as compared to the mid-depth or anterior stroma (Figure 2). The opposite was true, however, for the MCD cornea, with collagen fibril spacing clearly lower in the posterior stroma (Figure 2). This pattern was seen in the corneal mid-periphery in MCD too, although the collagen spacing values are higher overall than those in the corneal center as tends to be the case in human corneas.³⁶ In the central region of the MCD cornea, collagen spacing is 5.4% less in the posterior 100 μm of stroma compared to the anterior 100 μm ($p < 0.01$), while in the mid-periphery, the posterior 100 μm of the MCD stroma shows a collagen spacing that is 10.0% less than that in the anterior 100 μm ($p < 0.01$). Thus, the profile of collagen fibril spacing as a function of stromal depth in MCD—i.e., lower fibril spacing in the deep

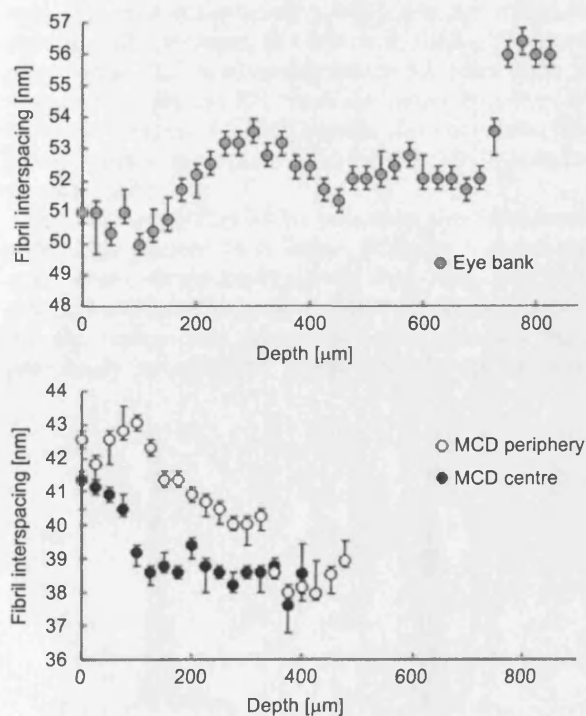


FIGURE 2 Center-to-center collagen fibril spacing measured in 25 μm steps across an eye bank cornea (top) and MCD cornea (bottom). In the eye bank, cornea fibril spacing is lower in the anterior stroma, while in the central and mid-peripheral regions of the MCD cornea, a clear decrease in collagen fibril spacing is evident in the deeper stroma.

stroma—is unlike that for a human cornea from the eye bank, which displays a lower fibril spacing in the anterior stroma.

Confirmation of more prevalent stromal alterations in the posterior cornea in MCD came from an electron microscopic examination of the cornea. This disclosed that the collagen fibrils appear structurally normal in the anterior cornea, but that the deep stroma possesses focal pockets of abnormally large diameter collagen fibrils (Figure 3). Fibrils ($n=802$) in the eye bank cornea examined here displayed a normal distribution of fibril diameters that ranged from 20.0–35.6 nm (Figure 4), and was centered on 26.4 nm ($SD \pm 2.6$ nm), similar to published values.³⁷ Measurement of 800 fibrils in

areas of the posterior MCD cornea, which contained congregations of large-diameter fibrils, on the other hand, indicated a larger spread of diameters 19.6 nm to 63.1 nm, with a distribution that was not normal (one-sample Kolmogorov-Smirnov test $p < 0.001$), but was skewed by the existence of fibrils with larger-than-normal diameters (Figure 4). Large-diameter collagen fibrils have been documented previously in MCD where they were reported to range in size from 20 nm to 60 nm.^{38,39} However, it was not indicated at what stromal depth they existed. In the MCD cornea studied here, abnormally large collagen fibrils were restricted to the deep stroma.

DISCUSSION

An abnormality in the biosynthetic pathway of KS occurs in MCD and causative mutations have been found in a gene, *CHST6*, which encodes the sulfotransferase enzyme *N*-acetylglucosamine 6-*O* sulfotransferase (CGn6ST).⁴⁰ KS is a linear carbohydrate chain comprised of a repeating series of disaccharides, in which each is composed of galactose (Gal) and *N*-acetylglucosamine (GlcNAc). CGn6ST and galactose 6-*O* sulfotransferase (G6ST) transfer sulphate onto the 6-*O* positions of GlcNAc and Gal,^{41,42} thus a mutation in *CHST6* adversely affects the production of a mature, sulphated KS. Since the initial discovery of the causative gene for MCD, molecular genetic studies have reported mutations in *CHST6* in MCD patients worldwide.^{43–57}

KS-PGs are believed to influence the ultrastructural arrangement of collagen fibrils in the cornea, and recent three-dimensional data from electron tomography have suggested that they do so by forming macromolecular structures more complex than previously believed.^{58,59} Fibril diameter in the cor-

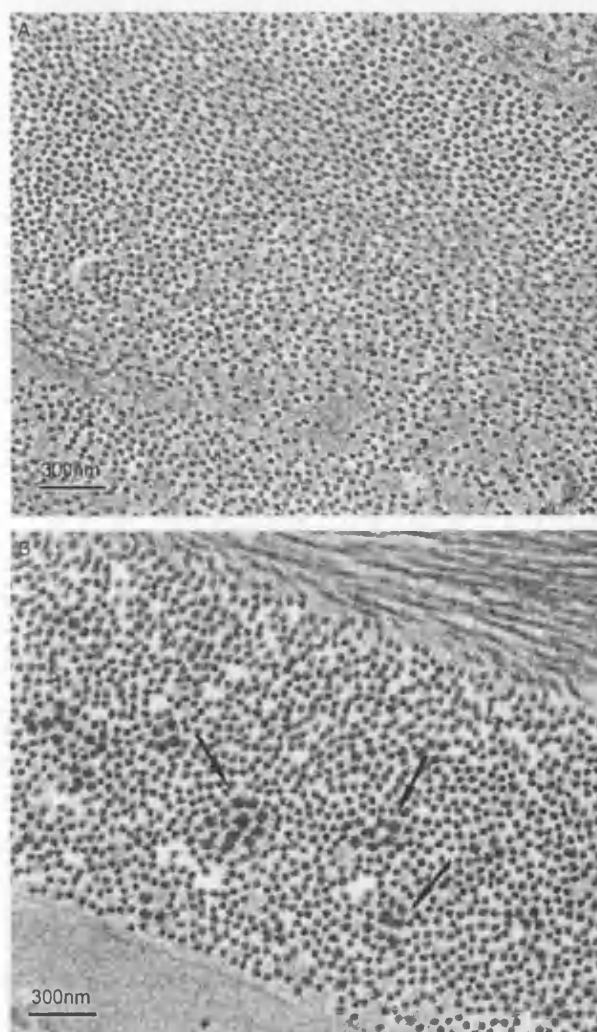


FIGURE 3 Transverse-section electron microscopic images of collagen fibrils in the anterior (A) and posterior (B) stroma in MCD. Focal pockets of collagen fibrils of abnormally large diameter are present in the posterior stroma. Magnification 32k.

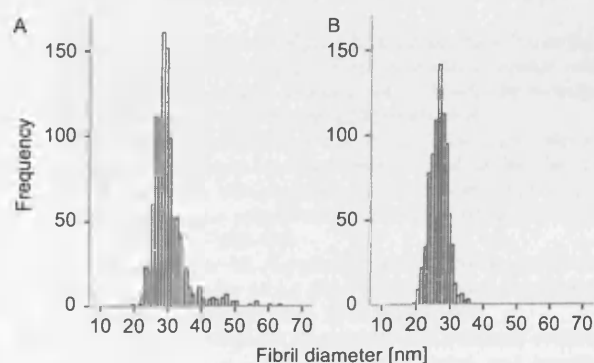


FIGURE 4 Histograms showing the range of collagen fibril diameters in deep regions of the MCD stroma, which contain abnormally large diameter fibrils (A), and in the eye bank cornea (B).

nea is controlled, in part, by the proportion of type V collagen molecules in the hybrid type I/V fibril, with higher proportions of collagen type V leading to narrower fibrils.⁶⁰ Evidence exists, too, for a role for KS-PGs in the regulation of fibril diameter and *in vitro* both lumican and decorin (a corneal PG with a hybrid chondroitin sulphate/dermatan sulphate [CS/DS] GAG) regulate collagen fibrillogenesis, although, interestingly, they do so with, as well as without, the GAG side chain.⁶¹ This suggests that the regulatory ability might lie with the core protein, and studies of the corneas of lumican-null mice show that collagen fibrils are sometimes abnormally large, presumably because of the reduction of this KS-PG in the stroma.⁶² The presence of unusually large collagen fibrils in the corneas of MCD patients is suggestive of a role for the GAG side chain of KS in the regulation of fibril diameter. Collagen intermolecular spacing appears to be unchanged within fibrils in MCD corneas.⁶³ We can, therefore, probably assign the larger fibril diameters to the aggregation of more molecules into fibrils, and even perhaps the merging of existing fibrils, rather than the existence of more widely spaced collagen molecules within fibrils. Studies on the corneas of gene-targeted mice with a mutation of *Chst5*, a murine equivalent of *CHST6* in humans, have reported a thin stroma and closer-than-normal collagen fibril spacing, but not pockets of abnormally large collagen fibrils in the corneal stroma.⁶⁴ The mouse cornea, however, contains KS GAG chains that are less sulphated than those in the human cornea,^{32,65} so perhaps the lack of KS sulfotransferase activity in the *Chst5*-null mouse has less of an impact on collagen fibril diameter because of the limited need for sulphated KS in the cornea of this species.

The low levels of sulphated KS in the mouse cornea have been attributed to the thinness of the cornea, into which oxygen readily diffuses to all layers of the stroma.³² It was postulated by Scott that proportionally higher levels of sulphated KS found in the deeper layers of the thicker corneas of larger animals is a direct consequence of the restricted oxygen supply, and that KS acts as a "stand-in" for CS/DS in conditions of lacking oxygen.^{66–68} This concept has support in other tissues, such as articular cartilage, in which a similarly increased incidence of KS is seen in thicker cartilages, accompanied by a greater abundance in deeper layers.^{69,70} KS is not found in sulphated form in the stroma in MCD I,^{10–14} but rather is present in unsulphated or low-sulphated form.^{71–73} The current finding that structural matrix changes (i.e., reduced collagen fibril spacing and large-diameter fibrils) are more prevalent in the deep stroma in MCD I might reflect the heightened importance of sulphated KS-PGs in this part of the tissue in the human cornea.

ACKNOWLEDGMENTS

Our research programs are funded by BBSRC Project Grant BB/D001919/1 (U.K.), NIH/NEI Research Grant EY014620 (U.S.A.), MRC Program Grant G0600755 (U.K.), EPSRC Project Grant EP/F034970/1 (U.K.), and beamtime access awards from The Japan Synchrotron Radiation Research Institute. B.P.P. is a graduate student sponsored by a BBSRC Doctoral Training Grant.

Declaration of interest: The authors report no conflicts of interest. The authors alone are responsible for the content and writing of the paper.

REFERENCES

- [1] Klintworth GK, Vogel FS. Macular corneal dystrophy. An inherited acid mucopolysaccharide storage disease of the corneal fibroblast. *Am J Pathol.* 1964;45:565–586.
- [2] Klintworth GK, Smith CF. Abnormalities of proteoglycans and glycoproteins synthesized by corneal organ cultures derived from patients with macular corneal dystrophy. *Lab Invest.* 1983;48:603–612.
- [3] Hassell JR, Newsome DA, Krachmer JH, et al. Macular corneal dystrophy: Failure to synthesize a mature keratan sulfate proteoglycan. *Proc Natl Acad Sci U S A.* 1980;77:3705–3709.
- [4] Nakazawa K, Hassell JR, Hascall VC, et al. Defective processing of keratan sulfate in macular corneal dystrophy. *J Biol Chem.* 1984;259:13751–13757.
- [5] Midura RJ, Hascall VC, MacCallum DK, et al. Proteoglycan biosynthesis by human corneas from patients with types 1 and 2 macular corneal dystrophy. *J Biol Chem.* 1990;265:15947–15955.
- [6] Plaas AH, West LA, Thonar EJ, et al. Altered fine structures of corneal and skeletal keratan sulfate and chondroitin/dermatan sulfate in macular corneal dystrophy. *J Biol Chem.* 2001;276:39788–39796.
- [7] Klintworth GK. Genetic disorders of the cornea. In: GK and A Garner (Eds.). *Pathobiology of Ocular Disease*, 3rd edition. New York: Klintworth, Informa Healthcare, 2008; pp. 615–713.
- [8] Caterson B, Christner JE, Baker JR. Identification of a monoclonal antibody that specifically recognizes corneal and skeletal keratan sulfate. Monoclonal antibodies to cartilage proteoglycan. *J Biol Chem.* 1983;258:8848–8854.
- [9] Mehmet H, Scudder P, Tang PW, et al. The antigenic determinants recognized by three monoclonal antibodies to keratan sulphate involve sulphated hepta- or larger oligosaccharides of the poly(N-acetyllactosamine) series. *Eur J Biochem.* 1986;157:385–391.
- [10] Thonar EJ, Meyer RF, Dennis RF, et al. Absence of normal keratan sulfate in the blood of patients with macular corneal dystrophy. *Am J Ophthalmol.* 1986;102:561–569.
- [11] Klintworth GK, Meyer R, Dennis R, et al. Macular corneal dystrophy. Lack of keratan sulfate in serum and cornea. *Ophthalmic Paediatr Genet.* 1986;7:139–143.
- [12] Yang CJ, SundarRaj N, Thonar EJ, et al. Immunohistochemical evidence of heterogeneity in macular corneal dystrophy. *Am J Ophthalmol.* 1988;106:65–71.

- [13] Edward DP, Yue BY, Sugar J, et al. Heterogeneity in macular corneal dystrophy. *Arch Ophthalmol*. 1988;106:1579–1583.
- [14] Klintworth GK, Oshima E, al-Rajhi A, et al. Macular corneal dystrophy in Saudi Arabia: A study of 56 cases and recognition of a new immunophenotype. *Am J Ophthalmol*. 1997;124:9–18.
- [15] Quantock AJ, Young RD, Akama TO. Structural and biochemical aspects of keratan sulphate in the cornea. *Cell Mol Life Sci*. 2010;67:89–906.
- [16] Blochberger TC, Vergnes JP, Hempel J, et al. cDNA to chick lumican (corneal keratan sulfate proteoglycan) reveals homology to the small interstitial proteoglycan gene family and expression in muscle and intestine. *J Biol Chem*. 1992;267:347–352.
- [17] Corpuz LM, Funderburgh JL, Funderburgh ML, et al. Molecular cloning and tissue distribution of keratocan. Bovine corneal keratan sulfate proteoglycan 37A. *J Biol Chem*. 1996;271:9759–9763.
- [18] Funderburgh JL, Corpuz LM, Roth MR, et al. Mimecan, the 25-kDa corneal keratan sulfate proteoglycan, is a product of the gene producing osteoglycin. *J Biol Chem*. 1997;272:28089–28095.
- [19] Scott JE, Haigh M. 'Small' proteoglycan:collagen interactions: Keratan sulphate proteoglycan associates with rabbit corneal collagen fibrils at the 'a' and 'c' bands. *Biosci Rep*. 1986;5:765–774.
- [20] Meek KM, Elliott GF, Nave C. A synchrotron X-ray diffraction study of bovine cornea stained with cupromeronic blue. *Coll Relat Res*. 1986;6:203–218.
- [21] Bettelheim FA, Plessy B. The hydration of proteoglycans of bovine cornea. *Biochim Biophys Acta*. 1975;381:203–214.
- [22] Bettelheim FA, Goetz D. Distribution of hexosamines in bovine cornea. *Invest Ophthalmol*. 1976;15:301–304.
- [23] Castoro JA, Bettelheim AA, Bettelheim FA. Water gradients across bovine cornea. *Invest Ophthalmol Vis Sci*. 1988;29:963–968.
- [24] Borcharding MS, Blacik LJ, Sittig RA, et al. Proteoglycans and collagen fibre organization in human corneal scleral tissue. *Exp Eye Res*. 1975;21:59–70.
- [25] Ehlers N, Bramsen T. Central thickness in corneal disorders. *Acta Ophthalmol*. 1978;56:412–416.
- [26] Donnenfeld ED, Cohen EJ, Ingraham HJ, et al. Corneal thinning in macular corneal dystrophy. *Am J Ophthalmol*. 1986;101:112–113.
- [27] Fullwood NJ, Tuft SJ, Malik NS, et al. Synchrotron x-ray diffraction studies of keratoconus corneal stroma. *Invest Ophthalmol Vis Sci*. 1992;33:1734–1741.
- [28] Meek KM, Tuft SJ, Huang Y, et al. Changes in collagen orientation and distribution in keratoconus corneas. *Invest Ophthalmol Vis Sci*. 2005;46:1948–1956.
- [29] Meek KM, Quantock AJ, Elliott GF, et al. Macular corneal dystrophy: The macromolecular structure of the stroma observed using electron microscopy and synchrotron x-ray diffraction. *Exp Eye Res*. 1989;49:941–958.
- [30] Quantock AJ, Meek KM, Ridgway AEA, et al. Macular corneal dystrophy: Reduction in both corneal thickness and collagen interfibrillar spacing. *Curr Eye Res*. 1990;9:393–398.
- [31] Scott JE, Haigh M, Ali P. Keratan sulphate is unevenly distributed from back to front of bovine cornea. *Biochem Soc Trans*. 1988;16:333–334.
- [32] Scott JE, Bosworth TR. A comparative biochemical and ultrastructural study of proteoglycan-collagen interactions in corneal stroma. *Biochem J*. 1990;270:491–497.
- [33] Meek KM, Quantock AJ. The use of x-ray scattering techniques to determine corneal ultrastructure. *Prog Ret Eye Res*. 2001;20:95–137.
- [34] Quantock AJ, Boote C, Young RD, et al. Small-angle fibre diffraction studies of corneal matrix structure: A depth-profiled investigation of the human eye-bank cornea. *J Appl Crystal*. 2007;40:335–340.
- [35] Worthington CR, Inouye H. X-ray diffraction study of the cornea. *Int J Biol Macromol*. 1985;7:2–8.
- [36] Boote C, Dennis S, Newton RH, et al. Collagen fibrils appear more closely packed in the prepupillary cornea: Optical and biomechanical implications. *Invest Ophthalmol Vis Sci*. 2003;44:2941–2948.
- [37] Quantock AJ, Meek KM, Fullwood NJ, et al. Scheie's syndrome: The architecture of corneal collagen and distribution of corneal proteoglycans. *Can J Ophthalmol*. 1993;28:266–272.
- [38] Quantock AJ, Meek KM, Thonar EJ-MA, et al. Synchrotron x-ray diffraction in atypical macular dystrophy. *Eye*. 1993;7:779–784.
- [39] Quantock AJ, Fullwood NJ, Thonar EJ-MA, et al. Macular corneal dystrophy type II: Multiple studies on a cornea with low levels of sulphated keratan sulphate. *Eye*. 1997;11:57–67.
- [40] Akama TO, Nishida K, Nakayama J, et al. Macular corneal dystrophy type I and type II are caused by distinct mutations in a new sulphotransferase gene. *Nat Genet*. 2000;26:237–241.
- [41] Akama TO, Nakayama J, Nishida K, et al. Human corneal GlcNAc 6-O-sulfotransferase and mouse intestinal GlcNAc 6-O-sulfotransferase both produce keratan sulfate. *J Biol Chem*. 2001;276:16271–16278.
- [42] Fukuta M, Inazawa J, Torii T, et al. Molecular cloning and characterization of human keratan sulfate Gal-6-sulfotransferase. *J Biol Chem*. 1997;272:32321–32328.
- [43] Liu NP, Dew-Knight S, Rayner M, et al. Mutations in corneal carbohydrate sulfotransferase 6 gene (CHST6) cause macular corneal dystrophy in Iceland. *Mol Vis*. 2000;6:261–264.
- [44] El-Ashry MF, Abd El-Aziz MM, Wilkins S, et al. Identification of novel mutations in the carbohydrate sulfotransferase gene (CHST6) causing macular corneal dystrophy. *Invest Ophthalmol Vis Sci*. 2002;43:377–382.
- [45] Niel F, Ellies P, Dighiero P, et al. Truncating mutations in the carbohydrate sulfotransferase 6 gene (CHST6) result in macular corneal dystrophy. *Invest Ophthalmol Vis Sci*. 2003;44:2949–2953.
- [46] Iida-Hasegawa N, Furuhashi A, Hayatsu H, et al. Mutations in the CHST6 gene in patients with macular corneal dystrophy: Immunohistochemical evidence of heterogeneity. *Invest Ophthalmol Vis Sci*. 2003;44:3272–3277.
- [47] Warren JF, Aldave AJ, Srinivasan M, et al. Novel mutations in the CHST6 gene associated with macular corneal dystrophy in southern India. *Arch Ophthalmol*. 2003;121:1608–1612.
- [48] Abbruzzese C, Kuhn U, Molina F, et al. Novel mutations in the CHST6 gene causing macular corneal dystrophy. *Clin Genet*. 2004;65:120–125.
- [49] Aldave AJ, Yellore VS, Thonar EJ, et al. Novel mutations in the carbohydrate sulfotransferase gene (CHST6) in American patients with macular corneal dystrophy. *Am J Ophthalmol*. 2004;137:465–473.
- [50] El-Ashry MF, Abd El-Aziz MM, Shalaby O, et al. Novel CHST6 nonsense and missense mutations responsible for macular corneal dystrophy. *Am J Ophthalmol*. 2005;139:192–193.
- [51] Liu NP, Bao W, Smith CF, et al. Different mutations in carbohydrate sulfotransferase 6 (CHST6) gene cause macular

- corneal dystrophy types I and II in a single sibship. *Am J Ophthalmol.* 2005;139:1118–1120.
- [52] Liu NP, Smith CF, Bowling BL, et al. Macular corneal dystrophy types I and II are caused by distinct mutations in the CHST6 gene in Iceland. *Mol Vis.* 2006;12:1148–1152.
- [53] Klintworth GK, Smith CF, Bowling BL. CHST6 mutations in North American subjects with macular corneal dystrophy: A comprehensive molecular genetic review. *Mol Vis.* 2006;12:159–176.
- [54] Liskova P, Veraitch B, Jirsova K, et al. Sequencing of the CHST6 gene in Czech macular corneal dystrophy patients supports the evidence of a founder mutation. *Br J Ophthalmol.* 2008;92:265–267.
- [55] Sultana A, Klintworth GK, Thonar EJ, et al. Immunophenotypes of macular corneal dystrophy in India and correlation with mutations in CHST6. *Mol Vis.* 2009;15:319–325.
- [56] Dang X, Zhu Q, Wang L, et al. Macular corneal dystrophy in a Chinese family related with novel mutations of CHST6. *Mol Vis.* 2009;15:700–705.
- [57] El-Ashry MF, Abd El-Aziz MM, Shalaby O, et al. Molecular genetic study of Egyptian patients with macular corneal dystrophy. *Br J Ophthalmol.* 2009;250–255.
- [58] Knupp C, Pinali C, Lewis PN, et al. The architecture of the cornea and structural basis of its transparency. *Adv Prot Chem Struct Biol.* 2009;78:25–49.
- [59] Parfitt GJ, Pinali C, Young RD, et al. Three-dimensional reconstruction of collagen-proteoglycan interactions in the mouse corneal stroma by electron tomography. *J Struct Biol.* 2010;170:392–397.
- [60] Birk DE, Fitch JF, Babiarz JP, et al. Collagen fibrillogenesis in vitro: Interaction of types I and V collagen regulates fibril diameter. *J Cell Sci.* 1990;95:649–657.
- [61] Rada J, Cornuet PK, Hassell JR. Regulation of corneal collagen fibrillogenesis in vitro by corneal proteoglycan (lumican and decorin) core proteins. *Exp Eye Res.* 1993;56:635–648.
- [62] Chakravarti S, Petroll WM, Hassell JR, et al. Corneal opacity in lumican-null mice: Defects in collagen fibril structure and packing in the posterior stroma. *Invest Ophthalmol Vis Sci.* 2000;41:3365–3373.
- [63] Quantock AJ, Meek KM, Thonar EJ-MA. Analysis of high-angle synchrotron x-ray diffraction patterns obtained from macular dystrophy corneas. *Cornea* 1992;11: 185–190.
- [64] Hayashida Y, Akama TO, Beecher N, et al. Matrix morphogenesis in cornea is mediated by the modification of keratan sulfate by GlcNAc 6-O sulfotransferase. *Proc Natl Acad Sci USA.* 2006;103:13333–13338.
- [65] Young RD, Tudor D, Hayes AJ, et al. Atypical composition and ultrastructure of proteoglycans in the mouse corneal stroma. *Invest Ophthalmol Vis Sci.* 2005;46:1973–1978.
- [66] Scott JE, Haigh M. Keratan sulphate and the ultrastructure of cornea and cartilage: A 'stand-in' for chondroitin sulphate in conditions of oxygen lack? *J Anat.* 1988;158: 95–108.
- [67] Scott JE. Chondroitin sulphate and keratan sulphate are almost isosteric. *Biochem J.* 1991;275:267–268.
- [68] Scott JE. Keratan sulphate—A 'reserve' polysaccharide. *Eur J Clin Chem Clin Biochem.* 1994;32:217–223.
- [69] Stockwell RA, Scott JE. Observations on the acid glycosaminoglycan (mucopolysaccharide) content of the matrix of aging cartilage. *Ann Rheum Dis.* 1965;24:341–350.
- [70] Stockwell RA. Morphometry of cytoplasmic components of mammalian articular chondrocytes and corneal keratocytes: Species and zonal variations of mitochondria in relation to nutrition. *J Anat.* 1991;175:251–261.
- [71] Lewis D, Davies Y, Nieduszyński IA, et al. Ultrastructural localization of sulfated and unsulfated keratan sulfate in normal and macular corneal dystrophy type I. *Glycobiology* 2000;10:305–312.
- [72] Young RD, Akama TO, Liskova P, et al. Differential immunogold localisation of sulphated and unsulphated keratan sulphate proteoglycans in normal and macular dystrophy cornea using sulphation motif-specific antibodies. *Histochem Cell Biol.* 2007;127:115–120.
- [73] Saito T, Nishida K, Nakayama J, et al. Sulfation patterns of keratan sulfate in different macular corneal dystrophy immunophenotypes using three different probes. *Br J Ophthalmol.* 2008;92:1434–1436.

Decorin Accumulation Contributes to the Stromal Opacities Found in Congenital Stromal Corneal Dystrophy

Cecilie Bredrup,^{1,2,3} Espen Stang,⁴ Ove Bruland,³ Barbara P. Palka,⁵ Robert D. Young,⁵ Jan Haavik,⁶ Per M. Knappskog,^{1,3} and Eyvind Rødahl^{1,2}

PURPOSE. Congenital stromal corneal dystrophy (CSCD) is characterized by stromal opacities that morphologically are seen as interlamellar layers of amorphous substance with small filaments, the nature of which has hitherto been unknown. CSCD is associated with truncating mutations in the decorin gene (*DCN*). To understand the molecular basis for the corneal opacities we analyzed the expression of decorin in this disease, both at the morphologic and the molecular level.

METHODS. Corneal specimens were examined after contrast enhancement with cuprolinic blue and by immunoelectron microscopy. Decorin protein from corneal tissue and keratocyte culture was studied by immunoblot analysis before and after O- and N-deglycosylation. The relative level of *DCN* mRNA expression was examined using Q-RT-PCR, and cDNA was sequenced. Recombinant wild-type and truncated decorin transiently expressed in HEK293 cells were analyzed by gel filtration and immunoblotting.

RESULTS. The areas of interlamellar filaments were stained by cuprolinic blue. Immunoelectron microscopy using decorin antibodies revealed intense labeling of these areas. Both wild-type and truncated decorin protein was expressed in corneal tissue and keratocytes of affected persons. When decorin expressed in HEK293 cells was examined by gel filtration, the truncated decorin eluted as high molecular weight aggregates.

CONCLUSIONS. Accumulation of decorin was found in the interlamellar areas of amorphous substance. The truncated decorin is present in CSCD corneas, and there is evidence it may aggregate in vitro. Thus, decorin accumulation appears to contribute to the stromal opacities that are characteristic of CSCD. (*Invest Ophthalmol Vis Sci.* 2010;51:5578–5582) DOI:10.1167/iops.09-4933

Congenital stromal corneal dystrophy (CSCD; Online Mendelian Inheritance in Man 610048) is a rare autosomal dominant disorder characterized by small opacities found

throughout the stroma. These small flakes and spots are present shortly after birth and are thought to be slowly progressive. Most patients will need bilateral corneal transplantations as young adults. By transmission electron microscopy, the opacities can be visualized as layers of thin filaments embedded in an amorphous material that separates apparently normal stromal lamellae. The nature of these opacities has hitherto been unknown. Genetic analysis in two CSCD families has revealed frameshift mutations in the C-terminal part of the decorin gene in affected persons.^{1,2} Both mutations (c.967delT and c.941delC) are predicted to introduce the same premature stop codon, causing the deletion of 33 amino acids in the C-terminal end of the decorin protein.^{1,2}

Decorin is a small leucine-rich proteoglycan (SLRP) involved in several important biological processes, including collagen fibrillogenesis and matrix assembly.^{3,4} Decorin-deficient mice have abnormal collagen morphology in skin and tendons but have clear corneas.⁵ This indicates that decorin is not essential for corneal transparency. To improve our understanding of why heterozygous truncating mutations in the decorin gene cause corneal clouding, we analyzed decorin expression in CSCD corneas morphologically and at a molecular level.

MATERIALS AND METHODS

Patients with CSCD and unaffected persons were invited to participate in the study. Informed written consent was obtained from all participants. The study was approved by the Regional Committee for Medical and Research Ethics, Western Norway (IRB 00001872) and adhered to the tenets of the Declaration of Helsinki.

Tissue Samples

Skin biopsy samples were obtained from the forearm skin of affected persons carrying the c.967delT mutation and from healthy family members. A CSCD corneal button was available after therapeutic corneal grafting. The clinical findings of the patient have previously been described (V-6 in Bredrup et al.¹). An unaffected cornea was obtained from an unrelated person who had an eye removed because of malignant choroidal melanoma.

Cuprolinic Blue Staining

CSCD and healthy corneal samples were plunge frozen and stored in liquid nitrogen. Thawed samples were fixed overnight in 2.5% glutaraldehyde in 25 mM sodium acetate buffer, pH 5.7, containing 0.1 M magnesium chloride and 0.05% cuprolinic blue (BioSciences, Warrington, PA). The samples were washed in 25 mM sodium acetate buffer, then transferred to aqueous 0.5% sodium tungstate for 15 minutes, followed by 50% ethanolic 0.5% sodium tungstate for 15 minutes. Specimens were dehydrated in an ascending ethanol series, followed by propylene oxide, and were infiltrated with Araldite resin. They were embedded in moulds with fresh resin and were cured for 24

From the Departments of ¹Clinical Medicine and ⁶Biomedicine, University of Bergen, Bergen, Norway; the ²Department of Ophthalmology and the ³Center for Medical Genetics and Molecular Medicine, Haukeland University Hospital, Bergen, Norway; the ⁴Department of Pathology, Oslo University Hospital, Rikshospitalet, Oslo, Norway; and the ⁵Structural Biophysics Group, School of Optometry and Vision Sciences, Cardiff University, Cardiff, Wales, United Kingdom.

Supported by grants from the Western Norway Regional Health Authority.

Submitted for publication November 16, 2009; revised March 26 and April 16, 2010; accepted May 8, 2010.

Disclosure: C. Bredrup, None; E. Stang, None; O. Bruland, None; B.P. Palka, None; R.D. Young, None; J. Haavik, None; P.M. Knappskog, None; E. Rødahl, None

Corresponding author: Eyvind Rødahl, Department of Ophthalmology, Haukeland University Hospital, 5021 Bergen, Norway; cyvind.rodahl@helse-bergen.no.

hours at 60°C. Ultrathin sections were cut with a diamond knife, collected on uncoated copper grids, stained with 1% phosphotungstic acid and saturated uranyl acetate solutions, and examined in a transmission electron microscope (EM208; Philips, Eindhoven, The Netherlands).

Immunoelectron Microscopy

Corneal specimens were fixed using 4% paraformaldehyde and 0.1% glutaraldehyde in 0.1 M phosphate buffer for 2 hours and processed for cryosectioning and immunolabeling essentially as previously described.⁶ Some sections were incubated with 0.4 U/mL chondroitinase ABC in 0.1 M Tris acetate, pH 6.8, for 1 hour at room temperature and washed in PBS before blocking and immunolabeling. Bound antibodies were visualized using protein A gold (G. Posthuma, Utrecht, The Netherlands). The sections were examined using an electron microscope (CM 120; Philips).⁷

Three decorin antibodies were used—goat anti-human decorin antibody AF143 (R&D Systems, Minneapolis, MN) and two rabbit antisera, LF-136 and LF-122, generously provided by Larry Fisher (Dept. of Health and Human Services, NIH, Bethesda, MD). The target for LF-136 is an N-terminal peptide,⁸ and that for LF-122⁹ and AF143 is recombinant human decorin. When labeling with the goat anti-decorin antibody, a rabbit anti-goat IgG antibody (Cappel; ICN Biochemicals Costa Mesa, CA) was used as secondary antibody before incubation with protein A gold.

Extraction of Decorin from Corneal Tissue

Untreated corneal samples that had been stored in liquid nitrogen were added to 200 μ L lysis buffer (5 mM EDTA, 150 mM NaCl, 0.002 M phenylmethylsulfonyl fluoride, 50 mM Tris-HCl, pH 7.5) containing 1 μ L protease inhibitor cocktail (P8340; Sigma-Aldrich, St. Louis, MO). The sample was homogenized (TissueLyser II; Qiagen, Hilden, Germany) for 200 seconds before the addition of 1 μ L Nonidet P-40, 1 μ L Tween 20, and 1 μ L 20% sodium dodecyl sulphate (SDS) and was incubated at 37°C for 30 minutes. The sample was centrifuged at 16000g for 10 minutes, and the supernatant was collected.

Keratocyte and Fibroblast Cultures

Skin biopsy specimens and part of the corneal buttons were cut into small pieces. Keratocytes and fibroblasts were cultivated (Amnionchrome II with Amnionchrome II Supplement modified; Lonza, Verviers, Belgium) at 37°C with 5% CO₂. When fully confluent, the cells were transferred (Amnionchrome II without Supplement; Lonza), and the medium was harvested after 6 hours. Cells were lysed using 50 mM Tris-HCl, pH 7.5, containing 200 mM NaCl, 5 mM EDTA, 1% Igepal, 1 μ g/mL aprotinin, 1 mM phenylmethylsulfonyl fluoride, complete protease inhibitor cocktail (Roche Diagnostics GmbH, Mannheim, Germany), 0.5% Tween, and 0.1% SDS.

RNA Analyses

Total RNA was purified from the corneal specimen and HEK293 cells (TissueLyser and RNeasy kits; Qiagen). The quality of the purified RNA was analyzed (Experion system; Bio-Rad, Hercules, CA), and cDNA synthesis was performed (TaqMan Reverse Transcription kit; ABI, Foster City, CA). *DCN* RNA expression was determined using quantitative reverse transcriptase-PCR (Q-RT-PCR) using ABI primers and probes (Assay on Demand; HS00266491) and was analyzed (7900 instrument; ABI). Expression of β -actin was used as an endogenous normalization control.

PCR amplification of *DCN* from cDNA of cultured corneal cells was performed with forward primer (5'-GAGGGAGCTTCACTTGGACAACA-3') and reverse primer (5'-GAATGGCAGAGCGCACGTAG-3'), and the PCR product was sequenced.

Construction of Plasmids

Both wild-type and mutant *DCN* from a heterozygous sample were cloned by PCR amplification of cDNA using forward primer (5'-cgcg-

gatccGCAAATTCGCGGATTAAA-3') and reverse primer (5'-ctagtctagaTGCATAATAAGTCATGTGGGTAA-3'), with sequences incorporating restriction sites facilitating cloning added at the 5'-end (lower caps). PCR products were digested and ligated into the pCDNA3.1(+) vector (Invitrogen, Carlsbad, CA) using the *Bam*HI and *Xba*I restriction enzymes (NEB; Ipswich, MA). All plasmids were verified by DNA sequencing.

Transient Transfection of Cells

Human embryonic kidney cells (HEK293) were grown in Dulbecco's modified Eagle medium (DMEM; Gibco, Auckland, New Zealand) supplemented with 10% fetal calf serum. Six million cells were plated onto 10-cm dishes the day before transfection to obtain 90% to 95% confluence at transfection. The transfection mixture contained 60 μ L reagent (Lipofectamine 2000; Invitrogen), 24 μ g expression vector (wild-type and mutated decorin), or empty vector as a negative control. Transfection was performed according to the manufacturer's recommendations. A GFP expression vector (pSiren RetroQ, 2.5 μ g; Clontech Laboratories, Mountain View, CA) was added as an internal control of transfection efficacy. The medium was changed daily. At 48 hours after transfection, the cells were transferred to serum-free DMEM for 6 hours, and the medium was then harvested.

N- and O-Deglycosylation Using Chondroitinase ABC and N-Glycosidase F

Homogenized corneal tissue or cell culture medium (50 μ L) with 1 μ L protease inhibitor cocktail P8340 and 10 μ L chondroitinase ABC (Sigma-Aldrich; 0.01 U/ μ L in 50 mM Tris-HCl buffer, pH 8.0, containing 60 mM sodium acetate and 0.02% bovine serum albumin [BSA]) was incubated at 37°C for 6 hours. After acetone precipitation, the pellet was dissolved in either 20 μ L sample buffer (Invitrogen) for immunoblotting or in 25 μ L of 20 mM sodium phosphate buffer, pH 7.2, containing 1% SDS for further N-deglycosidase F digestion.

For N-deglycosylation alone, a sample with acetone-precipitated cell culture medium (50 μ L) dissolved in 25 μ L of 20 mM sodium phosphate buffer, pH 7.2, containing 1% SDS was prepared. Both this and the sample that had previously undergone O-deglycosylation were denatured by heating to 100°C for 2 minutes. The reaction mixtures were then adjusted to contain 10 mM EDTA, 0.5% Nonidet P-40, 0.1% SDS, and 1% 2-mercaptoethanol in 20 mM sodium phosphate buffer, pH 7.2, in a total volume of 150 μ L. One unit of N-glycosidase F (Roche Diagnostics GmbH) was added, and the samples were incubated for 1 hour at 37°C. One additional unit of N-glycosidase F was then added, and the incubations continued for another hour.

Western Blot Analysis

Proteins were separated with a high-resolution gel system (12% Nu-PAGE Novex Bis-Tris Gel; Invitrogen) according to the manufacturer's instructions and were electrophoretically transferred to nitrocellulose membranes (Bio-Rad, Hercules, CA). After blocking with 5% nonfat dry milk (Bio-Rad), 1% glycine, and 1% BSA in PBS-T buffer (PBS containing 0.05% Tween 20), the membranes were incubated overnight at 4°C with goat anti-human decorin antibody (R&D Systems) at a dilution of 0.05 μ g/mL. Membranes were washed with PBS containing 0.05% Tween 20 and incubated with horseradish peroxidase-conjugated anti-goat IgG (Santa Cruz Biotechnology, Santa Cruz, CA) at a dilution of 0.2 μ g/mL for 2 hours at room temperature. Proteins were visualized (Super Signal West Pico system; Pierce, Rockford, IL), and protein standard (MagicMark; Invitrogen) was used as a molecular weight marker.

Gel Filtration of Decorin

Medium from transfected HEK293 cells was concentrated approximately 50 times with a centrifugal filter (Amicon Ultra, 10K NMWL; Millipore, Billerica, MA) and diluted in 10 mM HEPES buffer, pH 7.4,

containing 150 mM NaCl, 3.4 mM EDTA, and 0.005% (vol/vol) surfactant P20.

Samples (500 μ L) were run on a column (Superdex 200 HR 10/30; Amersham Biosciences, Piscataway, NJ) connected to a chromatography system (BioLogic HR; Bio-Rad) with absorbance detection at 280 nm and a flow rate of 0.2 mL/min at 4°C. The column was equilibrated in 10 mM HEPES buffer, pH 7.4, containing 150 mM NaCl, 3.4 mM EDTA, and 0.005% (vol/vol) surfactant P20. The column was calibrated using the following proteins as standards: catalase (MWt, 250 kDa), BSA (MWt, 66 kDa), and lysozyme (MWt, 14.3 kDa). Fractions (500 μ L) were collected and subjected to immunoblot analysis using affinity-purified antibodies against recombinant human decorin.

RESULTS

Cuprolinic Blue Staining

The healthy corneal sample had a normal ultrastructure. Some fracture lines, interpreted as freeze-thaw artifacts, were found (Fig. 1A). In contrast, the CSCD cornea was severely disorganized. Areas of amorphous substance with small filaments disrupted layers of apparently normal collagen fibrils. These areas were often located in the immediate vicinity of keratocytes. In some places, the lamellar structure of collagen fibrils appeared to disintegrate (Fig. 1B). The abnormal filaments seen in the CSCD cornea stained with cuprolinic blue, indicating the presence of sulfated glycosaminoglycans (GAGs; Fig. 1D). Cuprolinic blue staining was also found along the collagen fibrils in CSCD and in healthy corneas (Fig. 1).

Immunoelectron Microscopy

When examining normal and CSCD corneas by immunoelectron microscopy, decorin immunolabeling was located along collagen fibrils. This was particularly prominent when using the R&D System goat anti-decorin antibody (Fig. 2). A similar pattern was seen with antibody LF-136, whereas LF-122 did not

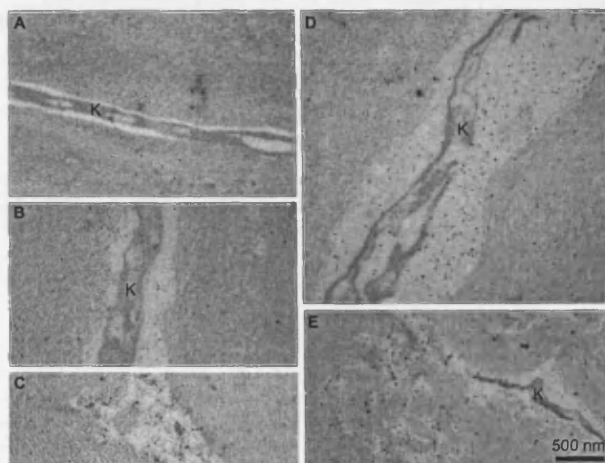


FIGURE 2. Electron micrographs of corneal stroma after labeling with an anti-decorin antibody. (A) Section of healthy cornea treated with chondroitinase ABC before labeling. Labeling is diffusely distributed along collagen fibrils. (B–E) Sections of CSCD cornea without (B, C) or with (D, E) chondroitinase ABC treatment before labeling. Labeling is localized to small filaments in the amorphous area near keratocytes (K; B, D), and in areas with abnormal filaments (C, E).

label the collagen fibrils (data not shown). In addition, strong decorin immunolabeling was found in the abnormal areas of CSCD cornea, particularly in the areas with abnormal filaments. This finding was similar for all three decorin antibodies. Decorin immunolabeling of keratocytes was not above background. Chondroitinase ABC treatment strongly increased decorin immunolabeling (Fig. 2), particularly for antibody LF-122 (data not shown).

Decorin Expression in Patient Samples

Primary keratocyte cultures from a person heterozygous for the c.967delT mutation (hetDCN) and from an unaffected person (normDCN) were established. No major differences regarding the morphology of the cells could be observed. Both cell types had to be fully confluent for high levels of decorin to be secreted into the medium. Sequencing of cDNA from cultured hetDCN corneal cells revealed that both wild-type transcripts and transcripts with the deletion were present (data not shown).

Supernatant from homogenized cornea and medium from cultured keratocytes were examined by immunoblot analysis before and after treatment with chondroitinase ABC and N-glycosidase F. In both hetDCN and normDCN samples, decorin was detected as a diffuse band with molecular weights of approximately 80 kDa and 90 kDa in the medium from keratocyte culture and homogenized cornea, respectively. The wild-type decorin expressed in hetDCN samples, particularly from corneal tissue, appeared to migrate slightly faster than that expressed in the normDCN samples. No difference in glycosylation was observed, as assessed by chondroitinase ABC or N-glycosidase F treatment between hetDCN and normDCN samples (Fig. 3).

After treatment with chondroitinase ABC and N-glycosidase F, a single band of approximately 41 kDa, as determined by molecular weight markers (MagicMark; Invitrogen) was observed in the normDCN samples, whereas two clearly distinguishable bands (41 and 37 kDa) were seen in the hetDCN samples (Fig. 3). The same pattern was seen in cultured fibroblasts (data not shown). Decorin was not detected by immunoblot analysis of normDCN and hetDCN keratocyte lysates (data not shown).

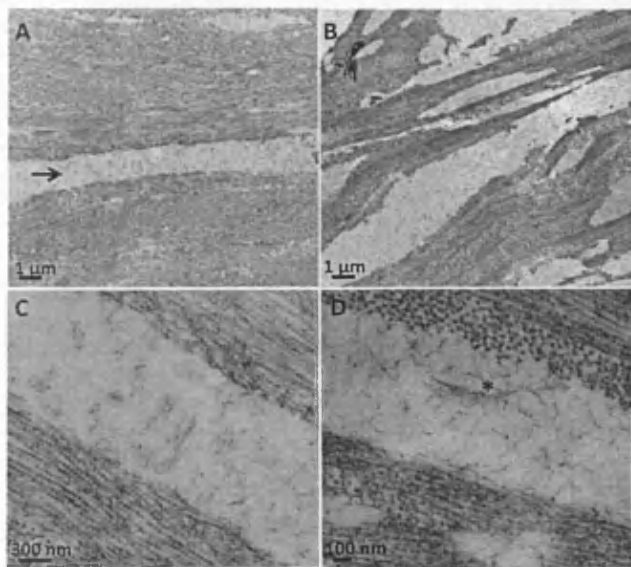


FIGURE 1. Electron micrographs of corneal stroma after cuprolinic blue staining. (A) Overview of healthy cornea showing normal stromal architecture with some freeze-thaw breaks (arrow). (B) CSCD cornea with areas of small filaments separating what appear to be normal lamellae. (C) Detail of a freeze-thaw break in healthy cornea showing minimal staining with cuprolinic blue. (D) Detail of an area with abnormal filaments showing strong staining with cuprolinic blue. Asterisk: in some places the filaments seem to form longer structures.

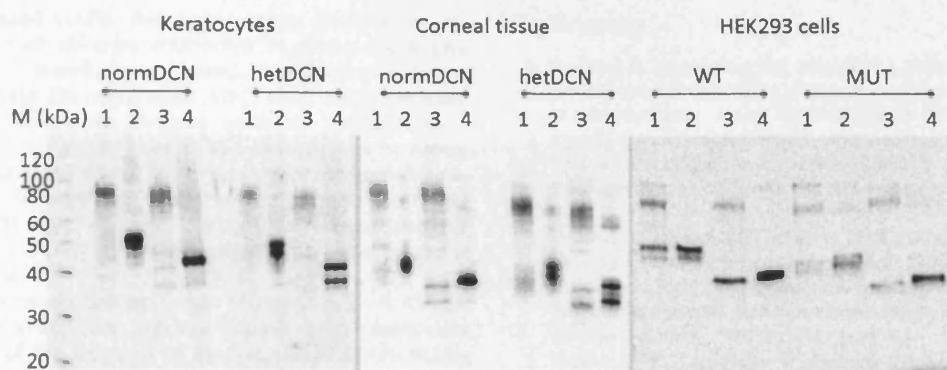


FIGURE 3. Western blot analysis of decorin. Shown are untreated samples (1), samples treated with chondroitinase ABC (2), N-glycosidase F (3), and samples treated with both chondroitinase ABC and N-glycosidase F (4) from keratocytes, corneal tissue, and HEK293 cells. Keratocytes and corneal tissue were obtained from either a healthy cornea (normDCN) or a CSCD cornea heterozygous for the c.967delT mutation (hetDCN). The HEK293 cells had been transfected with either WT or MUT *DCN* cDNA. Separate gels were used for samples from keratocytes, corneal tissue, and HEK293 cells. Different migration between gels is attributed to variation in electrophoresis time. M, molecular weight marker.

Transient Transfection of Cells

HEK293 cells were transfected with plasmids containing wild-type decorin (WT) or *DCN* cDNA with the c.967delT mutation (MUT). Low endogenous expression of decorin was found in HEK293 cells by Q-RT-PCR, with a cycle threshold of approximately 35. Decorin could not be identified by immunoblot analysis of cells transfected with GFP expression vector alone (data not shown). On immunoblot analysis, decorin was detected as four bands (80, 65, 48, and 45 kDa; Fig. 3). After complete N- and O-deglycosylation, a single band of 39 kDa and 35 kDa in the WT and MUT samples, respectively, was left. All bands in the MUT sample had slightly lower molecular weight corresponding to the expression of a truncated protein (Fig. 3).

Gel Filtration

Medium from WT- and MUT-transfected HEK293 cells were subjected to size exclusion chromatography using a high-resolution gel filtration column (Superdex 200 HR 10/30; Amersham Biosciences; Freiburg, Germany). The fractionation range for globular proteins on this column is between 10 and 600 kDa. The UV absorption profile was similar for WT and MUT media. Fractions were subjected to immunoblot analysis; in the WT medium, decorin was detected across 12 fractions in a broad molecular weight range. Medium from MUT-transfected cells showed a different pattern. Here decorin was found in only five fractions starting in the void volume of the column, corresponding to the presence of decorin as aggregates (Fig. 4).

Immunoblot analyses of early WT fractions showed decorin as a diffuse band with an estimated molecular weight around 80 kDa. The molecular weight was gradually reduced in later fractions, suggesting varying degrees of glycosylation of decorin. In all MUT fractions, decorin was detected as a major band with an estimated molecular weight of 40 kDa. Higher molecular weight bands were also observed (Fig. 4).

DISCUSSION

CSCD is characterized by stromal layers of abnormal filaments, randomly arranged and loosely embedded in an amorphous substance.^{1,10-12} In the present study a CSCD cornea, exhibiting these typical findings, was available for cuprolinic blue staining and immunoelectron microscopy. The abnormal filaments were found to stain with cuprolinic blue, indicating the

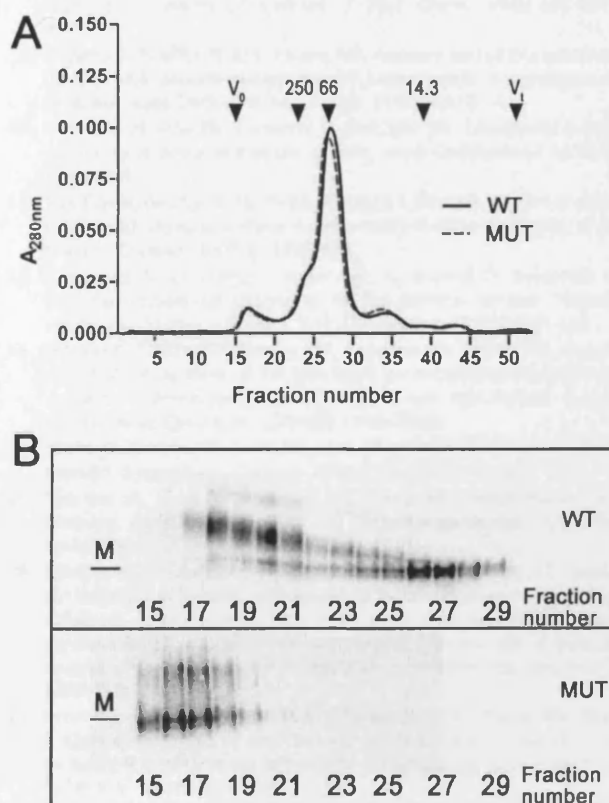


FIGURE 4. Size exclusion chromatography of medium from transfected HEK293 cells. (A) UV absorption of WT and MUT media. The fractionation range for globular proteins on this column is between 10 and 600 kDa. (B) Immunoblot analysis of WT and MUT fractions. In the WT medium, decorin is present in a broad molecular weight range, whereas in the MUT medium, decorin is found in a few early fractions, starting in the void volume of the column. Downward arrows: position of protein standards; molecular weights are shown above. Catalase (MWt, 250 kDa), BSA (MWt, 66 kDa), lysozyme (MWt, 14.3 kDa). Vo, void volume; Vp, total volume; M, molecular weight marker corresponding to 40 kDa.

presence of sulfated GAGs. Immunoelectron microscopy revealed staining with decorin antibodies in these areas and where disorganized lamellae were found. Staining was stronger after treatment with chondroitinase ABC, most likely because the GAG chain of decorin disturbs antibody recognition.¹³ Deposition of various substances in the keratocytes or extracellular matrix has been found in several other stromal dystrophies. Examples include the transforming growth factor- β -induced gene (*TGFBI*) corneal dystrophies, lattice corneal dystrophy type II, Schnyder corneal dystrophy, and macular corneal dystrophy.^{14,15}

The two decorin mutations found associated with CSCD, c.967delT and c.941delC, are predicted to produce a truncated protein because of the deletion of 33 C-terminal amino acids. Analyses of mRNA in a person carrying the c.967delT mutation showed that both the wild-type and the mutated allele are transcribed. By Western blot analysis, the presence of both WT and truncated decorin protein could be observed in corneal tissue and in keratocyte and fibroblast cell cultures. Decorin contains a single chondroitin/dermatan sulfate GAG chain attached to a serine residue near the N terminus¹⁶ and three N-linked oligosaccharides.¹⁷ These would theoretically not be affected by the C-terminal decorin truncation found in CSCD.

Decorin is a class I SLRP with a core of 12 leucine-rich repeats (LRR) flanked by cysteine-rich capping domains important for the stability of the protein.¹⁸ The LRR domain forms a curved solenoid fold, with the second-to-last LRR (the ear repeat) spanning away from the main solenoid and coming back at the last LRR. The truncation is likely to disrupt the disulfide bond between Cys283 and Cys316 in the mature protein (corresponding to amino acids 313–346 in the unprocessed gene product) that connects the last LRR to the top of the ear repeat. It is thought that this disulfide bond is important for folding the ear repeat back to complete the solenoid and thus to maintain the structure of the protein.^{17,18} The decorin mutations found associated with CSCD are, therefore, likely to result in an altered protein structure with other properties than WT.

When concentrated medium from WT HEK293 cells was subjected to size exclusion chromatography, decorin eluted over a broad molecular weight range. In contrast, when medium from MUT HEK293 cells was examined, decorin eluted in the void volume of the column. The finding of decorin from the MUT sample as high molecular weight complexes suggested that the truncated decorin was more likely than the WT decorin to aggregate *in vitro*. Decorin is known to form dimers¹⁹ and probably also larger protein complexes, and it interacts with a number of other proteins. The precise nature of the high molecular weight complexes observed in the MUT sample is unknown. Varying degrees of glycosylation were observed in the WT sample, a feature of HEK293 cells previously described by others.²⁰ The same pattern was not observed in the MUT sample, possibly because the presence of truncated decorin in aggregates prevented the separation of proteins with varying degrees of glycosylation.

In conclusion, we provide evidence that decorin accumulates in the amorphous areas with small filaments that cause the stromal opacities in CSCD. Truncated decorin is expressed in patients with CSCD and is more likely than WT to form high-molecular weight complexes. These altered molecular features could be important for the accumulation of decorin in CSCD.

Acknowledgments

The authors thank Helge Boman for valuable advice and continuous support throughout this work, Andrew Quantock and Ingeborg Winge for professional assistance, and Jorunn Bringsli for technical assistance.

References

- Bredrup C, Knappskog PM, Majewski J, Rødahl E, Boman H. Congenital stromal dystrophy of the cornea caused by a mutation in the decorin gene. *Invest Ophthalmol Vis Sci*. 2005;46:420–426.
- Rødahl E, Van Ginderdeuren R, Knappskog PM, Bredrup C, Boman H. A second decorin frame shift mutation in a family with congenital stromal corneal dystrophy. *Am J Ophthalmol*. 2006;142:520–521.
- Goldoni S, Seidler DG, Heath J, et al. An antimetastatic role for decorin in breast cancer. *Am J Pathol*. 2008;173:844–855.
- Goldoni S, Iozzo RV. Tumor microenvironment: modulation by decorin and related molecules harboring leucine-rich tandem motifs. *Int J Cancer*. 2008;123:2473–2479.
- Danielson KG, Baribault H, Holmes DF, Graham H, Kadler KE, Iozzo RV. Targeted disruption of decorin leads to abnormal collagen fibril morphology and skin fragility. *J Cell Biol*. 1997;136:729–743.
- Griffiths G, McDowall A, Back R, Dubochet J. On the preparation of cryosections for immunocytochemistry. *J Ultrastruct Res*. 1984;89:65–78.
- Stang E, Blystad FD, Kazacic M, et al. Cbl-dependent ubiquitination is required for progression of EGF receptors into clathrin-coated pits. *Mol Biol Cell*. 2004;15:3591–3604.
- Fisher LW, Termine JD, Young MF. Deduced protein sequence of bone small proteoglycan I (biglycan) shows homology with proteoglycan II (decorin) and several nonconnective tissue proteins in a variety of species. *J Biol Chem*. 1989;264:4571–4576.
- Fisher LW, Stubbs JT 3rd, Young MF. Antisera and cDNA probes to human and certain animal model bone matrix noncollagenous proteins. *Acta Orthop Scand Suppl*. 1995;266:61–65.
- Witschel H, Fine BS, Grutzner P, McTigue JW. Congenital hereditary stromal dystrophy of the cornea. *Arch Ophthalmol*. 1978;96:1043–1051.
- Van Ginderdeuren R, De Vos R, Casteels I, Foets B. Report of a new family with dominant congenital hereditary stromal dystrophy of the cornea. *Cornea*. 2002;21:118–120.
- Pouliquen Y, Lacombe E, Schreinzer C, Giraud JP, Savoldelli M. [Familial congenital dystrophy of the corneal stroma: Turpin's syndrome (author's transl)]. *J Fr Ophtalmol*. 1979;2:115–125.
- Bianco P, Fisher LW, Young MF, Termine JD, Robey PG. Expression and localization of the two small proteoglycans biglycan and decorin in developing human skeletal and non-skeletal tissues. *J Histochem Cytochem*. 1990;38:1549–1563.
- Weiss JS, Möller HU, Lisch W, et al. The IC3D classification of the corneal dystrophies. *Cornea*. 2008;27(suppl 2):S1–S83.
- Vincent AL, Patel DV, McGhee CN. Inherited corneal disease: the evolving molecular, genetic and imaging revolution. *Clin Exp Ophthalmol*. 2005;33:303–316.
- Chopra RK, Pearson CH, Pringle GA, Fackre DS, Scott PG. Dermatan sulphate is located on serine-4 of bovine skin proteodermatan sulphate: demonstration that most molecules possess only one glycosaminoglycan chain and comparison of amino acid sequences around glycosylation sites in different proteoglycans. *Biochem J*. 1985;232:277–279.
- Scott PG, McEwan PA, Dodd CM, Bergmann EM, Bishop PN, Bella J. Crystal structure of the dimeric protein core of decorin, the archetypal small leucine-rich repeat proteoglycan. *Proc Natl Acad Sci U S A*. 2004;101:15633–15638.
- McEwan PA, Scott PG, Bishop PN, Bella J. Structural correlations in the family of small leucine-rich repeat proteins and proteoglycans. *J Struct Biol*. 2006;155:294–305.
- Scott PG, Grossmann JG, Dodd CM, Sheehan JK, Bishop PN. Light and X-ray scattering show decorin to be a dimer in solution. *J Biol Chem*. 2003;278:18353–18359.
- Graham FL, Smiley J, Russell WC, Nairn R. Characteristics of a human cell line transformed by DNA from human adenovirus type 5. *J Gen Virol*. 1977;36:59–74.

References

- Abbruzzese C, Kuhn U, Molina F, Rama P, De Luca M (2004) Novel mutations in the CHST6 gene causing macular corneal dystrophy. *Clinical Genetics* 65: 120-125.
- Adachi E, Hayashi T (1986) In vitro formation of hybrid fibrils of type V collagen and type I collagen. Limited growth of type I collagen into thick fibrils by type V collagen. *Connective Tissue Research* 14: 257-266.
- Aguirre G, Raber I, Yanoff M, Haskins M (1992) Reciprocal corneal transplantation fails to correct mucopolysaccharidosis VI corneal storage. *Investigative Ophthalmology & Visual Science* 33: 2702-2713.
- Akama TO, Nakayama J, Nishida K, Hiraoka N, Suzuki M, McAuliffe J, Hindsgaul O, Fukuda M, Fukuda MN (2001) Human corneal GlcNAc 6-O-sulfotransferase and mouse intestinal GlcNAc 6-O-sulfotransferase both produce keratan sulfate. *Journal of Biological Chemistry* 276: 16271-16278.
- Akama TO, Nishida K, Nakayama J, Watanabe H, Ozaki K, Nakamura T, Dota A, Kawasaki S, Inoue Y, Maeda N, Yamamoto S, Fujiwara T, Thonar EJ, Shimomura Y, Kinoshita S, Tanigami A, Fukuda MN (2000) Macular corneal dystrophy type I and type II are caused by distinct mutations in a new sulphotransferase gene. *Nature Genetics* 26: 237-241.
- Akimoto Y, Yamakawa N, Furukawa K, Kimata K, Kawakami H, Hirano H (2002) Changes in distribution of the long form of type XII collagen during chicken corneal development. *Journal of Histochemistry and Cytochemistry* 50: 851-862.
- Alberts B, Johnson A, Lewis J, Raff M, Roberts K, Walter P (2002) Molecular biology of the cell. New York: Garland Science.
- Aldave AJ, Sonmez B (2007) Elucidating the molecular genetic basis of the corneal dystrophies: Are we there yet? *Archives of Ophthalmology* 125: 177-186.
- Algvere PV, Torstensson PA, Tengroth BM (1993) Light transmittance of ocular media in living rabbit eyes. *Investigative Ophthalmology & Visual Science* 34: 349-354.
- Alroy J, Haskins M, Birk DE (1999) Altered corneal stromal matrix organization is associated with mucopolysaccharidosis I, III and VI. *Experimental Eye Research* 68: 523-530.
- Alroy J, Orgad U, DeGasperi R, Richard R, Warren CD, Knowles K, Thalhammer JG, Raghavan SS (1992) Canine GM1-gangliosidosis. A clinical, morphologic, histochemical, and biochemical comparison of two different models. *American Journal of Pathology* 140: 675-689.
- Andrikopoulos K, Liu X, Keene DR, Jaenisch R, Ramirez F (1995) Targeted mutation in the col5a2 gene reveals a regulatory role for type V collagen during matrix assembly. *Nature Genetics* 9: 31-36.
- Anseth A (1961) Glycosaminoglycans in the developing corneal stroma. *Experimental Eye Research* 1: 116-121.
- Ashworth JL, Biswas S, Wraith E, Lloyd IC (2006) Mucopolysaccharidoses and the eye. *Survey of Ophthalmology* 51: 1-17.
- Beer T. 1892. Studien über die Accommodation des Vogelauges. *Pflügers Archiv European Journal of Physiology* 53: 175-237.
- Bella J, Eaton M, Brodsky B, Berman HM (1994) Crystal and molecular structure of a collagen-like peptide at 1.9 Å resolution. *Science* 266: 75-81.

- Bellhorn RW, Bellhorn MS (1975) The avian pecten. I. Fluorescein permeability. *Ophthalmic Research* 7: 1-7.
- Benedek GB (1971) Theory of the transparency of the eye. *Applied optics* 10: 459-473.
- Berg RA, Prockop DJ (1973) The thermal transition of a non-hydroxylated form of collagen. Evidence for a role for hydroxyproline in stabilizing the triple-helix of collagen. *Biochemical and Biophysical Research Communications* 52: 115-120.
- Bergmanson JP, Horne J, Doughty MJ, Garcia M, Gondo M (2005) Assessment of the number of lamellae in the central region of the normal human corneal stroma at the resolution of the transmission electron microscope. *Eye Contact Lens* 31: 281-287.
- Bergwerk KE, Falk RE, Glasgow BJ, Rabinowitz YS (2000) Corneal transplantation in a patient with mucopolysaccharidosis type VII (Sly disease). *Ophthalmic Genetics* 21: 17-20.
- Bettelheim FA, Ehrlich SH (1963) Water vapor sorption of mucopolysaccharides. *Journal of Physical Chemistry* 67: 1948-1953.
- Bettelheim FA, Goetz D (1976) Distribution of hexosamines in bovine cornea. *Investigative Ophthalmology & Visual Science* 15: 301-304.
- Bettelheim FA, Plessy B (1975) The hydration of proteoglycans of bovine cornea. *Biochimica et Biophysica Acta* 381: 203-214.
- Bianco P, Fisher LW, Young MF, Termine JD, Robey PG (1990) Expression and localization of the two small proteoglycans biglycan and decorin in developing human skeletal and non-skeletal tissues. *Journal of Histochemistry and Cytochemistry* 38: 1549-1563.
- Birk DE (2001) Type V collagen: heterotypic type I/V collagen interactions in the regulation of fibril assembly. *Micron* 32: 223-237.
- Birk DE, Fitch JM, Babiarz JP, Doane KJ, Linsenmayer TF (1990) Collagen fibrillogenesis in vitro: interaction of types I and V collagen regulates fibril diameter. *Journal of Cell Science* 95: 649-657.
- Birk DE, Fitch JM, Linsenmayer TF (1986) Organization of collagen types I and V in the embryonic chicken cornea. *Investigative Ophthalmology & Visual Science* 27: 1470-1477.
- Birk DE, Lande MA, Fernandez-Madrid FR (1981) Collagen and glycosaminoglycan synthesis in aging human keratocyte cultures. *Experimental Eye Research* 32: 331-339.
- Birk DE, Trelstad RL (1984) Extracellular compartments in matrix morphogenesis: collagen fibril, bundle, and lamellar formation by corneal fibroblasts. *Journal of Cell Biology* 99: 2024-2033.
- Birk DE, Zhang G, Simpson HC (2006) Dysfunctional regulation of fibril assembly and stromal organization in the compound decorin/biglycan-deficient cornea. *Investigative Ophthalmology & Visual Science* 47: E-abstract 2999.
- Birkenmeier EH, Davisson MT, Beamer WG, Ganschow RE, Vogler CA, Gwynn B, Lyford KA, Maltais LM, Wawrzyniak CJ (1989) Murine mucopolysaccharidosis type VII. Characterization of a mouse with beta-glucuronidase deficiency. *Journal of Clinical Investigation* 83: 1258-1266.
- Blaschke UK, Eikenberry EF, Hulmes DJS, Galla H-J, Bruckner P (2000) Collagen XI nucleates self-assembly and limits lateral growth of cartilage fibrils. *Journal of Biological Chemistry* 275: 10370-10378.

- Blaschke UK, Hedbom E, Bruckner P (1996) Distinct isoforms of chicken decorin contain either one or two dermatan sulfate chains. *Journal of Biological Chemistry* 271: 30347-30353.
- Blochberger TC, Cornuet PK, Hassell JR (1992a) Isolation and partial characterization of lumican and decorin from adult chicken corneas. A keratan sulfate-containing isoform of decorin is developmentally regulated. *Journal of Biological Chemistry* 267: 20613-20619.
- Blochberger TC, Vergnes JP, Hempel J, Hassell JR (1992b) cDNA to chick lumican (corneal keratan sulfate proteoglycan) reveals homology to the small interstitial proteoglycan gene family and expression in muscle and intestine. *Journal of Biological Chemistry* 267: 347-352.
- Bonaldo P, Russo V, Bucciotti F, Doliana R, Colombatti A (1990) Structural and functional features of the alpha 3 chain indicate a bridging role for chicken collagen VI in connective tissues. *Biochemistry* 29: 1245-1254.
- Bonanno JA (2003) Identity and regulation of ion transport mechanisms in the corneal endothelium. *Progress in Retinal and Eye Research* 22: 69-94.
- Boote C, Dennis S, Huang Y, Quantock AJ, Meek KM (2005) Lamellar orientation in human cornea in relation to mechanical properties. *Journal of Structural Biology* 149: 1-6.
- Boote C, Dennis S, Newton RH, Puri H, Meek KM (2003) Collagen fibrils appear more closely packed in the prepupillary cornea: optical and biomechanical implications. *Investigative Ophthalmology & Visual Science* 44: 2941-2948.
- Boote C, Hayes S, Jones S, Quantock AJ, Hocking PM, Inglehearn CF, Ali M, Meek KM (2008) Collagen organization in the chicken cornea and structural alterations in the retinopathy, globe enlarged (rge) phenotype--An X-ray diffraction study. *Journal of Structural Biology* 161: 1-8.
- Boote C, Hayes S, Young RD, Kamma-Lorger CS, Hocking PM, Elsheikh A, Inglehearn CF, Ali M, Meek KM (2009) Ultrastructural changes in the retinopathy, globe enlarged (rge) chick cornea. *Journal of Structural Biology* 166: 195-204.
- Borcherding MS, Blacik LJ, Sittig RA, Bizzell JW, Breen M, Weinstein HG (1975) Proteoglycans and collagen fibre organization in human corneal tissue. *Experimental Eye Research* 21: 59-70.
- Bourne WM, Nelson LR, Hodge DO (1997) Central corneal endothelial cell changes over a ten-year period. *Investigative Ophthalmology & Visual Science* 38: 779-782.
- Bozzola JJ, Russell LD. 1992. Electron microscopy. Principles and Techniques for Biologists. Boston: Jones and Bartlett Publishers.
- Bredrup C, Knappskog PM, Majewski J, Rodahl E, Boman H (2005) Congenital stromal dystrophy of the cornea caused by a mutation in the decorin gene. *Investigative Ophthalmology & Visual Science* 46: 420-426.
- Brown DC, Vogel KG (1989) Characteristics of the in vitro interaction of a small proteoglycan (PG II) of bovine tendon with type I collagen. *Matrix* 9: 468-478.
- Burgeson RE, Lunstrum GP, Rokosova B, Rimberg CS, Rosenbaum LM, Keene DR (1990) The structure and function of type VII collagen. *Annals of the New York Academy of Sciences* 580: 32-43.
- Butt WD, Keilin D (1962) Absorption spectra and some other properties of cytochrome c and of its compounds with ligands. *Proceedings of the Royal Society London B* 156: 429-458.
- Cai CX, Fitch JM, Svoboda KK, Birk DE, Linsenmayer TF (1994) Cellular invasion and collagen type IX in the primary corneal stroma in vitro. *Developmental Dynamics* 201: 206-215.

- Calabro A, Plaas AH, Midura RJ, Goodstone NJ, Roden L, Hascall VC (2000) Structure and biosynthesis of chondroitin sulfate and hyaluronan. In: Proteoglycans: structure, biology, and molecular interactions. Iozzo RV, editor. Philadelphia: Marcel Dekker Inc.
- Carlson EC, Liu C-Y, Chikama T-i, Hayashi Y, Kao CWC, Birk DE, Funderburgh JL, Jester JV, Kao WWY (2005) Keratocan, a cornea-specific keratan sulfate proteoglycan, is regulated by lumican. *Journal of Biological Chemistry* 280: 25541-25547.
- Castoro JA, Bettelheim AA, Bettelheim FA (1988) Water gradients across bovine cornea. *Investigative Ophthalmology & Visual Science* 29: 963-968.
- Caterson B, Christner JE, Baker JR (1983) Identification of a monoclonal antibody that specifically recognizes corneal and skeletal keratan sulfate. Monoclonal antibodies to cartilage proteoglycan. *Journal of Biological Chemistry* 258: 8848-8854.
- Caterson B, Mahmoodian F, Sorrell JM, Hardingham TE, Bayliss MT, Carney SL, Ratcliffe A, Muir H (1990) Modulation of native chondroitin sulphate structure in tissue development and in disease. *Journal of Cell Science* 97: 411-417.
- Cenedella RJ, Fleschner CR. 1990. Kinetics of corneal epithelium turnover in vivo. Studies of lovastatin. *Investigative Ophthalmology & Visual Science* 31: 1957-1962.
- Chakravarti S (2006) Focus on molecules: keratocan (KERA). *Experimental Eye Research* 82: 183-184.
- Chakravarti S, Petroll WM, Hassell JR, Jester JV, Lass JH, Paul J, Birk DE (2000) Corneal opacity in lumican-null mice: defects in collagen fibril structure and packing in the posterior stroma. *Investigative Ophthalmology & Visual Science* 41: 3365-3373.
- Chan CC, Green WR, Maumenee IH, Sack GH (1982) Ocular ultrastructural studies of two cases of the Hurler syndrome (systemic mucopolysaccharidoses I-H). *Ophthalmic Paediatrics Genetics* 2: 3-19.
- Chopra RK, Pearson CH, Pringle GA, Fackre DS, Scott PG (1985) Dermatan sulphate is located on serine-4 of bovine skin proteodermatan sulphate. Demonstration that most molecules possess only one glycosaminoglycan chain and comparison of amino acid sequences around glycosylation sites in different proteoglycans. *Biochemical Journal* 232: 277-279.
- Cintron C, Gregory JD, Damle SP, Kublin CL (1990) Biochemical analyses of proteoglycans in rabbit corneal scars. *Investigative Ophthalmology & Visual Science* 31: 1975-1981.
- Connon CJ, Meek KM, Kinoshita S, Quantock AJ (2004) Spatial and temporal alterations in the collagen fibrillar array during the onset of transparency in the avian cornea. *Experimental Eye Research* 78: 909-915.
- Connon CJ, Siegler V, Meek KM, Hodson SA, Caterson B, Kinoshita S, Quantock AJ (2003) Proteoglycan alterations and collagen reorganisation in the secondary avian cornea during development. *Ophthalmic Research* 35: 177-184.
- Conrad GW (1970) Collagen and mucopolysaccharide biosynthesis in the developing chick cornea. *Developmental Biology* 21: 292-317.
- Cornuet PK, Blochberger TC, Hassell JR (1994) Molecular polymorphism of lumican during corneal development. *Investigative Ophthalmology & Visual Science* 35: 870-877.
- Corpuz LM, Funderburgh JL, Funderburgh ML, Bottomley GS, Prakash S, Conrad GW (1996) Molecular cloning and tissue distribution of keratocan. *Journal of Biological Chemistry* 271: 9759-9763.

- Corsi A, Xu T, Chen XD, Boyde A, Liang J, Mankani M, Sommer B, Iozzo RV, Eichstetter I, Robey PG, Bianco P, Young MF (2002) Phenotypic effects of biglycan deficiency are linked to collagen fibril abnormalities, are synergized by decorin deficiency, and mimic Ehlers-Danlos-like changes in bone and other connective tissues. *Journal of Bone and Mineral Research* 17: 1180-1189.
- Coulombre AJ, Coulombre JL (1958a) Corneal development. I. Corneal transparency. *Journal of Cellular and Comparative Physiology* 51: 1-11.
- Coulombre AJ, Coulombre JL (1958b) The Role of Intraocular Pressure in the Development of the Chick Eye: IV. Corneal Curvature. *AMA Archives of Ophthalmology* 59: 502-506.
- Dang X, Zhu Q, Wang L, Su H, Lin H, Zhou N, Liang T, Wang Z, Huang S, Ren Q, Qi Y (2009) Macular corneal dystrophy in a Chinese family related with novel mutations of CHST6. *Molecular Vision* 15: 700-705.
- Danielson KG, Baribault H, Holmes DF, Graham H, Kadler KE, Iozzo RV (1997) Targeted disruption of decorin leads to abnormal collagen fibril morphology and skin fragility. *Journal of Cell Biology* 136: 729-743.
- Davanger M, Evensen A (1971) Role of the pericorneal papillary structure in renewal of corneal epithelium. *Nature* 229: 560-561.
- Del Monte MA, Maumenee IH, Green WR, Kenyon KR (1983) Histopathology of Sanfilippo's syndrome. *Archives of Ophthalmology* 101: 1255-1262.
- Di Iorio E, Barbaro V, Volpi N, Bertolin M, Ferrari B, Fasolo A, Arnaldi R, Brusini P, Prosdocimo G, Ponzin D, Ferrari S (2010) Localization and expression of CHST6 and keratan sulfate proteoglycans in the human cornea. *Experimental Eye Research* 91: 293-299.
- Donnenfeld ED, Cohen EJ, Ingraham HJ, Poleski SA, Goldsmith E, Laibson PR (1986) Corneal thinning in macular corneal dystrophy. *American Journal of Ophthalmology* 101: 112-113.
- Doutch J, Quantock AJ, Smith VA, Meek KM (2008) Light transmission in the human cornea as a function of position across the ocular surface: theoretical and experimental aspects. *Biophysical Journal* 95: 5092-5099.
- Dunlevy JR, Beales MP, Berryhill BL, Cornuet PK, Hassell JR (2000) Expression of the keratan sulfate proteoglycans lumican, keratocan and osteoglycin/mimecan during chick corneal development. *Experimental Eye Research* 70: 349-362.
- Dunlevy JR, Neame PJ, Vergnes J-P, Hassell JR (1998) Identification of the N-linked oligosaccharide sites in chick corneal lumican and keratocan that receive keratan sulfate. *Journal of Biological Chemistry* 273: 9615-9621.
- Edward DP, Yue BY, Sugar J, Thonar EJ, Sunder Raj N, Stock EL, Tso MO (1988) Heterogeneity in macular corneal dystrophy. *Archives of Ophthalmology* 106: 1579-1583.
- Ehlers N, Bramsen T (1978) Central thickness in corneal disorders. *Acta Ophthalmologica* 56: 412-416.
- El-Ashry MF, Abd El-Aziz MM, Shalaby O, Bhattacharya SS (2010) Molecular genetic study of Egyptian patients with macular corneal dystrophy. *British Journal of Ophthalmology* 94: 250-255.
- El-Ashry MF, Abd El-Aziz MM, Shalaby O, Wilkins S, Poopalasundaram S, Cheetham ME, Tuft SJ, Hardcastle AJ, Bhattacharya SS, Ebenezer ND (2005) Novel CHST6 nonsense and missense mutations responsible for macular corneal dystrophy. *American Journal of Ophthalmology* 139: 192-193.

- El-Ashry MF, El-Aziz MMA, Wilkins S, Cheetham ME, Wilkie SE, Hardcastle AJ, Halford S, Bayoumi AY, Ficker LA, Tuft S, Bhattacharya SS, Ebenezer ND (2002) Identification of novel mutations in the carbohydrate sulfotransferase gene (CHST6) causing macular corneal dystrophy. *Investigative Ophthalmology & Visual Science* 43: 377-382.
- Farrell RA, McCally RL (2000) Corneal transparency. In: Principles and practice of ophthalmology. Albert DM, Jakobiec FA, editors. Philadelphia: W.B. Saunders Company. pp 629-644.
- Farrell RA, McCally RL, Tatham PE (1973) Wave-length dependencies of light scattering in normal and cold swollen rabbit corneas and their structural implications. *Journal of Physiology* 233: 589-612.
- Feuk T (1970) On the transparency of the stroma in the mammalian cornea. *IEEE Transactions on Biomedical Engineering* 17: 186-190.
- Fisher LW, Hawkins GR, Tuross N, Termine JD (1987) Purification and partial characterization of small proteoglycans I and II, bone sialoproteins I and II, and osteonectin from the mineral compartment of developing human bone. *Journal of Biological Chemistry* 262: 9702-9708.
- Fitch J, Fini ME, Beebe DC, Linsenmayer TF (1998) Collagen type IX and developmentally regulated swelling of the avian primary corneal stroma. *Developmental Dynamics* 212: 27-37.
- Fitch JM, Birk DE, Linsenmayer C, Linsenmayer TF (1991) Stromal assemblies containing collagen types IV and VI and fibronectin in the developing embryonic avian cornea. *Developmental Biology* 144: 379-391.
- Fitch JM, Gordon MK, Gibney EP, Linsenmayer TF (1995) Analysis of transcriptional isoforms of collagen types IX, II, and I in the developing avian cornea by competitive polymerase chain reaction. *Developmental Dynamics* 202: 42-53.
- Fitch JM, Gross J, Mayne R, Johnson-Wint B, Linsenmayer TF (1984) Organization of collagen types I and V in the embryonic chicken cornea: monoclonal antibody studies. *Proceedings in the National Academy of Sciences of the United States of America* 81: 2791-2795.
- Fitch JM, Linsenmayer CM, Linsenmayer TF (1994) Collagen fibril assembly in the developing avian primary corneal stroma. *Investigative Ophthalmology & Visual Science* 35: 862-869.
- Fitch JM, Mentzer A, Mayne R, Linsenmayer TF (1988) Acquisition of type IX collagen by the developing avian primary corneal stroma and vitreous. *Developmental Biology* 128: 396-405.
- Forrester J, Dick A, McMenemin P, Lee W (2002) The eye : basic sciences in practice: Edinburgh ; New York : W.B. Saunders. pp1-98 .
- Freund DE, McCally RL, Farrell RA (1986) Direct summation of fields for light scattering by fibrils with applications to normal corneas. *Applied optics* 25: 2739-2746.
- Fukuta M, Inazawa J, Torii T, Tsuzuki K, Shimada E, Habuchi O (1997) Molecular cloning and characterization of human keratan sulfate gal-6-sulfotransferase. *Journal of Biological Chemistry* 272: 32321-32328.
- Fullwood NJ, Davies Y, Nieduszyński IA, Marcyniuk B, Ridgway AE, Quantock AJ (1996) Cell surface-associated keratan sulfate on normal and migrating corneal endothelium. *Investigative Ophthalmology & Visual Science* 37: 1256-1270.
- Fullwood NJ, Tuft SJ, Malik NS, Meek KM, Ridgway AE, Harrison RJ (1992) Synchrotron x-ray diffraction studies of keratoconus corneal stroma. *Investigative Ophthalmology & Visual Science* 33: 1734-1741.
- Funderburgh JL (2000) Keratan sulfate: structure, biosynthesis, and function. *Glycobiology* 10: 951-958.

- Funderburgh JL, Caterson B, Conrad GW (1986) Keratan sulfate proteoglycan during embryonic development of the chicken cornea. *Developmental Biology* 116: 267-277.
- Funderburgh JL, Corpuz LM, Roth MR, Funderburgh ML, Tasheva ES, Conrad GW (1997) Mimecan, the 25-kDa corneal keratan sulfate proteoglycan, is a product of the gene producing osteoglycin. *Journal of Biological Chemistry* 272: 28089-28095.
- Funderburgh JL, Funderburgh ML, Mann MM, Conrad GW (1991) Physical and biological properties of keratan sulphate proteoglycan. *Biochemical Society Transactions* 19: 871-876.
- Funderburgh JL, Hevelone ND, Roth MR, Funderburgh ML, Rodrigues MR, Nirankari VS, Conrad GW (1998) Decorin and biglycan of normal and pathologic human corneas. *Investigative Ophthalmology & Visual Science* 39: 1957-1964.
- Fyfe JC, Kurzhals RL, Lassaline ME, Henthorn PS, Alur PRK, Wang P, Wolfe JH, Giger U, Haskins ME, Patterson DF, Sun H, Jain S, Yuhki N (1999) Molecular basis of feline [beta]-glucuronidase deficiency: an animal model of mucopolysaccharidosis VII. *Genomics* 58: 121-128.
- Garrett DM, Conrad GW (1979) Fibroblast-like cells from embryonic chick cornea, heart, and skin are antigenically distinct. *Developmental Biology* 70: 50-70.
- Gealy EC, Kerr BC, Young RD, Tudor D, Hayes AJ, Hughes CE, Caterson B, Quantock AJ, Ralphs JR (2007) Differential expression of the keratan sulphate proteoglycan, keratocan, during chick corneal embryogenesis. *Histochemistry and Cell Biology* 128: 551-555.
- Gipson IK (1992) Adhesive mechanisms of the corneal epithelium. *Acta Ophthalmologica* 70: 13-17.
- Gipson IK, Spurr-Michaud SJ, Tisdale AS (1987) Anchoring fibrils form a complex network in human and rabbit cornea. *Investigative Ophthalmology & Visual Science* 28: 212-220.
- Gitzelmann R, Bosshard NU, Superti-Furga A, Spycher MA, Briner J, Wiesmann U, Lutz H, Litschi B (1994) Feline mucopolysaccharidosis VII due to beta-glucuronidase deficiency. *Veterinary Pathology Online* 31: 435-443.
- Glasser A, Troilo D, Howland HC (1994) The mechanism of corneal accommodation in chicks. *Vision Research* 34: 1549-1566.
- Goldman JN, Benedek GB, Dohlman CH, Kravitt B (1968) Structural alterations affecting transparency in swollen human corneas. *Investigative Ophthalmology & Visual Science* 7: 501-519.
- Goodfellow JM, Elliott GF, Woolgar AE (1978) X-ray diffraction studies of the corneal stroma. *Journal of Molecular Biology* 119: 237-252.
- Gordon M, Hahn R (2010) Collagens. *Cell and Tissue Research* 339: 247-257.
- Gordon MK, Fitch JM, Foley JW, Gerecke DR, Linsenmayer C, Birk DE, Linsenmayer TF (1997) Type XVII collagen (BP 180) in the developing avian cornea. *Investigative Ophthalmology & Visual Science* 38: 153-166.
- Gordon MK, Foley JW, Linsenmayer TF, Fitch JM (1996) Temporal expression of types XII and XIV collagen mRNA and protein during avian corneal development. *Developmental Dynamics* 206: 49-58.
- Gordon MK, Gerecke DR, Dublet B, Van Der Rest M, Sugrue SP, Olsen BR (1990) The structure of type XII collagen. *Annals of the New York Academy of Sciences* 580: 8-16.
- Gosh M, McCulloch C (1974) The Morquio syndrome - light and electron microscopic findings from two corneas. *Canadian Journal of Ophthalmology* 9: 445-452.

- Grubb JH, Vogler C, Sly WS (2010) New strategies for enzyme replacement therapy for lysosomal storage diseases. *Rejuvenation Research* 13: 229-236.
- Güntürkün O (1998) 1. Sensory physiology: vision. In: Sturkie's avian physiology, Sturkie PD, Whittow GC, editors. Academic Press. pp 1-20.
- Gwynn B, Lueders K, Sands MS, Birkenmeier EH (1998) Intracisternal A-particle element transposition into the murine beta -glucuronidase gene correlates with loss of enzyme activity: a new model for beta -glucuronidase deficiency in the C3H mouse. *Molecular and Cellular Biology* 18: 6474-6481.
- Habuchi O, Hirahara Y, Uchimura K, Fukuta M (1996) Enzymatic sulfation of galactose residue of keratan sulfate by chondroitin 6-sulfotransferase. *Glycobiology* 6: 51-57.
- Hahn RA, Birk DE (1992) beta-D xyloside alters dermatan sulfate proteoglycan synthesis and the organization of the developing avian corneal stroma. *Development* 115: 383-393.
- Hahnel C, Somodi S, Weiss DG, Guthoff RF (2000) The keratocyte network of human cornea: A three-dimensional study using confocal laser scanning fluorescence microscopy. *Cornea* 19: 185-193.
- Hamada R, Giraud JP, Graf B, Pouliquen Y (1972) [Analytical and statistical study of the lamellae, keratocytes and collagen fibrils of the central region of the normal human cornea. (Light and electron microscopy)]. *Archives d'ophtalmologie et revue generale d'ophtalmologie* 32: 563-570.
- Hamburger V, Hamilton HL (1992) A series of normal stages in the development of the chick embryo. *American Journal of Anatomy* 195: 231-272.
- Hardingham TE, Fosang AJ, Hey NJ, Hazell PK, Kee WJ, Ewins RJF (1994) The sulphation pattern in chondroitin sulphate chains investigated by chondroitinase ABC and ACII digestion and reactivity with monoclonal antibodies. *Carbohydrate Research* 255: 241-254.
- Hart GW (1976) Biosynthesis of glycosaminoglycans during corneal development. *Journal of Biological Chemistry* 251: 6513-6521.
- Hart RW, Farrell RA (1969) Light scattering in the cornea. *Journal of the Optical Society of America* 59: 766-774.
- Haskins ME, Aguirre GD, Jezyk PF, Patterson DF (1980) The pathology of the feline model of mucopolysaccharidosis VI. *American Journal of Pathology* 101: 657-674.
- Haskins ME, Desnick RJ, DiFerrante N, Jezyk PF, Patterson DF (1984) Beta-glucuronidase deficiency in a dog: a model of human mucopolysaccharidosis VII. *Pediatric Research* 18: 980-984.
- Hassell JR, Newsome DA, Hascall VC (1979) Characterization and biosynthesis of proteoglycans of corneal stroma from rhesus monkey. *Journal of Biological Chemistry* 254: 12346-12354.
- Hassell JR, Newsome DA, Krachmer JH, Rodrigues MM (1980) Macular corneal dystrophy: failure to synthesize a mature keratan sulfate proteoglycan. *Proceedings of the National Academy of Sciences of the United States of America* 77: 3705-3709.
- Hay ED, Revel JP (1969) Fine structure of the developing avian cornea. Wolsky A, Chen PS, editors. Basel: S. Karager. pp 1-144.
- Hayashida Y, Akama TO, Beecher N, Lewis P, Young RD, Meek KM, Kerr B, Hughes CE, Caterson B, Tanigami A, Nakayama J, Fukada MN, Tano Y, Nishida K, Quantock AJ (2006) Matrix morphogenesis in cornea is mediated by the modification of keratan sulfate by GlcNAc 6-O-sulfotransferase. *Proceedings of the National Academy of Sciences of the United States of America* 103: 13333-13338.

- Hayat MA (1989) Principles and techniques of electron microscopy. The MacMillan Press LTD.
- Hendrix MJ, Hay ED, von der Mark K, Linsenmayer TF (1982) Immunohistochemical localization of collagen types I and II in the developing chick cornea and tibia by electron microscopy. *Investigative Ophthalmology & Visual Science* 22: 359-375.
- Hirsch M, Noske W, Prenant G, Renard G (1999) Fine structure of the developing avian corneal stroma as revealed by quick-freeze, deep-etch electron microscopy. *Experimental Eye Research* 69: 267-277.
- Hodson S, Miller F (1976) The bicarbonate ion pump in the endothelium which regulates the hydration of rabbit cornea. *Journal of Physiology* 263: 563-577.
- Hogan MJ, Alvarado JA, Weddell JE (1971) The cornea. Histology of the human eye An atlas and textbook. Philadelphia: Saunders. pp 89.
- Holmes DF, Gilpin CJ, Baldock C, Ziese U, Koster AJ, Kadler KE (2001) Corneal collagen fibril structure in three dimensions: Structural insights into fibril assembly, mechanical properties, and tissue organization. *Proceedings of the National Academy of Sciences of the United States of America* 98: 7307-7312.
- Huang AJ, Tseng SC (1991) Corneal epithelial wound healing in the absence of limbal epithelium. *Investigative Ophthalmology & Visual Science* 32: 96-105.
- Huang Y, Bron AJ, Meek KM, Vellodi A, McDonald B (1996) Ultrastructural study of the cornea in a bone marrow-transplanted Hurler syndrome patient. *Experimental Eye Research* 62: 377-388.
- Ihanamäki T, Pelliniemi LJ, Vuorio E (2004) Collagens and collagen-related matrix components in the human and mouse eye. *Progress in Retinal and Eye Research* 23: 403-434.
- Iida-Hasegawa N, Furuhashi A, Hayatsu H, Murakami A, Fujiki K, Nakayasu K, Kanai A (2003) Mutations in the CHST6 gene in patients with macular corneal dystrophy: immunohistochemical evidence of heterogeneity. *Investigative Ophthalmology & Visual Science* 44: 3272-3277.
- Iwasaki S, Hosaka Y, Iwasaki T, Yamamoto K, Nagayasu A, Ueda H, Kokai Y, Takehana K (2008) The modulation of collagen fibril assembly and its structure by decorin: an electron microscopic study. *Archives of Histology and Cytology* 71: 37-44.
- Jakus MA (1956) Studies on the cornea. II. The fine structure of Descemet's membrane. *Journal of Biophysical and Biochemical Cytology* 2: 243-252.
- Jester JV (2008) Corneal crystallins and the development of cellular transparency. *Seminars in Cell & Developmental Biology* 19: 82-93.
- Jester JV, Moller-Pedersen T, Huang J, Sax CM, Kays WT, Cavangh HD, Petroll WM, Piatigorsky J (1999) The cellular basis of corneal transparency: evidence for 'corneal crystallins'. *Journal of Cell Science* 112: 613-622.
- Kadler KE, Hill A, Canty-Laird EG (2008) Collagen fibrillogenesis: fibronectin, integrins, and minor collagens as organizers and nucleators. *Current Opinion in Cell Biology* 20: 495-501.
- Kadler KE, Hojima Y, Prockop DJ (1987) Assembly of collagen fibrils de novo by cleavage of the type I pC-collagen with procollagen C-proteinase. Assay of critical concentration demonstrates that collagen self-assembly is a classical example of an entropy-driven process. *Journal of Biological Chemistry* 262: 15696-15701.
- Kadler KE, Holmes DF, Trotter JA, Chapman JA (1996) Collagen fibril formation. *Biochemical Journal* 316: 1-11.

- Kamata Y, Okuyama T, Kosuga M, O'Hira A, Kanaji A, Sasaki K, Yamada M, Azuma N (2001) Adenovirus-mediated gene therapy for corneal clouding in mice with mucopolysaccharidosis Type VII. *Molecular Therapy* 4: 307-312.
- Kamata Y, Tanabe A, Kanaji A, Kosuga M, Fukuhara Y, Li XK, Suzuki S, Yamada M, Azuma N, Okuyama T (2003) Long-term normalization in the central nervous system, ocular manifestations, and skeletal deformities by a single systemic adenovirus injection into neonatal mice with mucopolysaccharidosis VII. *Gene Therapy* 10: 406-414.
- Kamma-Lorger CS, Boote C, Hayes S, Moger J, Burghammer M, Knupp C, Quantock AJ, Sorensen T, Di Cola E, White N, Young RD, Meek KM (2010) Collagen and mature elastic fibre organisation as a function of depth in the human cornea and limbus. *Journal of Structural Biology* 169: 424-430.
- Kao WW, Liu C-Y (2003) The use of transgenic and knock-out mice in the investigation of ocular surface cell biology. *Ocular Surface* 1: 5-19.
- Kao WWY, Funderburgh JL, Xia Y, Liu C-Y, Conrad GW (2006) Focus on molecules: lumican. *Experimental Eye Research* 82: 3-4.
- Keene DR, Lunstrum GP, Morris NP, Stoddard DW, Burgeson RE (1991) Two type XII-like collagens localize to the surface of banded collagen fibrils. *The Journal of Cell Biology* 113: 971-978.
- Klintworth G (2009) Corneal dystrophies. *Orphanet Journal of Rare Diseases* 4: 7.
- Klintworth GF (1994) Disorders of glycosaminoglycans (mucopolysaccharides) and proteoglycans. In: Pathobiology of Ocular Disease, A Dynamic Approach. 2nd ed. Garner A, Klintworth GF, editors. New York, USA: Marcel Dekker Inc. pp 855-892.
- Klintworth GF, Meyer HJ, Dennis R, Hewitt AT, Stock EL, Lenz ME, Hassell JR, Stark WJJ, Kuettner KE, Thonar EJ (1986) Macular corneal dystrophy. Lack of keratan sulfate in serum and cornea. *Ophthalmic Paediatrics and Genetics* 7: 139-143.
- Klintworth GK, Oshima E, al-Rajhi A, al-Saif A, Thonar EJ, Karcioğlu ZA (1997) Macular corneal dystrophy in Saudi Arabia: a study of 56 cases and recognition of a new immunophenotype. *American Journal of Ophthalmology* 124: 9-18.
- Klintworth GK, Smith CF (1983) Abnormalities of proteoglycans and glycoproteins synthesized by corneal organ cultures derived from patients with macular corneal dystrophy. *Laboratory Investigation* 48: 603-612.
- Klintworth GK, Smith CF, Bowling BL (2006) CHST6 mutations in North American subjects with macular corneal dystrophy: a comprehensive molecular genetic review. *Molecular Vision* 12: 159-176.
- Klintworth GK, Vogel FS (1964) Macular corneal dystrophy. An inherited acid mucopolysaccharide storage disease of the corneal fibroblast. *American Journal of Pathology* 45 :565-586.
- Kobe B, Deisenhofer J (1993) Crystal structure of porcine ribonuclease inhibitor, a protein with leucine-rich repeats. *Nature* 366: 751-756.
- Kobe B, Deisenhofer J (1995) Proteins with leucine-rich repeats. *Current Opinion in Structural Biology* 5: 409-416.
- Koch M, Foley JE, Hahn R, Zhou P, Burgeson RE, Gerecke DR, Gordon MK (2001) $\alpha 1(X)$ collagen, a new member of the collagen subfamily, fibril-associated collagens with interrupted triple helices. *Journal of Biological Chemistry* 276: 23120-23126.

- Komai Y, Ushiki T (1991) The three-dimensional organization of collagen fibrils in the human cornea and sclera. *Investigative Ophthalmology & Visual Science* 32: 2244-2258.
- Kostyuk O, Nalovina O, Mubard TM, Regini JW, Meek KM, Quantock AJ, Elliott GF, Hodson SA (2002) Transparency of the bovine corneal stroma at physiological hydration and its dependence on concentration of the ambient anion. *Journal of Physiology* 543: 633-642.
- Krusius T, Finne J, Margolis RK, Margolis RU (1986) Identification of an O-glycosidic mannose-linked sialylated tetrasaccharide and keratan sulfate oligosaccharides in the chondroitin sulfate proteoglycan of brain. *Journal of Biological Chemistry* 261: 8237-8242.
- Kyle JW, Birkenmeier EH, Gwynn B, Vogler C, Hoppe PC, Hoffmann JW, Sly WS (1990) Correction of murine mucopolysaccharidosis VII by a human beta-glucuronidase transgene. *Proceedings in the National Academy of Sciences of the United States of America* 87: 3914-3918.
- Lauder RM, Huckerby TN, Brown GM, Bayliss MT, Nieduszynski IA (2001) Age-related changes in the sulphation of the chondroitin sulphate linkage region from human articular cartilage aggrecan. *Biochemical Journal* 358: 523-528.
- Lavery MA, Green WR, Jabs EW, Luckenbach MW, Cox JL (1983) Ocular histopathology and ultrastructure of Sanfilippo's syndrome, type III-B. *Archives of Ophthalmology* 101: 1263-1274.
- Leonard DW, Meek KM (1997) Refractive indices of the collagen fibrils and extrafibrillar material of the corneal stroma. *Biophysical Journal* 72: 1382-1387.
- Lerman S (1984) Biophysical aspects of corneal and lenticular transparency. *Current Eye Research* 3: 3-14.
- Levy GA (1953). beta-Glucuronidase and related enzymes. *British Medical Bulletin* 9: 126-130.
- Lewis D, Davies Y, Nieduszynski IA, Lawrence F, Quantock AJ, Bonshek R, Fullwood NJ (2000) Ultrastructural localization of sulfated and unsulfated keratan sulfate in normal and macular corneal dystrophy type I. *Glycobiology* 10: 305-312.
- Lewis PN, Pinali C, Young RD, Meek KM, Quantock AJ, Knupp C (2010) Structural Interactions between Collagen and Proteoglycans Are Elucidated by Three-Dimensional Electron Tomography of Bovine Cornea. *Structure* 18: 239-245.
- Li K, Tamai K, Tan EM, Uitto J (1993) Cloning of type XVII collagen. Complementary and genomic DNA sequences of mouse 180-kilodalton bullous pemphigoid antigen (BPAG2) predict an interrupted collagenous domain, a transmembrane segment, and unusual features in the 5'-end of the gene and the 3'-untranslated region of the mRNA. *Journal of Biological Chemistry* 268: 8825-8834.
- Li W, Vergnes J-P, Cornuet PK, Hassell JR (1992) cDNA clone to chick corneal chondroitin/dermatan sulfate proteoglycan reveals identity to decorin. *Archives of Biochemistry and Biophysics* 296: 190-197.
- Liles M, Palka BP, Harris A, Kerr B, Hughes C, Young RD, Meek KM, Caterson B, Quantock AJ (2010) Differential relative sulfation of keratan sulfate glycosaminoglycan in the chick cornea during embryonic development. *Investigative Ophthalmology & Visual Science* 51: 1365-1372.
- Linsenmayer TF, Bruns RR, Mentzer A, Mayne R (1986) Type VI collagen: immunohistochemical identification as a filamentous component of the extracellular matrix of the developing avian corneal stroma. *Developmental Biology* 118: 425-431.

- Linsenmayer TF, Fitch JM, Gordon MK, Cai CX, Igoe F, Marchant JK, Birk DE (1998) Development and roles of collagenous matrices in the embryonic avian cornea. *Progress in Retina and Eye Research* 17: 231-265.
- Linsenmayer TF, Gibney E, Igoe F, Gordon MK, Fitch JM, Fessler LI, Birk DE (1993) Type V collagen: molecular structure and fibrillar organization of the chicken alpha 1(V) NH2-terminal domain, a putative regulator of corneal fibrillogenesis. *Journal of Cell Biology* 121: 1181-1189.
- Liskova P, Veraitch B, Jirsova K, Filipce M, Neuwirth A, Ebenezer ND, Hysi PG, Hardcastle AJ, Tuft SJ, Bhattacharya SS (2008) Sequencing of the CHST6 gene in Czech macular corneal dystrophy patients supports the evidence of a founder mutation. *British Journal of Ophthalmology* 92: 265-267.
- Little PJ, Ballinger ML, Burch ML, Osman N (2008) Biosynthesis of Natural and Hyperelongated Chondroitin Sulfate Glycosaminoglycans: New Insights into an Elusive Process. *Open Biochemistry Journal* 2: 135-142.
- Liu C-Y, Shiraishi A, Kao CWC, Converse RL, Funderburgh JL, Corpuz LM, Conrad GW, Kao WWY (1998) The cloning of mouse keratocan cDNA and genomic DNA and the characterization of its expression during eye development. *Journal of Biological Chemistry* 273: 22584-22588.
- Liu N-P, Bao W, Smith CF, Vance JM, Klintworth GK (2005) Different mutations in carbohydrate sulfotransferase 6 (CHST6) gene cause macular corneal dystrophy types I and II in a single sibship. *American journal of ophthalmology* 139: 1118-1120.
- Liu NP, Dew-Knight S, Rayner M, Jonasson F, Akama TO, Fukuda MN, Bao W, Gilbert JR, Vance JM, Klintworth GK (2000) Mutations in corneal carbohydrate sulfotransferase 6 gene (CHST6) cause macular corneal dystrophy in Iceland. *Molecular Vision* 6: 261-264.
- Liu NP, Smith CF, Bowling BL, Jonasson F, Klintworth GK (2006) Macular corneal dystrophy types I and II are caused by distinct mutations in the CHST6 gene in Iceland. *Molecular Vision* 12: 1148-1152.
- Lorincz AE (1978) The mucopolysaccharidoses: advances in understanding and treatment. *Pediatric Annals* 7: 104-122.
- Mac A, Joy J (2000) Marijuana and glaucoma. Marijuana as medicine? The science beyond the controversy. Washington DC: National Academy Press. pp 124-128.
- Malley DS, Steinert RF, Puliafito CA, Dobi ET (1990) Immunofluorescence study of corneal wound healing after excimer laser anterior keratectomy in the monkey eye. *Archives of Ophthalmology* 108: 1316-1322.
- Marshall GE, Konstas AG, Lee WR (1993) Collagens in ocular tissues. *British Journal of Ophthalmology* 77: 515-524.
- Maurice DM (1957) The structure and transparency of the cornea. *Journal of Physiology* 136: 263-286.
- Maurice DM (1972) The location of the fluid pump in the cornea. *Journal of Physiology* 221: 43-54.
- McEwan PA, Scott PG, Bishop PN, Bella J (2006) Structural correlations in the family of small leucine-rich repeat proteins and proteoglycans. *Journal of Structural Biology* 155: 294-305.
- Meek KM, Blamires T, Elliott GF, Gyi TJ, Nave C (1987) The organisation of collagen fibrils in the human corneal stroma: a synchrotron X-ray diffraction study. *Current Eye Research* 6: 841-846.

- Meek KM, Elliott GF, Nave C (1986) A synchrotron X-ray diffraction study of bovine cornea stained with cupromeronic blue. *Collagen and Related Research* 6: 203-218.
- Meek KM, Elliott GF, Sayers Z, Whitburn SB, Koch MHJ (1981) Interpretation of the meridional X-ray diffraction pattern from collagen fibrils in corneal stroma. *Journal of Molecular Biology* 149: 477-488.
- Meek KM, Fullwood NJ (2001) Corneal and scleral collagens-a microscopist's perspective. *Micron* 32: 261-272.
- Meek KM, Leonard DW (1993) Ultrastructure of the corneal stroma: a comparative study. *Biophysical Journal* 64: 273-280.
- Meek KM, Leonard DW, Connon CJ, Dennis S, Khan S (2003a) Transparency, swelling and scarring in the corneal stroma. *Eye* 17: 927-936.
- Meek KM, Quantock AJ (2001) The use of X-ray scattering techniques to determine corneal ultrastructure. *Progress in Retinal and Eye Research* 20: 95-137.
- Meek KM, Quantock AJ, Boote C, Liu CY, Kao WWY (2003b) An X-ray scattering investigation of corneal structure in keratocan-deficient mice. *Matrix Biology* 22: 467-475.
- Meek KM, Quantock AJ, Elliott GF, Ridgway AEA, Tullo AB, Bron AJ, Thonar EJMA (1989) Macular corneal dystrophy: The macromolecular structure of the stroma observed using electron microscopy and synchrotron X-ray diffraction. *Experimental Eye Research* 49: 941-958.
- Meek KM, Tuft SJ, Huang Y, Gill PS, Hayes S, Newton RH, Bron AJ (2005) Changes in collagen orientation and distribution in keratoconus corneas. *Investigative Ophthalmology & Visual Science* 46: 1948-1956.
- Mehmet H, Scudder P, Tang P, W., Hounsell EF, Feizi T, Caterson B (1986) The antigenic determinants recognized by three monoclonal antibodies to keratan sulphate involve sulphated hepta- or larger oligosaccharides of the poly(N-acetyllactosamine) series. *European Journal of Biochemistry* 157: 385-391.
- Mendler M, Eich-Bender SG, Vaughan L, Winterhalter KH, Bruckner P (1989) Cartilage contains mixed fibrils of collagen types II, IX, and XI. *Journal of Cell Biology* 108: 191-197.
- Merline R, Schaefer R, Schaefer L (2009) The matricellular functions of small leucine-rich proteoglycans (SLRPs). *Journal of Cell Communication and Signaling* 3: 323-235.
- Michelacci YM (2003) Collagens and proteoglycans of the corneal extracellular matrix. *Brazilian Journal of Medical and Biological Research* 36: 1037-1046.
- Midura RJ, Hascall VC (1989) Analysis of the proteoglycans synthesized by corneal explants from embryonic chicken. II. Structural characterization of the keratan sulfate and dermatan sulfate proteoglycans from corneal stroma. *Journal of Biological Chemistry* 264: 1423-1430.
- Midura RJ, Hascall VC, MacCallum DK, Meyer RF, Thonar EJ, Hassell JR, Smith CF, Klintworth GK (1990) Proteoglycan biosynthesis by human corneas from patients with types 1 and 2 macular corneal dystrophy. *Journal of Biological Chemistry* 265: 15947-15955.
- Midura RJ, Toledo OM, Yanagishita M, Hascall VC (1989) Analysis of the proteoglycans synthesized by corneal explants from embryonic chicken. I. Characterization of the culture system with emphasis on stromal proteoglycan biosynthesis. *Journal of Biological Chemistry* 264: 1414-1422.

- Miller EJ, Matukas VJ (1969) Chick cartilage collagen: a new type of alfa chain not present in bone or skin of the species. *Proceedings of the National Academy of Sciences of the United States of America* 64: 1264-1268.
- Mollard RJ, Telegan P, Haskins ME, Aguirre GD (1996) Corneal endothelium in mucopolysaccharide storage disorders. Morphologic studies in animal models. *Cornea* 15: 25-34.
- Nagata K (1998) Expression and function of heat shock protein 47: A collagen-specific molecular chaperone in the endoplasmic reticulum. *Matrix Biology* 16: 379-386.
- Nakazawa K, Hassell JR, Hascall VC, Lohmander LS, Newsome DA, Krachmer J (1984) Defective processing of keratan sulfate in macular corneal dystrophy. *Journal of Biological Chemistry* 259: 13751-13757.
- Nakazawa K, Isomura T, Shimoeda S (1995) Proteoglycan synthesis by chicken corneal explants. *Journal of Biochemistry (Tokyo)* 117: 697-706.
- Neame PJ, Kay CJ (2000) Small leucine-rich proteoglycans. In: Proteoglycans: structure, biology and molecular interactions. Iozzo RV, editor. Philadelphia: Marcel Dekker Inc.
- Niel F, Ellies P, Dighiero P, Soria J, Sabbagh C, San C, Renard G, Delpech M, Valleix S (2003) Truncating mutations in the carbohydrate sulfotransferase 6 gene (CHST6) result in macular corneal dystrophy. *Investigative Ophthalmology & Visual Science* 44: 2949-2953.
- Odland M (1968) Dystrophia corneae parenchymatosa congenita. A clinical, morphological and histochemical examination. *Acta Ophthalmologica (Copenh)* 46: 477-485.
- Oeben M, Keller R, Stuhlsatz HW, Greiling H (1987) Constant and variable domains of different disaccharide structure in corneal keratan sulphate chains. *Biochemical Journal* 248: 85-93.
- Orgel JPRO, Wess TJ, Miller A (2000) The in situ conformation and axial location of the intermolecular cross-linked non-helical telopeptides of type I collagen. *Structure* 8: 137-142.
- Orgel JPRO, Eid A, Antipova O, Bella J, Scott JE (2009) Decorin core protein (Decoron) shape complements collagen fibril surface structure and mediates its binding. *PLoS ONE* 4: e7028.
- Oyster C (1999) The human eye : structure and function: Sunderland, Mass. : Sinauer Associates ; Basingstoke : Macmillan.
- Parfitt GJ, Pinali C, Young RD, Quantock AJ, Knupp C (2010) Three-dimensional reconstruction of collagen-proteoglycan interactions in the mouse corneal stroma by electron tomography. *Journal of Structural Biology* 170: 392-397.
- Petruska JA, Hodge AJ (1964) A subunit model for the tropocollagen macromolecule. *Proceedings of the National Academy of Sciences of the United States of America* 51: 871-876.
- Plaas AH, West LA, Thonar EJA, Karcioğlu ZA, Smith CJ, Klintworth GK, Hascall VC (2001) Altered fine structures of corneal and skeletal keratan sulfate and chondroitin/dermatan sulfate in macular corneal dystrophy. *Journal of Biological Chemistry* 276: 39788-39796.
- Plessy B, Bettelheim FA (1975) Water vapor sorption of keratan sulfate. *Molecular and Cellular Biochemistry* 6: 85-91.
- Prashar A, Hocking PM, Erichsen JT, Fan Q, Saw SM, Guggenheim JA (2009) Common determinants of body size and eye size in chickens from an advanced intercross line. *Experimental Eye Research* 89: 42-48.
- Quantock AJ, Boote C, Siegler V, Meek KM (2003) Collagen organization in the secondary chick cornea during development. *Investigative Ophthalmology & Visual Science* 44: 130-136.

- Quantock AJ, Boote C, Young RD, Hayes S, Tanioka H, Kawasaki S, Ohta N, Iida T, Yagi N, Kinoshita S, Meek KM (2007) Small-angle fibre diffraction studies of corneal matrix structure: a depth-profiled investigation of the human eye-bank cornea. *Journal of Applied Crystallography* 40(s1): 335-340.
- Quantock AJ, Fullwood NJ, Thonar EJ, Waltman SR, Capel MS, Ito M, Verity SM, Schanzlin DJ (1997) Macular corneal dystrophy type II: multiple studies on a cornea with low levels of sulphated keratan sulphate. *Eye (Lond)* 11: 57-67.
- Quantock AJ, Kinoshita S, Capel MS, Schanzlin DJ (1998) A synchrotron X-ray diffraction study of developing chick corneas. *Biophysical Journal* 74: 995-998.
- Quantock AJ, Meek KM, Fullwood NJ, Zabel RW (1993a) Scheie's syndrome: the architecture of corneal collagen and distribution of corneal proteoglycans. *Canadian Journal of Ophthalmology* 28: 266-272.
- Quantock AJ, Meek KM, Ridgway AE, Bron AJ, Thonar EJ (1990) Macular corneal dystrophy: reduction in both corneal thickness and collagen interfibrillar spacing. *Current Eye Research* 9: 393-398.
- Quantock AJ, Meek KM, Thonar EJ (1992) Analysis of high-angle synchrotron x-ray diffraction patterns obtained from macular dystrophy corneas. *Cornea* 11: 185-190.
- Quantock AJ, Meek KM, Thonar EJ, Assil KK (1993b) Synchrotron X-ray diffraction in atypical macular dystrophy. *Eye (Lond)* 7: 779-784.
- Rada JA, Achen VR, Perry CA, Fox PW (1997) Proteoglycans in the human sclera. Evidence for the presence of aggrecan. *Investigative Ophthalmology & Visual Science* 38: 1740-1751.
- Rada JA, Cornuet PK, Hassell JR (1993) Regulation of corneal collagen fibrillogenesis in vitro by corneal proteoglycan (lumican and decorin) core proteins. *Experimental Eye Research* 56: 635-648.
- Radner W, Zehetmayer M, Aufreiter R, Mallinger R (1998) Interlacing and cross-angle distribution of collagen lamellae in the human cornea. *Cornea* 17: 537-543.
- Ramshaw JAM, Shah NK, Brodsky B (1998) Gly-X-Y Tripeptide Frequencies in Collagen: A Context for Host-Guest Triple-Helical Peptides. *Journal of Structural Biology* 122: 86-91.
- Raspanti M, Viola M, Forlino A, Tenni R, Gruppi C, Tira ME (2008) Glycosaminoglycans show a specific periodic interaction with type I collagen fibrils. *Journal of Structural Biology* 164: 134-139.
- Rawe IM, Leonard DW, Meek KM, Zabel RW (1997) X-ray diffraction and transmission electron microscopy of Morquio syndrome type A cornea: a structural analysis. *Cornea* 16: 369-376.
- Ray J, Bouvet A, DeSanto C, Fyfe JC, Xu D, Wolfe JH, Aguirre GD, Patterson DF, Haskins ME, Henthorn PS (1998) Cloning of the canine [beta]-glucuronidase cDNA, mutation identification in canine MPS VII, and retroviral vector-mediated correction of MPS VII cells. *Genomics* 48: 248-253.
- Rødahl E, Van Ginderdeuren R, Knappskog PM, Bredrup C, Boman H (2006) A second decorin frame shift mutation in a family with congenital stromal corneal dystrophy. *American Journal of Ophthalmology* 142: 520-521.
- Rosenberg LC, Choi HU, Tang LH, Johnson TL, Pal S, Webber C, Reiner A, Poole AR (1985) Isolation of dermatan sulfate proteoglycans from mature bovine articular cartilages. *Journal of Biological Chemistry* 260: 6304-6313.

- Rózsa AJ, Beuerman RW (1982) Density and organization of free nerve endings in the corneal epithelium of the rabbit. *Pain* 14: 105-120.
- Ruggiero F, Burillon C, Garrone R (1996) Human corneal fibrillogenesis. Collagen V structural analysis and fibrillar assembly by stromal fibroblasts in culture. *Investigative Ophthalmology & Visual Science* 7: 1749-1760.
- Ruhland C, Schonherr E, Robenek H, Hansen U, Iozzo RV, Bruckner P, Seidler DG (2007) The glycosaminoglycan chain of decorin plays an important role in collagen fibril formation at the early stages of fibrillogenesis. *FEBS Journal* 274: 4246-4255.
- Rummelt V, Meyer HJ, Naumann GO (1992) Light and electron microscopy of the cornea in systemic mucopolysaccharidosis type I-S (Scheie's syndrome). *Cornea* 11: 86-92.
- Ruter ER, Kresse H (1984) Partial purification and characterization of 3'-phosphoadenylylsulfate:keratan sulfate sulfotransferases. *Journal of Biological Chemistry* 259: 11771-11776.
- Sage H, Trueb B, Bornstein P (1983) Biosynthetic and structural properties of endothelial cell type VIII collagen. *Journal of Biological Chemistry* 258: 13391-13401.
- Saika S, Shiraishi A, Saika S, Liu C-Y, Funderburgh JL, Kao CWC, Converse RL, Kao WWY (2000) Role of Lumican in the Corneal Epithelium during Wound Healing. *Journal of Biological Chemistry* 275: 2607-2612.
- Saito T, Nishida K, Nakayama J, Akama TO, Fukuda MN, Watanabe K, Quantock AJ, Maeda N, Watanabe H, Tano Y (2008) Sulfation patterns of keratan sulfate in different macular corneal dystrophy immunophenotypes using three different probes. *British Journal of Ophthalmology* 92: 1434-1436.
- Sampaio LdO, Bayliss MT, Hardingham TE, Muir H (1988) Dermatan sulphate proteoglycan from human articular cartilage. Variation in its content with age and its structural comparison with a small chondroitin sulphate proteoglycan from pig laryngeal cartilage. *Biochemical Journal* 254: 757-764.
- Sands MS, Barker JE, Vogler C, Levy B, Gwynn B, Galvin N, Sly WS, Birkenmeier EH (1993) Treatment of murine mucopolysaccharidosis type VII by syngeneic bone marrow transplantation in neonates. *Laboratory Investigation* 68: 676-686.
- Sands MS, Birkenmeier EH (1993) A single-base-pair deletion in the beta-glucuronidase gene accounts for the phenotype of murine mucopolysaccharidosis type VII. *Proceedings of the National Academy of Sciences of the United States of America* 90: 6567-6571.
- Sands MS, Vogler C, Kyle JW, Grubb JH, Levy B, Galvin N, Sly WS, Birkenmeier EH (1994) Enzyme replacement therapy for murine mucopolysaccharidosis type VII. *The Journal of Clinical Investigation* 93: 2324-2331.
- Sands MS, Vogler C, Torrey A, Levy B, Gwynn B, Grubb J, Sly WS, Birkenmeier EH (1997a) Murine mucopolysaccharidosis type VII: long term therapeutic effects of enzyme replacement and enzyme replacement followed by bone marrow transplantation. *The Journal of Clinical Investigation* 99: 1596-1605.
- Sands MS, Wolfe JH, Birkenmeier EH, Barker JE, Vogler C, Sly WS, Okuyama T, Freeman B, Nicholes A, Muzyczka N, Chang PL, Axelrod HR (1997b) Gene therapy for murine mucopolysaccharidosis type VII. *Neuromuscular Disorders* 7: 352-360.
- Sawada H, Konomi H, Hirosawa K (1990) Characterization of the collagen in the hexagonal lattice of Descemet's membrane: its relation to type VIII collagen. *Journal of Cell Biology* 110: 219-227.

- Schaefer L, Grone H-J, Raslik I, Robenek H, Ugorcakova J, Budny S, Schaefer RM, Kresse H (2000) Small proteoglycans of normal adult human kidney: Distinct expression patterns of decorin, biglycan, fibromodulin, and lumican. *Kidney International* 58: 1557-1568.
- Schaefer L, Iozzo RV (2008) Biological Functions of the Small Leucine-rich Proteoglycans: From Genetics to Signal Transduction. *Journal of Biological Chemistry* 283: 21305-21309.
- Schaefer L, Schaefer R (2010) Proteoglycans: from structural compounds to signaling molecules. *Cell and Tissue Research* 339: 237-246.
- Schaeffel F, Howland HC (1987) Corneal accommodation in chick and pigeon. *Journal of Comparative Physiology A: Neuroethology, Sensory, Neural, and Behavioral Physiology* 160: 375-384.
- Schwartz MF, Werblin TP, Green WR (1985) Occurrence of mucopolysaccharide in corneal grafts in the Maroteaux-Lamy syndrome. *Cornea* 4: 58-66.
- Scott JE (1972) Histochemistry of Alcian blue. 3. The molecular biological basis of staining by Alcian blue 8GX and analogous phthalocyanins. *Histochemie* 32: 191-212.
- Scott JE (1980) Collagen-proteoglycan interactions. Localization of proteoglycans in tendon by electron microscopy. *Biochemical Journal* 187: 887-891.
- Scott JE (1988) Proteoglycan-fibrillar collagen interactions. *Biochemical Journal* 252: 313-323.
- Scott JE (1991a) Proteoglycan: collagen interactions and corneal ultrastructure. *Biochemical Society transactions* 19: 877-881.
- Scott JE (1991b) Proteoglycan:collagen interactions in connective tissues. Ultrastructural, biochemical, functional and evolutionary aspects. *International Journal of Biological Macromolecules* 13: 157-161.
- Scott JE (1992) Morphometry of cupromeronic blue-stained proteoglycan molecules in animal corneas, versus that of purified proteoglycans stained in vitro, implies that tertiary structures contribute to corneal ultrastructure. *Journal of Anatomy* 180: 155-164.
- Scott JE (1994) Keratan sulphate--a 'reserve' polysaccharide? *European Journal of Clinical Chemistry and Clinical Biochemistry* 32: 217-223.
- Scott JE, Bosworth TR (1990) A comparative biochemical and ultrastructural study of proteoglycan-collagen interactions in corneal stroma. Functional and metabolic implications. *Biochemical Journal* 270: 491-497.
- Scott JE, Haigh M (1985) 'Small'-proteoglycan: collagen interactions: Keratan sulphate proteoglycan associates with rabbit corneal collagen fibrils at the 'a' and 'c' bands. *Bioscience Reports* 5: 765-774.
- Scott JE, Haigh M (1988a) Identification of specific binding sites for keratan sulphate proteoglycans and chondroitin-dermatan sulphate proteoglycans on collagen fibrils in cornea by the use of cupromeronic blue in 'critical-electrolyte-concentration' techniques. *Biochemical Journal* 253: 607-610.
- Scott JE, Haigh M (1988b) Keratan sulphate and the ultrastructure of cornea and cartilage: a 'stand-in' for chondroitin sulphate in conditions of oxygen lack? *Journal of Anatomy* 158: 95-108.
- Scott JE, Haigh M (1988c) Keratan sulphate is unevenly distributed from back to front of bovine cornea. *Biochemical Society Transactions* 16: 333-334.
- Scott JE, Orford CR (1981) Dermatan sulphate-rich proteoglycan associates with rat tail-tendon collagen at the d band in the gap region. *Biochemical Journal* 197: 213-216.

- Scott PG, McEwan PA, Dodd CM, Bergmann EM, Bishop PN, Bella J (2004) Crystal structure of the dimeric protein core of decorin, the archetypal small leucine-rich repeat proteoglycan. *Proceedings of the National Academy of Sciences of the United States of America* 101: 15633-15638.
- Scudder P, Tang PW, Hounsell EF, Mehmet H, Feizi T, Lawson AM (1986) Isolation and characterization of sulphated oligosaccharides released from bovine corneal keratan sulphate by the action of endo- β -galactosidase. *European Journal of Biochemistry* 157: 365-373.
- Shaw LM, Olsen BR (1991) FACIT collagens: diverse molecular bridges in extracellular matrices. *Trends in Biochemical Sciences* 16: 191-194.
- Shoulders MD, Raines RT (2009) Collagen structure and stability. *Annual Review of Biochemistry* 78: 929-958.
- Siegler V, Quantock AJ (2002) Two-stage compaction of the secondary avian cornea during development. *Experimental Eye Research* 74: 427-431.
- Silbert CK, Palmer ME, Humphries DE, Silbert JE (1989) Production of [^3H]hexosamine-labeled proteoglycans by cultures of normal and diabetic skin fibroblasts: Dilution of exogenous [^3H]glucosamine by endogenous hexosamine from glucose and other sources. *Archives of Biochemistry and Biophysics* 268: 393-397.
- Silverstein Dombrowski DC, Carmichael PK, Wang P, O'Malley TM, Haskins ME, Giger U (2004) Mucopolysaccharidosis type VII in a German Shepherd Dog. *Journal of the American Veterinary Medical Association* 224: 553-557, 532-533.
- Sly WS, Quinton BA, McAlister WH, Rimoin DL (1973) Beta glucuronidase deficiency: report of clinical, radiologic, and biochemical features of a new mucopolysaccharidosis. *The Journal of pediatrics* 82: 249-257.
- Sly WS, Vogler C, Grubb JH, Zhou M, Jiang J, Zhou XY, Tomatsu S, Bi Y, Snella EM (2001) Active site mutant transgene confers tolerance to human β -glucuronidase without affecting the phenotype of MPS VII mice. *Proceedings of the National Academy of Sciences of the United States of America* 98: 2205-2210.
- Smith JW (1969) The transparency of the corneal stroma. *Vision Research* 9: 393-396, IN313-IN314.
- Smith JW, Frame J (1969) Observations on the collagen and proteinpolysaccharide complex of rabbit corneal stroma. *Journal of Cell Science* 4: 421-436.
- Sorrell JM, Carrino DA, Caplan AI (1993) Structural domains in chondroitin sulfate identified by anti-chondroitin sulfate monoclonal antibodies. Immunosequencing of chondroitin sulfates. *Matrix* 13: 351-361.
- Sorrell JM, Mahmoodian F, Schafer IA, Davis B, Caterson B (1990) Identification of monoclonal antibodies that recognize novel epitopes in native chondroitin/dermatan sulfate glycosaminoglycan chains: their use in mapping functionally distinct domains of human skin. *Journal of Histochemistry and Cytochemistry* 38: 393-402.
- Speleman F, Vervoort R, van Roy N, Liebaers I, Sly WS, Lissens W (1996) Localization by fluorescence in situ hybridization of the human functional beta-glucuronidase gene (GUSB) to 7q11.21 --> q11.22 and two pseudogenes to 5p13 and 5q13. *Cytogenetics and Cell Genetics* 72: 53-55.
- Spencer WH (1996) Cornea: inherited systemic metabolic diseases with corneal involvement. Ophthalmic pathology. An atlas and textbook. 4th ed. Philadelphia, USA: W. B. Saunders. pp 282-299.

- Stein T, Keller R, Stuhlsatz HW, Greiling H, Ohst E, Muller E, Scharf HD (1982) Structure of the linkage-region between polysaccharide chain and core protein in bovine corneal proteokeratan sulfate. *Hoppe-Seyler's Zeitschrift fur physiologische Chemie* 363: 825-833.
- Stockwell RA (1991) Morphometry of cytoplasmic components of mammalian articular chondrocytes and corneal keratocytes: species and zonal variations of mitochondria in relation to nutrition. *Journal of Anatomy* 175: 251-261.
- Stockwell RA, Scott JE (1965) Observations on the acid glycosaminoglycan (mucopolysaccharide) content of the matrix of aging cartilage. *Annals of the Rheumatic Diseases* 24: 341-350.
- Sugar J (1997) Metabolic disorders of the cornea. In: The Cornea. 2nd ed. Kaufman HE, Barron BA, McDonald MB, editors. Oxford: Butterworth-Heinemann, pp 391-410.
- Sultana A, Klintworth GK, Thonar EJ, Vemuganti GK, Kannabiran C (2009) Immunophenotypes of macular corneal dystrophy in India and correlation with mutations in CHST6. *Molecular Vision* 15: 319-325.
- Svoboda KK, Nishimura I, Sugrue SP, Ninomiya Y, Olsen BR (1988) Embryonic chicken cornea and cartilage synthesize type IX collagen molecules with different amino-terminal domains. *Proceedings of the National Academy of Sciences of the United States of America* 85: 7496-7500.
- Tabone E, Grimaud JA, Peyrol S, Grandperret D, Durand L (1978) Ultrastructural aspects of corneal fibrous tissue in the Scheie syndrome. *Virchows Archiv B Cell Pathology* 27: 63-67.
- Takahashi I, Nakamura Y, Hamada Y, Nakazawa K (1999) Immunohistochemical analysis of proteoglycan biosynthesis during early development of the chicken cornea. *Journal of Biochemistry (Tokyo)* 126: 804-814.
- Tasheva ES, Koester A, Paulsen AQ, Garrett AS, Boyle DL, Davidson HJ, Song M, Fox N, Conrad GW (2002) Mimecan/osteoglycin-deficient mice have collagen fibril abnormalities. *Molecular Vision* 8: 407-415.
- Thonar EJ, Meyer RF, Dennis RF, Lenz ME, Maldonado B, Hassell JR, Hewitt AT, Stark WJJ, Stock EL, Kuettner KE (1986) Absence of normal keratan sulfate in the blood of patients with macular corneal dystrophy. *American Journal of Ophthalmology* 102: 561-569.
- Tomatsu S, Montañño AM, Dung VC, Grubb JH, Sly WS (2009) Mutations and polymorphisms in GUSB gene in mucopolysaccharidosis VII (Sly Syndrome). *Human Mutation* 30: 511-519.
- Tomatsu S, Orii KO, Vogler C, Grubb JH, Snella EM, Gutierrez M, Dieter T, Holden CC, Sukegawa K, Orii T, Kondo N, Sly WS (2003) Production of MPS VII mouse (Gustm(hE540A{middle dot}mE536A)Sly) doubly tolerant to human and mouse {beta}-glucuronidase. *Human Molecular Genetics* 12: 961-973.
- Tomino S, Paigen K, Tulsiani DR, Touster O (1975) Purification and chemical properties of mouse liver lysosomal (L form) beta-glucuronidase. *Journal of Biological Chemistry* 250: 8503-8509.
- Toole BP, Trelstad RL (1971) Hyaluronate production and removal during corneal development in the chick. *Developmental Biology* 26: 28-35.
- Topping TM, Kenyon KR, Goldberg MF, Maumenee AE (1971) Ultrastructural ocular pathology of Hunter's syndrome. Systemic mucopolysaccharidosis type II. *Archives of Ophthalmology* 86: 164-177.
- Tovee MJ (2008) An introduction to the visual system. New York: Cambridge university press.

- Trelstad RL, Coulombre AJ (1971) Morphogenesis of the collagenous stroma in the chick cornea. *Journal of Cell Biology* 50: 840-858.
- Trelstad RL, Kang AH (1974) Collagen heterogeneity in the avian eye: Lens, vitreous body, cornea and sclera. *Experimental Eye Research* 18: 395-406.
- Turpin R, Tisserand M, Serane (1939) Opacities corneennes hereditaires et congenitales reparties sur trois generations et atteignant deux jumelles monozygotes. *Archives of Ophthalmology (Paris)* 3: 109-111.
- Twersky V (1975) Transparency of pair-correlated, random distributions of small scatterers, with applications to the cornea. *Journal of the Optical Society of America* 65: 524-530.
- Uchimura K, Muramatsu H, Kadomatsu K, Fan Q-W, Kurosawa N, Mitsuoka C, Kannagi R, Habuchi O, Muramatsu T (1998) Molecular cloning and characterization of an N-acetylglucosamine-6-O-sulfotransferase. *Journal of Biological Chemistry* 273: 22577-22583.
- van der Rest M, Mayne R (1988) Type IX collagen proteoglycan from cartilage is covalently cross-linked to type II collagen. *Journal of Biological Chemistry* 263: 1615-1618.
- van der Rest M, Mayne R, Ninomiya Y, Seidah NG, Chretien M, Olsen BR (1985) The structure of type IX collagen. *Journal of Biological Chemistry* 260: 220-225.
- Van Ginderdeuren R, De Vos R, Casteels I, Foets B (2002) Report of a new family with dominant congenital heredity stromal dystrophy of the cornea. *Cornea* 21: 118-120.
- Veit G, Kobbe B, Keene DR, Paulsson M, Koch M, Wagener R (2006) Collagen XXVIII, a novel von Willebrand factor A domain-containing protein with many imperfections in the collagenous domain. *Journal of Biological Chemistry* 281: 3494-3504.
- Villone D, Fritsch A, Koch M, Bruckner-Tuderman L, Hansen U, Bruckner P (2008) Supramolecular interactions in the dermo-epidermal junction zone: anchoring fibril-collagen VII tightly binds to banded collagen fibrils. *Journal of Biological Chemistry* 283: 24506-24513.
- Vogel KG, Paulsson M, Heinegard D (1984) Specific inhibition of type I and type II collagen fibrillogenesis by the small proteoglycan of tendon. *Biochemical Journal* 223: 587-597.
- Vogel KG, Trotter JA (1987) The effect of proteoglycans on the morphology of collagen fibrils formed in vitro. *Collagen and Related Research* 7: 105-114.
- Vogler C, Barker J, Sands MS, Levy B, Galvin N, Sly WS (2001) Murine mucopolysaccharidosis VII: Impact of therapies on the phenotype, clinical course, and pathology in a model of a lysosomal storage disease. *Pediatric and Developmental Pathology* 4: 421-433.
- Vogler C, Levy B, Galvin NJ, Thorpe C, Sands MS, Barker JE, Baty J, Birkenmeier EH, Sly WS (1999) Enzyme replacement in murine mucopolysaccharidosis type VII: neuronal and glial response to beta-glucuronidase requires early initiation of enzyme replacement therapy. *Pediatric Research* 45: 838-844.
- Vogler C, Levy B, Grubb JH, Galvin N, Tan Y, Kakkis E, Pavloff N, Sly WS (2005) Overcoming the blood-brain barrier with high-dose enzyme replacement therapy in murine mucopolysaccharidosis VII. *Proceedings of the National Academy of Sciences of the United States of America* 102: 14777-14782.
- Warren JF, Aldave AJ, Srinivasan M, Thonar EJ, Kumar AB, Cevallos V, Whitcher JP, Margolis TP (2003) Novel mutations in the CHST6 gene associated with macular corneal dystrophy in southern India. *Archives of Ophthalmology* 121: 1608-1612.
- Weber IT, Harrison RW, Iozzo RV (1996) Model structure of decorin and implications for collagen fibrillogenesis. *Journal of Biological Chemistry* 271: 31767-31770.

- Wenstrup RJ, Florer JB, Brunskill EW, Bell SM, Chervoneva I, Birk DE (2004) Type V collagen controls the initiation of collagen fibril assembly. *Journal of Biological Chemistry* 279: 53331-53337.
- Wess TJ, Hammersley AP, Wess L, Miller A (1998) A consensus model for molecular packing of type I collagen. *Journal of Structural Biology* 122: 92-100.
- Witschel H, Fine BS, Grutzner P, McTigue JW (1978) Congenital hereditary stromal dystrophy of the cornea. *Archives of Ophthalmology* 96: 1043-1051.
- Worthington CR, Inouye H (1985) X-ray diffraction study of the cornea. *International Journal of Biological Macromolecules* 7: 2-8.
- Yang CJ, SundarRaj N, Thonar EJ, Klintworth GK (1988) Immunohistochemical evidence of heterogeneity in macular corneal dystrophy. *American Journal of Ophthalmology* 106: 65-71.
- Yee RW, Matsuda M, Schultz RO, Edelhauser HF (1985) Changes in the normal corneal endothelial cellular pattern as a function of age. *Current Eye Research* 4: 671-678.
- Ying S, Shiraishi A, Kao CWC, Converse RL, Funderburgh JL, Swiergiel J, Roth MR, Conrad GW, Kao WWY (1997) Characterization and Expression of the Mouse Lumican Gene. *Journal of Biological Chemistry* 272: 30306-30313.
- Young BB, Zhang G, Koch M, Birk DE (2002) The roles of types XII and XIV collagen in fibrillogenesis and matrix assembly in the developing cornea. *Journal of Cellular Biochemistry* 87: 208-220.
- Young RD (1985) The ultrastructural organization of proteoglycans and collagen in human and rabbit scleral matrix. *Journal of Cell Science* 74: 95-104.
- Young RD, Akama TO, Liskova P, Ebenezer ND, Allan B, Kerr B, Caterson B, Fukuda MN, Quantock AJ (2007a) Differential immunogold localisation of sulphated and unsulphated keratan sulphate proteoglycans in normal and macular dystrophy cornea using sulphation motif-specific antibodies. *Histochemistry and Cell Biology* 127: 115-120.
- Young RD, Gealy EC, Liles M, Caterson B, Ralphs JR, Quantock AJ (2007b) Keratan sulfate glycosaminoglycan and the association with collagen fibrils in rudimentary lamellae in the developing avian cornea. *Investigative Ophthalmology & Visual Science* 48: 3083-3088.
- Young RD, Tudor D, Hayes AJ, Kerr B, Hayashida Y, Nishida K, Meek KM, Caterson B, Quantock AJ (2005) Atypical composition and ultrastructure of proteoglycans in the mouse corneal stroma. *Investigative Ophthalmology & Visual Science* 46: 1973-1978.
- Yurchenco PD, Ruben GC (1988) Type IV collagen lateral associations in the EHS tumor matrix. Comparison with amniotic and in vitro networks. *The American journal of pathology* 132: 278-291.
- Zabel RW, MacDonald IM, Mintsoulis G, Addison DJ (1989) Scheie's syndrome. An ultrastructural analysis of the cornea. *Ophthalmology* 96: 1631-1638.
- Zhang G, Chen S, Goldoni S, Calder BW, Simpson HC, Owens RT, McQuillan DJ, Young MF, Iozzo RV, Birk DE (2009) Genetic evidence for the coordinated regulation of collagen fibrillogenesis in the cornea by decorin and biglycan. *Journal of Biological Chemistry* 284: 8888-8897.
- Zhang Y, Conrad AH, Tasheva ES, An K, Corpuz LM, Kariya Y, Suzuki K, Conrad GW (2005) Detection and quantification of sulfated disaccharides from keratan sulfate and chondroitin/dermatan sulfate during chick corneal development by ESI-MS/MS. *Investigative Ophthalmology & Visual Science* 46: 1604-1614.